DEVELOPING BIOMATERIAL-BASED STRATEGIES TO ENHANCE THE DELIVERY AND ACCESSIBILITY OF BACTERIOPHAGE THERAPEUTICS

DEVELOPING BIOMATERIAL-BASED STRATEGIES TO ENHANCE THE DELIVERY AND ACCESSIBILITY OF BACTERIOPHAGE THERAPEUTICS

By FERESHTEH BAYAT, B.A.Sc., M.A.Sc.

A Thesis Submitted to the School of Graduate Studies in Partial Fulfilment of the Requirements for the Degree Doctor of Philosophy

DOCTOR OF PHILOSOPHY (2023)

School of Biomedical Engineering, McMaster University

1280 Main St W, Hamilton, Ontario L8S 4L7

TITLE: DEVELOPING BIOMATERIAL-BASED STRATEGIES TO ENHANCE THE DELIVERY AND ACCESSIBILITY OF BACTERIOPHAGE THERAPEUTICS

AUTHOR: Fereshteh Bayat

B.A.Sc. (Iran University of Science and Technology, Iran)

M.A.Sc. (Iran University of Science and Technology, Iran)

SUPERVISOR: Dr. Tohid Didar

NUMBER OF PAGES: xxvi, 247

Lay Abstract

Antibiotic resistance is rapidly spreading worldwide, leading to a substantial loss of lives each year and imposing a significant economic burden. Bacteriophages, natural bactericidal viruses, are emerging as a promising solution due to their unique properties. This thesis focuses on the practical implementation of bacteriophages to address real-world challenges linked to antibiotic resistance. I worked on facilitating the process of selecting phages for personalized phage therapy through detecting phage-mediated release of bacteria encoded biomolecules. I also developed phage-loaded injectable hydrogels and phage-conjugated liquid infused coatings to combat bone and implant-related infections. Moreover, I have shown the promise of phage biocontrol beyond biomedical application by demonstrating its effectiveness in restoring a heavily biofouled sensor used for measuring dissolved oxygen, a critical water quality indicator.

Abstract

The primary goal of this research is to engineer solutions facilitating the utilization of bacteriophages as naturally occurring bactericidal agents for combatting multidrug-resistant (MDR) bacterial infections. Bacteriophages, which are bacterial viruses, represent self-replicating antibacterial agents known for their remarkable specificity in targeting bacterial cells. This specificity stands in sharp contrast to the indiscriminate and broad-spectrum actions of many currently employed antimicrobials across various sectors. Specificity of bacteriophages is a double-sided sword, often requiring large-scale phage hunting and phage biobank screening. This, combined with the lack of a global phage biobank can significantly limit access to phage therapeutics. I have developed a rapid, high-throughput platform focused on the detection of phage-mediated adenosine triphosphate (ATP) release via enzymatic ATP bioluminescence assay to identify highly lytic phages targeting MDR bacterial pathogens. I also used pullulan-trehalose sugar mixture to stabilize the ATP bioluminescence assay components at physiological temperatures. The sugar mixture also enhanced the desiccation tolerance of the ATP assay components along with phage, enabling the creation of all-inclusive shelf-stable tablets. The resulting tablets proved effectiveness and reliability in tracking phage-mediated bacterial cell lysis, and the pullulan-trehalose encapsulation significantly enhanced both the signal and desiccation tolerance of the phage and assay components.

Next, I developed a bi-functional phage delivering nanoclay-based injectable hydrogel that can serve as both antibacterial and osteoinductive therapeutic hydrogel for treating bone and implant associated infections. The *in vitro* results for phage-loaded injectable hydrogels confirmed strong antimicrobial action against bacterial biofilms, in both biofilm prevention and biofilm dispersion challenges. Continuing the phage biomaterials research, I also co-developed a combination of phage-collagen conjugated liquid infused coating on titanium implant that enhanced osteointegration and was remarkably effective against implant-associated infections as a prophylactic measure *in vivo*. Lastly, and as a proof of the utility of phage biocontrol beyond biomedical applications, I demonstrated biofilm removal and full signal regeneration for dissolved oxygen (DO) sensors using a phage cocktail.

Acknowledgements

First and foremost, I would like to express my profound gratitude to Dr. Tohid Didar for his continuous support and guidance throughout this journey. I thank him for providing me with all the required resources, trusting me with new ideas and giving me the freedom to explore different topics in the field of biomedical engineering. I am very grateful to Dr. Hosseinidoust for providing me with the chance to enter the extraordinary field of bacteriophages, offering comprehensive training, continuous help, and guidance to delve into this research area and acquire additional skills. I appreciate the opportunities to learn and grow as a researcher under their mentorship.

I extend my appreciation to Dr. Kyla Sask, my committee member, for her insightful feedback and constructive criticisms throughout my PhD studies. I also express my heartfelt appreciation to Dr. Carlos Filipe for his kind and generous support during my PhD studies.

I am grateful to the wonderful McMaster community for providing an equitable and inclusive learning environment for all the students. Special thanks to my amazing labmates and collaborators, specifically Martin Villegas, Sara Rahmani, Dr. Maryam Badv, Noor Abu Jarad, Mathura Thirugnanasampanthar, Dr. Lei Tian, Kyle Jackson, Mellissa Gomez and all the other present and previous Didar Lab and Hosseinidoust Lab members.

Above all, I want to express my deepest gratitude to my family for their unwavering love and support. They have consistently believed in me, encouraged me to embrace new opportunities, and instilled in me the commitment to always strive to do my best. Thank you for always having my back.

Last but not least, to my friend and partner in life and science, Pooya Torab Ahmadi. Thanks for empowering me, cheering for me along the way, and helping me to look at everything from a different perspective. None of this could have happened without your unconditional love and support. Thank you for everything, I am very lucky to have you by my side on the journey of life.

This Thesis is dedicated to my family.

Contents

Lay Abstract iv
Abstract v
Acknowledgements vi
List of Figures xii
List of Tables xxii
List of Abbreviations xxiii
Declaration of Academic Achievement xxv
First-author publications xxv
Patents xxv
Co-author publications xxv
Conference Presentations xxvi
Chapter 1: Objectives and outline 1
1.1 Thesis objectives 1
1.2 Thesis outline 2
Chapter 2: Introduction 5
2.1 Antimicrobial resistance, a global challenge 6
2.2 Bacteriophages, natural bactericidal agents 6
2.3 Bacteriophage applications for biocontrol and human therapy 10
2.3.1 Characteristics of bacteriophages 10
2.3.2 History and principles of phage therapy 11
2.3.3 Different methods for phage susceptibility testing 14
2.3.4 Challenges of using phage for biocontrol and human therapeutics 15
2.4 Conclusion 19
2.5 References 20
Chapter 3: High throughput platform technology for rapid target identification in personalized phage therapy 24
3.1 Abstract 25
3.2 Introduction 26
3.3 Results and discussion 28
3.3.1 Phage-mediated bacteria lysis 28
3.3.2 Increasing signal-to-noise ratio and end-point detection of phage-mediated bacteria lysis 32
3.3.3 One-pot biochemistry for detection of phage lytic activity 35

3.3.4 Optimizing detection of phage-mediated lysis in a stabilizing sugar polymer matrix 37
3.3.5 Screening the stabilized phage library against clinical bacterial isolates 40
3.4 Discussion 42
3.5 Materials 43
3.6 Methods 43
3.6.1 Bacterial culture and phage propagation 43
3.6.2 XTT metabolic assay 45
3.6.3 Optical density assay (OD_{600}) 45
3.6.4 Transmission electron microscopy (TEM) 46
3.6.5 ATP Bioluminescence assay 46
3.6.6 Stabilization in sugar polymer matrices 47
3.7 References 48
3.8 Supplementary Information 50
Chapter 4: Phage-loaded Injectable hydrogel for treating bone and implant associated infection 55
4.1. Abstract 56
4.2. Introduction 57
4.3. Results and discussion 59
4.3.1 Hydrogel polymer interactions 59
4.3.2 Physical characterization of hydrogel 63
4.3.3 Rheological Characterization of hydrogels 64
4.3.4 In vitro bacterial assays 67
4.3.5 In vitro cell culture. 71
4.4. Conclusion 73
4.5. Materials 73
4.6. Methods 74
4.6.1 Hydrogel preparation 74
4.6.2 Rheological analysis 74
4.6.3 Swelling and degradation experiments 75
4.6.4 Scanning Electron Microscopy (SEM) 75
4.6.5 Transmission Electron Microscopy (TEM) 75
4.6.6 Fourier Transform Infrared Spectroscopy (FTIR) 76
4.6.7 Dynamic Light Scattering (DLS) 76
4.6.8 Bacterial culture and phage propagation 76
4.6.9 Phage cocktail design 77
4.6.10 In vitro antibacterial assessment 77
4.6.11 In vitro cell studies 78
4.7. References 79
4.8. Supplementary Information 83

Chapter 5: Phage-Conjugated Liquid-Infused Implants Prevent Mortality Against an Implant-Associated-Infection in a Mouse Mode 90
5.1. Abstract 91
5.2. Introduction 92
5.3. Results and discussion 95
5.3.1 Liquid-Infused Layer Testing 96
5.3.2 Establishing a Mouse Sepsis Model 101
5.3.3 Bacteriophage-LIS Testing in Mouse Sepsis Model 104
5.4. Conclusion 107
5.5. Materials 108
5.6. Methods 109
5.6.1 Preparation of combined Bacteriophage and Collagen Liquid-Infused Coating 109
5.6.2 Contact Angle and Sliding Angle Measurements 110
5.6.3 *In vitro* cell studies 110
5.6.4 Bacterial culture and phage propagation 112
5.6.5 Mice Sepsis Model 114
5.6.6 Scanning Electron Microscopy 117
5.6.7 Statistical analysis 117
5.7. References 117
5.8. Supplementary Information 123
Chapter 6: Regenerating Heavily Biofouled Dissolved Oxygen Sensors using Bacterial Viruses 126
6.1. Abstract 127
6.2. Introduction 128
6.3. Results and discussion 130
6.3.1 Biofilm removal with phage 132
6.3.2 Sensor signal recovery 136
6.4. Conclusion 138
6.5. Materials 140
6.6. Methods 140
6.6.1 Bacterial strain, phage, and culture conditions 140
6.6.2 Biofilm formation and quantification 140
6.6.3 Phage treatment 141
6.6.4 Bleach treatment 141
6.6.5 Sensitivity readings 141
6.6.6 Fluorescence microscopy 141
6.6.7 Scanning electron microscopy (SEM) 142
6.6.8 Statistical analysis 142

6.7. References 142
6.8. Supplementary Information 147
Chapter 7. Concluding remarks and Future Direction 148
7.1. Conclusions 148
7.2. Recommendations for future work 150
APPENDIX I: Bacteriophages as Engineering Nano Tools for Monitoring and Detection of Pathogen in Water and Wastewater 152
1. Abstract 153
2. Introduction 153
3. Bacteriophages as sensing probes 158
3.1. Waterborne bacterial pathogens and their significance in quality monitoring 159
3.2. Phage-based biosensors and bioassays for water-borne pathogens 161
3.3. Different categories of phage-based sensors 164
3.4. Sensor design using phage display technology 168
3.5. Design parameters for phage-based biosensors 168
4. Specific considerations for phage-based detection/monitoring in wastewater 176
4.1. Sewage as a source of phage 176
4.2. Deactivation and interference 178
4.3. Horizontal gene transfer 179
4.4. Detection and monitoring of bacteria in biofilm mode 179
5. Outlook and future directions 181
6. References 185
APPENDIX II: Strategies to Prevent Bacterial Infections on Titanium-BASED Orthopedic and Dental Implants 197
1. Abstract 198
2. Introduction 198
3. Anti-adhesion Coatings 204
3.1. Superhydrophobic coatings 204
3.2. Liquid infused coatings 207
3.3. Polymeric coatings 211
4. Bactericidal Coatings 215
4.1. Metallic coatings 216
4.2. Antibiotic coatings 222

4.3. Bacteriophages 226
5. Animal Studies 230
6. Commercialization of antibacterial coatings 235
7. Conclusion 236
8. References 237

List of Figures

Chapter 2

Figure 1. Phages classified based on morphology and genetic material (double stranded DNA: dsDNA, single stranded RNA: ssRNA, and single stranded DNA: ssDNA). **(A)** tailed phages, **(B)** icosahedral phage, (C) filamentous phage.[11] 7
Figure 2. Different phage replication cycles. **(A)** The lytic cycle starts by (1) phage adsorption, (2) phage genome insertion into bacterial cell, (3) synthesis of new virions (progeny phages), and 4) bacterial lysis (5) and release of new phage into the surrounding environment. **(B)** Lysogenic cycle starts with phage adsorption (1) and genome insertion (2); however, the phage genome is incorporated into the bacterial genome, forming a prophage (3) that is replicated through the bacterial reproduction cycle (4). The lysogenic cycle could be induced to start the lytic cycle which ultimately leads to cell lysis (shown by the dashed arrow). **(C)** The phage chronic lifestyle starts with phage adsorption (1) and genome insertion (2). After new virions (progeny phages) are synthesized inside the bacterial cell (3), they are released without lysing bacterial cells (4). Some chronic phages can also adopt a lysogenic lifestyle, in which the phage genome is incorporated into the bacterial genome forming a prophage (3′) and is replicated through the bacterial reproduction cycle (4′) until the chronic cycle is induced (shown by the dashed arrow).[11] 9
Figure 3. Common framework for personalized phage therapy. Antibiotic resistant bacteria are isolated from the patient, screened through a phage library, and effective phages are identified. Subsequently, the selected phages are produced in high titers and purified to be free from endotoxins. In addition, all phages in the library should be lytic without carrying any toxic genes. 13

Chapter 3

Figure 1. (A) Personalized phage therapy. The first step in personalized phage therapy is isolation of treatment-resistant bacterial strain from patient (i), followed by employing slow culture-based, spot test method to screen and select therapeutic phages (ii). We propose a single-tablet technology for rapid, high-throughput screening of therapeutic phages (iii). **(B)** Phage-mediated ATP release and detection. Phage-mediated lysis of bacterial cell starts when a phage virion encounters the host cell and attaches to specific

phage receptors (i), this is followed by phage genome insertion into the host bacteria (ii). This starts a cascade of events leading to hijacking of bacteria replication machinery for synthesis of new progeny phage(iii), which ultimately leads to host cell lysis (iv), and release of progeny virions along with a burst of ATP (v). ATP reacts with luciferin to form luciferin adenylate, which is oxidized by the luciferase enzyme in the presence of magnesium to form oxyluciferin, CO_2 and adenosine monophosphate (AMP), which results in light emission (vi). **(C)** Transmission electron micrographs of P32 (i), JG004 (iii), and PP7 (v). Plaque formation on Pa lawns created by P32 (ii), JG004 (iv), and PP7 (vi). **(D)** Metabolic activity of uninfected and infected (MOI = 10, 1, 0.1, 0.01, 0.001) Pa cultures (n=3, mean ± SD). All reported values are the mean of three biological replicates and associated error bars shown as dashed lines represent standard deviation from the mean. 30
Figure 2. (A) Workflow schematic. Bacterial cultures were infected with phage at different concentration (i) and incubated at 37ºC (ii), at different time intervals, ATP was measured at room temperature by adding ATP reagent solution which contains luciferin and luciferase as main components (iii), and bioluminescence signal was measured (iv). Concentration of ATP was calculated for bioluminescence signal measured from Pa infected with P32, JG004, and PP7 at different MOIs: **(B)** MOI = 10, **(C)** MOI = 1, **(D)** MOI = 0.1, **(E)** MOI = 0.01, **(F)** MOI = 0.001. All reported values are the mean of three biological replicates and associated error bars represent standard deviation from the mean. Significance levels include *P < 0.05, **P < 0.01, ***P < 0.001, and ****P < 0.0001. 34
Figure 3. **(A**) One-pot ATP bioluminescence assay. Workflow schematic (i) which includes adding all ATP bioluminescence assay reagents (luciferin and luciferin as major components) and phage, followed by adding bacterial suspension and incubating the plate at 37ºC for real-time measurement of phage-induced ATP release. Kinetic ATP measurement for Pa infected with P32, JG004, and PP7 at MOI = 10 and uninfected Pa (ii). Time to peak signal for P32 and JG004 at different MOIs (iii) **(B**) Signal at peak for Pa cultures infected with P32, JG004, and PP7 at different MOIs including (i) MOI=10, (ii) MOI=1, (iii) MOI=0.1, (iv) MOI=0.01, (v) MOI=0.001. All reported values are the mean of three biological replicates. 36
Figure 4. (A) Workflow schematic. Bacterial suspensions are added to 96 well plate containing phages mixed with ATP reagents in sugar mixture. Bioluminescence signal at peak and assay end point of 6 hours for P32 **(B)** and JG004 **(C)** infected Pa cultures in the presence versus absence of sugar mixture in fresh liquid one-pot ATP assay. **(D)** Continuous measurement of bioluminescence signal for Pa infected with P32, JG004, and PP7 in fresh liquid sugar mix solutions. **(E)** Kinetic measurement of bioluminescence signal for Pa infected with P32, JG004, and PP7 in reconstituted one-week old tablets. **(F)** Kinetic measurement of bioluminescence signal for Pa infected with P32, JG004, and PP7 in rehydrated phage and enzymes dried in the absence of sugar polymers showing complete loss of signal after one week storage. **(G)** Same data as pert F but with a narrower y-axis scale, clearly showing the loss of signal. Error bars in B and C graphs show the statistical analysis based on unpaired t-test, associated error bars represent standard deviation from the mean. Significance levels include *P < 0.05 and **P < 0.01. Dashed line in D, E, and G show standard deviation from the mean for at least 3 replicates. 39
Figure 5. (A) proposed workflow for screening a bacterial isolate against a phage library using our platform technology, where the phage library is redesigned as solid, all-inclusive

tablets, each containing phage along with the detection biochemistry. The microtiter plate can be stored at room temperature, or shipped to point of use and once the need arises to find phage targets for a bacterial isolate of interest, a drop of bacterial culture is added to each tablet resulting in a bioluminescence signal. (B) The urinary tract infection isolate C0335 (i) was screened against a week-old library of all-inclusive tablets. Bioluminescence signal was recorded every 5 mins (ii) and the peak signal is shown after 60 min for each well (iii), which corresponds to spot tests of representative *P. aeruginosa* phages (iv). (C) The arm infection isolate C0072 (i) was screened against a week-old library of all-inclusive tablets. Bioluminescence signal was recorded every 5 mins (ii) and the peak signal is shown after 60 min for each well (iii), which corresponds to spot tests of representative *P. aeruginosa* phages (iv). Data points represent results for at least 3 technical replicates.. 41

Chapter 4

Figure 1. Molecular Structure of Laponite Nanoparticles and the Formation Mechanism of a Multifunctional Phage-Loaded Injectable Hydrogel with Antibacterial Properties. a) Molecular structure of a single Laponite nanoparticle, composed of tetrahedral and octahedral layers of lithium magnesium silicates. b) Schematic representation of the self-interaction of Laponite nanoparticles in water, leading to the formation of a "house of cards" structure at higher concentrations. c) Illustration of the interactions between Laponite and carboxymethyl cellulose (CMC), involving hydrogen bonds and electrostatic interactions. d) The application of phage-loaded Laponite-CMC injectable hydrogels for the treatment of osteomyelitis." 62
Figure *2*. Physical Characterization of NC-CMC Hydrogel. a) Schematic of phage-loaded injectable hydrogel formation by mixing CMC and NC. b) Image of the physically cross-linked hydrogel. c) Injectability of the NC-CMC hydrogel. d) Free-standing hydrogel, e) Freeze dried hydrogel. f) SEM images of the 2.5%NC-CMC hydrogel. g) FTIR spectrum of CMC, NC, and NC-CMC hydrogel. h) Storage (G′) and loss (G″) moduli of NC-CMC hydrogels. i) frequency sweep in the range of 1-100 Hz at 0.2% strain at 25°C. j) Viscosity versus shear rate for 0, 1.5, 2, 2.5% NC-at constant 1%CMC hydrogels at 25°C k) Yield stress of NC-CMC hydrogels at 38°C. l) Recovery test of the hydrogels by applying consecutive cyclic low (0.2%) and high (500%) strains up to 6 cycles at 38°C. 65
Figure 3. *In vitro* bacterial assays. **a)** Transmission electron microscopy (TEM) images of phages (P32 and JG004) and scanning electron microscopy (SEM) images of P. aeruginosa (PAO1). **b)** Kill curves depicting the effects of individual and binary phage infections on PAO1 bacterial cells (OD_{600} assay). **c)** Schematic representation of phage-loaded injectable hydrogel preparation, along with an image illustrating the antibacterial effect of the hydrogel after being injected onto bacterial lawn. The cleared zone surrounding the injected hydrogel signifies bacterial growth inhibition. **d)** Schematic illustrating the steps of the bacterial prevention assay (a prophylactic measure). **e)** Biofilm prevention performance is analyzed after 24 hours of incubation by measuring CFU counts. **f)** representative images of MacConkey agar plates after culturing 100 µL supernatants from each well containing hydrogel with phage and control no phage hydrogel. **g)** Metabolic activity of bacterial cells in both the supernatant and adhered biomass of each well within a 24-well plate using the XTT assay. **h)** The assay protocol for biofilm dispersion **i)** CFU counts of biofilm

dispersion assay. **j)** Representative images of MacConkey agar plates after culturing 100 µL supernatants from each well containing hydrogel with phage and control no phage hydrogel. **k)** Metabolic activity of bacterial cells in supernatant and adhered biomass using XTT assay in biofilm dispersion assay. (****p < 0.0001, **p < 0.01, *p < 0.05)..... 68
Figure 4. *In vitro* cell culture. a) Indirect cytotoxicity assay conducted after 48 hours of incubating SaOS-2 cells with extracts of hydrogels immersed in complete media for 5 and 7 days at 37°C in 5% CO2, in comparison to cells grown in fresh complete cell culture media as a control. None of the hydrogels exhibited any cytotoxic effects on the SaOS-2 cell line. b) ALP assay performed after incubating cells with hydrogels for 3 days, revealing significantly higher levels of ALP induction in cells incubated with hydrogels when compared to control cells cultured in complete cell culture media alone. (****p < 0.0001, ***p < 0.001, **p < 0.01, *p < 0.05) 72

Chapter 5

Figure 1. Implant Infection Prevention, Device Fabrication, and Wettability. a) Biofilm formation scheme. **b)** Infection Prevention scheme displaying bacterial cell repulsion, lubricant penetration, and cell lysis due to bacteriophage infection and propagation mechanism. **c)** The surface fabrication process displays the surface's hydroxylation, mixed silane deposition, and collagen-bacteriophage layer addition. Finally, the coated surfaces are lubricated with a fluorinated lubricant to form a liquid-infused layer. **d)** Water contact angle between pristine titanium (Ti), Ti after fluorosilanization (FS), and Ti with the addition of collagen, fluorosilane, and bacteriophages (Phage-FS). **e)** Water sliding angle for the coated titanium surfaces, both bare or lubricated with PFPP. Part d) and e) were analyzed using an ANOVA, n=4 for part d) and n=5 independent samples for part e). '***' represent a p-value of P < 0.001, and '*' represent a p-value of P < 0.05 96
Figure 2. In vitro surface testing with mammalian and bacteria cells. a) Image representation of SaOS-2 cell population and morphology after a 3-day incubation period. **b)** SaOS-2 Cell count after a 3-day incubation period. n=4 independent surface for all surfaces. **c)** Cell cytotoxicity assay after a 3-day incubation period of SaOS-2 cells. n= 5 independent surfaces. **d)** Alkaline phosphatase activity after a 3-day incubation of SaOS-2 cells. n= 4 independent surfaces n=4). **e)** Colony Forming Units (CFU) of P. aeruginosa on the surface of Ti and treated Ti samples. **f)** Planktonic CFU of P. aeruginosa left in a solution containing Ti and treated Ti samples (n=4). **g)** Plaque Forming Units (PFU) of phage-coated samples on the surface and in solution (n=4). **h)** Optical density growth curve of PAO1 bacteria with bacteriophages P32, E79 and synergistic combination of P32-E79. Parts b), c), d), e), and f) ANOVA were analyzed using an ANOVA, and part g) was analyzed using a student t-test. '****' represent a p-value of P < 0.0001, '***' represent a p-value of P < 0.001, '**' represent a p-value of P < 0.01, and '*' represent a p-value of P < 0.05, ns denotes a no statistical difference. 100
Figure 3. In vivo Optimization of Bacterial Load for Sepsis Model. Mice were implanted with a bare titanium surface, and bioluminescent PAO1-lux bacteria were introduced into the subcutaneous cavity with the following concentrations: $1x10^7$, $1x10^6$, $1x10^5$, $1x10^4$, $1x10^3$ CFU, and PBS as control. **a)** Representative bioluminescent imaging of female mice with bacteria concentrations $1x10^7$ CFU for LL and RR and 1x106 CFU

for mice labeled 0, L, and R. Missing mice represent mice that have reached the endpoint. **b)** Kaplan-Meier curve denoting the survival probabilities of each group of mice. **c)** Bioluminescent signal from mice with different bacterial loads. **d)** Average weight for male mice with different bacterial loads. **e)** Average weight for female mice with different bacterial loads. **f)** Average health score was given to mice for their appearance and attitude during their daily survey, as explained in Table S1, located in the supporting information section. Note: a score of 3 or lower in either category represented a mouse reaching the endpoint. The '#' symbol denotes the number of mice reaching the endpoint at different times. Part b) was analyzed using a Log-rank test. '**' represents a p-value of $P < 0.01$. 103

Figure 4. In vivo Results for Titanium and Coated Titanium Surfaces. Mice were implanted with either bare titanium, liquid infused (LIS), or Phage-LIS coated surface, and PAO1 bacteria was introduced into the subcutaneous cavity at a concentration of 1x108 CFU. **a)** Representative images of wounds created by the bacteria seven days post-infection. **b)** Average weight for male and female mice for Ti, LIS, and Phage-LIS groups. **c)** Average health scores given to mice for their appearance and attitude during their daily survey, as explained in Table S1, located in the supporting information section. Note: a score of 3 or lower in either category represented a mouse reaching the endpoint. **d)** Scanning Electron Microscopy images of excised titanium implants for Ti, LIS, and Phage-LIS groups. **e)** Kaplan-Meier curve denoting the survival probabilities of each group of mice. **f)** Colony Forming Units (CFU) found in blood samples of mice at the endpoint. g) Bacteriophage's Plaque Forming Units (PFU) found in blood samples of mice treated with phage-LIS coated implants at the endpoint. Note: the '#' symbol in figures b-c) denotes the number of mice reaching the endpoint at different time points. Part e) was analyzed using a Log-rank test, and part f) was analyzed using an ANOVA. '**' represents a p-value of $P < 0.01$ and n.s. for no statistical difference. 107

Chapter 6

Figure 1. (A) Schematic diagram showing the workflow for artificially fouling the membranes of DO sensors and subsequent phage treatment. After baseline measurement with the DO sensor, the membranes were incubated with a PA culture for 4 days to form a thick bacterial biofilm, then treated with phage overnight before subsequent DO measurements. **(B)** A simplified diagram of the phage lytic cycle that leads to lysis and destruction of the bacterial cells comprising the biofilm on the sensor membrane. First, phage attaches to specific receptors on the bacteria cell surface and injects its genome into the bacterium, thus taking over the cell reproduction machinery. Hundreds of phage particles are synthesized and assembled in each bacterium and the bacterium is subsequently lysed to release the new phages into the environment to infect more bacterial cells. 131

Figure 2. (**A)** Amount of PA biofilm grown in a microtiter plate for the duration of one to four days, quantified as absorbance of re-solubilized crystal violet stain at 590 nm. Each data point represents an average of 20 technical replicates (n=3). **(B)** SEM images of PA biofilm grown on DO sensor membranes for one, two, three, and four days. White arrows indicate some of the water channels visible in the matrix structure. **(C)** Schematic of a PA

biofilm lifecycle: (i) initial attachment of cells to the surface; (ii) lateral spreading of cells and production of EPS, leading to irreversible attachment; (iii) early development of biofilm structure; (iv) mature biofilm architecture; (v) dispersion of cells from the biofilm and continuation of the cycle. 133
Figure 3. (A) Fluorescence intensity of biofouled and phage treated membranes for 6 hr and overnight phage treatments, stained with Hoechst dye and quantified with ImageJ software. Significant difference in fluorescence intensity was observed between biofouled and phage treated membranes. Overnight phage treatment resulted in a significantly lower fluorescence signal, compared to 6 hr treated phage. Significant difference when comparing biofouled membranes with 6 hr and overnight phage treated membranes (* $P<0.05$, ** $P<0.001$). (B) Fluorescence micrographs of biofouled, 6 hr- and overnight phage treated membranes. The fluorescence signal does not differentiate between intracellular and extracellular DNA. (C) SEM images depicting a clean DO sensor membrane, a biofouled membrane with a 4-day PA biofilm, and a biofouled membrane subjected to an overnight phage treatment..... 135
Figure 4. (A) DO measurement for clean, biofouled, phage treated, and bleached sensor membranes in DI water. **(B)** Response time of DO sensor measured with clean, biofouled, phage treated and bleached membranes. The data points show the average of three measurements with each membrane. Experiments were performed in triplicates, and for each replicate, 2 membranes were used, bringing the total number of membranes used for each condition to six. Different color shades have been used to differentiate the data points for each biological replicate. Significant difference when comparing phage treated membranes with biofouled and clean membranes (* $P<0.05$, ** $P<0.01$). 138

Appendix I

Figure 1. Phages classified based on morphology and genetic material (double stranded DNA: dsDNA, single stranded RNA: ssRNA, and single stranded DNA: ssDNA). **(A)** tailed phages, **(B)** icosahedral phage, (C) filamentous phage..... 155
Figure 2. Different phage replication cycles. **(A)** The lytic cycle starts by (1) phage adsorption, (2) phage genome insertion into bacterial cell, (3) synthesis of new virions (progeny phages), and 4) bacterial lysis (5) and release of new phage into the surrounding environment. **(B)** Lysogenic cycle starts with phage adsorption (1) and genome insertion (2); however, the phage genome is incorporated into the bacterial genome, forming a prophage (3) that is replicated through the bacterial reproduction cycle (4). The lysogenic cycle could be induced to start the lytic cycle which ultimately leads to cell lysis (shown by the dashed arrow). **(C)** The phage chronic lifestyle starts with phage adsorption (1) and genome insertion (2). After new virions (progeny phages) are synthesized inside the bacterial cell (3), they are released without lysing bacterial cells (4). Some chronic phages can also adopt a lysogenic lifestyle, in which the phage genome is incorporated into the bacterial genome forming a prophage (3′) and is replicated through the bacterial reproduction cycle (4′) until the chronic cycle is induced (shown by the dashed arrow). 157
Figure 3. Overview of areas of application of phages in detection and/or monitoring of bacterial contamination in water and wastewater. (1) Natural water resources such as rivers

and lakes and ground water can become contaminated through environmental factors such as heavy rainfalls or flooding or with waste from municipal wastewater, waste from industrial plants or factory farms due to treatment deficiencies. Bacteriophages can be used to monitor the health of natural water resources. (2) Water treatment plants deliver clean water to houses and industry, the quality of treated drinking water delivered from water treatment plants can be monitored using phage. (3) Wastewater from manufacturing plants, agricultural activities, and households could enter ground water and natural water resources. Using phages, we can monitor wastewater to catch contamination at the source. (4) The efficiency of wastewater treatment process in wastewater treatment plants can be monitored to prevent the release and spread of pathogenic bacteria through plant effluents. 158
Figure 4. Phages used as bio-probes in different bioassays and biosensors. **(A)** Phage infection assays. These assays can use wild type or engineered phage. With wild type phage, progeny phages (by phage typing or through phage amplification assays) or the intracellular components released from the bacterial cell during cell lysis can be detected using different detection platforms. With engineered phage, the expressed reporter gene or released reporter enzyme is detected using optical, electrochemical, etc. detection platforms. **(B)** Phage amplification assay used in conjunction with infection-based assays consists of four steps. (1) Phage is added to sample, and if the target host cell is present, phage infection occurs. (2) The remaining phages are destroyed before release of progeny phages by adding a viricide which is then neutralized. (3) Helper cells (healthy host cells) are then introduced to the solution to provide the chance for progeny phages to amplify, (4) which could be simply detected by top agar plaque assay. **(C)** Phage binding assays. These assays use the process of phage binding (usually without the use of an extra transduction platform) for bacteria detection. Common approaches are staining phage with nucleic acid dye (detecting with flow cytometer or microscopy) or conjugating phage with micro/nanoparticles to separate/detect host cells coupled with PCR or optical, electrochemical detection platforms. **(D)** Phages can be immobilized on a substrate to form a bioactive surface that can be used as the sensing layer in biosensors. Binding phages to target host cells causes a change in conductivity, optical properties, or mass. In this case, the electrical, fluorescent, colorimetric, or luminescent signal generated by phage-host binding or host lysis is transduced using the sensor platform. 165
Figure 5. Approaches to improve the limit of the detection of phage-based bioassays. **(A)** Example of enrichment effect on phage-based colorimetric assay to detect *E. coli* BL21 in drinking water. (1) T7 reporter conjugated magnetic beads used for phage-mediated lysis and release of β-galactosidase enzyme, which was then detected using a substrate to produce a colorimetric readout. (2) Image and colorimetric readout for samples, which gives LOD qual to 10^4 CFU/mL. (3) Photographs and colorimetric readout for samples containing 10 and 100 CFU/mL of *E. coli* after enrichment for 5-8 hours, leading to decrease the LOD form 10^4 CFU/mL to 10 CFU/mL. Reprinted with permission from J. Chen et al.,[65] copy right (2015) American chemical society. **(B)** Example of phage-based colorimetric and bioluminescence assay combined with filtration and enrichment. (1) 100 mL of water sample is filtered using a filter membrane (47 mm diameter with a 0.22 μm pore size), (2) the filter was then removed and incubated on an absorbent pad allow further bacteria growth. (3) Engineered phages were added to infect target bacterial cells (*E. coli*) to express desired reporter enzymes genetically fused to a protein capable of binding to

cellulose filter upon release (CMB), that (4) can be detected with a suitable substrate to provide colorimetric or luminescent signal. Reprinted with permission from T. Hinkley et al.,[55] copy right (2018) Springer Nature **(C)** Example of filter-based detection of *E. coli* in drinking water using engineered phage. (1) 100 mL of water sample is filtered using 0.22 µm cellulose filter to separate the bacteria, (2) the filter is removed and placed on LB media, and (3) engineered phages (grey) are added to infect target bacterial cells and result in subsequent release of reporter enzyme NanoLuc (blue) fused to CMB (orange) with specificity to cellulose that is detected with a luminescence assay. Reprinted with permission from T. Hinkley et al.,[67] copy right (2020) MDPI. 170

Appendix II

Figure 1. Schematic representation of antibacterial coatings. a) Schematic representation of biofilm formation and development. b) Schematic representation of different antibacterial coating strategies. Figure adapted with permission.[30] Copyright 2019 American Chemical Society. 200
Figure 2. anti-adhesion coatings. **ai**) SEM images of control (Ti) and superhydrophobic titania nanoflower (NF-s) surfaces before bacterial incubation and 24 hours after bacterial incubation. Bacterial cell adhesion area percentage for live **aii)** S. aureus and **aiii)** E. coli. Figure 2a was adapted with permission.[33] **bi)** Schematic representation of chitosan-conjugated liquid-infused coatings on titanium. **bii**) Crystal violet evaluation of *S. aureus* biofilm formation. **biii)** Fluorescent microscopy images of SaOS-2 cell proliferation after seven-day cell cultures (nuclei: blue; microfilaments: red). Figure 2b was adapted with permission.[7] **ci)** Schematic representation of substrate coated with tannic acid and PEG. **cii)** Fluorescent images of bacteria adhesion for *E. coli* and *S. aureus*. **ciii)** Mean fluorescent intensity values of adherent bacteria for *E. coli* and *S. aureus.* Figure 2c was adapted with permissions.[43] 207
Figure 3. Bactericidal coatings. **ai**) Schematic representation of silver imbedded in a polymer coated on Ti. **aii)** Colony forming units (CFU) assay for *E. coli* and *S. aureus*. **aiii)** Fluorescent live/dead assay of osteoblast cells. Figure 3a was adapted with permission.[53]. **bi)** Schematic representation of vancomycin binded to polymer brush linker. **bii**) SEM images of *S. aureus* on Ti control and antibiotic coated surface. **biii)** Bioluminescent quantification of live bacteria. Figure 3b was adapted with permission. [114] **ci)** Schematic representation of the bacteriophage's lytic life cycle. **cii)** Bacteriophages physically or covalently bonded to Ti. **ciii)** Bacteriophages loaded into polymeric coating. Figure 3c was created in biorender.com. 221
Figure 4. In vivo studies for antibacterial coatings. a) Doxycycline coating titanium was implanted into the tibia of a rabbit model and showed an increased bone formation toward the titanium screw using a 3D micro-CT technique. Figures 4a. were modified with permissions.[57] b) Mesoporous polydopamine nanoparticles were loaded with osteogenic peptide RGD and indocyanine green (ICG) to enhance osseointegration and eradicated biofilms upon near infrared (NIR) stimulus, respectively. When exposed to NIR, the ICG in the nanoparticles produced photothermal and photodynamic therapies to destroy biofilms and kill S. aureus with 99.7% efficiency. Scale bar in 5biii. represents 5 µm. Figures 5b. were modified with permissions.[66] c) Titanium coated with a hyperbranched

poly-L-lysine promoted osseointegration (ii, iii) and lysed bacteria (iv) in a rat animal model. Figures 4c. were modified with permissions.[46] 234

Chapter 3 – Supplementary Information

Figure S1. Optical density (OD_{600}) or growth curve of PAO1 infected with P32 (**A**), JG004 (**B**), and PP7 (**C**). P32 shows a strong performance in preventing bacterial growth by decreasing the culture turbidity even at lower MOIs (0.001). JG004 was also able to suppress the bacterial growth effectively, while PP7 shows week performance which aggravates by decreasing the initial concentration of phage (lower MOIs). 50
Figure S2. Schematics of Phage life cycles. **(A)** Lytic life cycle of phage starts with (i) phage recognition and attachment to bacterial cell receptors, (ii) genome insertion, (iii) taking control of bacterial replication machinery and producing new virions, and (iv) release of progeny phages by bacterial cell lysis. **(B)** In lysogenic life cycle, phage is adsorbed to cell receptors (i) and inserts its genome inside bacterial cell (ii); however, the phage genome is incorporated into the bacterial genome, forming a prophage (iii) that is replicated through the bacterial reproduction cycle (iv). The lysogenic cycle could be induced to start the lytic cycle with environmental triggers such as high temperature and UV exposure which can ultimately lead to cell lysis (as shown by the dashed arrow). **(C)** Similar to other phage life cycles, the chronic lifestyle (mostly seen in filamentous phages) starts with recognition and adsorption to bacterial cell receptors (i) and genome insertion (ii). By taking control of bacterial replication machinery, new virions are synthesized inside the bacterial cell (iii) and are released through budding or extrusion without lysing bacterial cells (iv). Similar to tailed phages, some chronic phages can also adopt a lysogenic lifestyle, in which the phage genome is incorporated into the bacterial genome forming a prophage (iii′) and is replicated through the bacterial reproduction cycle and staying dormant (iv′) until the chronic cycle is induced by environmental stimuli (shown by the dashed arrow). 51
Figure S3. ATP background in phage solutions at different stages of purification (A) and after dilution in cell media (B). The effect of diluting phage samples is comparable to purifying phage suspensions. Depending on the availability, either diluted sterile filtered phages in cell media/buffer or purified phages can be used to reduce the effect of the background bioluminescence signal intensity. 52
Figure S4. Stability of dried *Pseudomonas* phages **A**) P32, **B**) JG004, **C**) PP7 in ambient conditions in 10 wt% pullulan + 0.5 M trehalose in comparison with no sugars. Sugar polymers helped to retain higher infectivity after 30 days. 52
Figure S5. Antibiotic resistance profile of the clinical isolates C0072 and C00335, isolated form patients with urinary tract and arm infections, respectively.[1] 53
Figure S6. Optical density assay of C0335 (**A**) and C0072 (**B**) infected with P32, JG004, and PP7 at MOI ~ 10 compared to uninfected strains. None of the phages infect C0335, while C0072 is infected with P32 as turbidity of the culture decreases compared to uninfected C0072. 53
Figure S7. Metabolic activity measurement of phage infected and uninfected C0335 (**A**) and C0072 (**B**) at MOI ~ 10. Metabolic activity of phage infected C0335 shows no

significant changes compared to uninfected cultures, while metabolic activity of C0072 decrease after 2 hours for C0072 infected with P32. 53
Figure S8. Zoomed in image of the phage library screening, showing a delayed increase in bioluminescence signal for C0035 infected with JG004 appearing after 2 hours. 54

Chapter 4 – Supplementary Information

Figure S1. DLS and zeta potential measurements 83
Figure S2. SEM images of 1.5% and 2%NC hydrogel formulations 84
Figure S3. Swelling ratio of freeze dried 1.5, 2, 2.5 %NC hydrogels at different time intervals recorded up to 24 hours. 84
Figure S4. Strain sweep at 10Hz for hydrogels containing 1.5, 2, and 2.5% NC at 38°C. 85
Figure S5. Stress sweep at 10Hz for hydrogels containing 1.5, 2, and 2.5% NC at 38°C. 85
Figure S6. Kill curves of individual and binary phage cocktails. OD600 assay results of infecting PAO1 bacterial strain with single P. aeruginosa phages including P32, JG004, PO4, E79 and PP7 and binary combinations of P32-JG004, P32-PO4, P32-E79 and P32-PP7, PO4-JG004, PO4-E79, PO4-PP7, JG004-PP7 and E79-PP7 in comparison to uninfected PAO1 (gray graph). Dashed line shows standard deviation from the mean of n=6 samples. 86
Figure S7. Kill curves of P32 and JG004 phages combination at MOIs of 10, 1, 0.1, 0.01, 0.001, 0.0001 using OD600 assay 87
Figure S8. Turbidity measurement of the supernatant in biofilm prevention assay 88
Figure S*9*. Turbidity measurement of the supernatant in biofilm dispersion assay 88
Figure S*10*. Representative images of wells for metabolic activity measurements using XTT assay. The metabolic activity of adhered biomass and the supernatant solution in each well was measured for both biofilm dispersion and prevention. Color change in wells containing hydrogels after removing the supernatant and adding the XTT reaction solution to measure the metabolic activity of adhered biofilm after 24 hours treatment with phage loaded hydrogels in comparison with POA1 and no phage containing hydrogel (A). Color change correlated to metabolic activity of cells in the supernatant of the wells containing phage compared to POA1 and no phage containing hydrogel after mixing the supernatant and XTT reaction solution 1:1 volume ratio (B). 89
Figure S11. Concentration of phage at the end of biofilm prevention and dispersion ... 89

Chapter 5 – Supplementary Information

Figure S1. *In Vitro* Bacteriophage Screening. a) Screening of bioluminescent *P. aeruginosa* PAO1-Lux against five strong lytic bacteriophages showing phage activity from E79 and JG004. b) Screening of non-bioluminescence *P. aeruginosa* PAO1 against five strong lytic bacteriophages showing phage activity from P32, P04, PP7, E79 and JG004. c) Bacteriophage activity from the treated titanium samples against PAO1 bacteria. A strong lysis zone can be seen in the presence or absence of PFPP lubricant. d) Optical

density kill curve between PAO1-Lux and JG004 bacteriophage. e) Optical density kill curve between PAO1-Lux and E79 bacteriophage. f) Optical density kill curve between PAO1-Lux and combined E79- JG004 bacteriophages. Note: the color legend in c-e) represents the Multiplicity of Infection (MOI) or the ratio between bacteriophage to bacteria. The color legend is denoted as black – No phage control, grey – MOI=0.0001, orange – MOI=0.001, magenta – MOI=0.01, red – MOI=0.1, blue – MOI=1, green – MOI=10. 124
Figure S2. *Ex Vivo* Bacteria and Bacteriophage Quantification from Samples Taken at Endpoint. a) Bacteria Colony forming unit (CFU) from retrieved titanium implants at the endpoint. b) PAO1 bacteria CFU retrieved from liver samples at the endpoint. c) PAO1 bacteria CFU from retrieved spleen samples at the endpoint. d) Bacteriophage Plaque forming units (PFU) from titanium, liver, spleen, and blood samples obtained at the endpoint..... 125
Figure S3. McConkey Agar Plates from Ex Vivo Titanium Samples. Representative images of McConkey agar plates with bacteria obtained from recovered titanium discs for untreated Ti, LIS-coated Ti, and Phage-LIS coated Ti. Notably, bacteria colonies obtained from Phage-LIS samples display phage activity, as noted by the dying colonies in the 0^{th} and 1^{st} dilutions. These colonies were lysed entirely within a few days. 125

Chapter 6 – Supplementary Information

Figure S1. PA biofilm removal (compared to the no-phage control) in a microtiter plate after treating a 4-day PA biofilm with single phages or a phage mixture, quantified as absorbance of re-solubilized crystal violet stain at 590 nm. Shown are the data point (the average of 10 technical replicates) for three independent biological replicates. 147

List of Tables

Appendix I

Table 1. Major bacterial pathogens in drinking-water and associated diseases*..... 160
Table 2. Phage-based biosensor and bioassays to detect waterborne bacterial pathogens 163
Table 3. Summary of studies that have used phage as a pathogen and operational biocontrol for wastewater and sludge..... 178

Appendix II

Table 1. Different categories of antibacterial coatings. 201

List of Abbreviations

AMR: Antimicrobial Resistance
ATP: Adenosine triphosphate
DO: Dissolved Oxygen
LIS: Liquid Infused surface
CMC: carboxymethyl cellulose
DNA: Deoxyribonucleic acid
dsDNA: double stranded DNA: dsDNA
ssDNA: single stranded DNA
RNA: Ribonucleic acid
ssRNA: single stranded DNA
ECM: extracellular matrix
EPS: exopolysaccharides
ARGs: antimicrobial resistant genes
EPS: extra cellular polymeric substance
FDA: Food and Drug Administration
PFU: Plaque-forming unit
LPS: lipopolysaccharide
XTT: 2,3-bis-(2-methoxy-4-nitro-5-sulfophenyl)-2H-tetrazolium-5-carboxanilide
CCEM: Canadian Center for Electron Microscopy
SEM: Scanning Electron Microscopy
TEM: Transition Electron Microscopy
MOI: multiplicity of infection
P32: vB_Pae-Tbilisi32
PEG: Polyethylene glycol
P. aeruginosa: Pseudomonas aeruginosa
Pa: *P. aeruginosa* PAO1
LB: Luria-Bertani
EOP: Efficiency of plating
CFU: Colony-forming unit
E. coli: *Escherichia coli*
Optical Density: OD
RLU: Relative Luminescence Unit
ALP: Alkaline phosphatase
AUP: Animal Utilization Protocol
DLS: Dynamic Light Scattering
MDR: multi-drug-resistant
UV: Ultraviolet
NC: Laponite nanoclay
FTIR: Fourier transform infrared
PBS: Phosphate-buffered saline
S. aureus: *Staphylococcus aureus*
TSB: Tryptic Soy Broth
G′: Storage modulus
G″: Loss modulus

LVE: Linear Viscoelastic
FBS: fetal bovine serum
ABX: Antibiotics
AREB: Animal Research Ethics Board
BIZ: Bacterial inhibition zone
BMP-2: Bone Morphogenetic Protein-2
BSA: Bovine Serum Albumin
CV: Crystal Violet
CVD: Chemical Vapor Deposition
DI: Deionized
EP: Endpoint
FS: Fluorosilane
GPTMS: 3-glycidyloxypropyl)trimethoxysilane
HA: Hydroxyapatite
IAI: Implant associated infection
LPD: Liquid Phase Deposition
MAO: Micro arc oxidation
MIC: Minimum Inhibitory Concentration
MMRI: McMaster Manufacturing Research Institute
MRSA: Methicillin-Resistant Staphylococcus aureus
Lux: Bacterial Luciferase Gene Cassette
PDMS: Polydimethylsiloxane
PFD: Perfluorodecalin
PFOCTS: Perfluorooctyl trichlorosilane
PFPP: Perfluoroperhydrophenanthrene
Phage: Bacteriophage
PS: Polystyrene
RF: Radiofrequency
ROS: radiofrequency
SAM: Self-assembled monolayer
SD: Standard deviation
SLIPS: Slippery-liquid-infused surfaces
SS: Stainless Steel
Ti: Titanium
TPFS: Trichloro(1H,1H,2H,2H-perfluorooctyl)
wt%: Percent weight
w/v%: weight per volume percent
XPS X-ray: Photoelectron Spectroscopy
ZOI: Zone of Inhibition

Declaration of Academic Achievement

This Ph.D. dissertation is organized in a "sandwich style" based on articles published, submitted and in preparation for submission.

First-author publications

1. **F. Bayat**, A. Hilal, M. Thirugnanasampanthar, C. Filipe, T. F. Didar, Z. Hosseinidoust; Portable, high throughput platform technology for rapid target identification in personalized phage therapy, Nature communications, 2023, under revision, NCOMMS-23-19146-T

2. **F. Bayat**, M. Villegas, S. Rahmani, L. Tian, M. Thirugnanasampanthar, F. Aguilar, Z. Hosseinidoust, T. F. Didar; Phage-loaded Injectable hydrogel for treating bone and implant associated infection, in preparation for submission.

3. **F. Bayat**, D. Maddiboina, T. F. Didar, Z Hosseinidoust; Regenerating heavily biofouled dissolved oxygen sensors using bacterial viruses, RSC Advances, 2021, 11, 8346-8355.

4. M. Villegas [Ψ], **F. Bayat** [Ψ], S. Rahmani, M. Thirugnanasampanthar, T. Kramer, E. Schwarz, D. Wilson, Z. Hosseinidoust, T. F. Didar; Phage-Conjugated Liquid-Infused Implants Prevent Mortality Against an Implant-Associated-Infection in a Mouse Model, ready to submit
   [Ψ] Equal contribution

5. **F. Bayat**, T. F. Didar & Z. Hosseinidoust, Emerging investigator series: bacteriophages as nano engineering tools for quality monitoring and pathogen detection in water and wastewater. Environ. Sci. Nano 8, 367–389 (2021).

Patents

1. T. F. Didar, Z. Hosseinidoust, **F. Bayat**; Methods for bacteriophage susceptibility screening, US Provisional patent has been filed.

Co-author publications

1. M. Villegas, **F. Bayat**, T. Kramer, E. Schwarz, D. Wilson, Z. Hosseinidoust, T. F. Didar, Strategies to Prevent Bacterial Infections on Titanium-Based Orthopedic and Dental Implants. ChemRxiv. Cambridge: Cambridge Open Engage; 2023; This content is a preprint and has not been peer reviewed.

2. M. Badv, **F. Bayat**, J. I. Weitz, T. F. Didar, Single and multi-functional coating strategies for enhancing the biocompatibility and tissue integration of blood-

contacting medical implants, Biomaterials, 2020, 258, 120291

3. E. Afonso, **F. Bayat**, L. Ladouceur, S. Khan, A. M. Gómez, J. I. Weitz, Z. Hosseinidoust, P. Tiemblo, N. García, and T. F. Didar; Highly Stable Hierarchically Structured All-Polymeric Lubricant-Infused Films Prevent Thrombosis and Repel Multidrug-Resistant Pathogens, ACS Appl. Mater. Interfaces, 2022, 14, 53535−53545

4. N. Abu Jarad, K. Rachwalski, **F. Bayat**, S. Khan, A. Shakeri, R. MacLachlan, M. Villegas, E. D. Brown, L. Soleymani, and T. F. Didar; An Omniphobic Spray Coating Created from Hierarchical Structures Prevents the Contamination of High-Touch Surfaces with Pathogens, Small, 2023, 19, 2205761

5. N. Abu Jarad, K. Rachwalski, **F. Bayat**, S. Khan, A. Shakeri, R. MacLachlan, M. Villegas, E. D. Brown, Z. Hosseinidoust, T. F. Didar, and L. Soleymani; A Bifunctional Spray Coating Reduces Contamination on Surfaces by Repelling and Killing Pathogens, ACS Appl. Mater. Interfaces 2023, 15, 16253−16265

Conference Presentations

1. *Canadian Chemistry Conference and Exhibition (CSC), July 2023, Vancouver, British Columbia, Canada.;* Bioluminescent all-inclusive platform for bacteriophage susceptibility testing of multi-drug resistant clinical bacterial isolates; **F. Bayat**, A. Hilal, M. Thirugnanasampanthar, C. Filipe, T. F. Didar, Z. Hosseinidoust. (**Oral presentation**)
2. *Oxford Bacteriophage Conference-Phages, September 2021, United Kingdom, virtual conference*; Phage Treatment Removes Biofilm and Recovers Sensitivity for Biofouled Dissolved Oxygen Sensors**; F. Bayat**, D. Maddiboina, T. F. Didar, Z. Hosseinidoust. (**Oral presentation**)
3. *71st Canadian Chemical Engineering Conference (CCEC), October 2021, Montreal, Quebec, Canada, virtual conference*; Phage Treatment Removes Biofilm and Recovers Sensitivity for Biofouled Dissolved Oxygen Sensors; **F. Bayat**, D. Maddiboina, T. F. Didar, Z. Hosseinidoust. (**Oral presentation**)
4. *12th annual biomedical engineering symposium, April 2023, McMaster University, Hamilton, Ontario, Canada***;** Comparing XTT and optical density as high throughput liquid assays to select for lytic bacteriophages for therapeutic applications**. F. Bayat**, A. Hilal, T. F. Didar, Z. Hosseinidoust. (**Poster presentation**)

Chapter 1: Objectives and outline

1.1 Thesis objectives

This work aims to advance engineering strategies for harnessing bacteriophages as natural antibacterial agents for the treatment and prevention of bacterial infections. Initially, the thesis emphasizes the creation of comprehensive sugar-based tablets containing phages and Adenosine triphosphate (ATP) bioluminescence assay reagents, expediting the phage selection process for tailored bacterial eradication in personalized phage therapy. Subsequently, two distinct methodologies were explored to harness the potential of phages in addressing bone and implant-related infections. Firstly, nanoclay-based phage-loaded injectable hydrogels were developed, offering dual functionality in treating and preventing infections while simultaneously promoting bone formation. In the second approach, phage-conjugated liquid-infused coatings were engineered for orthopedic implants, providing protection against bacterial infection and biofilm formation through the synergistic effects of anti-adhesion liquid-infused coatings and the antibacterial properties of phages. Finally, the study also explored the potential of phages in addressing biofouling in marine environments. This was demonstrated by the successful use of phage treatments to restore heavily biofouled Dissolved Oxygen (DO) sensors. These findings highlight the versatility of phage biocontrol which be expanded to a wide range of applications.

This thesis follows a "sandwich" format, comprising six chapters. Chapter 1 includes the objectives and outline, and Chapter 2 provides an introduction to the conducted research. Chapters 3 to 6 comprise journal articles, which have either been published, submitted for publication, or are in the process of being prepared for submission. Chapter 7 contains the concluding remarks and future directions. Appendix I includes a first-author review paper depicting the potential of phage in designing detection tools for environmental monitoring. Appendix II comprises a second-author review paper focusing on strategies to prevent bacterial infection and biofilm formation on Titanium orthopedic implants.

Following objectives have been pursued in this thesis:

1. Expediting the phage selection process with the creation of innovative sugar-based phage-ATP bioluminescence assay tablets.
2. Introducing phage-loaded osteoinductive injectable hydrogels to combat bone and implant-related infections.
3. Developing phage-conjugated liquid-infused surface (LIS) coatings for the prevention of biofouling on orthopedic implants, leveraging both phage bactericidal properties and LIS repellency.
4. Extending the antimicrobial potential of phages from the biomedical sector to address biofouling challenges in marine environments.

1.2 Thesis outline

Chapter 1 – Thesis outline and Objectives

This chapter explains the objectives of the projects and a brief overview of research conducted in each subsequent chapter.

Chapter 2 – Introduction

This chapter provides a concise overview of bacteriophages, delving into their distinctive characteristic for biocontrol and human therapeutics. Additionally, it explores the hurdles inherent in their application and provides potential solutions.

Chapter 3 - High throughput platform technology for rapid target identification in personalized phage therapy.

The phage selection process is a critical aspect of phage therapy, necessitated by the high specificity of phages in targeting bacterial cells. Adenosine triphosphate (ATP) serves as a universal energy source found in all living cells, including bacteria, and can be readily detected via a bioluminescence reaction in the presence of luciferin and luciferase enzymes. ATP offers a direct means of detecting lytic phages through phage-mediated cell lysis. In

this work, we stabilized all the components of the ATP bioluminescence assay, alongside each phage, within a sugar-based matrix. Sugars serve to prevent thermo-inactivation and desiccation tolerance of enzymes and phage. The all-inclusive desiccated tablets can also facilitate the storage and global transport of phages.

Chapter 4 – Phage-loaded Injectable hydrogel for treating bone and implant associated infection

Injectable hydrogels are promising biomaterials for drug delivery, tissue engineering, and wound healing applications owing to their minimally invasive administration, matching irregular defects, and delivering cargo molecules such as growth factors, chemokines, and therapeutic drugs. Here, we propose developing multifunctional phage-loaded injectable hydrogels based on physical cross-linking of laponite nanoclay and carboxymethyl cellulose (CMC). This dual capability makes them promising candidates for addressing bone and implant-related infections while simultaneously promoting bone formation.

Chapter 5 – Phage-Conjugated Liquid-Infused Implants Prevent Mortality Against an Implant-Associated-Infection in a Mouse Mode

In this context, we propose a synergistic approach by conjugating phage and collagen into a liquid-infused coating to deliver dual antibacterial functionality. This approach leverages the bacterial cell lysis capabilities of phages while harnessing the surface repellency of the liquid-infused coating to prevent bacterial attachment and colonization on the surface of orthopedic implants. These surfaces demonstrated promising results in both *in vitro* and *in vivo* mouse models.

Chapter 6 – Regenerating Heavily Biofouled Dissolved Oxygen Sensors using Bacterial Viruses

We have shown the effectiveness of lytic bacteriophages, or bacterial viruses, as a non-invasive approach to remove bacterial biofilms from the gas-permeable membrane of electrochemical dissolved oxygen sensors. Our findings reveal a near-complete restoration and signal recovery for the dissolved oxygen sensor, enabling the reuse of the biofouled

sensor without the need for harsh chemicals that could damage the delicate sensor membrane.

Chapter 7 – Conclusions and Future Direction

This chapter provides concluding remarks by summarizing the primary contributions of this thesis and outlining areas for future research.

Appendix I – Bacteriophages as Engineering Nano Tools for Monitoring and Detection of Pathogen in Water and Wastewater

In Appendix I, we explore the use of bacteriophages as a unique tool for developing detection and monitoring systems for environmental applications, with a specific focus on detecting pathogens in water and wastewater. Bacteriophages have garnered significant attention in the biomedical sector, but they remain relatively unknown to researchers in other fields. The information presented in this chapter provides valuable insights for a diverse audience interested in creating detection and monitoring methods that involve the application of phages.

Appendix II – Strategies to Prevent Bacterial Infections on Titanium-BASED Orthopedic and Dental Implants

In Appendix II, we explored antibacterial strategies to prevent biofilm formation on titanium-based orthopedic and dental implants. These strategies fall into two main categories: anti-adhesion and bactericidal coatings, both aimed at combating biofouling and bacterial infections. We discussed various techniques for surface modification, including chemical and physical methods, as well as polymer-based coatings, to create surfaces that resist bacterial adhesion and colonization. Furthermore, we investigated the incorporation of different bactericidal agents, such as metallic coatings (e.g., Ag, Zinc, copper), antibiotics, bactericidal chemicals, polymers, and bacteriophages, into coating strategies designed to eliminate bacteria, reduce bacterial load, and decrease virulence.

Chapter 2: Introduction

Preface: This chapter provides a concise background information regarding the global antibiotic resistance crisis, followed by introducing bacteriophages as natural bactericidal agents and their potential role in combating multidrug-resistant bacterial pathogens. It also introduces the utilization of phages for biocontrol and human therapeutics (phage therapy), discusses the challenges associated with their use, and explores potential solutions.

I have published a review paper on the use of phage in biosensing (**Appendix I**). For information regarding applications of phage for bone and implant associated infections, please refer to the review paper in **Appendix II, "section 4.3. bacteriophages"**.

Citations:

1. **Bayat, F.,** Didar, T. F. & Hosseinidoust, Z. Emerging investigator series: bacteriophages as nano engineering tools for quality monitoring and pathogen detection in water and wastewater. Environ. Sci. Nano 8, 367–389 (**2021**).

- Contribution: I performed the literature review and wrote the original draft. The manuscript was revised and approved by Dr. Hosseinidoust and Dr. Didar.
- Significance: This paper was selected for the Journal cover in recognition of the quality and significance of our research.
- *Parts of this review paper has been reproduced and cited in this chapter.*

2. Villegas M, **Bayat F**, Kramer T, Schwarz E, Wilson D, Hosseinidoust Z, et al. Strategies to Prevent Bacterial Infections on Titanium-Based Orthopedic and Dental Implants. ChemRxiv. Cambridge: Cambridge Open Engage; **2023**; This content is a preprint and has not been peer reviewed.

- Contribution: I contributed to Collecting relevant research papers, articles, and other sources, figure design, and writing. Notably, I authored the entire "3.3. Bacteriophages" section.

2.1 Antimicrobial resistance, a global challenge

In the early 20th century, Alexander Fleming discovered the first antibiotic, penicillin, when mold of Penicillium notatum cleared *Staphylococcus aureus* (*S. aureus*) from his plate. In 1943, penicillin became the first publicly available antibiotic, saving millions of lives during the second world war. The advancements that had paved the way to commercialization of penicillin, led to the rapid discovery of novel antibiotics over the next few decades.[1] Despite the initial effectiveness of antibiotics, overuse and misuse of these medications led to emergence and spread of antibiotic resistance and once again bacterial infections became life-threatening. In 2019, a comprehensive analysis revealed that approximately 4.95 million deaths were associated with drug-resistant bacterial infections, with 1.27 million directly attributable to bacterial Antimicrobial Resistance (AMR). The Centers for Disease Control has identified six primary pathogens responsible for death linked with the AMR burden including *Escherichia coli, Staphylococcus aureus, Klebsiella pneumoniae, Streptococcus pneumoniae, Acinetobacter baumannii*, and *Pseudomonas aeruginosa.*[2] Despite the critical situation where more and more bacterial pathogens are developing resistance towards antibiotics, the discovery of new antibiotics has become very slow and extremely costly during the past few decades due to various scientific, economic and regulatory obstacles and has not been able to keep up with the high rates of antibacterial resistance emergence and spread.[3,4] Discovery of new antibiotics takes more than 10 years and the overall cost exceeds $1 billion.[4] Considering all the above-mentioned hurdles to discover new antibiotics, researchers have been investigating alternative options to fight against the ongoing life-threatening bacterial AMR. Among different approaches to address the continuing crisis of AMR, natural bacteria targeting viruses, known as bacteriophages (or phage for short), have garnered considerable attention recently. The application of these bacteria targeting viruses as natural antibacterial agents to address the global challenge of bacterial AMR will be discussed in more detail throughout this chapter.

2.2 Bacteriophages, natural bactericidal agents

The alarming rates of antibiotic resistance spread around the world once again has turned bacterial infections into a major challenge, leading to increased rates of infection treatment

failures.[5,6] Bacteriophages, also known as phages for short, are bacterial viruses which have been around as antibacterial agents to treat bacterial infections for almost 100 years. With increased prevalence of chronic bacterial infections due to spread of antimicrobial resistance as a global threat, phages have regained attention after being overshadowed for a long time by antibiotics' discovery in 1940s.[7,8] These bacteria targeting viruses are the most abundant entities on the planet with a population 10 times larger than the bacterial population, meaning we have a ready to mine resource in the nature to select suitable phages for various applications.[9,10] So far, a diverse spectrum of phages with different morphology and genetic material (DNA or RNA) from various families and genera have been identified. Phages are mainly categorized by the nature of their nucleic acid (genetic material) and capsid morphology. **Figure 1** shows a few different families of phages. Two of the most extensively researched groups of phages include tailed phages, like T4 and T7, and filamentous phages, such as M13.[11]

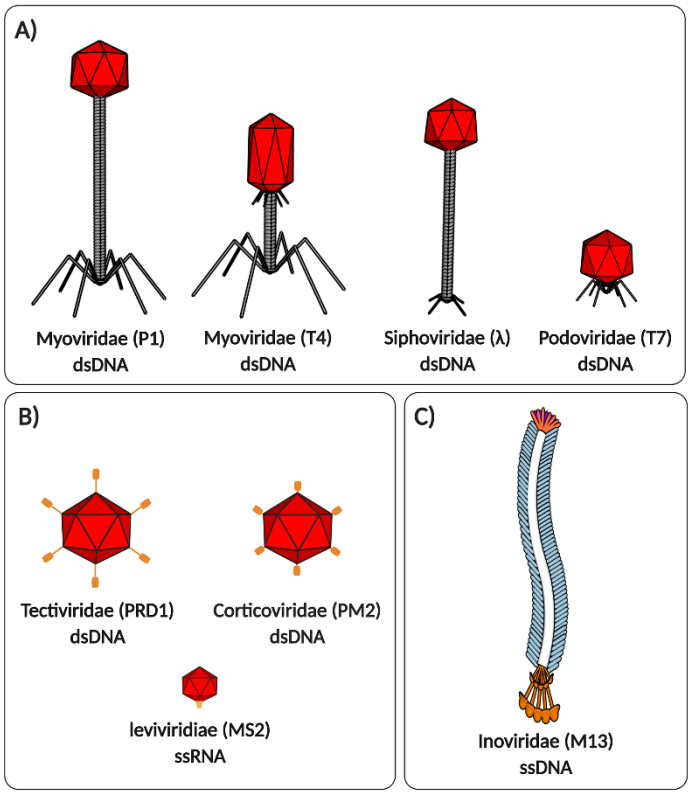

Figure 1. Phages classified based on morphology and genetic material (double stranded DNA: dsDNA, single stranded RNA: ssRNA, and single stranded DNA: ssDNA). **(A)** tailed phages, **(B)** icosahedral phage, (C) filamentous phage.[11]

Phages, similar to other viruses, are parasites which can replicate by hijacking the bacterial replications machinery by injecting their genetic material into bacteria. The overall process of phage infection includes adsorption, infection, and release. Phage infection can lead to the formation and release of new virions, called progeny phages, in a process called lytic life cycle. These phages are called lytic or virulent phages, are the most favorable options for applications of phage in biocontrol applications for offering immediate bactericidal actions. On the other hand, lysogenic or temperate phage infections can result in either inserting the phage's genome into the bacterial host chromosome, forming what is known as a prophage, remaining in a dormant state until environmental triggers induce it to enter the lytic cycle. Although release of progeny phages leads to bacterial cell death in most cases, the release of progeny phages from filamentous phages occurs without causing any major disruption to the bacterial cell wall, and this generally non-bactericidal phage infection is called chronic infection/cycle. **Figure 2** presents different steps of phage infection for each of the describes life cycles. [11]

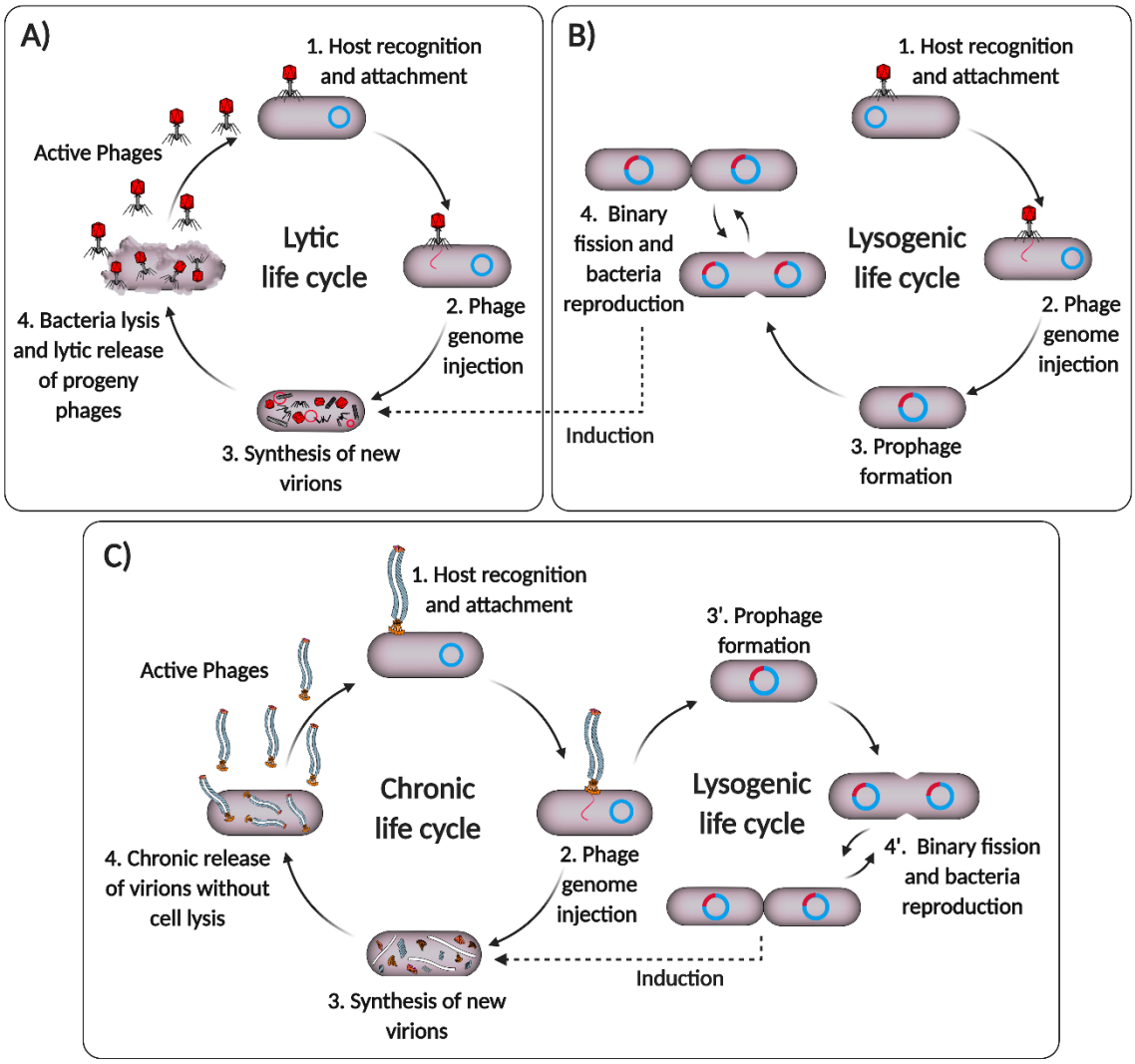

Figure 2. Different phage replication cycles. **(A)** The lytic cycle starts by (1) phage adsorption, (2) phage genome insertion into bacterial cell, (3) synthesis of new virions (progeny phages), and 4) bacterial lysis (5) and release of new phage into the surrounding environment. **(B)** Lysogenic cycle starts with phage adsorption (1) and genome insertion (2); however, the phage genome is incorporated into the bacterial genome, forming a prophage (3) that is replicated through the bacterial reproduction cycle (4). The lysogenic cycle could be induced to start the lytic cycle which ultimately leads to cell lysis (shown by the dashed arrow). **(C)** The phage chronic lifestyle starts with phage adsorption (1) and genome insertion (2). After new virions (progeny phages) are synthesized inside the bacterial cell (3), they are released without lysing bacterial cells (4). Some chronic phages can also adopt a lysogenic lifestyle, in which the phage genome is incorporated into the bacterial genome forming a prophage (3′) and is replicated through the bacterial reproduction cycle (4′) until the chronic cycle is induced (shown by the dashed arrow).[11]

2.3 Bacteriophage applications for biocontrol and human therapy

There is a direct relationship between the use of antimicrobials and the AMR spread. Antibiotics used in healthcare settings, animal husbandry, agriculture, aquaculture, and waste from industrial and domestic activities find their ways to the environment easily, and exacerbate the crisis of AMR worldwide.[12,13] Besides, in many natural or artificial environments, bacterial species form complex and irreversible assemblies called biofilms, to protect themselves against the surrounding hazards and to survive in diverse environments.[14] Biofilms are aggregates of bacterial cells embedded in a self-produced polymeric extracellular matrix (ECM) composed of exopolysaccharides (EPS), extracellular DNA and proteins[15]. It has been reported that biofilms show 10 to 1,000 times more resistance to antimicrobial treatments compared to planktonic bacteria and are extremely hard to eradicate. They could also perform as environmental reservoir of antimicrobial resistant genes (ARGs).[14,16] The ability to control and eradicate opportunistic microorganisms is also important for a large number of industries.[17–19] For instance, microbial control in water is of great importance not only to prevent infectious disease transmission through contaminated water, but also to reduce the biofouling in water and wastewater treatment plants which leads to infrastructure corrosion and water filtration membranes' malfunction.[20] Plant disease caused by pathogenic microorganisms, including more than 200 plant pathogenic bacteria, leads to 10% loss in global food production.[21] Phages as bacteria targeting viruses are natural antibacterial agents. Since the risk of antibiotic resistant bacteria as a global menace has raised, phages have regained attention globally to target bacterial pathogens in different settings.[8] To date, the antibacterial potential of phages has been harnessed in diverse applications, spanning from human, livestock, and poultry therapeutics to the biocontrol of pathogenic bacteria in food, agriculture, aquaculture, water, and wastewater.[20,22–26]

2.3.1 Characteristics of bacteriophages

Phages have distinctive characteristics that set them apart from other antibacterial agents in the treatment of bacterial infections. Apart from their abundance and extensive diversity, phages are regarded as self-sustaining antibacterial agents. This is because their population can increase exponentially by infecting the target pathogen and replicating on-site by taking

advantage of bacterial reproduction machinery.[27] They also offer high specificity in attacking bacterial species which helps protect the human microflora by selectively targeting troublesome bacteria.[28] In contrast, antibiotics have a broader spectrum, affecting a wider range of bacterial cell, eradicating both detrimental and beneficial bacteria and subsequently disturbing the balance of human microbiota. The imbalanced microbiota has been known to cause detrimental health conditions including gastrointestinal diseases, obesity, cancer, etc. Additionally, there are also some reports of direct toxic effects of antibiotics on host cells and tissue.[29] On the other hand, phages are safe and well tolerated as they are actually an important part of the microbiome and colonize different parts of human body, such as skin, oral cavity, gut, urinary tract and lungs.[16] Phages exclusively target bacterial cells and to date there has been no report of mammalian cell infection by phage. Furthermore, serious adverse events following phage therapy have been reported to be non-existent or extremely rare.[30,31] However, it is worth mentioning that the interactions of phage and human host is very complicated, not comprehensively understood by researchers and needs further exploration.[32] In addition to the previously mentioned traits, certain phages have been documented as potent biofilm eradicators. They achieve this by generating endolysins and extracellular polymeric substance (EPS) depolymerases, which can disrupt the structural matrix of the biofilm. This disruption creates the potential to penetrate the biofilm's inner layers, ultimately enabling the elimination of concealed bacteria.[33]

2.3.2 History and principles of phage therapy

Phage therapy was initially introduced in 1900s and is defined as the use phages, bacteria targeting viruses, to fight against pathogenic bacteria responsible for infectious diseases.[34,35] Félix d'Hérelle was the first scientist who used phages as therapeutics to treat children with severe dysentery (a gastrointestinal disease) in 1919, 20 years before the first clinical use of antibiotics.[36] During the 1930s and early 1940s, phage therapeutics were being commercialized. d'Herelle started producing five phage therapeutic products in Paris at L'Oréal, while Eli Lilly Company in the United States attempted to produce seven phage therapeutic preparations. Unfortunately, the latter effort encountered substantial technical difficulties and was ultimately discontinued, largely due to the increasing use of antibiotic

drugs.[10] Although the utilization of phage for treating bacterial infection was eclipsed in most parts of the world after the discovery and widespread use of antibiotics in the 1940s, it continued to persist in the Soviet Union and Eastern Europe in countries such as Poland and Georgia till today.[10] The revival of interest in phage therapy in the Western world can be attributed to controlled animal studies published in English-language scientific literature during the 1980s. In recent years, Western European countries, including Belgium and France, have approved the therapeutic applications of phage. In the United States, various organizations are in the process of developing phage therapeutics for clinical use, awaiting approval from the US Food and Drug Administration.[10] Recent FDA-approved "expanded access" experimental phage treatments, often referred to as compassionate use, for severely ill human patients afflicted by antibiotic-resistant bacterial infections have attracted substantial attention.[37]

There are two primary approaches to implementing phage therapy: standardized (general) and personalized phage therapy. In standardized phage therapy, a phage formula comprising a mix of different phages (e.g., phage cocktail) is developed that can address the need of a larger population of people infected with a specific bacterium. This approach is not restricted to a specific strain of bacteria.[38] Considering the fact that most patients have different microbiomes, and each infection could be different from the other, this approach may not apply to most cases. The other treatment approach that has been shown to be more effective is called personalized phage therapy in which the phage formula (single or a cocktail of phages) is designed to target the patient's specific infection.[39] For decades, phage therapy centers like the ones at the Eliava Institute in Tbilisi, Georgia, and in Wroclaw, Poland, have implemented a personalized approach to phage therapy. This individualized approach is now also being embraced in the United States through organizations like Adaptive Phage Therapeutics, Inc.[10]

Although there are many benefits associated with high specificity of bacteriophage, this trait adds complexity to the process of selecting appropriate phages for therapeutic applications. The common steps involved in personalized phage therapy are shown in **Figure 3**. First, the resistant bacterial pathogen is identified and isolated from the patient in the hospital. Afterwards, the related phage library is screened to find the suitable

phage/phages to attack the target pathogen. It is worth mentioning that this process requires high levels of collaboration and communications between research institutes, industry and army research centers as there is still no universal public phage libraries and different groups of phage researchers have their own local libraries.[38] The selected phage is then propagated, purified and sterilized based on FDA guidelines. The phage intended to be used as therapeutics should have some specifications such as being strictly lytic, having no sign of toxic genes or virulence factors, low levels of chloroform, cesium (left from phage purification step), etc. Finally, the phage or phage cocktail is sent to its destination for being administered properly (topical, intravenous, transnasal, and oral). If the treatment results are not satisfactory, further steps may involve additional phage isolation or phage training (i.e., phage evolution and selection), designing phage cocktails and phage and antibiotic combinatory treatment. Throughout the treatment process, it is essential to maintain ongoing vigilance for the emergence of resistant bacterial isolates and any interference with the host's response to treatment.[40]

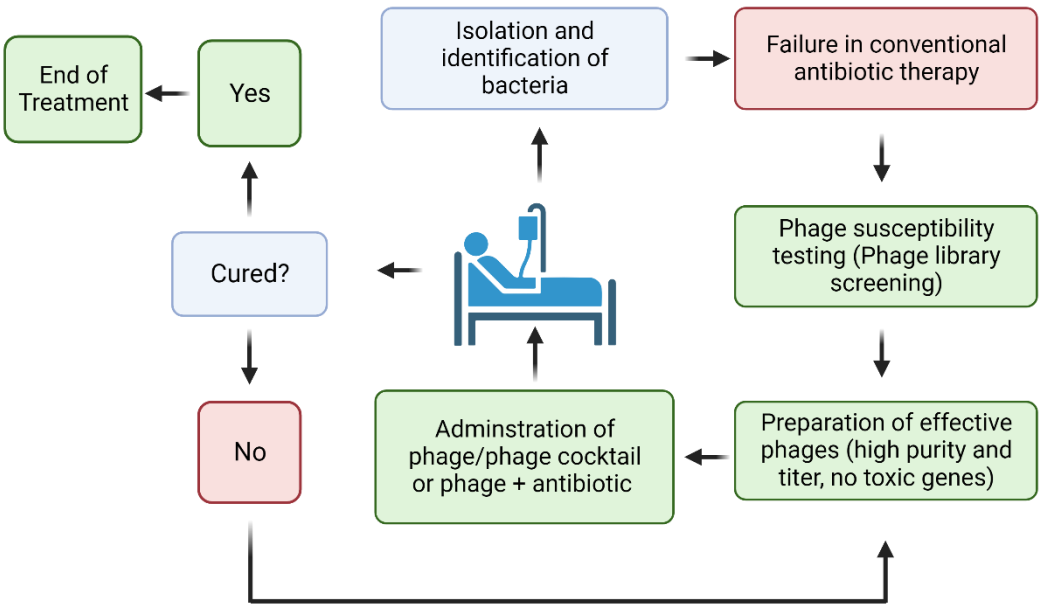

Figure 3. Common framework for personalized phage therapy. Antibiotic resistant bacteria are isolated from the patient, screened through a phage library, and effective phages are identified. Subsequently, the selected phages are produced in high titers and purified to be free from endotoxins. In addition, all phages in the library should be lytic without carrying any toxic genes.

2.3.3 Different methods for phage susceptibility testing

Due to high specificity of bacteriophages to bacterial species and even particular strains, customizing therapeutic phage cocktails for each patient to target the bacterial strains responsible for infection has been shown to be more effective than standardized phage cocktails.[41] For therapeutic applications, strictly lytic bacteriophages are needed to lyse and destroy the bacterial cells. The use of lysogenic phages is not recommended for therapeutic applications due their lack of immediate bactericidal effects and their potential involvement in horizontal transfer of antibiotic resistance genes and spread of virulence factors.[42,43] There are also a few characteristics of phages that can be considered to maximize the therapeutic action of phage including high concentration of phage (known as phage titer), shorter latent period (the duration from phage attachment to release of progeny phages), large burst size (number of released phages per lytic cycle), and high stability for long term storage.[44]

Plaque assay is the conventional and commonly used method to enumerate bacteriophage. In this methos, mixtures of phages and their corresponding bacterial host cells are mixed with molten soft agar and poured onto a nutrient-rich agar layer that supports bacterial growth. After overnight incubation (or longer for specific bacteria), the bacteria continue to grow until they reach the stationary phase, creating a continuous, opaque layer often referred to as a bacterial lawn. In areas where phages are present, the progeny phages released from phage infecting the nearby bacteria will create a zone observable by naked eye, commonly referred to as a "plaque," within the otherwise continuous bacterial lawn. These plaques are quantified, and the concentration or titer of phages is typically expressed as the number of plaque-forming units per milliliter (PFU/mL).[45,46] Aside from phage concentration, the morphology and plaque shapes can provide additional information about phage virulency.

There are various methods available for identifying the target phages to infect bacteria. These methods can be broadly classified into two categories: semi-solid medium assays and liquid assays.[47] Spot test is the most common example of semi-solid medium method

in which small volume droplets of phage are spotted over bacterial lawn and incubated for extended periods at a temperature suitable for bacteria growth. Although spot test is the gold standard method used in microbiology to identify phage infection, it is time-consuming, inefficient, and labor-intensive. However, it is still commonly used as an initial step of identifying target phages in the first round of phage library screening. Liquid assays to monitor bacteria lysis as a result of phage infection include tracking the bacteria culture turbidity (optical density) as a result of phage lysis[28], and bacterial cellular respiration.[47] These methods provide the opportunity to monitor the bacterial growth kinetic under phage predation and detect the long term efficacy of phage action, and pick up any secondary rise of a phage resistance mutants. The main hurdle of monitoring optical density of a bacteria culture is that bacteria cell debris, aggregates and clumps of lysates can contribute to turbidity of the culture and affect the results negatively. In addition, it cannot differentiate between dead and viable bacteria.[47] On the other hand, tracking the metabolic activity of bacteria under phage attack is not sensitive to aggregation and cell debris. In this method, a color change based on reduction of a redox-sensitive dye, such as tetrazolium, as result of bacterial cellular respiration is monitored. The drawbacks of this method are the irreversibility of the tetrazolium dye, which may not be able to detect lysis after growth, requiring additional compounds, and might be limited to aerobic bacteria.[40,48] However, a drawback of growth kinetic monitoring using the above-mentioned liquid assays is that scaling up demands costly equipment, such as multiple high-throughput robotic plate readers.[40] In addition to these approaches, detecting the enzymes released as a result of phage-mediated cell lysis such as adenylate kinase, adenosine triphosphate (ATP), or β-galactosidase have been reported for *E. coli* phages, mainly for biosensing purposes and not phage library screening.[11,48]

2.3.4 Challenges of using phage for biocontrol and human therapeutics

Despite many cases with successful treatment outcomes, the utilization of phages for biocontrol and therapeutic purposes is not without its challenges. The regulatory approval process for phage therapy has been complex and time-consuming due to the diversity of phages and phage cocktails, co-evolution of phage and its bacterial host, and complicated

in vivo behavior. The absence of well-controlled clinical trial data and the presence of intricate regulatory frameworks have led to compassionate use on a case-by-case basis for patients without a better treatment option.[49] Large scale manufacturing of high purity phages (e.g. endotoxin <0.5 EU/ml for subcutaneous injections) under current good manufacturing practice might be challenging as well.[50] Some additional challenges associated with phage therapy along with some potential solutions are detailed below.

Limited spectrum of activity (high specificity). As discussed in section 2.3.2, high specificity of phages can limit their spectrum of activity to infecting a single strain of a specific bacterial species. To expand the range of phage activity, it is possible to design phage cocktails capable of infecting different strains of the same bacterial species or even multiple bacterial species.[51] Another common approach to tackle this challenge is personalized phage therapy, wherein phages or phage cocktails are carefully selected based on the specific infection of a patient through the screening of phage libraries. It is noteworthy that certain phages exhibit the ability to infect multiple species or genera (polyvalent phages), whereas many phages exhibit specificity towards a single strain or a limited number of strains within a bacterial species.[52]

Phage activity is dependent on bacterial growth rate. Another critical factor to take into account is the bacterial growth rate, as it can significantly impact the efficiency of phage infectivity. Phages are essentially bacterial parasites; their replication depends on the bacterial replication machinery. As a result, the effectiveness of phage may differ in logarithmic and stationary growth phase of bacteria. It is recommended to examine the phage infectivity in both logarithmic and stationary states and, ideally, select phages that demonstrate effective performance in both stages of bacterial growth.[40]

Phage resistance. One of the main hurdles of phage therapy is the development of bacterial resistance to phages.[44] Utilizing a phage cocktail not only expands the range of phage infectivity but also acts as a potential preventive measure against the emergence of phage resistance. By having phages targeting different bacterial receptors, and having counter-defense mechanisms towards phage resistance, the phage cocktail can effectively overcome or bypass the defense mechanisms employed by the target bacteria.[53] Each phage can

employ slightly different infection mechanisms and as a result, bacteria may face a major challenge when attempting to prevent all the infection strategies employed by different phages. Additionally, phages often bind to crucial surface proteins as receptors. Phages carry binding proteins that identify and adhere to sites on the exterior of a bacterial cell. They can attach to bacterial structures like pili, flagella, porins, or efflux pumps. There have also been reports of phages binding to particular sugar components in lipopolysaccharide (LPS).[8] The mutation or loss of these receptors may prevent phage attachment but can impose a fitness cost on the bacterium and they might experience a reduced fitness, a reduction in the expression of that virulence factor, and increased vulnerability to the immune system when they develop resistance to phages.[54] This selective pressure against virulence factors can have several beneficial effects. For example, some virulence factors, like capsules, offer a degree of resistance to antibiotics, and hinder phagocytosis by macrophages.[8] Moreover, selection against other virulence factors that can act as phage receptors, such as adhesins, pili, or secretion systems, may prevent bacterial attachment and the invasion of epithelial cells. Similarly, phages that use an antibiotic efflux pump for infection can drive a reduction in the expression of the efflux pump, making the bacteria more susceptible to antibiotics that were previously being pumped out.[8] This leads us to the alternative approach for addressing phage resistance, which involves employing a combination therapy using both phages and antibiotics simultaneously.[55] If selected carefully, phage treatment of antibiotic-resistant bacteria can potentially restore their sensitivity to the antibiotic through above-mentioned mechanisms.[56]

Phage neutralization. Another challenge in the effective implementation of phage therapy is the risk of neutralization or elimination within the *in vivo* environment, attributed to factors such as extreme pH or immune responses.[48] Phages can be delivered to infection site either in saline/buffer-based solutions, or immobilized/encapsulated into nano/biomaterials. While the latter is less common, incorporating biomaterials could provide opportunities for developing multifunctional biomaterials that can serve for more than just bactericidal purposes. There are a range of biomaterials and coatings that can be combined with phage as natural bactericidal agent to offer additional functionalities attributed to the implemented bio/nanomaterial. Bio/nano materials could offer unique

properties including promoting cell proliferation/adhesion, osteoinductive properties, hemostatic effects, controlled release profile, etc. Phages can be immobilized onto the surface of medical devices such as grafts and implants using physical or chemical immobilization techniques. Different types of nano-biomaterials in various shapes and forms including hydrogels, nanoparticles, nanovesicles, nanofibers, etc. can be used to encapsulate/immobilize phage.[57–59] These methods can retain the phage for longer at the site of infection by increasing its stability by protecting it against harsh pH conditions, enzymatic and immune system neutralization and clearance.[57]

Complicated pharmacokinetics. There are significant complexities associated with pharmacokinetics (how the body processes phages) utilizing phage therapy to combat bacterial infections in both animals and humans. Pharmacokinetic obstacles are internal factors that impede a drug's ability to reach and sustain effective concentrations in specific target tissues for a sufficient duration. These obstacles are traditionally categorized into absorption (entry into the bloodstream), distribution (movement into various body tissues from the bloodstream), excretion (drug removal from the body), and metabolism (inactivation of drugs within the body). "Phage clearance," a collective term for excretion and metabolism, can present a significant challenge in the context of phage therapy. Shortcomings in phage absorption, dispersion, or overly rapid elimination or deactivation can impede the effectiveness of phage therapy.[60] For phages to act as effective antibacterial agents, they must first reach the target bacteria in adequate quantities. The route of this movement can vary in complexity; it may be straightforward, as in some topical applications, or more intricate, especially in the context of systemic phage application targeting bacteria in non-blood tissues.[60,61] When phages are administered through injections (parenteral) or orally, they primarily enter the bloodstream. The parenteral route is expected to be more efficient in terms of absorption, reducing the risk of phage loss compared to oral delivery. When administered orally, phages have to navigate the complex environment of the gastrointestinal tract. On the other hand, topical application minimizes losses in absorption and distribution, which enhances the antibacterial effectiveness of phages. Another method involves directly injecting phages into infection sites, further minimizing losses.[62]

2.4 Conclusion

Phages are one of the promising antibacterial agents in the era of global spread of AMR. These abundant natural bacteria-targeting viruses are easily accessible in the environment, and can be identified and propagated by processing various types of environmental samples, such as water, sewage, soil, etc. Phages have unique characteristics such as high specificity, self-dosing, and are generally safe and well-tolerated by humans and animals. Although several successful phage therapy cases in treating a wide range of infections in different body parts have been reported so far, there are complexities associated with their utilizations and needs to be explored and circumvented. The intricate pharmacodynamics and pharmacokinetics of phages have posed challenges for regulatory approval and extended use; however, several phage therapy centers are implementing these viruses to save lives through compassionate use in patients with severe antibiotic resistance infections. Incorporating phages into different biomedical engineering designs could contribute effectively to enhancing their performance. Specifically, proposing new ways of stabilizing phages, encapsulating phage into biomaterials, and immobilizing them on the surface of biomedical devices are some of the aspects that can be engineered to facilitate their incorporation in real-life applications.

In the following chapters, I have explored various applications of phages in biocontrol and therapeutics. My PhD research encompasses the following projects: the development of a novel approach for phage susceptibility testing using an ATP bioluminescence (Chapter 3), the creation of a phage-loaded injectable hydrogel for addressing bone and implant-associated infections (Chapter 4), the utilization of phage-conjugated liquid-infused coatings on titanium implants (Chapter 5), and the eradication of biofilms from the surface of dissolved oxygen sensors (Chapter 6). In Appendix I, you will find my review paper discussing the general properties of phages and their potential application in biosensors for environmental monitoring. Appendix II delves into various antibacterial coatings for titanium implants, including the potential incorporation of phages as natural antibacterial agents.

2.5 References

1. Kardos, N. & Demain, A. L. Penicillin: the medicine with the greatest impact on therapeutic outcomes. *Appl. Microbiol. Biotechnol.* **92**, 677–687 (2011).
2. Murray, C. J. L. *et al.* Global burden of bacterial antimicrobial resistance in 2019: a systematic analysis. *Lancet* **399**, 629–655 (2022).
3. Ventola, C. L. The antibiotic resistance crisis: part 1: causes and threats. *P T* **40**, 277–83 (2015).
4. Iskandar, K. *et al.* Antibiotic Discovery and Resistance: The Chase and the Race. *Antibiotics* **11**, 1–38 (2022).
5. Gibb, B. P. & Hadjiargyrou, M. Bacteriophage therapy for bone and joint infections an instructional review. *Bone Jt. J.* **103 B**, 234–244 (2021).
6. Li, B. & Webster, T. J. Bacteria antibiotic resistance: New challenges and opportunities for implant-associated orthopedic infections. *J. Orthop. Res.* **36**, 22–32 (2018).
7. Merril, C. R., Scholl, D. & Adhya, S. L. The prospect for bacteriophage therapy in Western medicine. *Nat. Rev. Drug Discov.* **2**, 489–497 (2003).
8. Kortright, K. E., Chan, B. K., Koff, J. L. & Turner, P. E. Phage Therapy: A Renewed Approach to Combat Antibiotic-Resistant Bacteria. *Cell Host Microbe* **25**, 219–232 (2019).
9. Mushegian, A. R. Are There 1031 Virus Particles on Earth, or More, or Fewer? *J. Bacteriol.* **202**, 2192–2197 (2020).
10. Nikolich, M. P. & Filippov, A. A. Bacteriophage therapy: Developments and directions. *Antibiotics* **9**, (2020).
11. Bayat, F., Didar, T. F. & Hosseinidoust, Z. Emerging investigator series: bacteriophages as nano engineering tools for quality monitoring and pathogen detection in water and wastewater. *Environ. Sci. Nano* **8**, 367–389 (2021).
12. Venter, H., Henningsen, M. L. & Begg, S. L. Antimicrobial resistance in healthcare, agriculture and the environment: the biochemistry behind the headlines. *Essays Biochem.* **61**, 1–10 (2017).
13. Singer, A. C., Shaw, H., Rhodes, V. & Hart, A. Review of antimicrobial resistance in the environment and its relevance to environmental regulators. *Front. Microbiol.* **7**, 1–22 (2016).
14. Balcázar, J. L., Subirats, J. & Borrego, C. M. The role of biofilms as environmental reservoirs of antibiotic resistance. *Front. Microbiol.* **6**, 1–9 (2015).
15. Rabin, N. *et al.* Biofilm formation mechanisms and targets for developing antibiofilm agents. *Future Med. Chem.* **7**, 493–512 (2015).
16. Hall-Stoodley, L., Costerton, J. W. & Stoodley, P. Bacterial biofilms: From the natural environment to infectious diseases. *Nat. Rev. Microbiol.* **2**, 95–108 (2004).
17. Cozad, A. & Jones, R. D. Disinfection and the prevention of infectious disease. *Am. J. Infect. Control* **31**, 243–254 (2003).
18. Preena, P. G., Swaminathan, T. R., Kumar, V. J. R. & Singh, I. S. B. Antimicrobial resistance in aquaculture: a crisis for concern. *Biologia (Bratisl).* (2020). doi:10.2478/s11756-020-00456-4
19. Połaska, M. & Sokołowska, B. Bacteriophages — a new hope or a huge problem in the food industry. **5**, 324–346 (2019).
20. Mathieu, J., Yu, P., Zuo, P., Da Silva, M. L. B. & Alvarez, P. J. J. Going Viral:

Emerging Opportunities for Phage-Based Bacterial Control in Water Treatment and Reuse. *Acc. Chem. Res.* **52**, 849–857 (2019).
21. Buttimer, C. *et al.* Bacteriophages and bacterial plant diseases. *Front. Microbiol.* **8**, 1–15 (2017).
22. Ye, M. *et al.* A review of bacteriophage therapy for pathogenic bacteria inactivation in the soil environment. *Environ. Int.* **129**, 488–496 (2019).
23. Svircev, A., Roach, D. & Castle, A. Framing the future with bacteriophages in agriculture. *Viruses* **10**, 1–13 (2018).
24. Dy, R. L., Rigano, L. A. & Fineran, P. C. Phage-based biocontrol strategies and their application in agriculture and aquaculture. *Biochem. Soc. Trans.* **46**, 1605–1613 (2018).
25. Gigante, A. & Atterbury, R. J. Veterinary use of bacteriophage therapy in intensively-reared livestock. *Virol. J.* **16**, 155 (2019).
26. Culot, A., Grosset, N. & Gautier, M. Overcoming the challenges of phage therapy for industrial aquaculture: A review. *Aquaculture* **513**, 734423 (2019).
27. Petrovic Fabijan, A. *et al.* Phage therapy for severe bacterial infections: a narrative review. *Med. J. Aust.* **212**, 279–285 (2020).
28. Xie, Y., Wahab, L. & Gill, J. J. Development and validation of a microtiter plate-based assay for determination of bacteriophage host range and virulence. *Viruses* **10**, (2018).
29. Patangia, D. V., Anthony Ryan, C., Dempsey, E., Paul Ross, R. & Stanton, C. Impact of antibiotics on the human microbiome and consequences for host health. *Microbiologyopen* **11**, 1–23 (2022).
30. Principi, N., Silvestri, E. & Esposito, S. Advantages and limitations of bacteriophages for the treatment of bacterial infections. *Front. Pharmacol.* **10**, 1–9 (2019).
31. Liu, D. *et al.* The safety and toxicity of phage therapy: A review of animal and clinical studies. *Viruses* **13**, 1–20 (2021).
32. Van Belleghem, J. D., Dąbrowska, K., Vaneechoutte, M., Barr, J. J. & Bollyky, P. L. Interactions between bacteriophage, bacteria, and the mammalian immune system. *Viruses* **11**, (2019).
33. Akanda, Z. Z., Taha, M. & Abdelbary, H. Current review—The rise of bacteriophage as a unique therapeutic platform in treating peri-prosthetic joint infections. *J. Orthop. Res.* **36**, 1051–1060 (2018).
34. Loc-Carrillo, C. & Abedon, S. T. Pros and cons of phage therapy. *Bacteriophage* **1**, 111–114 (2011).
35. Reindel, R. & Fiore, C. R. Phage therapy: Considerations and challenges for development. *Clin. Infect. Dis.* **64**, 1589–1590 (2017).
36. Abedon, S. T., Kuhl, S. J., Blasdel, B. G. & Kutter, E. M. Phage treatment of human infections. *Bacteriophage* **1**, 66–85 (2011).
37. Dickey, J. & Perrot, V. Adjunct phage treatment enhances the effectiveness of low antibiotic concentration against Staphylococcus aureus biofilms in vitro. *PLoS One* **14**, 1–17 (2019).
38. Ganeshan, S. D. & Hosseinidoust, Z. Phage Therapy with a Focus on the Human Microbiota. (2019).
39. Cui, Z., Guo, X., Feng, T. & Li, L. Exploring the whole standard operating procedure

for phage therapy in clinical practice. *J. Transl. Med.* **17**, 1–7 (2019).
40. Gelman, D. *et al.* Clinical Phage Microbiology: a suggested framework and recommendations for the in-vitro matching steps of phage therapy. *The Lancet Microbe* **2**, e555–e563 (2021).
41. Mattila, S., Ruotsalainen, P. & Jalasvuori, M. On-demand isolation of bacteriophages against drug-resistant bacteria for personalized phage therapy. *Front. Microbiol.* **6**, 1–7 (2015).
42. Melo, L. D. R., Oliveira, H., Pires, D. P., Dabrowska, K. & Azeredo, J. Phage therapy efficacy: a review of the last 10 years of preclinical studies. *Crit. Rev. Microbiol.* **46**, 78–99 (2020).
43. Lin, D. M., Koskella, B. & Lin, H. C. Phage therapy: An alternative to antibiotics in the age of multi-drug resistance. *World J. Gastrointest. Pharmacol. Ther.* **8**, 162 (2017).
44. Oromí-Bosch, A., Antani, J. D. & Turner, P. E. Developing Phage Therapy That Overcomes the Evolution of Bacterial Resistance. *Annu. Rev. Virol.* **10**, 1–22 (2023).
45. Ács, N., Gambino, M. & Brøndsted, L. Bacteriophage Enumeration and Detection Methods. *Front. Microbiol.* **11**, (2020).
46. Letarov, A. V. & Kulikov, E. E. Determination of the bacteriophage host range: Culture-Based approach. *Methods Mol. Biol.* **1693**, 75–84 (2018).
47. Henry, M. *et al.* Development of a high throughput assay for indirectly measuring phage growth using the OmniLog TM system . *Bacteriophage* **2**, 159–167 (2012).
48. Pires, D. P., Costa, A. R., Pinto, G., Meneses, L. & Azeredo, J. Current challenges and future opportunities of phage therapy. *FEMS Microbiology Reviews* **44**, 684–700 (2020).
49. Vázquez, R. *et al.* Essential Topics for the Regulatory Consideration of Phages as Clinically Valuable Therapeutic Agents: A Perspective from Spain. *Microorganisms* **10**, 1–20 (2022).
50. Cooper, C. J., Mirzaei, M. K. & Nilsson, A. S. Adapting drug approval pathways for bacteriophage-based therapeutics. *Front. Microbiol.* **7**, 1–15 (2016).
51. Abedon, S. T., Danis-Wlodarczyk, K. M. & Wozniak, D. J. Phage cocktail development for bacteriophage therapy: Toward improving spectrum of activity breadth and depth. *Pharmaceuticals* **14**, (2021).
52. Ross, A., Ward, S. & Hyman, P. More is better: Selecting for broad host range bacteriophages. *Front. Microbiol.* **7**, 1–6 (2016).
53. Torres-Barceló, C. Phage therapy faces evolutionary challenges. *Viruses* **10**, (2018).
54. Green, S., Ma, L. & Maresso, A. Phage Therapy. *Ref. Modul. Biomed. Sci.* 1–11 (2018). doi:10.1016/B978-0-12-801238-3.66117-2
55. Diallo, K. & Dublanchet, A. Benefits of Combined Phage–Antibiotic Therapy for the Control of Antibiotic-Resistant Bacteria: A Literature Review. *Antibiotics* **11**, 1–11 (2022).
56. Chan, B. K. *et al.* Phage selection restores antibiotic sensitivity in MDR Pseudomonas aeruginosa. *Sci. Rep.* **6**, 1–8 (2016).
57. Loh, B. *et al.* Encapsulation and Delivery of Therapeutic Phages. *Appl. Environ. Microbiol.* **87**, 1–13 (2021).
58. Yang, Y. *et al.* Encapsulation and delivery of phage as a novel method for gut flora manipulation in situ: A review. *J. Control. Release* **353**, 634–649 (2023).

59. Kim, H. Y., Chang, R. Y. K., Morales, S. & Chan, H. K. Bacteriophage-delivering hydrogels: Current progress in combating antibiotic resistant bacterial infection. *Antibiotics* **10**, 1–17 (2021).
60. Dąbrowska, K. & Abedon, S. T. Pharmacologically Aware Phage Therapy: Pharmacodynamic and Pharmacokinetic Obstacles to Phage Antibacterial Action in Animal and Human Bodies. *Microbiol. Mol. Biol. Rev.* **83**, (2019).
61. Dąbrowska, K. Phage therapy: What factors shape phage pharmacokinetics and bioavailability? Systematic and critical review. *Med. Res. Rev.* **39**, 2000–2025 (2019).
62. Qadir, M. I., Mobeen, T. & Masood, A. Phage therapy: Progress in pharmacokinetics. *Brazilian J. Pharm. Sci.* **54**, 1–9 (2018).

Chapter 3: High throughput platform technology for rapid target identification in personalized phage therapy

Preface: In this chapter, a tablet-based system has been developed to facilitate and accelerate the process of target phage identification for personalized phage therapy. In this method the ATP released as a result of phage-mediated cell lysis has been implemented to track the lytic activity of phages. In order to enhance the thermal stability of the ATP assay components, namely luciferase and its substrate luciferin, a sugar mix comprising pullulan and trehalose has been used. Finally, dry sugar-based tablets containing phage, ATP assay components, and phage have been developed to improve the shelf stability at room temperature and ease up the transportation process of the local phage libraries globally.

Contribution: I conducted the experiments, analyzed the results, and wrote the original draft of the manuscript. Arwa Hilal contributed to phage propagation and enumeration and metabolic activity measurements using XTT assay. Mathura Thirugnanasampanthar has contributed to optimizing the XTT assay protocol used in this study. The SEM and TEM imaging was conducted at Canadian Center for Electron Microscopy (CCEM). Carmen Andrei helped with TEM imaging of the samples. Dr. Tohid Didar and Dr. Zeinab Hosseinidoust conceptualized and supervised the project. Dr. Zeinab Hosseinidoust revised the manuscript. Dr. Carlos D. M. Filipe provided scientific support. All the authors read and approved the final version.

Citation: This research presented in this chapter has been submitted and is under revision in *Nature Communications* journal.

High throughput platform technology for rapid target identification in personalized phage therapy**,** Fereshteh Bayat, Arwa Hilal, Mathura Thirugnanasampanthar, Carlos D. M. Filipe, Tohid F Didar, Zeinab Hosseinidoust, *Nature Communications*, **2023**, *under revision*, NCOMMS-23-19146-T

3.1 Abstract

As bacteriophages continue to gain regulatory approval for personalized human therapy against antibiotic-resistant infections, there is a clear need for transformative technologies that address century-old challenges, specifically for rapid target identification through multiple, large, decentralized therapeutic phages libraries. Combining materials technology and biochemistry, we designed a high throughput phage screening platform comprised of a library of shelf-stable, ready-to-use, portable, all-inclusive solid tablets. Each tablet encapsulates phage along with the biochemistry of detection, stabilized in a matrix of sugar polymers that confer heat stability to detection enzymes, increasing the generated bioluminescence signal by ~90 % and allowing for phage susceptibility screening in as low as 30 mins, as well as enhancing desiccation tolerance of all components, promising easier and cheaper transportation of this technology around the world and as a result, increased accessibility to therapeutic phage. High throughput screening was demonstrated using an in-house library of all-inclusive solid tablets to identify target phages for selecting multidrug-resistant clinical isolates of Pseudomonas aeruginosa within 30 mins. This technology is a paradigm shift from the century-old, slow, and labor-intensive plaque assay, offering the promise of enhanced accessibility and potentially lowering mortality rates for patients with antibiotic-resistant infections through rapid personalized phage therapy.

Keywords: healthcare accessibility, antibiotic resistance, phage susceptibility, as, point-of-care

3.2 Introduction

The spread of antimicrobial resistance (AMR) is considered a major global challenge, claiming more than 700,000 lives per year, with a projected death toll of 10 million by 2050.[1] The looming global crisis of AMR and urgency to identify new therapeutics to fight against acute and chronic bacterial infections has garnered the attention of researchers, clinicians, and regulatory bodies towards bacteriophage therapy (*i.e.*, the use of bacteriophages to fight bacterial infections). Bacteriophages, or phages for short, are viruses that exclusively infect bacteria in a highly targeted manner.[2] This targeted killing action is in stark contrast to the indiscriminate sledge-hammer action of antibiotics and is a major advantage of phages over antibiotics, promising minimal disruption to our precious microbiota,[3–5] while simultaneously challenging decades of experience in development of antimicrobial therapies.

Phage therapy relies on century-old methods that while adequate for phage research labs, fall short when a human life hangs in the balance. Design and administration of phage therapeutics requires a fundamental shift in the way we think about antimicrobial therapies as well as a collection of custom-designed tools and technologies that meet the standard of care in modern medicine. One of the challenges in clinical practice of phage therapy is that owing to the targeted action of phage, human phage therapy is most effective when implemented as a personalized therapy, as demonstrated by an increasing number of clinical case reports.[5–7] Personalized phage therapy begins with isolating bacteria deemed to be resistant to all available antibiotics and screening the antibiotic-resistant bacterial isolate against large libraries of therapeutic phage and/or libraries of environmental samples expected to contain phage (**Figure 1A-i**). These libraries can contain hundreds of phages and thus require susceptibility profiling technologies that can be implemented rapidly and in a high throughput format. The current gold standard in susceptibility testing, which has remained unchanged for over a century, is the spot test,[8] a culture-based method which involves a long incubation period of overnight to several days (**Figure 1A-ii**).[9] Although widely used in research labs, the spot test method is laborious, slow, and not amenable to high throughput implementation. The second challenge is that a universal phage library is

nonexistent and patients, researchers and clinicians pursuing phage therapy depend on libraries maintained by local and, in very few cases, national or military research labs.[3] Successful implementation of personalized phage therapy therefore requires streamlined communication and sharing between curators of small and large phage libraries at the national and international level.[10] We envision a platform technology that addresses both aforementioned challenges in personalized phage therapy, namely a reliable high throughput technology that can be implemented rapidly with shelf-stable and portable assay reagents that can be readily shipped around the world to be employed at the point of care with minimal infrastructure or training. To meet these design criteria, we re-imagined a therapeutic phage library in the physical format of stable and all-inclusive solid tablets, each tablet encapsulating a stock phage along with the biochemistry of detection (**Figure 1A-iii**).

Plaque assay is the conventional and commonly used method to evaluate the phage infection of bacterial cells. In plaque assay, the formation of clear zones called plaques on a lawn of bacteria is monitored. As a result of phage lysing bacterial cells and release of progeny phages, these clear zones are formed[9]. However, this process is time-consuming, expensive, laborious, and not scalable for high throughput screening. Liquid assays to monitor bacteria lysis as a result of phage infection include tracking the bacteria culture turbidity (optical density) as a result of phage lysis[11], and phenotypic/metabolic analysis. The main hurdle of monitoring optical density of a bacteria culture is that bacteria cell debris can contribute to turbidity of the culture and affect the results negatively. The phenotypic/metabolic microarray assays have gained much attention recently and can be used to analyze properties related to phenotypes, namely cell growth and respiration.[12] However, these assays are detecting the phage-mediated bacterial cell lysis indirectly. We built our technology based on detection of released adenosine triphosphate (ATP) during phage-mediated bacteria lysis (**Figure 1B**) by overcoming two major barriers in biochemistry of detection. ATP can be readily detected with firefly luciferase, [13] which is a heat labile enzyme and quickly deactivated at temperatures above 30ºC.[14] For human therapeutic applications, however, lytic activity of bacteriophages must be detected at 37ºC, which is optimal for metabolic activity of clinical bacterial isolates and thus for phage lytic

action. In addition, commercially available ATP detection assays require stagewise addition of reaction components, complicating high throughput implementation.

To overcome these barriers in detection, we utilized materials technology and stabilized and encapsulated all reagents required for ATP detection along with each phage in a sugar-based matrix that prevented thermo-inactivation of enzymes. Optimizing the biochemical rection in the presence of this matrix enabled realization of a hassle-free, one-pot biochemical reaction, stabilized in the form of a solid tablet that preserved the activity of enzymes at physiological temperatures and the activity of phage along with the enzymes under desiccation. The latter promises easier and cheaper transportation around the world and as a result, easier screening of decentralized phage libraries and increased accessibility to phage therapy. We demonstrated the utility of this platform technology for high throughput implementation by phage susceptibility screening of selected multidrug-resistant clinical isolates of *Pseudomonas aeruginosa* from an in-house library.

3.3 Results and discussion

3.3.1 Phage-mediated bacteria lysis

To develop a one-tablet assay based on detection of phage-mediated lysis, we selected three phages from our in-house phage library with different levels of bacteria lysis ability. Bacteriophages vB_Pae-Tbilisi32 (P32), JG004, and PP7 were propagated using the host bacterial strain, *P. aeruginosa* PAO1 (Pa). Transmission Electron micrographs of the three phages are shown in **Figure 1C**. P32 belongs to the *Podoviridae* family and has a very short tail (**Figure 1C-i)**.[15] JG004 is a tailed *Myoviridae* phage,[16] with an isometric head and a contractile tail (**Figure 1C-iii)**. PP7 belongs to *Leviviridae* family and has an icosahedral capsid with an approximate diameter of 30 nm (**Figure 1C-v)**.[17] **Figure 1C** also depicts plaques generated by each of the three phages on Pa bacterial lawn, indicative of the ability of these phages to successfully infect and lyse Pa. A phage plaque is a clearing caused by phage-mediated killing of bacteria, usually cultured as a lawn on a semi-solid agar-matrix.[18,19] Plaque morphology can provide qualitative yet important information regarding phage characteristics. For example, larger plaques are usually indicative of a larger burst size (number of progeny phages released from the infection of a single bacterial cell)[20] and

shorter latent period (period between phage adsorption and release of progeny virions).[21] As seen in **Figure 1C-ii**, P32 generates the largest plaque, followed by JG004 (**Figure 1C-iv)**, and then PP7 (**Figure 1C-vi)**. To further characterize phage-mediated bacteria lysis, we generated kinetic kill curves which showed the change in metabolic activity of bacterial culture challenged with the three phages, using the XTT colorimetric assay (**Figure 1D**).

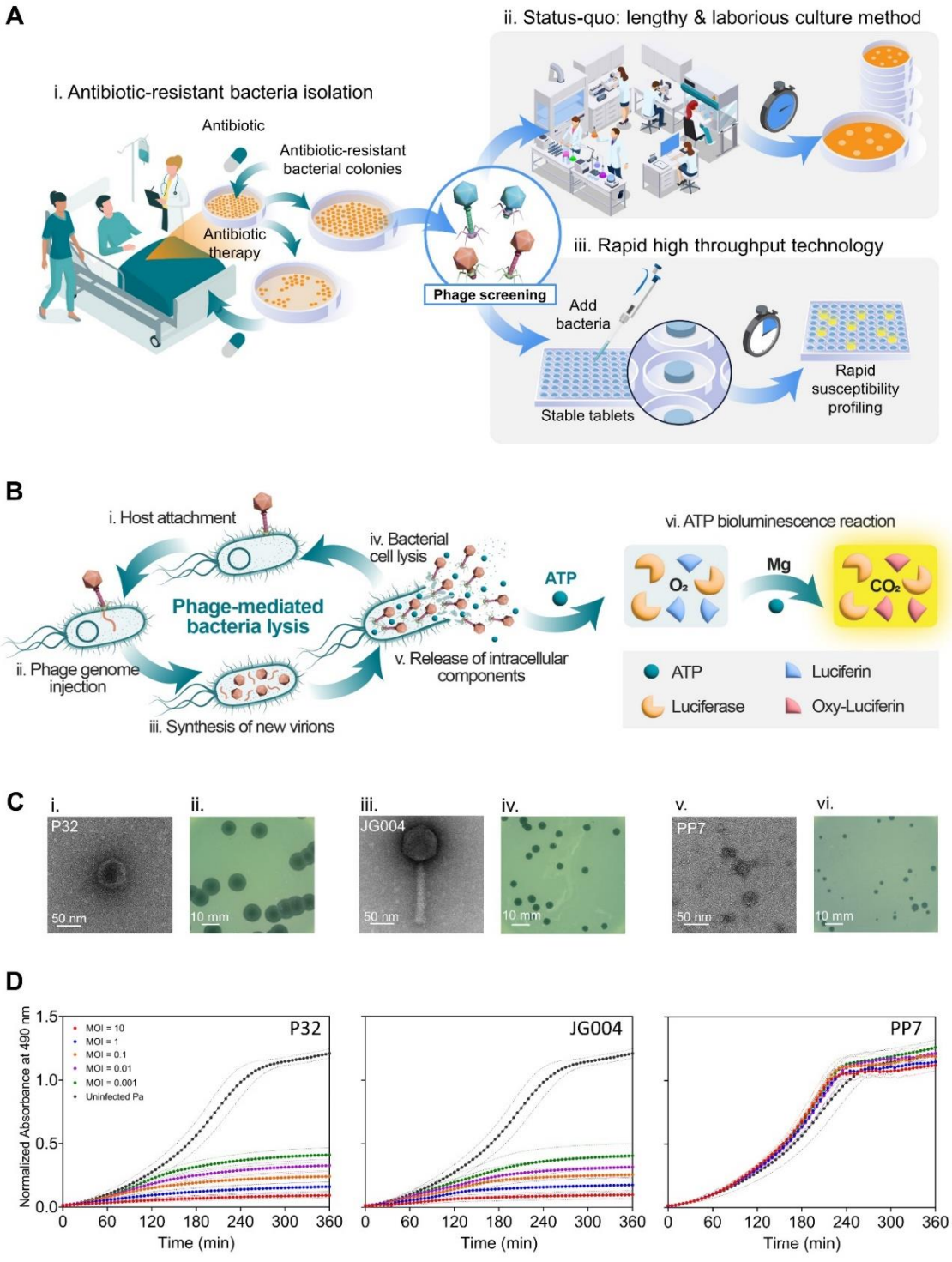

Figure 1. (A) Personalized phage therapy. The first step in personalized phage therapy is isolation of treatment-resistant bacterial strain from patient (i), followed by employing slow culture-based, spot test method to screen and select therapeutic phages (ii). We propose a single-tablet technology for rapid, high-throughput screening of therapeutic phages (iii). **(B)** Phage-mediated ATP release and detection. Phage-mediated lysis of bacterial cell starts

when a phage virion encounters the host cell and attaches to specific phage receptors (i), this is followed by phage genome insertion into the host bacteria (ii). This starts a cascade of events leading to hijacking of bacteria replication machinery for synthesis of new progeny phage(iii), which ultimately leads to host cell lysis (iv), and release of progeny virions along with a burst of ATP (v). ATP reacts with luciferin to form luciferin adenylate, which is oxidized by the luciferase enzyme in the presence of magnesium to form oxyluciferin, CO_2 and adenosine monophosphate (AMP), which results in light emission (vi). **(C)** Transmission electron micrographs of P32 (i), JG004 (iii), and PP7 (v). Plaque formation on Pa lawns created by P32 (ii), JG004 (iv), and PP7 (vi). **(D)** Metabolic activity of uninfected and infected (MOI = 10, 1, 0.1, 0.01, 0.001) Pa cultures (n=3, mean ± SD). All reported values are the mean of three biological replicates and associated error bars shown as dashed lines represent standard deviation from the mean.

Pa was infected at different MOIs (multiplicity of infection, commonly defined as the ratio of infectious virions to bacterial cells in a culture).[22] For all experiments, starting concentration of bacteria was kept constant (~ 10^7 CFU/mL). Both P32 and JG004 (**Figure 1D-i, ii**) significantly suppressed bacterial growth, as indicated by a low metabolic activity. The decrease in bacterial metabolic activity was slower by at lower MOIs, as expected. It is noteworthy that although PP7 formed visible plaques on Pa lawns, it did not show effective bacterial growth suppression (**Figure 1D-iii)**. These trends agree with Pa kill curves based on optical density Pa (**Figure S1**) and highlight a very important bias of the current gold standard method in phage susceptibility testing, specifically as it pertains to phage application for therapy and biocontrol that a clearing on a bacterial lawn (plaque or spot test) does not necessarily signal the ability of a phage to control the population of bacteria in a liquid culture, and as some studies have indicated, in *in vivo* models.[23]

It is important to note here that phages have three different lifecycles, namely lytic, lysogenic, and chronic (**Figure S2**). Through the lytic lifecycle (**Figure S2A**) a bacteriophage can lyse and destroy a bacterial cell in as short as ~20 minutes, leading to release of a range of biomolecules in addition to hundreds progeny phage.[24] Regulatory agencies have historically only approved strictly lytic phages for human therapeutic use and environmental biocontrol because of outstanding concerns regarding horizontal gene transfer through the lysogenic lifecycle (**Figure S2B, C**).[25] Keeping in mind that our aim was to screen phage libraries for phages with therapeutic potential, in this work we focused on detection of phages capable of bacterial lysis.

3.3.2 Increasing signal-to-noise ratio and end-point detection of phage-mediated bacteria lysis

The next step towards realizing the high throughput, one-pot detection of phage-mediated bacteria lysis was to filter out the background signal. Phage stocks are obtained through the infection and lysis of bacterial cells leading to the release of progeny phages along with other intracellular components, including ATP. Therefore, we hypothesized that phage suspensions must be treated to reduce residual ATP molecules which can otherwise give rise to a strong background signal. The goal was to diminish the background bioluminescent signal at time zero, *i.e.*, at the point of phage addition to the bacterial culture, which would in turn decrease the assay time and allow a signal to be discernable as soon as phage-mediated lysis of bacterial cells occurs. **Figure S3A** shows the background bioluminescence signal in phage suspensions at different stages of purification (including sterile filtration with 0.2 μm filters, PEG purification, supernatant and filtrate of ultra-filtration with 10 KDa and 3 KDa filters) and after diluting phage in culture media. After PEG purification, the ATP concentration decreased significantly; however, ultrafiltration with 3 KDa filters failed to reduce ATP levels. As shown in **Figure S3B**, simply diluting concentrated phage suspensions in cell media was found to be equally effective for reducing background ATP signal as the labor-intensive PEG purification technique. Based on these results, we used the dilution method to reduce background bioluminescence signal and recommend dilution for preparing large phage libraries. While the dilution method reduced the signal, it did not eliminate the signal and so the background bioluminescence signal due to residual ATP was deducted from the data for better visualization of the signal resulting from phage-induced ATP release.

For end point detection of phage lysis, each phage was mixed with a culture of host bacteria at physiological temperature. Aliquots were collected periodically and added to ATP assay reagents in a stagewise manner at room temperature, before measuring the bioluminescence signal **(Figure 2A)**. Exponentially growing bacteria were infected with phage at MOIs of 10, 1, 0.1, 0.01, 0.001. **Figures 2B-F** show ATP release as a result of phage-mediated lysis, measured over a 3-hr period. At MOI~10, bioluminescence signal was detected within 30 mins after the addition of P32 or JG004 to the bacterial culture (**Figure 2B**). At lower MOIs (lower phage to bacterial cell ratio), bioluminescence signal became detectable at later time

points. The phage with the weakest lytic activity, PP7, showed significant bioluminescence signal only at MOI=10 and after 60 to 120 mins, while at lower MOIs, the signal was not significantly different from the control, uninfected Pa, demonstrating the ability of the assay in endpoint format at physiological temperature to differentiate strong and week lytic activity. Another trend to note is that for P32 and JG004 phages at MOIs of 0.01 and 0.001 (**Figure 2E, F**), the signal intensity at the end of 3 hrs was visibly higher than the same timepoint at MOI=10. This can be explained by the lower number of phages at the beginning of infection, which provides enough times for bacterial cells to grow and increase their population, leading to higher bacterial concentration which can be infected and release ATP at later timepoints. **Figure 2G** clearly shows the overall trend that the minimum time to detect a signal that is significantly higher than the control decreased with increase of phage to bacteria ratio or MOI.

Another noteworthy trend and one that is of high significance for real-life application of phage is that even at very low phage to bacteria ratio of 1:1000 (MOI=0.001), signal intensity from phage infected samples is significantly different from uninfected samples 2 hrs post-infection (**Figure 2F**). This shows the ability of the ATP detection biochemistry to discriminate between phage-mediated lysis and bacterial autolysis at very low phage to bacterial cell ratios. It is important to keep in mind that the concentration of phages curated in libraries is quantified in terms of plaque forming units, which reflects the number of infective particles capable of infecting the known host bacteria used to propagate the library phages at the stage of making the library. When screening for therapeutic phages against an unknown strain of bacteria (*e.g.*, a multidrug resistant clinical or environmental isolate), the number of infective particles against this unknown strain may be orders of magnitude lower than the original host strain, a concept known as efficiency of plaquing.[26] Therefore, demonstrating that any susceptibility profiling technique works at low MOI and thus low efficacy of plaquing, is critical for real-life applications.

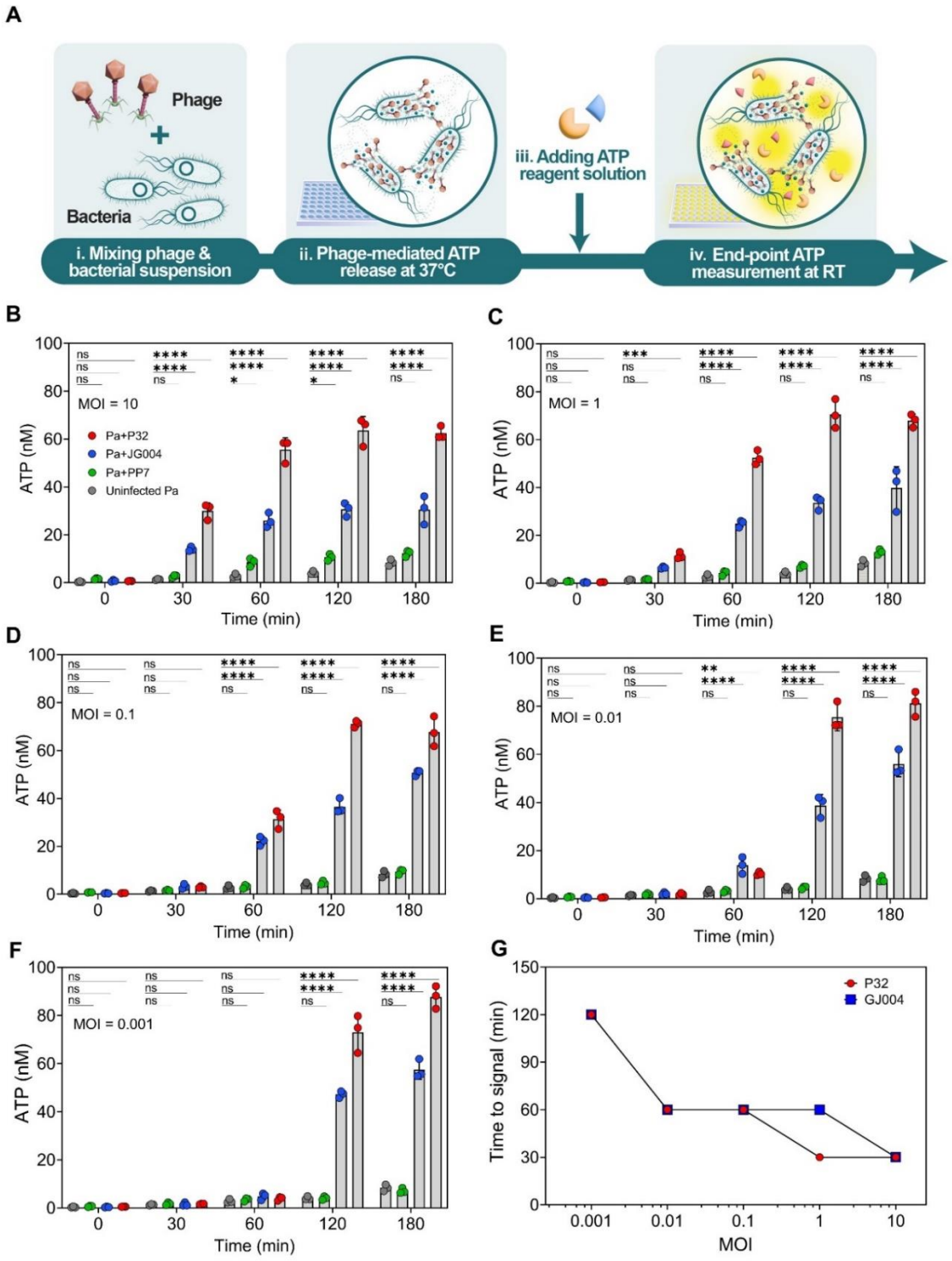

Figure 2. (A) Workflow schematic. Bacterial cultures were infected with phage at different concentration (i) and incubated at 37ºC (ii), at different time intervals, ATP was measured at room temperature by adding ATP reagent solution which contains luciferin and luciferase as main components (iii), and bioluminescence signal was measured (iv). Concentration of ATP was calculated for bioluminescence signal measured from Pa infected with P32,

JG004, and PP7 at different MOIs: **(B)** MOI = 10, **(C)** MOI = 1, **(D)** MOI = 0.1, **(E)** MOI = 0.01, **(F)** MOI = 0.001. All reported values are the mean of three biological replicates and associated error bars represent standard deviation from the mean. Significance levels include *$P < 0.05$, **$P < 0.01$, ***$P < 0.001$, and ****$P < 0.0001$.

3.3.3 One-pot biochemistry for detection of phage lytic activity

End-point detection of phage-mediated bacteria lysis involves periodic sampling of bacterial cultures, mixing with ATP reagents at room temperature, before measuring the bioluminescence signal. This technique is time-consuming and laborious, making it incompatible for high throughput screening applications. A one-pot format in which assay reagents are mixed with bacterial cultures at the start of phage infection cycle (**Figure 3A-i**) is therefore a more desirable and practical approach when designing a high throughput screening technology. **Figure 3A-ii** shows the bioluminescence kinetic curve for cultures infected with P32 and JG003 at MOI=10 in a one-pot format. Notably, a detectable signal appears ~30 mins post infection and peaks at 60 mins. Thereafter, the signal decays quickly until it becomes undetectable ~ 4 hrs post-infection. Signal detected from cultures infected with PP7, known to have weak lytic activity, was indistinguishable from uninfected cultures (**Figure 3A-ii**). The major shortcoming of the one-pot biochemistry of ATP detection, however, was that the bioluminescence signal produced under these conditions started to decay after 1 hr (**Figure 3A-ii**). The signal decay is a result of thermal inactivation of luciferin and luciferase at 37ºC, which can decrease assay fidelity, resulting in false negatives.

Despite the heat deactivation of luciferase, our data show that the one-pot format not only discriminates between uninfected and infected cultures but can also differentiate between strong (P32), moderate (JG004), and weak (PP7) lytic activity of different phages even at lower concentration of phage (lower MOIs) (**Figure 3B**). This capability to resolve lytic activity makes our method as powerful as the gold standard plaque assay, which has remained unchallenged for over a century, while offering the obvious advantage of being amenable to high throughout format. A re-examination of **Figure 1C (ii, iv, and vi)** shows that the plaque morphology for each phage, which shows the combined effect of phage burst size and latent period and is thus a good indicator (although not the only indicator) for phage biocontrol efficacy, agrees with the trends observed in **Figure 3A-ii and B**.

Latent periods and burst size of phages are two of the phage characteristics which are commonly used to evaluate the phage virulency.[27] P32 is reported to have a 20-minute latent period and a burst size of 210 progeny phages on *P. aeruginosa*. [15] JG004 is reported to have a 31-minute latent period and a burst size of 13 progeny phages *P. aeruginosa*. [16] Latent period and burst size numbers may vary depending on host bacterial strain, stage of bacterial growth, and nutrient source; however, the general trend should hold. **Figure 3A-ii** shows 25-30 mins are required from the time of phage addition to the time to detect bioluminescence signal, which matches closely with the latent period of P32 and JG004.[20] As seen in **Figure 3A-ii**, the time to peak signal decreases as concentration of phage increases (higher MOIs) as expected. Additionally, the phage burst size appears to correlate with the intensity of peak signal, with P32 generating a stronger peak signal as compared to JG004 **(Figure 3A-ii)**. Taken altogether, these findings confirm the feasibility of the one-pot chemistry for the detection of phage-mediated cell lysis and thus showing promise to form the basis of a high throughput susceptibility profiling technology.

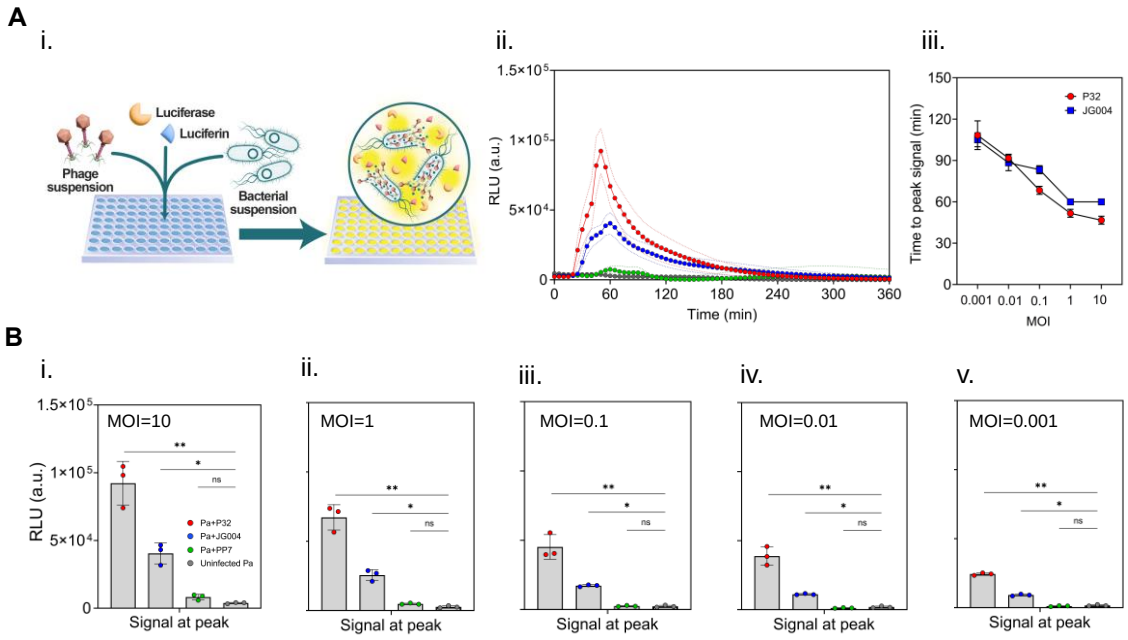

Figure 3. **(A)** One-pot ATP bioluminescence assay. Workflow schematic (i) which includes adding all ATP bioluminescence assay reagents (luciferin and luciferin as major components) and phage, followed by adding bacterial suspension and incubating the plate at 37ºC for real-time measurement of phage-induced ATP release. Kinetic ATP measurement for Pa infected with P32, JG004, and PP7 at MOI = 10 and uninfected Pa (ii). Time to peak signal for P32 and JG004 at different MOIs (iii) **(B)** Signal at peak for Pa

cultures infected with P32, JG004, and PP7 at different MOIs including (i) MOI=10, (ii) MOI=1, (iii) MOI=0.1, (iv) MOI=0.01, (v) MOI=0.001. All reported values are the mean of three biological replicates.

3.3.4 Optimizing detection of phage-mediated lysis in a stabilizing sugar polymer matrix

The next step towards a reliable susceptibility assay was to address the rapid enzyme deactivation at physiological temperatures. To address this challenge, we selected pullulan, based on previously reported thermo-protective effects towards biomolecules,[29,30] and trehalose based on reported desiccation protection towards viruses.[31,32] Pullulan and trehalose were added to a mixture of phage suspension and lyophilized ATP detection reagents and homogenized before the addition of bacteria (**Figure 4A**). As shown in **Figure 4D**, a discernable signal appeared 25-30 mins after all assay components were mixed with the bacterial suspension. Time to signal detection in the presence of the sugar mixture was comparable to the sugar-free mixture (**Figure 3B, C).** This confirmed that the addition of sugar polymers did not interfere with the function of assay reagents or with phage infectivity. Moreover, addition of sugars did not significantly affect the peak bioluminescence signal, whereas the signal at 6 hours post infection in cultures infected with P32 (**Figure 4B**) and JG004 (**Figure 4C**) containing pullulan-trehalose mixture was ~ 99% and 95% higher, respectively, than the negative control. In summary, addition of pullulan-trehalose to the mixture stabilized the assay signal and significantly reduced signal decay.

We further demonstrated that the sugar mixture can be dried and cast into a tablet format, encasing all the assay components into a sugar matrix **(Figure 4E)**. As shown in **Figure S4**, titer loss for phage encased in the sugar polymer matrix was less than one log for all three phages after a 30-day storage under ambient condition. In the absence of the sugar polymer matrix, phages showed weak desiccation tolerance, with PP7 being the least stable one with a 3-log reduction after being aged for 30 days, demonstrating a clear desiccation protective effect. We then evaluated the stability of all assay reagents in a dehydrated tablet form. ATP assay components were first mixed with pullulan-trehalose and then phage suspensions in a well plate and dried under nitrogen airflow. Following a week-long storage under vacuum, dried tablets were reconstituted. As shown in **Figure 4E**, the rate of rise in

bioluminescence signal from the reconstituted tablet assay was slower compared to the liquid assays. The rate of rise in signal intensity depends on the dissolution rate of the tablets in water, which in turn controls the release of phage and ATP reagents into the mixture. The slower rise of signal from the reconstituted tablet is a small trade-off for the portability, improved storage, and ease of use afforded by the solid tablet format (**Figure 4D**). Lastly, it should be noted that drying the ATP reagents and phage in the absence of sugar polymers led to complete loss of signal after the one-week storage period, as shown in **Figure 4F, G**. This clearly shows the importance of sugar polymers in preserving the phage and ATP assay components, which is particularly advantageous for ease of transportation and point-of-use accessibility of our phage screening technology, especially in remote regions.

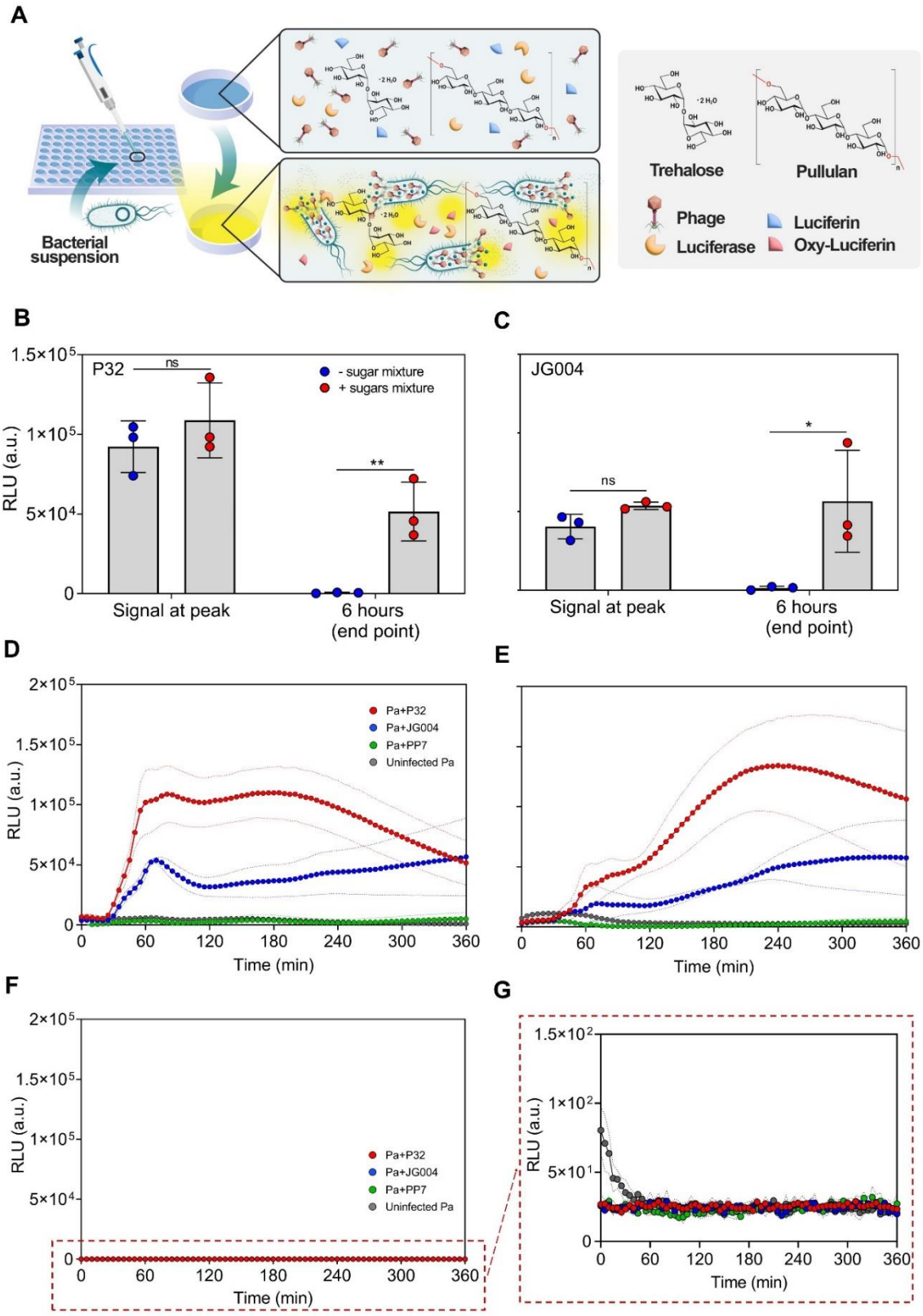

Figure 4. (A) Workflow schematic. Bacterial suspensions are added to 96 well plate containing phages mixed with ATP reagents in sugar mixture. Bioluminescence signal at

peak and assay end point of 6 hours for P32 **(B)** and JG004 **(C)** infected Pa cultures in the presence versus absence of sugar mixture in fresh liquid one-pot ATP assay. **(D)** Continuous measurement of bioluminescence signal for Pa infected with P32, JG004, and PP7 in fresh liquid sugar mix solutions. **(E)** Kinetic measurement of bioluminescence signal for Pa infected with P32, JG004, and PP7 in reconstituted one-week old tablets. **(F)** Kinetic measurement of bioluminescence signal for Pa infected with P32, JG004, and PP7 in rehydrated phage and enzymes dried in the absence of sugar polymers showing complete loss of signal after one week storage. **(G)** Same data as pert F but with a narrower y-axis scale, clearly showing the loss of signal. Error bars in B and C graphs show the statistical analysis based on unpaired t-test, associated error bars represent standard deviation from the mean. Significance levels include *P < 0.05 and **P < 0.01. Dashed line in D, E, and G show standard deviation from the mean for at least 3 replicates.

3.3.5 Screening the stabilized phage library against clinical bacterial isolates

We selected two multidrug resistant clinical isolates of *P. aeruginosa* from an in-house library of isolates from Hamilton Health Sciences. The antibiotic resistance profile for these strains is shown in **Figure S5**.[33] The two strains were given the designations C0335 and C0072 and were isolated from patients with urinary tract infection (**Figure 5B-i**) and arm wound infection (**Figure 5C-i**). We conducted susceptibility screening against our in-house phage library containing seventeen different phages using one week-old, all-inclusive tablets stored under ambient conditions. Results of the tablet-based, one-pot assay shows a significant, but slow rise in bioluminescence signal in 60 mins for C0072 infected with P32 (**Figure 5B-ii and iii**). As shown in **Figure 5C-ii**, for the clinical isolate C0335, the bioluminescence assay did not show any rise in signal with any of the phages in the library. However, a faint signal was observed for one of the phages (JG004) with a delay. Phage susceptibility was confirmed with a spot test (representative images shown in **Figure 5B-iv and C-iv**), as well as optical density (**Figure S6**), and XTT kill curves (**Figure S7**). Isolate C0072 showed an obvious clearance with P32 (**Figure 5B-iii**) but isolate C0335 did not show susceptibility to any of the phages in the library, although a very faint clearing was observed with JG004 (**Figure 5C-iii**), which may correspond to the faint signal after 180 min **(Figure S8)**. The identified phage for C0335 is clearly very weak and thus not recommended for phage therapy/biocontrol applications. We calculated the efficiency of plaquing the identified phage on C0072 to be 0.77, confirming a high production efficiency.[34] These data clearly demonstrate that aged tablets, stored under ambient conditions, could identify phages capable of infecting clinical bacterial isolates. The solid

tablet format of detection biochemistry, as well as the all-inclusive feature (detection biochemistry stabilized alongside each phage) enables point-of-use applications with minimal infrastructure and training. This highlights the compatibility of this engineered assay format for rapid screening of phage libraries against MDR isolates in clinical settings, even in remote and hard to access regions across the world.

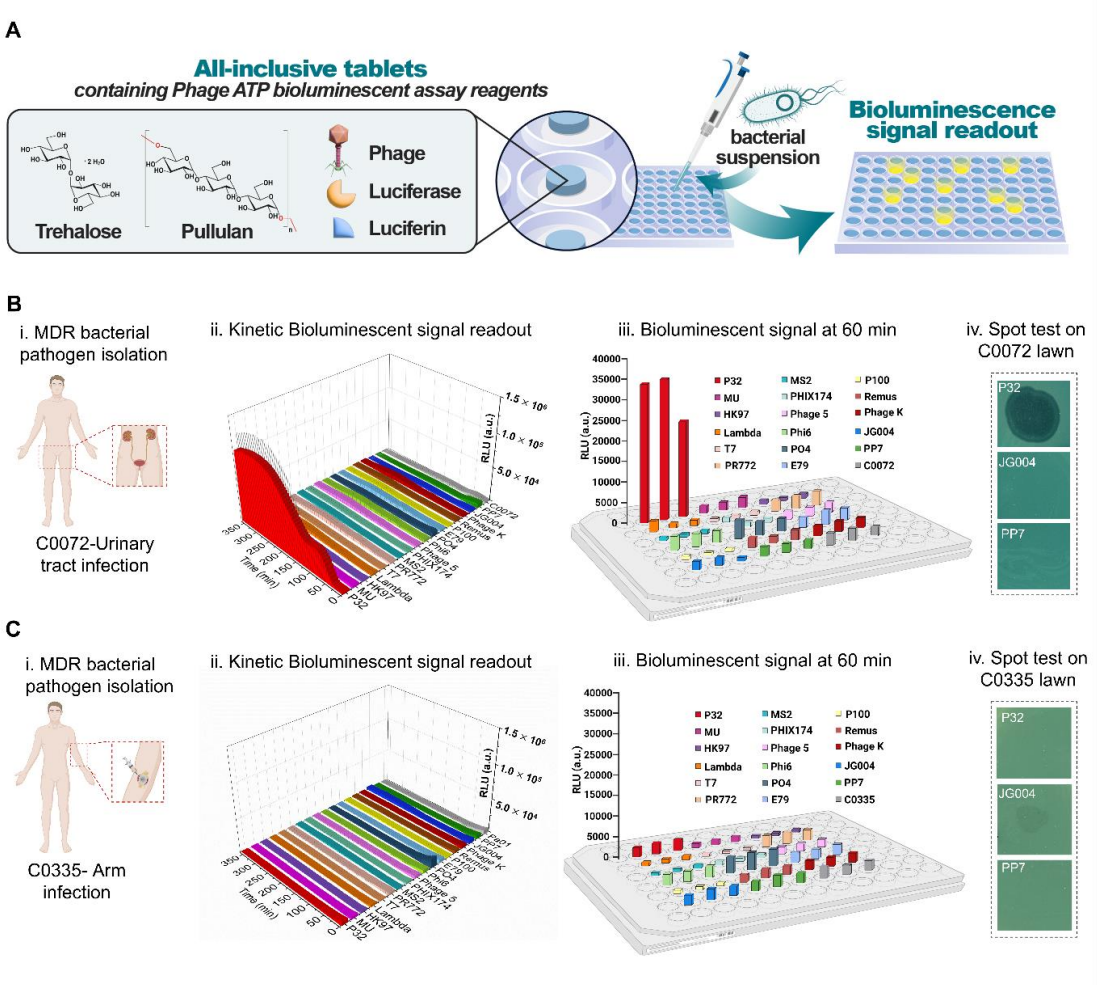

Figure 5. (A) proposed workflow for screening a bacterial isolate against a phage library using our platform technology, where the phage library is redesigned as solid, all-inclusive tablets, each containing phage along with the detection biochemistry. The microtiter plate can be stored at room temperature, or shipped to point of use and once the need arises to find phage targets for a bacterial isolate of interest, a drop of bacterial culture is added to each tablet resulting in a bioluminescence signal. (B) The urinary tract infection isolate C0335 (i) was screened against a week-old library of all-inclusive tablets. Bioluminescence signal was recorded every 5 mins (ii) and the peak signal is shown after 60 min for each well (iii), which corresponds to spot tests of representative *P. aeruginosa* phages (iv). (C) The arm infection isolate C0072 (i) was screened against a week-old library of all-inclusive tablets. Bioluminescence signal was recorded every 5 mins (ii) and the peak signal is shown

after 60 min for each well (iii), which corresponds to spot tests of representative *P. aeruginosa* phages (iv). Data points represent results for at least 3 technical replicates.

3.4 Discussion

Personalized phage therapy is the last hope for many patients suffering from infections resistant to all known antibiotics. However, access to phage therapy is challenged by the lack of a universal phage library. There have been efforts in curating phage libraries around the world, but due to the remarkable diversity in the phage world, the more realistic forecast is that we may always need to screen multiple decentralized libraries, likely curated in different parts of the world, each containing thousands of phages, to find suitable phage(s) against a resistant infection. This is challenged not only by the fact that there is not a clear library sharing mechanism and workflow (most these libraries are liquid lysates or frozen stocks), but also by the lack of rapid screening methods, which are laborious, time-consuming, with an extremely slow response time. We address both the challenges and in doing so present a path towards routine practice of personalized phage therapy worldwide. We re-imagined phage libraries not in the form of liquid lysates in a fridge, or even frozen stocks in a deep freezer, but as solid tablets packed in microtiter plates, stored on a shelf, ready for rapid high throughput screening with a plate reader when needed, or to ship around the world with a moment's notice. Each tablet contains a phage stock along with enzymes and ions needed to detect the burst of ATP release during phage-mediated bacteria lysis, all stabilized in a sugar polymer matrix that protects the enzymes against degradation at physiological temperatures needed for rapid phage susceptibility detection. The matrix also offers desiccation protection to phage and enzymes, making the tablets shelf stable and easy to store and ship around the world. In addition, the solid, all-inclusive tablet format eliminates the need for stage-wise addition of reagents, enabling high throughput screening. Our technology has obvious advantages over the status quo (culture techniques) for phage susceptibility profiling, namely a faster response time and compatibility with high throughput implementation, as well as environmental stability, eliminating the need for a cold chain or special packaging. All this makes the proposed phage susceptibility profiling technology suitable for point-of-use implementation with minimal infrastructure and training, which will be particularly impactful in remote, hard to access, and underdeveloped

regions. This addresses one of the major roadblocks for widespread practice of personalized phage therapy, which has been proven time and time again to save lives. Our technology goes beyond binary susceptibility profiling and can semi-quantitatively resolve phage ability for biocontrol. With personalized phage therapy being increasingly practiced as the last resort for treating antibiotic resistant infections, or work is a much-needed effort in developing powerful tools and technologies that address historic challenges in the field are essential to tackle the ever-rising tide of antibiotic resistance.

3.5 Materials

Pullulan (PI20 food grade, 200 kDa) from Hayashibara Co, Ltd., Okayama, Japan was kindly provided by Dr. Carlos Filipe, Department of Chemical Engineering, McMaster University. D-(+)-Trehalose dehydrate, and XTT tetrazolium sodium salt, menadione, and acetone were purchased from Sigma Aldrich. Phosphate-buffered saline (PBS) tablets were purchased from VWR (Mississauga, ON, CA). Luria Broth (LB) was purchased from Fisher Scientific (ON, CA). ATP bioluminescence Assay Kit CLS II was purchased from Millipore Sigma (Sigma-Aldrich, Oakville, ON). vB_Pae-Tbilisi32 or for short P32 and JG004 phages, and Pa strain were purchased from DSMZ (Germany), and PP7 phage from Université Laval (QC, Canada). Two clinical strains including C0072, isolated from patients with urinary tract infections, and C0335, isolated from arm infection site, were obtained from IIDR database at McMaster University. Antibiotic resistance profile for C0335 includes ampicillin, amoxicillin clavulanic acid, cefazolin, cephalothin, cefixime, nitrofurantoin, tetracycline, trimethoprim sulfamethoxazole, cefoxitin, ceftriaxone, and for C0072 includes ampicillin, amoxicillin clavulanic acid, cefazolin, cephalothin, cefixime, nitrofurantoin, tetracycline, trimethoprim sulfamethoxazole, cefoxitin, ceftriaxone.[33]

3.6 Methods

3.6.1 Bacterial culture and phage propagation

Pa was stored at -80°C in 25% v/v glycerol. Overnight bacterial cultures were prepared by inoculating 3 mL of LB media with Pa glycerol stock. The inoculated media was incubated

at 37°C and 180 rpm for 16-18 hours to promote bacterial growth. Overnight cultures were subsequently diluted 1:100 in 50 mL of fresh LB media and incubated for 2-3 hours to allow bacterial cells to reach the mid-exponential growth phase. 10 µL of phage was introduced to bacterial cells at mid-exponential phase and the cultures were incubated for a further 6 hours to allow for phage lysis of bacterial cells. The lysate was centrifuged for 20 min at 7000 rcf, and the supernatant was sterilized using a 0.2-µm-pore-sized filters and stored at 4°C. Phage concentration (number of plaque forming units per milliliter, PFU/mL) was determined using the overlay technique.[35] Phage stock was serially diluted in LB media and plated on bacterial lawns to enumerate the number of infectious virions present in the stock. All phages used in this paper were sterile filtered unless otherwise stated.

3.6.1.1 Efficiency of plating (EOP).

Efficiency of plating measures the titer of phage infecting a non-host bacterial strain. Phage overlay assay was conducted in triplicates to obtain the PFUs on the test strain (C0072) and the host strain (Pa). EOP was calculated using the following formula.[34]

$$\text{EOP} : \frac{\text{Average PFU on the test strain}}{\text{Average PFU on the host bacterium (Pa)}}$$

Infection efficiency:

EOP $\geq$ 0.5 (high production efficiency)

0.1$\leq$ EOP <0.5 (moderate production efficiency)

0.001< EOP <0.1 (Low production efficiency)

EOP $\leq$ 0.001 (inefficient)

3.6.1.2 Phage purification

The aqueous two-phase method was used to purify filter-sterilized phage suspension.[36] Briefly, sterile 20 (w/v)% Poly(ethylene glycol) containing 2.5 M NaCl solution was added to the phage stock suspension at a ratio of 1:6 v/v followed by overnight incubation at 4ºC. Phages in suspension was pelleted by centrifugation at 5000 rcf for 45 minutes and resuspended in 10 mL of RO Millipore water and subjected to mild agitation at 4ºC for at least 2 hours. PEG purified samples went through further purification using Amicon Ultra centrifugal filters (Millipore Sigma, Ultra-15, MWCO 10 KDa, and 3 KDa). ATP

background signal was measured at different stages of purification and compared with starting phage suspension to monitor the change in background signal. For all liquid phage infection assays, the initial titer of each phage was determined using the double agar layer method by three independent experiments.

3.6.2 XTT metabolic assay

XTT assay is commonly used to measure metabolic activity of cells using a tetrazolium salt which is a formazan compound in the presence of metabolically active cells followed by a detectable change of color. Assays were conducted in clear, flat-bottom, 96-well plates with total volume of 100 µL in each well. 12 µL of phage suspensions (~10^9-10^5 PFU/mL) were mixed with 38 µL bacteria at OD_{600} ~ 0.1 and added to wells at the final multiplicity of infection (MOI) of 10, 1, 0.1, 0.01, and 0.001 which indicates the ratio of phage to bacterial cells. XTT solution was prepared in LB media to contain 0.2 mg/mL of XTT and 0.1 mM menadione. 50 µL of the XTT solution was added to all wells, followed by the addition of 50 µL of LB media as negative control, 12 µL media with 38 µL bacterial suspension as positive control, and 12 µL phage with 38 µL bacterial suspension as phage-infected sample. Absorbance was measured at 490 nm wavelength every 5 minutes for at least16 hours using Synergy Neo2 BioTek plate reader set to 37ºC. The absorbance value from wells containing XTT solution with LB media was subtracted from bacteria-containing wells.

3.6.3 Optical density assay (OD_{600})

Overnight culture was added to fresh LB media at 1:100 v/v ratio and incubated until the sub-culture reached OD_{600} ~ 0.1. Assays were conducted in transparent flat bottom 96-well plate with total assay volume of 200 µL per well. 45 µL of Phage solutions (~10^9 to 10^5 PFU/mL) with 155 µL of bacteria at OD_{600} ~ 0.1 (~ 3×10^7 CFU/mL) were added to specific wells at the final multiplicity of infection (MOI) of 10, 1, 0.1, 0.01, and 0.001. Control wells contained 155 µL bacteria and 45 µL media. Absorbance was measured at 600 nm wavelength using Synergy Neo2 BioTek plate reader. Data was collected every 5 minutes for at least 16 hours at 37ºC.

3.6.4 Transmission electron microscopy (TEM)

Phages with concentration of 10^9 PFU/mL were absorbed onto plasma-cleaned carbon-coated copper grids and negatively stained with 1% uranyl acetate. Stained grids were dried at room temperature and imaged using Talos L120C transmission electron microscope at the Canadian Centre for Electron Microscopy (CCEM), McMaster University (ON, CA).

3.6.5 ATP Bioluminescence assay

ATP assay reagent solution was by reconstituting the lyophilized ATP reagent solution using bioluminescence Assay Kit CLS II (Sigma-Aldrich, Oakville, ON) based on manufacturer's instruction. For conducting ATP assay in pullulan-trehalose sugar solution, lyophilized ATP reagents of the ATP bioluminescence Assay Kit CLS II were reconstituted with the sterile sugar solution containing 10 wt% pullulan and 0.5 M trehalose, at the same liquid volume as manufacturer's instruction.

Assays were conducted in white flat bottom 96-well plate with total assay volume of 100 µL per well. Bioluminescence signal was detected from wells containing 50 µL of ATP reagent solution mixed with 50 µL of the sample (phage infected or uninfected bacterial suspension). 12 µL of phage suspensions with ~10^9 to 10^5 PFU/mL and 38 µL of bacteria at OD_{600} ~ 0.1 (~ 3×10^7 CFU/mL) was used for obtaining MOIs of 10, 1, 0.1, 0.01. 0.001. For end-point ATP bioluminescent assay, the ATP reagent solutions have been added at the end point to samples and the signal was measured at room temperature. The RLU signal was measured at times 0, 30-, 60-, 120-, and 180-minutes using Synergy Neo2 BioTek plate reader. The ATP standard curves were prepared per manufacturer's instruction to calculate the ATP amounts.

For one-pot ATP bioluminescent assay, 50 µL of ATP reagent solution was added to specified wells, followed by 12 µL of phage suspensions at different concentrations (10^9-10^5 PFU/mL) and 38 µL bacterial sub-cultures at OD_{600}=0.1 respectively, to obtain specific MOIs (10, 1, 0.1, 0.01, 0.001) within 100 µL assay volume. The plate containing ATP assay reagent solution, phage-infected and uninfected bacterial cultures was incubated inside Synergy Neo2 BioTek plate reader at 37ºC and the RLU signal was recorded every 5 minutes in stationary state without any shaking to prevent damaging the sensitive ATP

assay enzymes. Wells with uninfected bacterial suspensions, and wells containing phage only were used as controls. The RLU values from phage-only wells were used to normalize the data.

3.6.6 Stabilization in sugar polymer matrices

Sugar solutions containing 10 wt% pullulan and 0.5 M trehalose was dissolved in milli-Q water and autoclaved to sterilize.

3.6.6.1 Phage stability

Phage suspensions were diluted in sugar solution to achieve a concentration of 10^9 PFU/mL, and 100 μL of the phage suspension was added to 24-well plates and air-dried. Stability of phages incorporated within dried pullulan-trehalose matrix was tested. Phage titer was calculated 1-, 7-, and 30-days after storage at room temperature using the plaque overlay assay method.

3.6.6.2 All-inclusive dried tablet-based ATP assay

To stabilize the ATP reagents and the phage particles in a dried format, the plate containing phages (15 μL of 10^9 PFU/mL) and ATP reagent solution (50 μL) in sugars solution was added to specified wells. The plate was dried under nitrogen flow in a glove bag for at least 4 hours, followed by storage under vacuum at −0.08 MPa. The Stability of dried tablets containing ATP reagent solution and different phages in 96 well-plate was assessed after one week storage at room temperature. For conducting the assay, the dried tablet containing the ATP reagents and phage particles embedded in sugar polymer matrix were rehydrated using 50 μL of sterile milli-Q water, followed by addition of 50 μL bacteria sub-culture at OD_{600} = 0.1 (~ 3×10^7 CFU/mL), and reading the signal every 5 minutes at 37ºC. As a control, a plate containing phages and ATP reagent solution was prepared without addition of sugar polymers, and dried/stored under same conditions. The plate was rehydrated and tested following the same process used for assessing the phage-ATP reagent solution encased in sugar matrices.

3.7 References

1. Soleymani, L. *et al.* Hierarchical nanotextured microelectrodes overcome the molecular transport barrier to achieve rapid, direct bacterial detection. *ACS Nano* **5**, 3360–3366 (2011).
2. Wang, F. *et al.* Bioinspired micro/nano fabrication on dental implant-bone interface. *Appl. Surf. Sci.* **265**, 480–488 (2013).
3. Zhao, X. *et al.* Hierarchically engineered membrane surfaces with superior antifouling and self-cleaning properties. *J. Memb. Sci.* **441**, 93–101 (2013).
4. Zhu, Y., Zhang, Q., Shi, X. & Han, D. Hierarchical Hydrogel Composite Interfaces with Robust Mechanical Properties for Biomedical Applications. *Adv. Mater.* **31**, 1–5 (2019).
5. Peivandi, A., Tian, L., Mahabir, R. & Hosseinidoust, Z. Hierarchically Structured, Self-Healing, Fluorescent, Bioactive Hydrogels with Self-Organizing Bundles of Phage Nanofilaments. *Chem. Mater.* **31**, 5442–5449 (2019).
6. Pan, L. *et al.* Hierarchical nanostructured conducting polymer hydrogel with high electrochemical activity. *Proc. Natl. Acad. Sci. U. S. A.* **109**, 9287–9292 (2012).
7. Liu, K. *et al.* Coordination-triggered hierarchical folate/zinc supramolecular hydrogels leading to printable biomaterials. *ACS Appl. Mater. Interfaces* **10**, 4530–4539 (2018).
8. Sagbas, S. & Sahiner, N. Modifiable natural gum based microgel capsules as sustainable drug delivery systems. *Carbohydr. Polym.* **200**, 128–136 (2018).
9. Lv, C. *et al.* Humidity-responsive actuation of programmable hydrogel microstructures based on 3D printing. *Sensors Actuators, B Chem.* **259**, 736–744 (2018).
10. De France, K. J. *et al.* 2.5D Hierarchical Structuring of Nanocomposite Hydrogel Films Containing Cellulose Nanocrystals. *ACS Appl. Mater. Interfaces* **11**, 6325–6335 (2019).
11. Ma, X. *et al.* A Biocompatible and Biodegradable Protein Hydrogel with Green and Red Autofluorescence: Preparation, Characterization and in Vivo Biodegradation Tracking and Modeling. *Sci. Rep.* **6**, 1–12 (2016).
12. Peivandi, A. *et al.* Inducing Microscale Structural Order in Phage Nanofilament Hydrogels with Globular Proteins. *ACS Biomater. Sci. Eng.* In press (2021).
13. Levalley, P. J. *et al.* Fabrication of Functional Biomaterial Microstructures by in Situ Photopolymerization and Photodegradation. *ACS Biomater. Sci. Eng.* **4**, 3078–3087 (2018).
14. Liu, J., Gao, D., Li, H. F. & Lin, J. M. Controlled photopolymerization of hydrogel microstructures inside microchannels for bioassays. *Lab Chip* **9**, 1301–1305 (2009).
15. Franzesi, G. T., Ni, B., Ling, Y. & Khademhosseini, A. A controlled-release strategy for the generation of cross-linked hydrogel microstructures. *J. Am. Chem. Soc.* **128**, 15064–15065 (2006).
16. Kim, D. N., Lee, W. & Koh, W. G. Micropatterning of proteins on the surface of three-dimensional poly(ethylene glycol) hydrogel microstructures. *Anal. Chim. Acta* **609**, 59–65 (2008).
17. Widawski, G. & Rawiso, M. Self-organized honeycomb morphology of star-polymer polystyrene films. *Nature* **369**, 387–389 (1994).

18. Zhu, C., Tian, L., Liao, J., Zhang, X. & Gu, Z. Fabrication of Bioinspired Hierarchical Functional Structures by Using Honeycomb Films as Templates. *Adv. Funct. Mater.* **28**, 1–8 (2018).
19. Kyoung, J. & Basavaraja, K. C. Preparation and characterization of smart hydrogel nanocomposites sensitive to oxidation – reduction. *Polym. Bull.* **70**, 207–220 (2013).
20. Online, V. A., Jang, J. H., Orba, M., Wang, S. & Huh, D. S. Adsorption–desorption oscillations of nanoparticles on a honeycomb-patterned pH-responsive hydrogel surface in a closed reaction system. *Phys. Chem. Chem. Phys.* **16**, 25296–25305 (2014).
21. Bronze-Uhle, E. S., Costa, B. C., Ximenes, V. F. & Lisboa-Filho, P. N. Synthetic nanoparticles of bovine serum albumin with entrapped salicylic acid. *Nanotechnol. Sci. Appl.* **10**, 11–21 (2017).
22. Caraceni, P., Tufoni, M. & Bonavita, M. E. Clinical use of albumin. *Blood Transfus.* **11**, s18 (2013).
23. Guruvenket, S., Rao, G. M., Komath, M. & Raichur, A. M. Plasma surface modification of polystyrene and polyethylene. *Appl. Surf. Sci.* **236**, 278–284 (2004).
24. Chan, Y. *et al.* Solution-processed wrinkled electrodes enable the development of stretchable electrochemical biosensors. *Analyst* **144**, 172–179 (2019).
25. Keskin, D., Mergel, O., Van Der Mei, H. C., Busscher, H. J. & Van Rijn, P. Inhibiting Bacterial Adhesion by Mechanically Modulated Microgel Coatings. *Biomacromolecules* **20**, 243–253 (2019).
26. Shanks, R. M. Q. *et al.* Genetic evidence for an alternative citrate-dependent biofilm formation pathway in Staphylococcus aureus that is dependent on fibronectin binding proteins and the grars two-component regulatory system. *Infect. Immun.* **76**, 2469–2477 (2008).

3.8 Supplementary Information

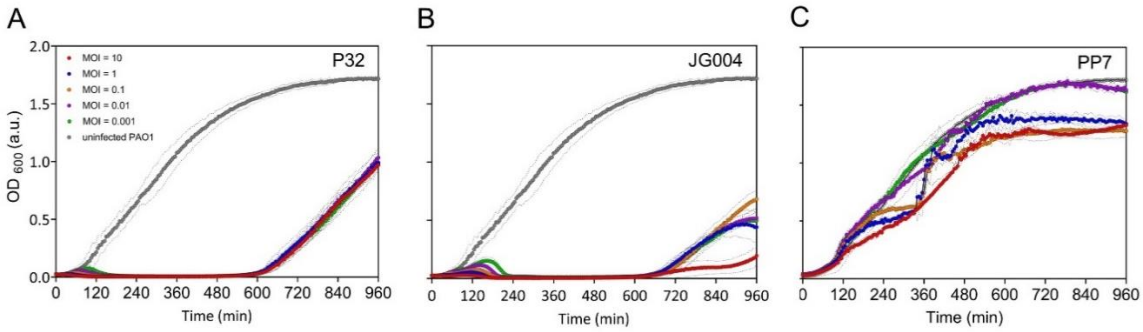

Figure S1. Optical density (OD_{600}) or growth curve of PAO1 infected with P32 (**A**), JG004 (**B**), and PP7 (**C**). P32 shows a strong performance in preventing bacterial growth by decreasing the culture turbidity even at lower MOIs (0.001). JG004 was also able to suppress the bacterial growth effectively, while PP7 shows week performance which aggravates by decreasing the initial concentration of phage (lower MOIs).

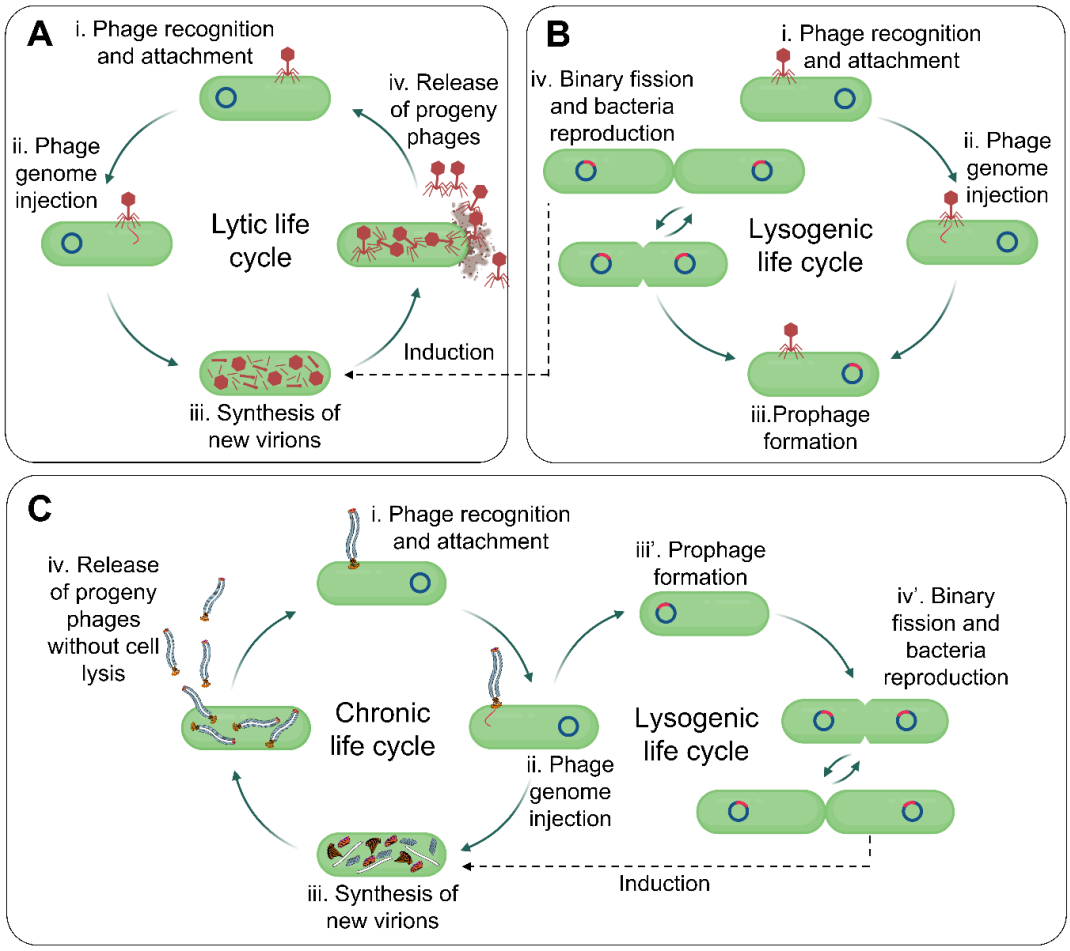

Figure S2. Schematics of Phage life cycles. **(A)** Lytic life cycle of phage starts with (i) phage recognition and attachment to bacterial cell receptors, (ii) genome insertion, (iii) taking control of bacterial replication machinery and producing new virions, and (iv) release of progeny phages by bacterial cell lysis. **(B)** In lysogenic life cycle, phage is adsorbed to cell receptors (i) and inserts its genome inside bacterial cell (ii); however, the phage genome is incorporated into the bacterial genome, forming a prophage (iii) that is replicated through the bacterial reproduction cycle (iv). The lysogenic cycle could be induced to start the lytic cycle with environmental triggers such as high temperature and UV exposure which can ultimately lead to cell lysis (as shown by the dashed arrow). **(C)** Similar to other phage life cycles, the chronic lifestyle (mostly seen in filamentous phages) starts with recognition and adsorption to bacterial cell receptors (i) and genome insertion (ii). By taking control of bacterial replication machinery, new virions are synthesized inside the bacterial cell (iii) and are released through budding or extrusion without lysing bacterial cells (iv). Similar to tailed phages, some chronic phages can also adopt a lysogenic lifestyle, in which the phage genome is incorporated into the bacterial genome forming a prophage (iii′) and is replicated through the bacterial reproduction cycle and staying dormant (iv′) until the chronic cycle is induced by environmental stimuli (shown by the dashed arrow).

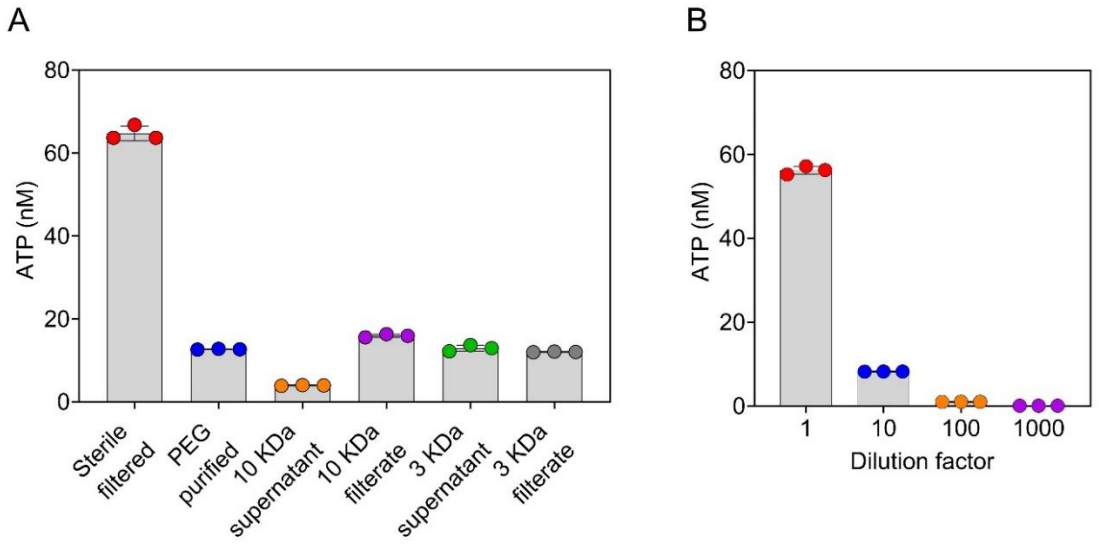

Figure S3. ATP background in phage solutions at different stages of purification (A) and after dilution in cell media (B). The effect of diluting phage samples is comparable to purifying phage suspensions. Depending on the availability, either diluted sterile filtered phages in cell media/buffer or purified phages can be used to reduce the effect of the background bioluminescence signal intensity.

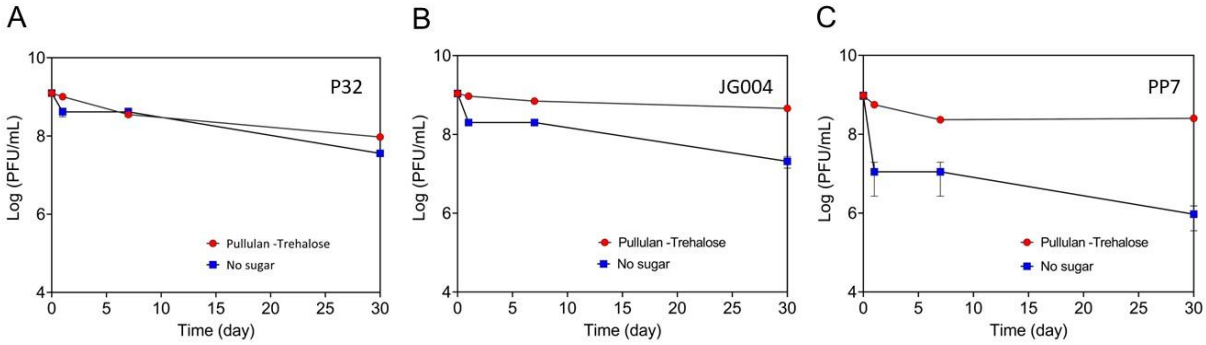

Figure S4. Stability of dried *Pseudomonas* phages **A**) P32, **B**) JG004, **C**) PP7 in ambient conditions in 10 wt% pullulan + 0.5 M trehalose in comparison with no sugars. Sugar polymers helped to retain higher infectivity after 30 days.

Strain	Antibiotic resistance profile	Source (body location)
C0072	ampicillin, amoxicillin clavulanic acid, cefazolin, cefalotin, cefixime, nitrofuratoin, tetracycline, trimethoprim sulfamethoxazole, cefoxitin, ceftriaxone	urine
C0335	ampicillin, amoxicillin clavulanic acid, cefazolin, cefalotin, cefixime, nitrofuratoin, tetracycline, trimethoprim sulfamethoxazole, cefoxitin, ceftriaxone	Arm

Figure S5. Antibiotic resistance profile of the clinical isolates C0072 and C00335, isolated form patients with urinary tract and arm infections, respectively.[1]

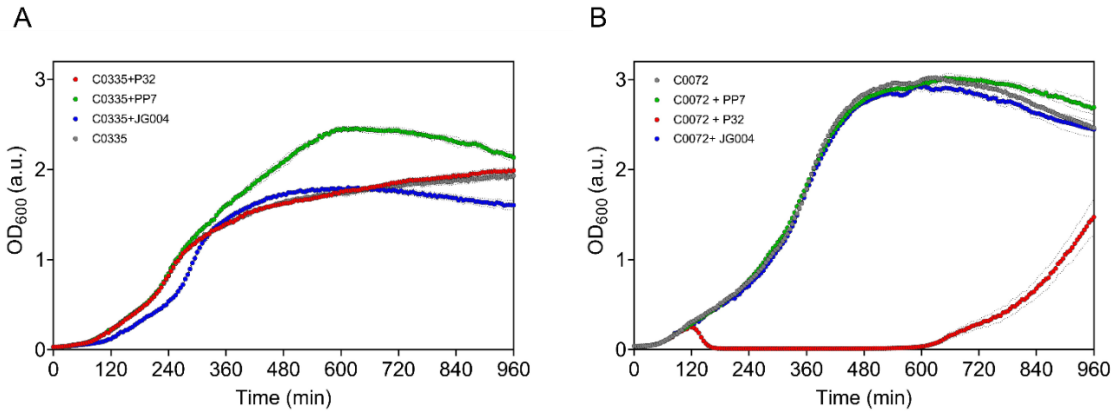

Figure S6. Optical density assay of C0335 (**A**) and C0072 (**B**) infected with P32, JG004, and PP7 at MOI ~ 10 compared to uninfected strains. None of the phages infect C0335, while C0072 is infected with P32 as turbidity of the culture decreases compared to uninfected C0072.

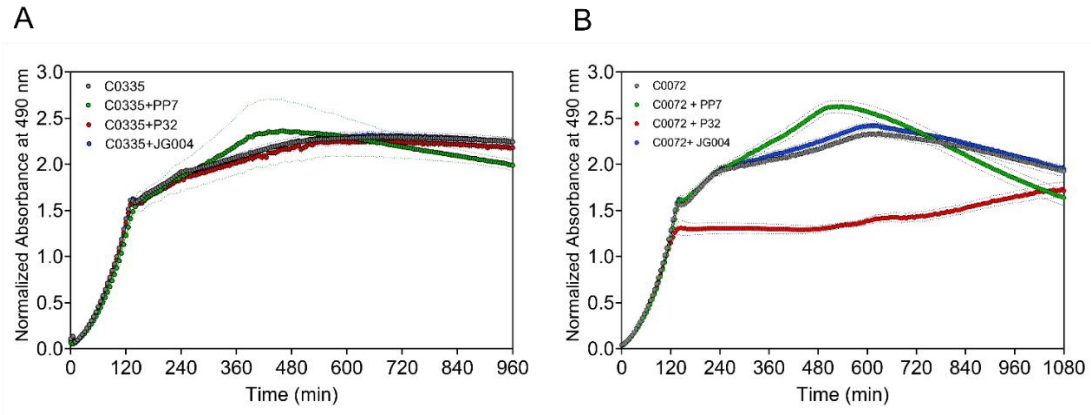

Figure S7. Metabolic activity measurement of phage infected and uninfected C0335 (**A**) and C0072 (**B**) at MOI ~ 10. Metabolic activity of phage infected C0335 shows no significant changes compared to uninfected cultures, while metabolic activity of C0072 decrease after 2 hours for C0072 infected with P32.

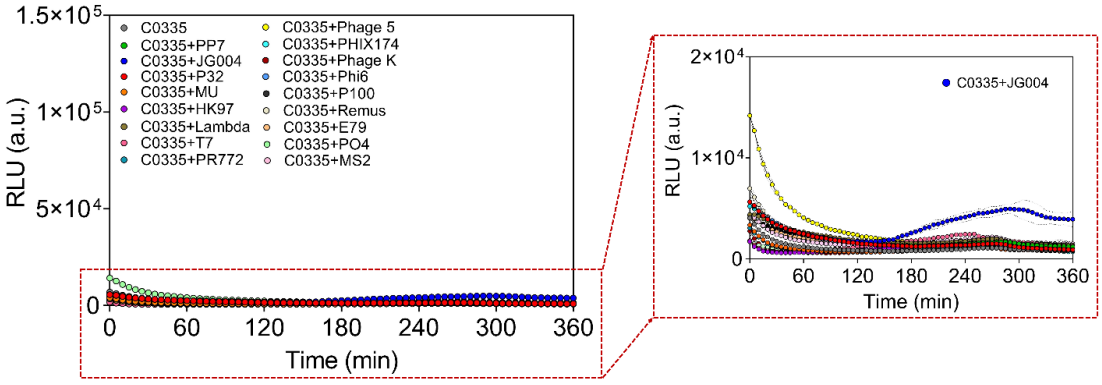

Figure S8. Zoomed in image of the phage library screening, showing a delayed increase in bioluminescence signal for C0035 infected with JG004 appearing after 2 hours.

Chapter 4: Phage-loaded Injectable hydrogel for treating bone and implant associated infection

Preface: In this chapter, we report a phage loaded injectable hydrogel based on physical crosslinking of laponite nanoclay (silicate-based nano discs) and carboxy methyl cellulose (CMC) for treating bone and implant associated infections. The hydrogel showed compatibility with phage infectivity and enhanced the production of Alkaline phosphatase (ALP) enzyme, which is an osteogenic biomarker, providing an antibacterial hydrogel suitable for bone healing and osteointegration of orthopedic implants.

Contribution: I conceptualized the project, conducted experiments, analyzed the data, and prepared the original draft under supervision of Dr. Tohid Didar and Dr. Zeinab Hosseinidoust. Sara Rahmani conducted *in vitro* mammalian cell culture and cytotoxicity assay. I conducted ALP assays. Lei Tian performed DLS and zeta potential analysis. Mathura Thirugnanasampanthar provided optimized XTT assay protocol and prepared the assay reagent solution. Fiorelle Aguilar contributed to phage propagation and purification. Martin Villegas developed Animal Utilization Protocol (AUP) and will contribute directly to animal studies in the next step. The SEM and TEM imaging was conducted at Canadian Centre for Electron Microscopy (CCEM), McMaster university. Chris Butcher and Carmen Andrei helped with SEM and TEM imaging, respectively.

Citation: This work is in preparation for submission.

Phage-loaded Injectable hydrogel for treating bone and implant associated infection, **Fereshteh Bayat**, Martin Villegas, Sara Rahmani, Lei Tian, Mathura Thirugnanasampanthar, Fiorelle Aguilar, Zeinab Hosseinidoust, Tohid F. Didar, Manuscript in preparation for submission.

4.1. Abstract

Injectable hydrogels loaded with antibacterial agents offer a minimally invasive approach for tackling recurrent bone and implant-associated infections. Pseudomonas aeruginosa (P. aeruginosa), a prominent Gram-negative multi-drug resistant (MDR) bacterial pathogen, plays a significant role in refractory bacterial infections related to bone diseases. Bacteriophages, commonly known as phages, are natural bactericidal agents that have demonstrated successful outcomes in the treatment of various bone-related infections, including osteomyelitis. This study introduces a shear-thinning injectable hydrogel loaded with phages, composed of laponite nanoclay and carboxymethyl cellulose (CMC), designed for the treatment of bone and implant-associated infections. The laponite and CMC interact through hydrogen bonding and electrostatic interactions, forming biocompatible shear-thinning physically crosslinked hydrogels. To enhance the bactericidal effectiveness of phage therapy, we have selected a binary cocktail of P. aeruginosa phages. These phage-loaded hydrogels have demonstrated exceptional antibacterial performance in both in vitro biofilm prevention and biofilm dispersion assays. Metabolic activity assays and bacterial load assessments (CFU counts) have revealed a highly effective inhibition of bacterial growth. This was evidenced by a remarkable reduction in bacterial cell activity by more than 99% and a substantial decrease in bacterial load of at least 5 logarithmic units in the in vitro setting. Moreover, the laponite-cellulose hydrogel loaded with phages exhibited not only effective antibacterial performance driven by phage activity but also an approximately 50% increase in the production of alkaline phosphatase (ALP) enzyme, a key early biomarker for osteogenic differentiation, in SaOS-2 cell line.

Keywords: Injectable, AMR, Phage, Bone, Implant, Bacterial infection, osteomyelitis

4.2. Introduction

Difficult to treat bone infections, also known as osteomyelitis, can develop in non-injured bone (e.g., septic arthritis), fractured bone, diabetic foot, and implanted devices such as peri-prosthetic joint infection.[1] Despite proper medical and surgical procedures in place for osteomyelitis treatment, the rate of infection relapse is around 20-30%, resulting in elevated mortality and morbidity rates, as well as a substantial economic burden on healthcare systems.[2] Furthermore, as the prevalence of antibiotic resistance escalates among both Gram-positive and Gram-negative pathogenic bacteria, the management of bone and implant-related infections is evolving into a significant global challenge.[3,4] *Staphylococcus aureus* and *Pseudomonas aeruginosa* are the most common gram positive and gram negative bacterial pathogens causing orthopedic infection.[1,5]

Bacteriophages, or phages for short, are bacterial viruses which have been around as antibacterial agents to treat bacterial infections for almost 100 years. With increased prevalence of chronic bacterial infections due to spread of antimicrobial resistance (AMR) as a global threat, phages have regained attention after being overshadowed for a long time by antibiotics' discovery in 1940s.[6,7] Phages can attack bacterial cells and replicate themselves on-site by taking advantage of bacterial reproduction machinery.[8] This unique self-dosing characteristic sets phage apart from the rest of antibacterial agents as phages can be implemented as self-sustained antibacterial agents. Another intriguing aspect of bacteriophages is their specificity in attacking bacterial species down to strain levels which mitigates the damage to the human microflora as opposed to antibiotics which can affect both good and troublesome bacteria.[9] There have been several successful cases of phage therapy in treating bone-related infections including osteomyelitis, bone and joint infections, implant associated infections, and fracture-based infections.[10–13]

Bioactive injectable hydrogels, capable of passing through small size needles, are intriguing candidates for regeneration of small non-load bearing infected bone defects, and implant associated infections.[14] They can also be used as local cell-, protein- and drug-delivery systems with no to minimal surgical procedures required. Additionally, injectable hydrogels have the potential of efficiently filling the irregular tissue defects and cavities.

Injectable hydrogels can be designed to cross-link in situ or cross-link before injection with shear-thinning or shape memory properties.[14] Some of the challenges regarding on-site gelation include non-uniform hydrogel formation with the liquid precursor solution penetrating into the surrounding tissue and gelation kinetics control which is also influenced by specific physiological conditions of the treated site.[15] Physically cross-linked shear-thinning hydrogel have the potential of addressing these challenges by showing viscos flow under shear stress (shear thinning property), and recovery of the structure following the stress release.[16]

Phages can get cleared by the immune system or degrade by enzymes and proteins present in body.[17–19] Phage-loaded hydrogels present numerous advantages, such as protecting phages from harsh pH condition, enzymatic degradation, host immune cell responses, and mammalian cell infiltration.[20–23] When designing phage-loaded biomaterials, it is imperative to prioritize phage compatibility in the selection and processing of biomaterials and minimize any interference with phage infectivity.[24] Specifically with hydrogels, any harsh chemical procedure, long term exposure to high temperatures and UV light would potentially damage the phages.[25] Hydrogels seem to be ideal carrier for phage delivery, as long as the crosslinking strategy is phage friendly and does not inactivate or interfere with the phage infection process.

Nanoclays as non-toxic, biologically active, and environmentally friendly components have been extensively studied for biomedical applications. In particular, disk-shaped laponite nanoclay with $(Na^{+}_{0.7}[(Si_8Mg_{5.5}Li_{0.3})\ O_{20}(OH)_4]^{-0.7}$ formulation with 20–50 nm diameter and 1–2 nm thickness have been used as an important bioactive gel forming component in many different hydrogel.[26] These nanoparticles have dual charge distribution by having permanently negative charge on the surface and a positive charge along the edges, making them capable of forming house of card structures when dispersed in water at high enough concentration.[26] The applications of these hydrogels extends from drug delivery systems,[27–29] to bone cements and musculoskeletal injury treatment,[30,31] tissue engineering,[26] and as hemostatic biomaterials for hemorrhage control.[32] Laponite specifically can interact with polymers through hydrogen bonding, electrostatic and hydrophobic interactions to form biocompatible physically crosslinked hydrogels. Laponite has proven to be osteoinductive

in a growth factor-free manner.[33] The degradation products of nanosilicate include magnesium, orthosilicic acid and Lithium which are non-toxic as well as beneficial for bone tissue engineering.[33] Implementing laponite-based hydrogels for treating bone-associated diseases has been extensively studied due to osteogenic potential of laponite degradation products.[26,34,35] On the other hand, cellulose-based hydrogels have been widely used in skin, bone and cartilage tissue engineering applications.[36] Carboxy methyl cellulose (CMC) is commercialized and widely used cellulose ether, offering non-toxicity, biocompatibility, and biodegradability. CMC is an anionic biopolymer which has been used as an important component of biomaterials used for bone tissue regeneration.[36–40]

Here, we have developed a bi-functional phage-loaded injectable hydrogel based on physical cross-linking of CMC and laponite nano-discs for bone-infection treatment. The physically cross-linked hydrogel has shown to be biocompatible and to preserve the phage infectivity, meaning not to interfere with bactericidal effect of phage. Furthermore, when the hydrogel degrades, it promotes the bone healing process in vitro by stimulating the production of alkaline phosphatase (ALP) enzyme in bone-like SaOS-2 cell lines. Additionally, our phage-loaded hydrogels effectively reduce bacterial load and successfully disperse/prevent the *P. aeruginosa* biofilms.

4.3. Results and discussion

4.3.1 Hydrogel polymer interactions

Laponite is a two-dimensional phyllosilicate composed of stacked tetrahedral and octahedral sheets in a 2:1 ratio. A positive charge is created a the edges by a charge imbalance caused by Magnesium/lithium atoms in the octahedral layer, while the surface is negatively charged due to the presence of silicate tetrahedral[41] (**Figure 1a**). The anisotropic charge distribution on the surface and edges of laponite can result in reversible electrostatic interactions between nanoclay particles. At higher concentrations, these interactions can lead to the formation of structures commonly referred to as "house of cards". (**Figure 1b**). Due to these opposite charges, and presence of hydroxyl and silanol groups on its crystals, laponite can interact with other anionic, cationic, and neutral

polymers by electrostatic, covalent and hydrogen bonding.[42,43] Biopolymers and nanoclay can have a fairly complicated interactions, but it is well-known that electrostatic and hydrogen bonds play a significant role in these interactions due to the presence of the opposite charges on the surface and edges of the nanoclay particles and the hydroxyl groups in nanoclay and most biopolymers.[26]

To create the nanocomposite injectable hydrogel, disc-shaped Laponite solutions were formed in milli-Q water using a vortexer and then mixed vigorously with CMC stock solutions to prevent clump formation. From this point, laponite nanoclay is referred to as NC. The hydrogels were formulated at constant concentration of 1 w/v% CMC and three different laponite nanoclay concentrations of 1.5, 2, 2.5 w/v%, and the final hydrogel formulations were simply labeled as 1.5% NC, 2%NC, and 2.5%NC. Right after mixing the components, the CMC polymer chains physically cross-links with laponite nano-discs. Hydrogen bonds between silanol groups of laponite (Si-O) and hydroxyl groups (-OH) of CMC.[43,44] As previously mentioned, there are electrostatic interactions among NCs as well. CMC is also an anionic biopolymer that can electrostatically interact with positive edges of the NC. As a result, CMC can get absorbed to the surface of NC and also interact with the positive edges through both hydrogen and electrostatic bonds.[43] **Figure 1c** shows a schematic representation of NC interacting with each other and CMC polymer chains through electrostatic and hydrogen bonding, to form a physically cross-linked injectable hydrogel. The phage loaded NC-CMC injectable hydrogel can then be implemented to different types of osteomyelitis affecting non-injured bone, fractured bone, diabetic foot, and bone implant associated infections (**Figure 1d**).

The interactions between carboxymethyl cellulose (CMC) and nanoclay (NC) were investigated using dynamic light scattering (DLS) analysis. In the presence of low concentrations of NC (0.2 w/v%) with fully dispersed NC particles in Milli-Q water, varying concentrations of CMC were introduced to the solution and vigorously mixed. The DLS results, illustrated in **Figure S1**, demonstrated that the hydrodynamic size of 0.2 w/v% NC was initially 60 nm. With the addition of 0.1, 0.2, 0.3, and 0.5 w/v% CMC, the hydrodynamic size progressively increased to 137 nm, 293 nm, 632 nm, and 1370 nm, respectively. Simultaneously, the standard deviation exhibited a notable increase,

indicating the nonuniform formation of NC and CMC aggregates. Furthermore, the solutions containing 0.2 w/v% NC, 0.2 w/v% CMC, and a combination of 0.2 w/v% NC and 0.2 w/v% CMC displayed zeta potentials of -31, -28, and -50 mV, respectively (see **Figure S1**). This suggests that the mixing of CMC and NC leads to the adsorption of CMC polymer chains onto the surface of NC through hydrogen bonding. Additionally, the anionic negatively charged CMC interacts with the positively charged edges of the NC, contributing to the observed variations in zeta potential.

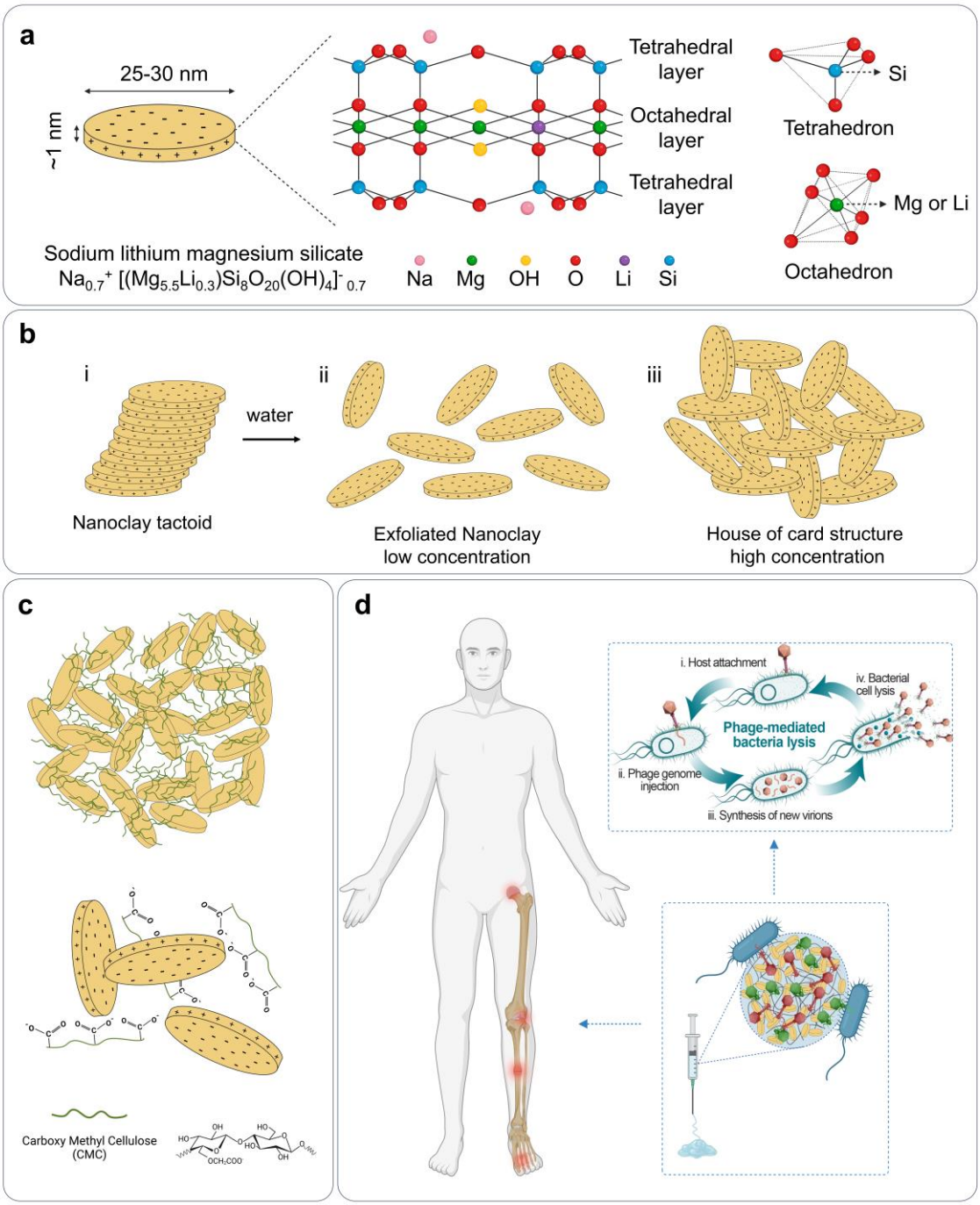

Figure 1. Molecular Structure of Laponite Nanoparticles and the Formation Mechanism of a Multifunctional Phage-Loaded Injectable Hydrogel with Antibacterial Properties. a) Molecular structure of a single Laponite nanoparticle, composed of tetrahedral and octahedral layers of lithium magnesium silicates. b) Schematic representation of the self-interaction of Laponite nanoparticles in water, leading to the formation of a "house of cards" structure at higher concentrations. c) Illustration of the interactions between Laponite and carboxymethyl cellulose (CMC), involving hydrogen bonds and electrostatic interactions.

d) The application of phage-loaded Laponite-CMC injectable hydrogels for the treatment of osteomyelitis."

4.3.2 Physical characterization of hydrogel

Free-standing injectable hydrogels were prepared by simple mixing of the NC and CMC in milli-q water, which led to instant interaction between NC and CMC due to the electrostatic and hydrogen bonding (**Figure 2a, b, d**). The hydrogels were easily injected through needles as seen in **Figure 2c** due to the reversible electrostatic and hydrogen bonds. To characterize the microstructure of the hydrogels using Scanning Electron Microscopy (SEM), samples were freeze dried (**Figure 2e**). As seen in SEM micrographs (**Figure 2f)**, the 2.5%NC hydrogel formed uniform pore size distribution with irregular pore shape. SEM images of the 1.5 and 2%NC hydrogels showed similar microstructure, with slightly larger feature sizes (**Figure S2**). Swelling test was conducted using PBS (pH 7.4) at 37°C on freeze dried samples, which showed high swelling ratios (3500-4500 g/g%) for all formulations. The dried aerogels absorbed PBS to their full capacity after 2 hours, and the amount of swelling ratio stayed constant for the rest of measurements till 24 hours. The Swelling ratio showed to be increasing by lowering the NC concentration from 2.5 to 1.5 w/v%, and there was no significant difference between 2.5%NC and 2%NC formulations (**Figure S3**). The Fourier transform infrared (FTIR) spectroscopy of laponite, CMC and NC-CMC aerogel is shown in **Figure 2g**. In the Laponite spectrum, the broad band shown at around 3427 cm^{-1} is due to –OH stretching vibration of the surface hydroxyl groups, and 1631 cm^{-1} is attributed to H-OH flexion (absorbed water).[45] The bands seen at 973 and 641 cm^{-1} of laponite spectrum can be attributed to bending and asymmetric stretching of Si–O and vibration of Mg–O bonds.[45] In the FTIR spectrum of CMC, the characteristic picks seen at 3281 cm^{-1}, 2891 cm^{-1}, 1319 cm^{-1}, and 1020 cm^{-1} are attributed to -OH, CH stretching, CH bending, C-O bonds, respectively.[46] The bonds at 1595 cm^{-1}, 1441 cm^{-1} are also indicators of symmetric and asymmetric C=O stretching vibrations of carboxylate ions, respectively. In the NC-CMC spectrum, the broadening and displacement of 3427 cm^{-1} to 3395 cm^{-1} and the displacement of the H-OH flexion pick from 1631 cm^{-1} to 1595 cm^{-1} can be attributed to intramolecular hydrogen bonding interactions between laponite and CMC.[45] Similarly, the Si-O band has been displaced from 973 to 983 $cm^{-1}$and also

broadened, along with displacement of asymmetric C=O stretching vibrations of carboxylate ions and C-O bonds, when comparing the laponite spectrum to laponite-CMC hydrogel, indicating the interactions between Si–O groups in laponite and the C-O, C=O groups in CMC.

4.3.3 Rheological Characterization of hydrogels

Quantitative measurements of viscosity and storage and loss moduli are crucial in determining the shear-thinning behavior and injectability of the hydrogel. The storage (G′) and loss (G″) moduli of a material in response to oscillatory shear measures its ability to either absorb (solid-like behavior) or dissipate the energy (liquid-like behavior), respectively. The amplitude sweep results revealed that in all hydrogel formulations, G′ exceeded G″, indicating the formation of a hydrogel network with solid-like behavior, resulting in the creation of a free-standing hydrogel (**Figure S4**). The region were G′ and G″ are independent of applied stress is called linear viscoelastic (LVE) region.[47,48]As expected, the elevation of NC concentrations resulted in an increased storage modulus. The resulting G′ were 446.47 ± 41 Pa, 573.6 ± 60 Pa, and 977.2 ± 88.4 Pa for the 1.5%, 2%, and 2.5% NC hydrogels, respectively. The G″ of the hydrogels were significantly smaller than the G′ (**Figure 2h**). A strain of 0.2%, within the linear viscoelastic (LVE) region of all hydrogels during the amplitude sweep, was selected and used for the frequency sweep test. This rheology test is used to investigate the viscoelastic properties of a hydrogel over a range of low to high frequencies to evaluate how the hydrogel respond to different rates of deformation or stress. As seen in (**Figure 2i**), across the frequency range of 0.01-100 Hz, G′ consistently exceeded G″, signifying a solid-like behavior maintained at all frequencies. This behavior suggests strong interactions between polymer chains and NC particles within the hydrogel network by maintaining its solid-like behavior (G′>G″) across low to high frequency range. As the oscillation frequency increased, both G′ and G″ showed an increase (frequency dependency), a phenomenon that has been reported to occur when there are physical entanglements within the hydrogel network.[49] This is due to the presence of a dynamic network structure formed by non-covalent interactions, such as hydrogen bonds or electrostatic forces between hydrogel components and polymer chains.

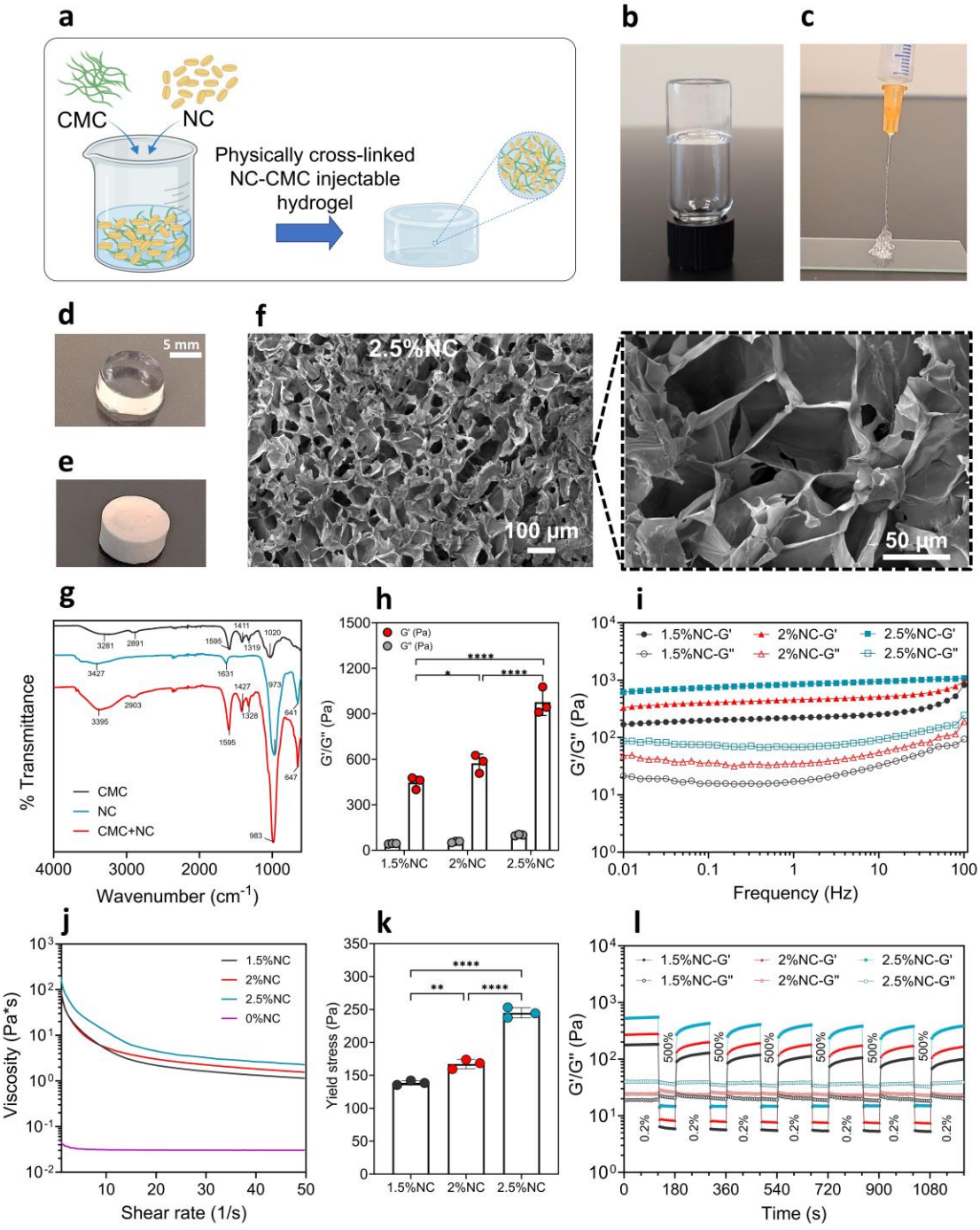

Figure 2. Physical Characterization of NC-CMC Hydrogel. a) Schematic of phage-loaded injectable hydrogel formation by mixing CMC and NC. b) Image of the physically cross-linked hydrogel. c) Injectability of the NC-CMC hydrogel. d) Free-standing hydrogel, e) Freeze dried hydrogel. f) SEM images of the 2.5%NC-CMC hydrogel. g) FTIR spectrum of CMC, NC, and NC-CMC hydrogel. h) Storage (G′) and loss (G″) moduli of NC-CMC hydrogels. i) frequency sweep in the range of 1-100 Hz at 0.2% strain at 25°C. j) Viscosity versus shear rate for 0, 1.5, 2, 2.5% NC-at constant 1%CMC hydrogels at 25°C k) Yield

stress of NC-CMC hydrogels at 38°C. l) Recovery test of the hydrogels by applying consecutive cyclic low (0.2%) and high (500%) strains up to 6 cycles at 38°C.

When a material is exposed to shear stress, monitoring the viscosity changes can show the ability of the material to resist deformation.[47] In shear-thinning hydrogels, viscosity decreases upon shear stress application due to the presence of reversible cross-linking mechanisms. As seen in **Figure 2j**, in all hydrogel formulations 1.5, 2 and 2.5% NC (all made at constant 1w/v% CMC), the viscosity decreased by increasing the shear rate, indicating the presence of shear-thinning behavior. By increasing NC amounts, relatively higher viscosities were observed due to the presence of more electrostatic and hydrogen bonding between NC and CMC polymer chains. In 0%NC (which is 1w/v% CMC) sample, the viscosity stayed constant and did not change with shear rate increase, indicating a Newtonian fluid behavior. The 0%NC (1%CMC) sample also showed significantly lower viscosity compared to NC-CMC hydrogels. The stress sweep test shows in which applied stress hydrogel transitions from a linear, elastic behavior to a more nonlinear, viscoelastic behavior. Th stress sweep result is presented in **Figure S5**. The point at which the hydrogel transitions from a linear to a nonlinear region is commonly referred to as the yield stress. Beyond this threshold, the hydrogel may begin to flow or exhibit plastic deformation. The results of the stress sweep test conducted at a constant frequency of 10 Hz indicated an increase in the yield stress, with values measured at 138.5 Pa, 167.2 Pa, and 244.9 Pa for the 1.5%, 2%, and 2.5% NC hydrogels, respectively (**Figure 2k**). This could be due to increased interactions between NC and CMC at higher NC concentration. Another significant feature of shear-thinning hydrogels is their capacity for rapid recovery after injection, which can be assessed by subjecting them to cyclic low and high strains and monitoring changes in G′ and G″ over time. As seen in **Figure 2l**, at lower strain levels within LVE region (0.2%), G′ surpasses G″, indicating the presence of a solid-like structure. However, when subjected to a high strain outside the LVE region (500%), the hydrogel network becomes compromised, with G″ surpassing G′, resulting in a loss of structural integrity. By lowering the applied strain to 0.2% again, there is a swift recovery of the hydrogel network as shown by immediate increase of G′ to levels higher than G″. These successive low and high strain cycles demonstrate the remarkable capacity of the hydrogel to recover after complete disintegration, a crucial attribute for shear-thinning

injectable hydrogels. In summary, the system containing 2.5% NC displayed the highest yield strength and elasticity. It's worth noting that NC concentrations exceeding 2.5% were not assessed due to the excessively high viscosity of the mixture, which made it impractical to achieve uniform hydrogels.

4.3.4 *In vitro* bacterial assays

Due to high specificity of phages, the utilization of purposefully designed phage cocktails has shown to enhance bacterial eradication and treatment efficacy.[50] Phage cocktails broaden the spectrum of phage antibacterial activity, allowing them to target a wider range of bacterial strains, and they may also mitigate the risk of phage resistance emergence.[51,52] As a proof of concept, we examined the bactericidal activity of six distinct P. aeruginosa phages, namely P32, JG004, PO4, PP7, and E79, against the P. aeruginosa laboratory strain, PAO1. These phages were tested both individually and in binary combinations. Based on turbidity monitoring (OD_{600} assay) of phage infected and uninfected bacterial cultures (kill curves) shown in **Figure S6**, by infecting the bacterial strain with individual phages, phage resistant mutants rise after ~8 hours. However, some binary phage infections showed promising results in terms of bacterial eradication performance. The Four phage pairs including P32-JG004, P32-E79, PO4-JG004, PO4-E79, were able to successfully eradicate bacteria and prevent phage-resistant mutants arise for up to 24 hours *in vitro*. The results of this experiment underscore the potential for enhancing the effectiveness of phage therapy through the deliberate formulation of phage cocktails. As a proof of concept, the combination of two specific phages, P32 and JG004, was selected for the development of phage-loaded injectable hydrogels for the subsequent experiments. In all phage-loaded hydrogel formulations, the term 'phage' refers to the P32-JG004 combination.

Figure 3a displays electron micrographs of phages, using transmission electron microscopy (TEM), and PAO1 bacterial cells, visualized through scanning electron microscopy (SEM). To assess this phage pair's efficacy, PAO1 cultures were exposed to varying phage concentrations. The ratio between the number of phages and the number of bacterial cells is referred to as the Multiplicity of Infection (MOI). **Figure 3b** illustrates that the P32-JG004 pair at MOI=0.1 effectively suppressed bacterial growth, whereas the use of individual P32 and JG004 phages led to the emergence of resistant mutants after 8-

10 hours. At all other examined MOIs (10, 1, 0.01, 0.001, 0.0001), a noticeable and effective reduction in bacterial growth was observed when compared to the control and single-phage infections (**Figure S7**). Injectable bactericidal hydrogels were created by incorporating a phage cocktail (composed of a 50:50 ratio of P32 and JG004) into the NC-CMC hydrogel. The resultant hydrogel contained a final phage concentration of approximately ~10^9 PFU/ml (Plaque Forming Units per milliliter). When this phage-loaded hydrogel was injected onto a bacterial lawn and incubated at 37°C overnight, a clear zone of bacterial clearance was observed around the injected hydrogel, demonstrating its effectiveness in eliminating bacterial cells. (**Figure 3c**).

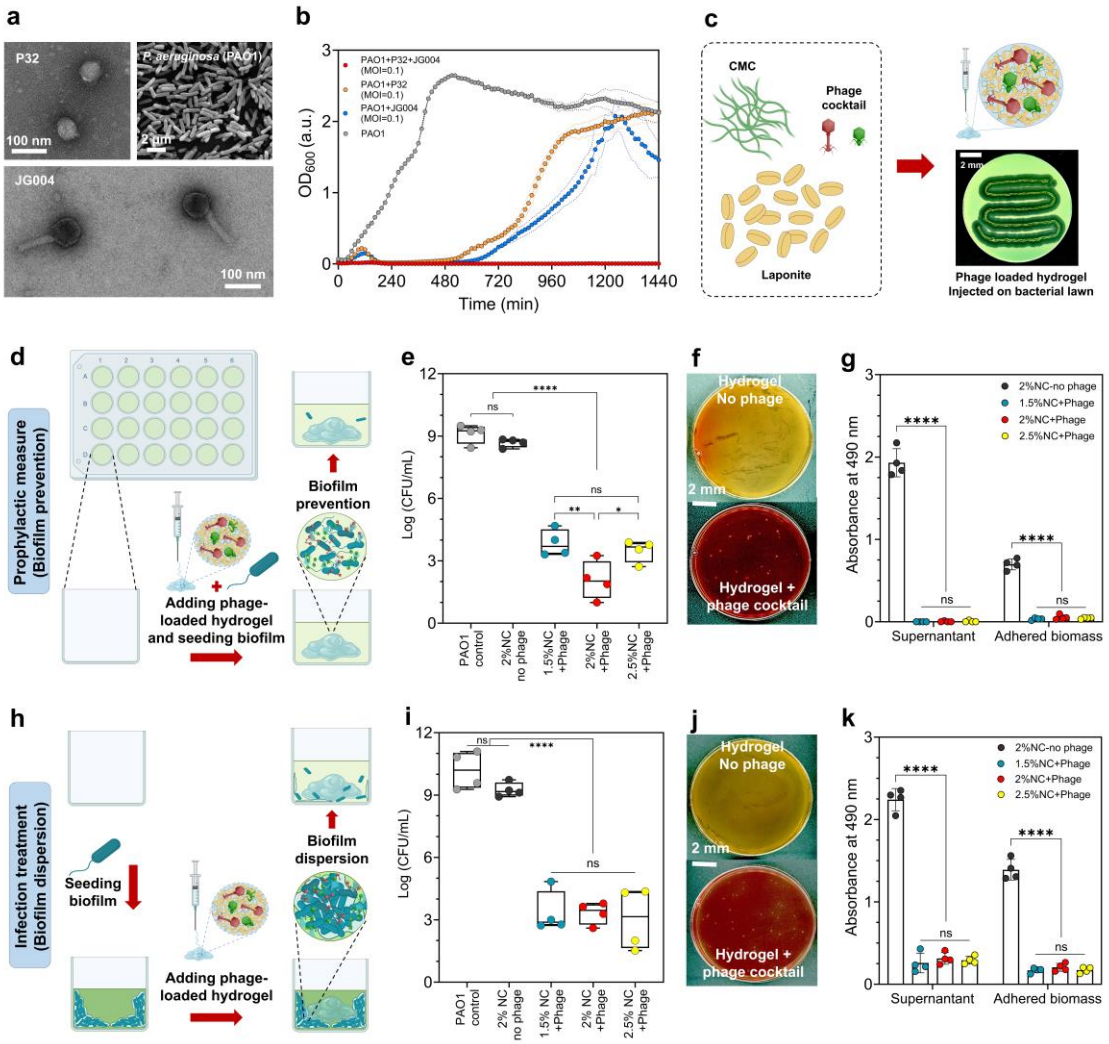

Figure 3. *In vitro* bacterial assays. **a)** Transmission electron microscopy (TEM) images of phages (P32 and JG004) and scanning electron microscopy (SEM) images of P. aeruginosa (PAO1). **b)** Kill curves depicting the effects of individual and binary phage infections on PAO1 bacterial cells (OD_{600} assay). **c)** Schematic representation of phage-loaded injectable

hydrogel preparation, along with an image illustrating the antibacterial effect of the hydrogel after being injected onto bacterial lawn. The cleared zone surrounding the injected hydrogel signifies bacterial growth inhibition. **d)** Schematic illustrating the steps of the bacterial prevention assay (a prophylactic measure). **e)** Biofilm prevention performance is analyzed after 24 hours of incubation by measuring CFU counts. **f)** representative images of MacConkey agar plates after culturing 100 µL supernatants from each well containing hydrogel with phage and control no phage hydrogel. **g)** Metabolic activity of bacterial cells in both the supernatant and adhered biomass of each well within a 24-well plate using the XTT assay (a tetrazolium salt undergoes reduction to an orange soluble formazan dye in response to cellular metabolic activity). **h)** The assay protocol for biofilm dispersion **i)** CFU counts of biofilm dispersion assay. **j)** Representative images of MacConkey agar plates after culturing 100 µL supernatants from each well containing hydrogel with phage and control no phage hydrogel. **k)** Metabolic activity of bacterial cells in supernatant and adhered biomass using XTT assay in biofilm dispersion assay. (****$p < 0.0001$, **$p < 0.01$, *$p < 0.05$)

The effectiveness of phage-loaded hydrogels in preventing and dispersing biofilms was assessed through various liquid bacterial assays, including colony-forming unit (CFU) counts, assessment of metabolic activity via the XTT assay (tetrazolium sodium salt) in both the supernatant and adhered biomass, as well as turbidity measurements (OD_{600} assay) of the supernatant within each well. In biofilm prevention assay, hydrogels were placed within sterile untreated flat bottom 24-well plate and bacterial cells were seeded at an initial concentration of 10^5 CFU/mL in each well (**Figure 3d**). The plate was incubated at 37°C at 120 rpm shaking for 24 hours to allow bacterial biofilm growth. Bacterial concentrations were assessed for each condition by creating serial dilutions of the supernatant from each well and then culturing on McConkey (a selective medium for gram-negative bacteria) agar plates. **Figure 3e** presents the concentration of viable bacterial cells in Log (CFU/mL) for each condition. A comparison between the PAO1 blank control (no hydrogel) and the 2%NC hydrogel without phage reveals that the hydrogel did not exhibit any bactericidal effect, as the number of viable bacterial cells remained the same. In contrast, phage-loaded hydrogels with various formulations (1.5%, 2%, and 2.5% NC) reduced the bacterial load by approximately 5 logs when compared to the control PAO1 blank and the hydrogel without phage. By spreading 100 µL of the supernatant from each well onto MacConkey agar plates and incubating them overnight, it was observed that phage-loaded hydrogels led to the growth of only a few colonies. In contrast, the hydrogel without phage was densely covered with bacteria, as illustrated in the representative plate images in **Figure 3f**. The

metabolic activity of bacterial cells in both the supernatant and adhered biomass from each well was assessed using the XTT assay, a cell proliferation assay employed to measure cellular metabolic activity as an indicator of cell viability. XTT is a tetrazolium salt that undergoes reduction to an orange soluble formazan dye in response to cellular metabolic activity. An increase in the metabolic activity of bacterial cells leads to the reduction of tetrazolium salt into formazan dye, resulting in increased absorbance.[53,54] After introducing 100 µL of the XTT solution to an equal volume of the supernatant from each well (resulting in a total volume of 200 µL) and incubating for one hour at 37°C, the metabolic activity of bacterial cells was assessed to compare hydrogels loaded with a phage cocktail to hydrogels without phages. To measure the metabolic activity of bacterial cells within the adhered biomass, all the supernatant solution was removed from each well without disturbing the adhered biomass. Subsequently, 1000 µL of XTT solution was added to each well (without removing the hydrogel), and the plate was incubated for one hour at 37°C. Subsequently, 200 µL of the solution was transferred to a 96-well plate, and the absorbance was measured at 490 nm. The absorbance values were significantly reduced for phage-loaded hydrogels compared to hydrogels without phages in both the supernatant and adhered biomass. These results affirm the successful antibacterial performance of the phage-loaded hydrogels in preventing the formation of bacterial biofilms (**Figure 3g**). The turbidity of the supernatant was also measured for each well and as shown in **Figure S8.** Phage-loaded hydrogels resulted in lower absorbance numbers (OD_{600}), that the presence of phages effectively prevented bacterial growth and biofilm formation.

For biofilm dispersion assay, PAO1 was seeded into the wells of a 24-well plate and allowed to grow biofilms for 24 hours at 37°C with agitation at 120 rpm. After the 24 hours of biofilm growth, half of the supernatant from each well was carefully removed. Subsequently, hydrogels were introduced into the wells, and the volume of supernatant that was previously removed was replaced with fresh growth media. The plates were then incubated for an additional 24 hours to assess the hydrogel's dispersion abilities (**Figure 3h**). Similar trends were observed in the biofilm dispersion assay. The results from the CFU count assay indicated a remarkable decrease in bacterial load (approximately 6 logs) in biofilms treated with phage-loaded hydrogels when compared to the PAO1 blank control and hydrogels without phages (**Figure 3i**). Representative images of the overnight growth

of 100 µL of the supernatant from each condition, which was spread on MacConkey agar plates, are presented in **Figure 3j.** The introduction of phage-loaded hydrogels resulted in a substantial reduction in bacterial load, with only a few bacterial colonies observed. In contrast, the supernatant from wells with hydrogels lacking phages was able to completely cover the plate. The XTT assay results demonstrated a significant decrease in bacterial metabolic activity in both the supernatant and adhered biomass of the phage-loaded hydrogels when compared to hydrogels without phages (**Figure 3k**). Turbidity measurements of the supernatant in each well validated the findings from CFU counts and the XTT assay by revealing lower absorbance values in the presence of phage-loaded hydrogels **(Figure S9).** Representative images of the wells of biofilm prevention/dispersion experiments after conducting XTT assay are shown in **Figure S10.**

An intriguing characteristic of phages as bactericidal agents is their self-dosing ability. They can replicate on-site by utilizing bacterial reproduction machinery to multiply. In both the biofilm prevention and dispersion assays, the concentration of phages was determined by serially diluting and plating the supernatant from samples of phage-loaded hydrogels on a PAO1 bacterial lawn. The phage population increased to approximately ~10^9 and ~10^{11} PFU/mL in the biofilm prevention and biofilm dispersion assays, respectively (see **Figure S11**). The final concentration of phages in the biofilm dispersion assay was notably higher than in the biofilm prevention assay, as the bacterial cell density in each well was greater due to the pre-existing 24-hour biofilm growth when the hydrogels were introduced.

4.3.5 In vitro cell culture.

In vitro cell culture studies were conducted on phage-loaded injectable hydrogels using the SaOS-2 osteoblast cell line. The cytocompatibility of the hydrogels was evaluated through an indirect approach, wherein seeded cells were exposed to standard complete media and complete media containing extracts from phage-loaded hydrogels. These hydrogel extracts were derived from hydrogels incubated in standard complete media for 5 and 7 days. As depicted in **Figure 4a**, the hydrogels exhibited biocompatibility, with no signs of cytotoxicity. Cells exposed to extracts from hydrogels with a longer incubation period (7

days) also displayed enhanced cell proliferation compared to cells cultured in regular complete medium.

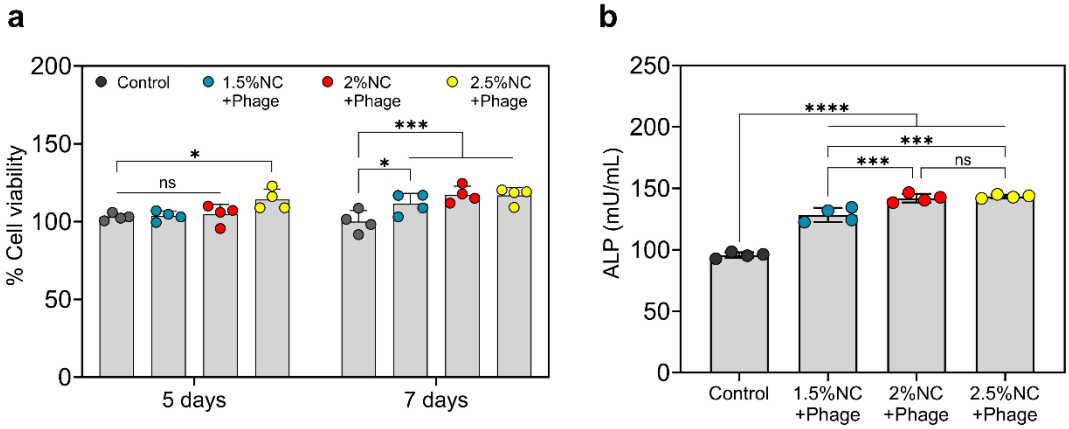

Figure 4. *In vitro* cell culture. a) Indirect cytotoxicity assay conducted after 48 hours of incubating SaOS-2 cells with extracts of hydrogels immersed in complete media for 5 and 7 days at 37°C in 5% CO2, in comparison to cells grown in fresh complete cell culture media as a control. None of the hydrogels exhibited any cytotoxic effects on the SaOS-2 cell line. b) ALP assay performed after incubating cells with hydrogels for 3 days, revealing significantly higher levels of ALP induction in cells incubated with hydrogels when compared to control cells cultured in complete cell culture media alone. (****p < 0.0001, ***p < 0.001, **p < 0.01, *p < 0.05)

Osteomyelitis, a severe form of bone infection, is renowned for causing localized bone loss and destruction. The prevalence of antibiotic-resistant infections and biofilm formation has significantly reduced the success rate of treatment in such cases.[50] To improve the management of osteomyelitis, the creation of a biomaterial with dual functionality for infection control and bone regeneration is imperative. As previously mentioned, the hydrogel utilized in this study incorporates laponite and CMC, both of which have shown promise in promoting bone formation in various research studies.[26,33–40] The SaOS-2 cells used in this study are human osteosarcoma cells exhibiting osteoblastic characteristics, including the expression of alkaline phosphatase (ALP), osteonectin, and a response to mineralization activation.[55] ALP serves as an early marker of osteogenic differentiation in osteoblast cells. It is expressed on the extracellular matrix and stimulates bone mineralization by releasing phosphorus.[40] "In this study, we assessed the ALP activity after culturing SaOS-2 cells in the presence of hydrogels for 3 days. The ALP activity increased

by 34%, 48%, and 50% in the presence of 1.5%, 2%, and 2.5% NC hydrogels, respectively (**Figure 4b)**.

4.4. Conclusion

In this study, we successfully developed an injectable hydrogel for delivering phages to infected bone tissue. This hydrogel was created by simply blending NC and CMC, resulting in physical cross-linking driven by electrostatic and hydrogen bonds. The presence of reversible electrostatic and hydrogen bonds conferred shear-thinning behavior and self-healing properties to the injectable hydrogel, as demonstrated by rheological assessments. The hydrogels were loaded with a binary *P. aeruginosa* phage cocktail, which exhibited significantly stronger antibacterial performance compared to individual phages. The phage-loaded hydrogels demonstrated excellent antibiofilm performance in both biofilm prevention and dispersion assays. Furthermore, these biocompatible hydrogels displayed enhanced osteogenic activity in SaOS-2 osteoblast cells, underscoring their considerable potential for promoting bone healing and osteointegration. In summary, the phage-loaded NC-CMC injectable hydrogel, with its dual functionality of antibiofouling and bone healing properties, holds promising potential for the treatment of bone and implant-associated infections.

4.5. Materials

Carboxy methyl cellulose (CMC) with average Molecular weight of ~250,000 and degree of substitution 0.9 was purchased from Millipore Sigma (Oakville, ON, Canada). Laponite XLG Nanoclay (NC) was generously provided by BYK Additives Inc., USA. Phosphate-buffered saline (PBS) tablets were purchased from VWR (Mississauga, ON, CA). Luria Broth (LB) was purchased from Fisher Scientific (ON, CA). vB_Pae-Tbilisi32 or for short P32 and JG004 phages, and Pseudomonas aeruginosa (PAO1) strain were purchased from DSMZ (Germany). E79, PO4 and PP7 phage from Université Laval (QC, Canada). XTT tetrazolium sodium salt, menadione, and acetone were purchased from Sigma Aldrich. Phosphate-buffered saline (PBS) tablets were purchased from VWR (Mississauga, ON, CA). Luria Broth (LB) was purchased from Fisher Scientific (ON, CA). Alkaline

Phosphatase Assay Kit (ab138887) and PrestoBlue™ HS Cell Viability Reagent (Invitrogen P50200) were purchased from Abcam (Abcam.com) and Fisher Scientific (ON, CA), respectively.

4.6. Methods

4.6.1 Hydrogel preparation

Solutions of CMC and Laponite were prepared in milli-q water under vigorous agitation. CMC required a heating process at 50°C for at least 5 hours to obtain homogenized solutions, while laponite formed transparent solutions after a few minutes of stirring at room temperature. Laponite nanoclay particles (NC) were stirred at 700 rpm and after 2 minutes, CMC solutions was added to it, followed by a vertexing for 5 minutes to obtain a homogenized hydrogel. The concentration of CMC was kept constant at 1 w/v% and NC concentrations increased to obtain hydrogels with 1.5, 2, 2.5w/v % NC. All hydrogel formulations were aged for 48 hours at room temperature after preparation.

Phage loaded hydrogels were prepared the same way described above by mixing Laponite, CMC and phage cocktail to obtain the final concentration of phages at ~10^9 PFU/mL. The original phage cocktail was prepared by mixing equal volumes of both phages at 10^{11} PFU/mL to obtain 5×10^{10} PFU/mL in the final mixed solution.

4.6.2 Rheological analysis

Rheological properties were assessed using a Discovery HR-2 hybrid rheometer (TA Instruments, USA) with a cone-plate geometry with 40 mm diameter, 1°cone angle, and 50 µm truncation gap. To prevent evaporation, mineral oil was applied around the circumference of the plates in all measurements to obtain consistent results. The hydrogels were equilibrated for 2 minutes prior testing under steady shear of 0.2% strain at 10 Hz to remove the mechanical history of handling the hydrogel. Frequency sweeps were conducted from 0.01 to 100 Hz at 25°C, and strain sweeps were performed from 0.01% to 1000% strain at 10 Hz at 37°C by 10 points per decade measurements. The recovery test was performed at 10 Hz 37°C under 500% strain for 60 seconds, a value outside the linear viscoelastic region, followed by applying a 0.2% strain for 120 seconds. The low and high

strain cycle was repeated 6 times for a cyclic strain test to assess the ability of the hydrogel to recover itself. The flow ramp was performed at shear rates from 0 to 50 s^{-1} over 150 seconds at 25°C.

4.6.3 Swelling and degradation experiments

Freeze dried hydrogels (n=4) inside a cell strainer were submerged in PBS and incubated at 37°C. Samples were removed at different time intervals, including 2, 4, 6, 8 and 24 hours. Before weighing the samples, the excess water was removed carefully using a Kim wipe. The swelling ratio was measured using the formula: Swelling ratio = $(W_w\text{-}W_d)/W_d \times 100$. W_w represent the swollen weight after incubation in PBS, and W_d is the original dry weight.

4.6.4 Scanning Electron Microscopy (SEM)

Bacterial cells were grown on steel coupons overnight and fixed using 30% glutaraldehyde for 30 min at 4 °C. Fixed samples were dehydrated by sequentially immersing in ethanol gradient solutions (10%, 30%, 50%, 70%, 90%, 100%) for 10 min. Samples were then dried using a Leica EM CPD300 critical point dryer (Leica Mikrosysteme GmbH, Austria). Dried samples were coated with 20 nm of gold using a Polaron Model E5100 sputter coater (Polaron Equipment Ltd., UK). SEM images were taken using a Tecan VEGA II LSU SEM (Tecan USA, PA, USA). In order to prepare hydrogels for SEM imaging, hydrogel samples were freeze dried for 24 hours, sputter coated with a 15 nm gold layer and fixed on SEM stubs using double sided carbon tape. The samples were then imaged using a JEOL 6610LV SEM instrument at the Canadian Centre for Electron Microscopy (CCEM), McMaster University (ON, CA).

4.6.5 Transmission Electron Microscopy (TEM)

First, carbon-coated copper grids were plasma treated shortly to help spread the liquid on it properly. Afterwards, phages with an initial concentration of 10^9 PFU/mL were absorbed onto the prepared carbon coated copper grids and negatively stained with 1% uranyl acetate. Stained grids were dried at room temperature and imaged using Talos L120C transmission electron microscope at the Canadian Centre for Electron Microscopy (CCEM), McMaster University (ON, CA).

Transmission election microscopy (TEM) images of the phages were obtained using Talos L120C transmission electron microscope at the Canadian Centre for Electron Microscopy (CCEM), McMaster University (ON, CA).

4.6.6 Fourier Transform Infrared Spectroscopy (FTIR)

FTIR spectra were obtained for laponite XLG powder (NC), CMC powder and powdered lyophilized hydrogel (1%CMC-2%NC) in the range of 4000-400 cm^{-1}, at 2 cm^{-1} resolution with 32 scans (Bruker instrument, model Vertex70)

4.6.7 Dynamic Light Scattering (DLS)

DLS measurements were performed at a backscattering angle of 173° and a laser wavelength of 633 nm. First, the hydrodynamic size of 0.2% NC was assessed using DLS. In order to analyze the interaction between CMC and NC, 0.1, 0.2, 0.3, and 0.5% CMC was introduced to the 0.2% NC dispersions, and the measurements were conducted after 60 seconds of high-speed vortex. Fresh samples were prepared for every measurement. Zeta potential and DLS measurements were performed using Malvern Zetasizer Nano.

4.6.8 Bacterial culture and phage propagation

Overnight cultures of bacteria were prepared by streaking a frozen glycerol stock of *Pseudomonas aeruginosa* PAO1 strain (stored at -80°C) and inoculating LB media, followed by incubation under 180 rpm at 37°C for 14-16 hours. *Pseudomonas aeruginosa* phages including JG004 (JG004), vB_Pa2-Tbilisi32 (P32), PO4, PP7, and E79 were propagated on their host (PAO1), by introducing a single plaque of each phage to a bacterial subculture at mid-exponential phase of growth (OD_{600} = 0.3) and incubating at 37°C at 180 rpm for 6 hours. Crude phage lysates were then pelleted down at 7000 rcf, at 4°C for 15 minutes, the solution on top was decanted to a new tube, and the pellet containing bacterial debris was discarded. The phage containing solutions were then sterile filtered using 0.45 µm and 0.22 µm syringe filters consecutively. To further concentrate the phage solutions in some cases 100 KDa, and 30 KDa Amicon ultra filters were used.

4.6.9 Phage cocktail design

Phage Cocktail designs were conducted by measuring turbidity of phage infected cultures compared to un-infected cultures using OD_{600} assay. Binary combinations of phages (including P32-JG004, P32-PO4, P32-PP7, P32-E79, PO4-JG004, PO4-PP7, PO4-E79, JG004-PP7, PP7-E79) were introduced to PAO1 cultures at OD_{600} ~0.1 at MOI=10 (multiplicity of infection or phage to bacteria ratio), at total volume of 200 µL in a sterile flat bottom transparent 96 well plate. The plate was incubated for 24 hours at 37°C under orbital shaking inside a Synergy Neo2 BioTek plate reader and absorbance was recorded every 5 minutes at 600 nm. Phage pairs which successfully suppressed the bacterial growth and had absorbance values similar to media controls were introduced as effective combinations. The selected phage pair (P32-JG004) were further analyzed by repeating the above explained experiments at different MOIs including 10, 1, 0.1, 0.01, 0.001. The final OD_{600} results were graphed using GraphPad Prism 10 software.

4.6.10 In vitro antibacterial assessment

In order to evaluate the biofilm prevention ability of the phage loaded hydrogels, quadruplicates of phage cocktail-loaded hydrogels with 3 different formulations (1.5%NC, 2%NC, 2.5%NC+phage) with a final concentration of 10^9 PFU/mL of phage cocktail containing P32,JG004 (1:1 v/v) and a hydrogel formulation without phage (2%NC-no phage) as a negative control were placed in a sterile untreated flat bottom 24 well plate. LB media only wells and PAO1 only wells were also used controls. Hydrogel volume was kept constant at 400 µL for all conditions. Having added 1 mL of bacterial cultures of PAO1 at 10^5 CFU/mL to each well, bacterial biofilms were grown for 24 hours under 120 rpm agitation at 37°C. At the end of 24 hours biofilm growth, optical density of 200 µL of the supernatant was measured at 600 nm (OD_{600}) in a 96 well plate, comparing the turbidity of the samples. Afterwards, CFU counts of the supernatant was calculated by taking samples from the wells containing hydrogels with and without phage and serially diluted in sterile PBS solution (10 folds serial dilutions) and plating on MacConkey agar (selective for gram negative bacteria) plates to obtain CFU/mL. The metabolic activity of the planktonic bacterial cells was also measured by adding 100 µL of solution from each well and added to 100 µL of XTT solution in a 96 well plate and incubated for an hour. The absorbance

was then recorded at 490 nm using Synergy Neo2 BioTek plate reader. The metabolic activity of the adhered biomass was also evaluated by carefully removing all the planktonic bacteria and adding 1500 of XTT solution, followed by one hour incubation in the dark under 120 rpm agitation at 37°C. The absorbance was recorded for all samples by adding 200 µL of the XTT containing solutions from each well to a 96 well plate and recording the absorbance at 490 nm.

For assessing the **biofilm dispersing** ability of the injectable hydrogels, 24-hour biofilms were first seeded inside a sterile 24 well plate under 120 rpm agitation at 37°C in a total volume of 1000 µL per well by initial concentration of PAO1 at 10^5 CFU/mL. Having removed 500 µL from each well at the end of 24-hour incubations, and replacing it with 500 µL of fresh media, different hydrogel formulations with and without phage cocktails, were introduced to each well in quadruplicates. The plates were then incubated for another 24 hours, followed by measuring the turbidity of the supernatant (OD_{600}), metabolic activity of the supernatant and the adhered biomass using XTT assay, CFU counts, and turbidity measurements as discussed above. Synergy Neo2 BioTek plate reader was used to record absorbance data in both XTT and OD_{600} assays.

4.6.11 *In vitro* cell studies

The cytotoxicity of the phage-loaded NC-CMC hydrogels was evaluated using an indirect method. First, hydrogels with three different Lapointe concentrations (1.5, 2, 2.5% NC) loaded with a mixture of P32-JG004 phages at a final concentration of 10^9 PFU/ml were emersed in 700ul SaOS-2 growth medium (McCoy's 5A medium supplemented with fetal bovine serum (FBS)) and intubated at 37°C in 5% CO2 for 3, 5, and 7 days. In the meanwhile, SaOS-2 cells were seeded at a density of 2×10^5 cells per well into each well of a tissue culture treated 24-well plate. The SaOS-2 cells were exposed to hydrogel extracts by replacing the complete media in cell seeded wells with 700 µL of the extract form each hydrogel group. The cells were incubated for an additional 48 hours in elution media containing hydrogel extracts. The cells exposed to fresh complete media were regarded as a control group. After 48h of incubation, cytotoxicity assay was conducted using PrestoBlue™ HS Cell Viability Reagent (Invitrogen P50200) according to the manufacturer's instructions. Briefly, having removed the medium from each well of the 24-

well plate containing cells, a 10-fold dilution of the cell viability reagent in cell culture medium was added to each well. The plate was incubated for 3 h at 37°C in 5% CO2. After incubation, 200 µL of the solution was added to black well plates (Greiner Bio-One 655086) and fluorescence measurements were taken at excitation and emission wavelengths of 560±5 nm and 590±5 nm, respectively using Synergy Neo2 BioTek plate reader. To assess the ALP activity of cells exposed to hydrogels, SaOS-2 cells were seeded at a density of 2×10^5 cells per well into each well of a tissue culture treated 24-well plate. Hydrogels with 1.5, 2, 2.5% NC loaded with phage cocktail (P32, JG004) were placed onto seeded wells, and incubated for 3 days. The ALP activity was measured at the end of incubation in the supernatant of each sample using Alkaline Phosphatase Assay Kit (ab138887, Abcam.com), based on manufacturer's instructions. All measurements were performed in quadruplicates.

4.7. References

1. Masters, E. A. *et al.* Skeletal infections: microbial pathogenesis, immunity and clinical management. *Nat. Rev. Microbiol.* **20**, 385–400 (2022).
2. Garcia Del Pozo, E., Collazos, J., Carton, J. A., Camporro, D. & Asensi, V. Factors predictive of relapse in adult bacterial osteomyelitis of long bones. *BMC Infect. Dis.* **18**, 1–11 (2018).
3. Gibb, B. P. & Hadjiargyrou, M. Bacteriophage therapy for bone and joint infections an instructional review. *Bone Jt. J.* **103 B**, 234–244 (2021).
4. Li, B. & Webster, T. J. Bacteria antibiotic resistance: New challenges and opportunities for implant-associated orthopedic infections. *J. Orthop. Res.* **36**, 22–32 (2018).
5. Wang, B. *et al.* Trends in microbiological epidemiology of orthopedic infections: a large retrospective study from 2008 to 2021. *BMC Infect. Dis.* **23**, 1–12 (2023).
6. Merril, C. R., Scholl, D. & Adhya, S. L. The prospect for bacteriophage therapy in Western medicine. *Nat. Rev. Drug Discov.* **2**, 489–497 (2003).
7. Kortright, K. E., Chan, B. K., Koff, J. L. & Turner, P. E. Phage Therapy: A Renewed Approach to Combat Antibiotic-Resistant Bacteria. *Cell Host Microbe* **25**, 219–232 (2019).
8. Petrovic Fabijan, A. *et al.* Phage therapy for severe bacterial infections: a narrative review. *Med. J. Aust.* **212**, 279–285 (2020).
9. Xie, Y., Wahab, L. & Gill, J. J. Development and validation of a microtiter plate-based assay for determination of bacteriophage host range and virulence. *Viruses* **10**, (2018).
10. Fish, R., Kutter, E., Bryan, D., Wheat, G. & Kuhl, S. Resolving digital staphylococcal osteomyelitis using bacteriophage—A case report. *Antibiotics* **7**, 1–6 (2018).
11. Doub, J. B. *et al.* Salvage bacteriophage therapy for a chronic MRSA prosthetic joint

infection. *Antibiotics* **9**, 1–6 (2020).
12. Clarke, A. L., Soir, S. De & Jones, J. D. The safety and efficacy of phage therapy for bone and joint infections: A systematic review. *Antibiotics* **9**, 1–11 (2020).
13. Khatami, A. *et al.* Bacterial lysis, autophagy and innate immune responses during adjunctive phage therapy in a child. *EMBO Mol. Med.* **13**, 1–9 (2021).
14. Koons, G. L., Diba, M. & Mikos, A. G. Materials design for bone-tissue engineering. *Nat. Rev. Mater.* **5**, 584–603 (2020).
15. Uman, S., Dhand, A. & Burdick, J. A. Recent advances in shear-thinning and self-healing hydrogels for biomedical applications. *J. Appl. Polym. Sci.* **137**, 1–20 (2020).
16. Guvendiren, M., Lu, H. D. & Burdick, J. A. Shear-thinning hydrogels for biomedical applications. *Soft Matter* **8**, 260–272 (2012).
17. Dąbrowska, K. & Abedon, S. T. Pharmacologically Aware Phage Therapy: Pharmacodynamic and Pharmacokinetic Obstacles to Phage Antibacterial Action in Animal and Human Bodies. *Microbiol. Mol. Biol. Rev.* **83**, (2019).
18. Bichet, M. C. *et al.* Bacteriophage uptake by mammalian cell layers represents a potential sink that may impact phage therapy. *iScience* **24**, 102287 (2021).
19. Dąbrowska, K. Phage therapy: What factors shape phage pharmacokinetics and bioavailability? Systematic and critical review. *Med. Res. Rev.* **39**, 2000–2025 (2019).
20. Onsea, J. *et al.* Bacteriophage Therapy for the Prevention and Treatment of Fracture-Related Infection Caused by Staphylococcus aureus: a Preclinical Study. *Microbiol. Spectr.* **9**, 1–14 (2021).
21. Yang, Y. *et al.* Encapsulation and delivery of phage as a novel method for gut flora manipulation in situ: A review. *J. Control. Release* **353**, 634–649 (2023).
22. Loh, B. *et al.* Encapsulation and Delivery of Therapeutic Phages. *Appl. Environ. Microbiol.* **87**, 1–13 (2021).
23. Malik, D. J. *et al.* Formulation, stabilisation and encapsulation of bacteriophage for phage therapy. *Adv. Colloid Interface Sci.* **249**, 100–133 (2017).
24. Shen, H. Y. *et al.* Controlled-release of free bacteriophage nanoparticles from 3D-plotted hydrogel fibrous structure as potential antibacterial wound dressing. *J. Control. Release* **331**, 154–163 (2021).
25. Kim, H. Y., Chang, R. Y. K., Morales, S. & Chan, H. K. Bacteriophage-delivering hydrogels: Current progress in combating antibiotic resistant bacterial infection. *Antibiotics* **10**, 1–17 (2021).
26. Gaharwar, A. K. *et al.* 2D Nanoclay for Biomedical Applications: Regenerative Medicine, Therapeutic Delivery, and Additive Manufacturing. *Adv. Mater.* **31**, 1–28 (2019).
27. Davis, R., Urbanowski, R. A. & Gaharwar, A. K. 2D layered nanomaterials for therapeutics delivery. *Curr. Opin. Biomed. Eng.* **20**, 100319 (2021).
28. Stealey, S. T., Gaharwar, A. K., Pozzi, N. & Zustiak, S. P. Development of Nanosilicate-Hydrogel Composites for Sustained Delivery of Charged Biopharmaceutics. *ACS Appl. Mater. Interfaces* **13**, 27880–27894 (2021).
29. Kiaee, G. *et al.* Laponite-Based Nanomaterials for Drug Delivery. *Adv. Healthc. Mater.* **11**, 1–21 (2022).
30. Peña-Parás, L., Sánchez-Fernández, J. A. & Vidaltamayo, R. Nanoclays for biomedical applications. *Handb. Ecomater.* **5**, 3543–3471 (2019).

31. Shi, P. *et al.* Self-Assembling Nanoclay Diffusion Gels for Bioactive Osteogenic Microenvironments. *Adv. Healthc. Mater.* **7**, (2018).
32. Gaharwar, A. K. *et al.* Shear-Thinning Nanocomposite Hemorrhage. *ACS Nano* **8**, 9833–9842 (2014).
33. Xavier, J. R. *et al.* Bioactive nanoengineered hydrogels for bone tissue engineering: A growth-factor-free approach. *ACS Nano* **9**, 3109–3118 (2015).
34. Erezuma, I. *et al.* Nanoclay Reinforced Biomaterials for Mending Musculoskeletal Tissue Disorders. *Advanced Healthcare Materials* **10**, 1–20 (2021).
35. Zandi, N. *et al.* Nanoengineered shear-thinning and bioprintable hydrogel as a versatile platform for biomedical applications. *Biomaterials* **267**, 120476 (2021).
36. Chen, C., Xi, Y. & Weng, Y. Recent Advances in Cellulose-Based Hydrogels for Tissue Engineering Applications. *Polymers (Basel).* **14**, (2022).
37. Tang, L. *et al.* Study on synergistic effects of carboxymethyl cellulose and LIPUS for bone tissue engineering. *Carbohydr. Polym.* **286**, 119278 (2022).
38. Matinfar, M., Mesgar, A. S. & Mohammadi, Z. Evaluation of physicochemical, mechanical and biological properties of chitosan/carboxymethyl cellulose reinforced with multiphasic calcium phosphate whisker-like fibers for bone tissue engineering. *Mater. Sci. Eng. C* **100**, 341–353 (2019).
39. Gaihre, B. & Jayasuriya, A. C. Fabrication and characterization of carboxymethyl cellulose novel microparticles for bone tissue engineering. *Mater. Sci. Eng. C* **69**, 733–743 (2016).
40. Deng, J. *et al.* Advanced applications of cellulose-based composites in fighting bone diseases. *Compos. Part B Eng.* **245**, 110221 (2022).
41. Stealey, S. T., Gaharwar, A. K. & Zustiak, S. P. Laponite-Based Nanocomposite Hydrogels for Drug Delivery Applications. *Pharmaceuticals* **16**, (2023).
42. Jin, Y., Liu, C., Chai, W., Compaan, A. & Huang, Y. Self-Supporting Nanoclay as Internal Scaffold Material for Direct Printing of Soft Hydrogel Composite Structures in Air. *ACS Appl. Mater. Interfaces* **9**, 17456–17465 (2017).
43. Corzo, I. J. M., da Fonsêca, J. H. L. & d'Ávila, M. A. Influence of carboxymethyl cellulose solutions on rheological properties of Laponite dispersions. *Rheol. Acta* **62**, 393–404 (2023).
44. Xu, P. *et al.* Osmotic-Pressure-Induced Nematic Ordering in Suspensions of Laponite and Carboxy Methyl Cellulose. (2020). doi:10.1021/acs.jpcb.0c06674
45. Pálková, H., Madejová, J., Zimowska, M. & Serwicka, E. M. Laponite-derived porous clay heterostructures: II. FTIR study of the structure evolution. *Microporous Mesoporous Mater.* **127**, 237–244 (2010).
46. Garai, S. & Sinha, A. Biomimetic nanocomposites of carboxymethyl cellulose-hydroxyapatite: Novel three dimensional load bearing bone grafts. *Colloids Surfaces B Biointerfaces* **115**, 182–190 (2014).
47. Cooke, M. E. & Rosenzweig, D. H. The rheology of direct and suspended extrusion bioprinting. *APL Bioeng.* **5**, (2021).
48. Chen, M. H. *et al.* Methods to Assess Shear-Thinning Hydrogels for Application As Injectable Biomaterials. *ACS Biomater. Sci. Eng.* **3**, 3146–3160 (2017).
49. Stojkov, G., Niyazov, Z., Picchioni, F. & Bose, R. K. Relationship between structure and rheology of hydrogels for various applications. *Gels* **7**, (2021).
50. Wu, S. *et al.* Mini Review Therapeutic Strategies Targeting for Biofilm and Bone

Infections. *Front. Microbiol.* **13**, 1–14 (2022).
51. Abedon, S. T., Danis-Wlodarczyk, K. M. & Wozniak, D. J. Phage cocktail development for bacteriophage therapy: Toward improving spectrum of activity breadth and depth. *Pharmaceuticals* **14**, (2021).
52. Chan, B. K., Abedon, S. T. & Loc-Carrillo, C. Phage cocktails and the future of phage therapy. *Future Microbiol.* **8**, 769–783 (2013).
53. Aguiar, P. H. N., Fernandes, N. M. G. S., Zani, C. L. & Mourão, M. M. A high-throughput colorimetric assay for detection of Schistosoma mansoni viability based on the tetrazolium salt XTT. *Parasites and Vectors* **10**, 1–10 (2017).
54. Xu, Z. *et al.* Crystal Violet and XTT Assays on Staphylococcus aureus Biofilm Quantification. *Curr. Microbiol.* **73**, 474–482 (2016).
55. Neufurth, M. *et al.* Engineering a morphogenetically active hydrogel for bioprinting of bioartificial tissue derived from human osteoblast-like SaOS-2 cells. *Biomaterials* **35**, 8810–8819 (2014).

4.8. Supplementary Information

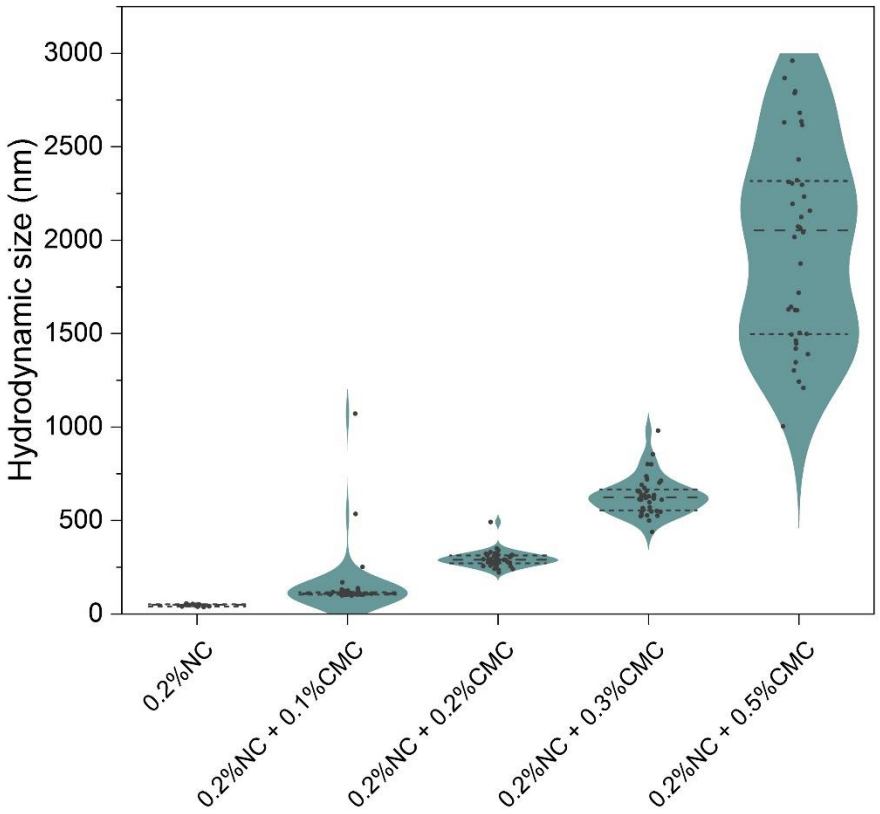

Table 1. Zeta potential

Sample	0.2%CMC	0.2%NC	0.2%NC+ 0.2%CMC
Zeta potential (mV)	-28.4 ±0.8	-31.4 ±0.5	-50 ±2.3

Figure S1. DLS and zeta potential measurements

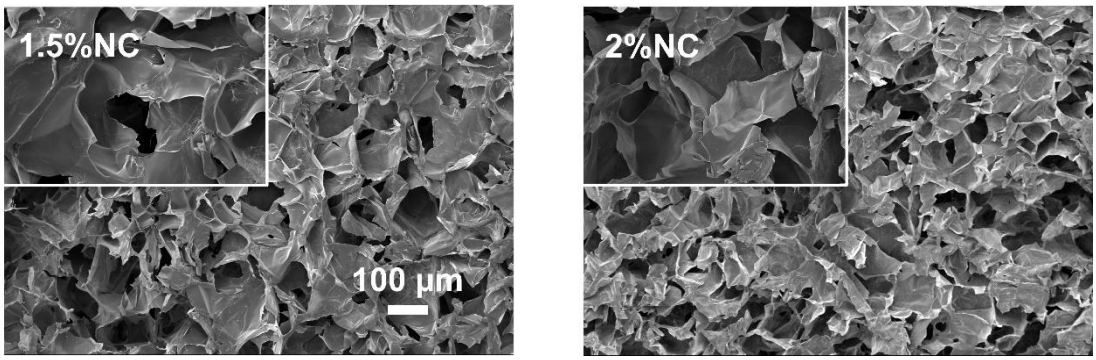

Figure S2. SEM images of 1.5% and 2%NC hydrogel formulations

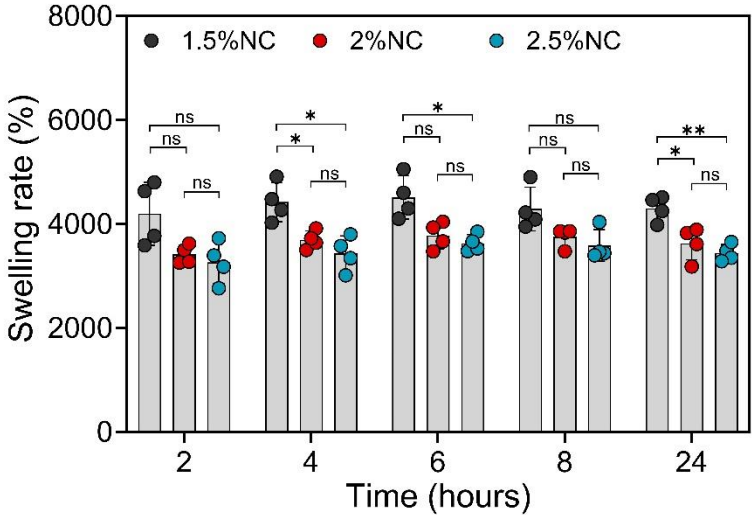

Figure S3. Swelling ratio of freeze dried 1.5, 2, 2.5 %NC hydrogels at different time intervals recorded up to 24 hours.

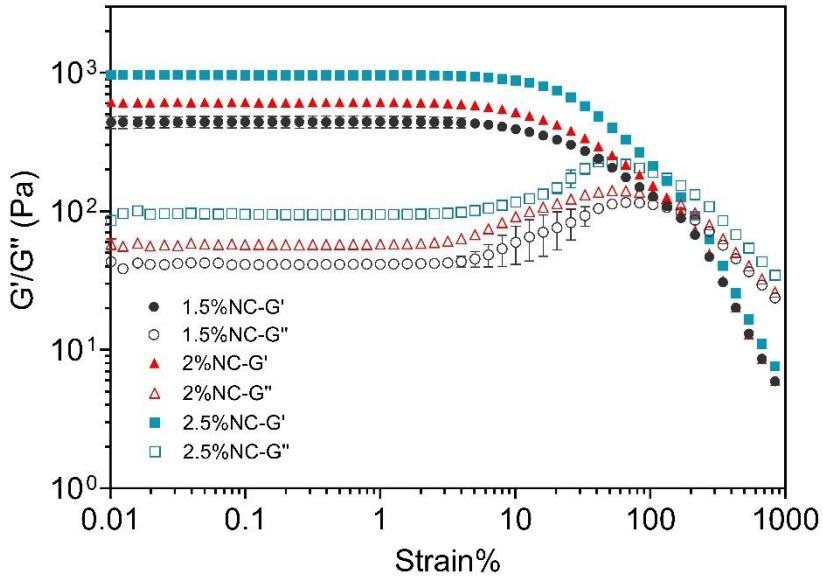

Figure S4. Strain sweep at 10Hz for hydrogels containing 1.5, 2, and 2.5% NC at 38°C.

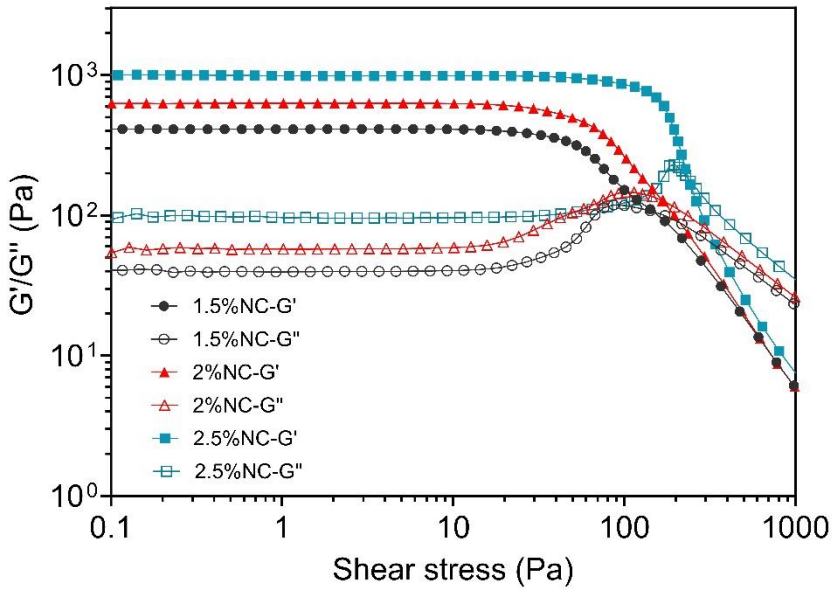

Figure S5. Stress sweep at 10Hz for hydrogels containing 1.5, 2, and 2.5% NC at 38°C.

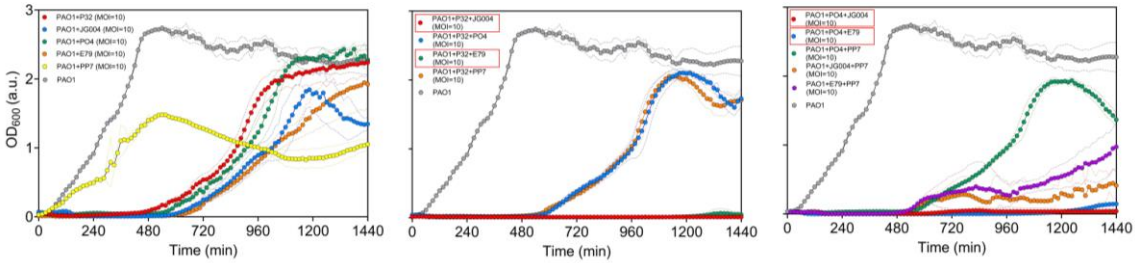

Figure S6. Kill curves of individual and binary phage cocktails. OD600 assay results of infecting PAO1 bacterial strain with single P. aeruginosa phages including P32, JG004, PO4, E79 and PP7 and binary combinations of P32-JG004, P32-PO4, P32-E79 and P32-PP7, PO4-JG004, PO4-E79, PO4-PP7, JG004-PP7 and E79-PP7 in comparison to uninfected PAO1 (gray graph). Dashed line shows standard deviation from the mean of n=6 samples.

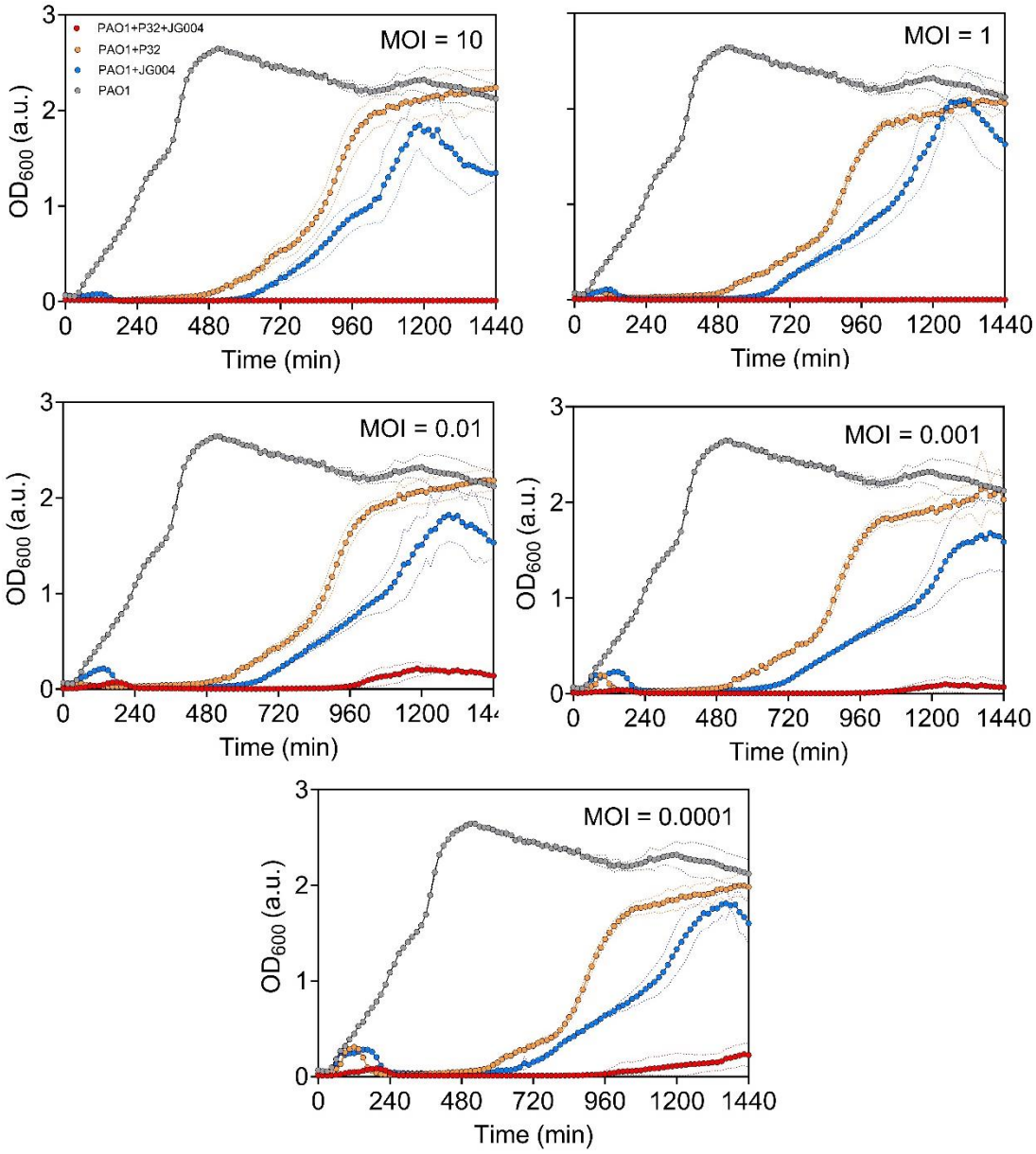

Figure S7. Kill curves of P32 and JG004 phages combination at MOIs of 10, 1, 0.1, 0.01, 0.001, 0.0001 using OD600 assay

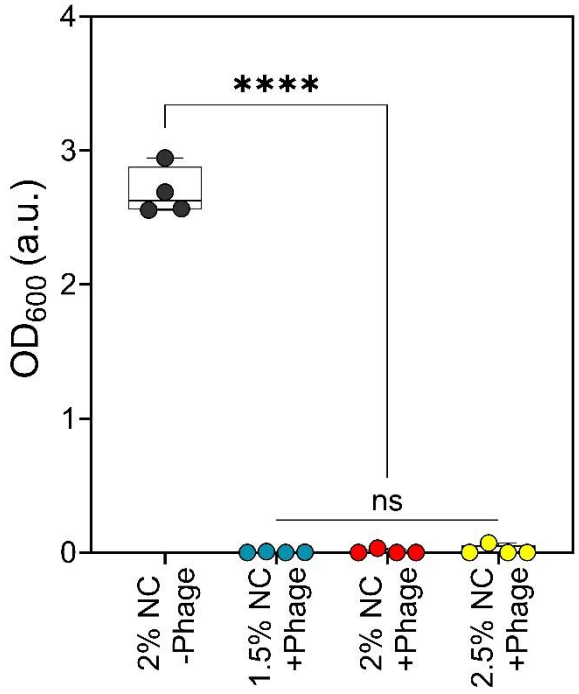

Figure S8. Turbidity measurement of the supernatant in biofilm prevention assay

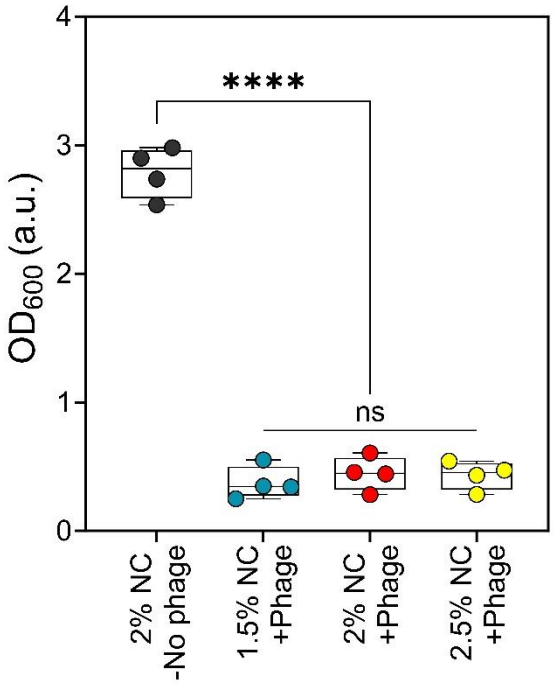

Figure S9. Turbidity measurement of the supernatant in biofilm dispersion assay

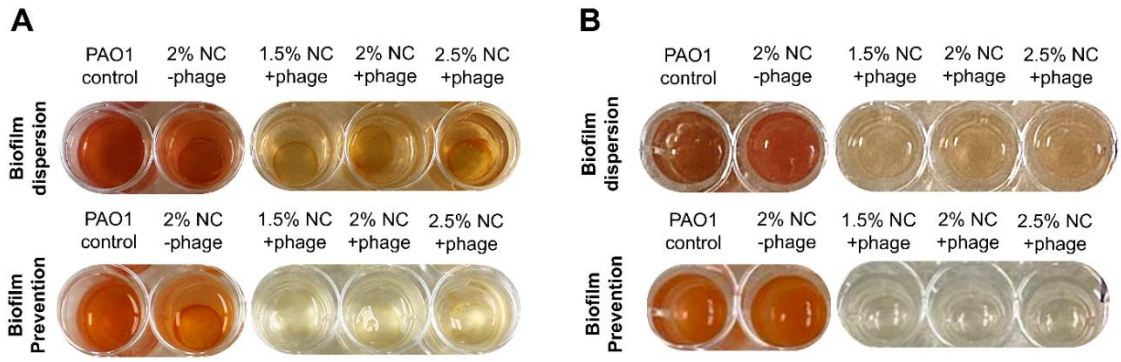

Figure S10. Representative images of wells for metabolic activity measurements using XTT assay. The metabolic activity of adhered biomass and the supernatant solution in each well was measured for both biofilm dispersion and prevention. Color change in wells containing hydrogels after removing the supernatant and adding the XTT reaction solution to measure the metabolic activity of adhered biofilm after 24 hours treatment with phage loaded hydrogels in comparison with POA1 and no phage containing hydrogel (A). Color change correlated to metabolic activity of cells in the supernatant of the wells containing phage compared to POA1 and no phage containing hydrogel after mixing the supernatant and XTT reaction solution 1:1 volume ratio (B).

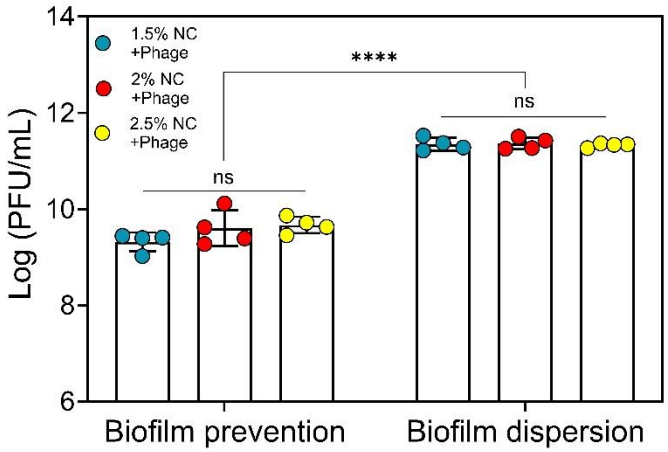

Figure S11. Concentration of phage at the end of biofilm prevention and dispersion

Chapter 5: Phage-Conjugated Liquid-Infused Implants Prevent Mortality Against an Implant-Associated-Infection in a Mouse Mode

Preface: In this chapter, a phage-conjugated liquid infused coating was developed to prevent bacterial infection and biofilm formation on the surface of orthopedic implants. The developed coating harnesses a dual functionality, combining the anti-adhesion properties of a liquid-infused surface with the bactericidal effects of phages. The biocompatibility and efficacy of this coating were tested in both *in vitro* and *in vivo* mouse model.

Contribution: This work was an equal collaboration between me and Martin Villegas. Martin Villegas developed the Liquid Infused Coatings, conducted *in vitro* mammalian cell culture and *in vivo* animal studies with help of Sara Rahmani and two undergraduate students, Taylor Kramer and Elise Schwarz. I helped with sample preparation, propagated, and purified different phages, conducted all the bacterial cultures, *in vitro* bacterial and phage assays. I analyzed the samples collected from animals and conducted bacterial assays on them with help from Mathura Thirugnanasampanthar. Martin Villegas wrote the original draft with input from me and others. Both Martin Villegas and I analyzed the results and edited the manuscript. The project was conceptualized by Dr. Tohid Didar and conducted under supervision of Dr. Tohid Didar and Dr. Zeinab Hosseinidoust. Dr. David Wilson provided scientific support from a clinical perspective.

Citation: This work is in preparation for submission.

Phage-Conjugated Liquid-Infused Implants Prevent Mortality Against an Implant-Associated-Infection in a Mouse Mode, Martin Villegas,[Ψ] **Fereshteh Bayat,**[Ψ] Sara Rahmani, Mathura Thirugnanasampanthar, Taylor Kramer, Elise Schwarz, David Wilson, Zeinab Hosseinidoust, Tohid F. Didar.

[Ψ] Equal contribution

5.1. Abstract

Implant-associated infections (IAIs) continue to be one of the top medical complications in modern medicine. Eradicating an IAI can be difficult due to the bacteria's ability to form a biofilm on the medical device. A biofilm is a surface-bound bacterial community encapsulated in an extracellular matrix, which promotes bacterial attachment and creates a protective barrier against antibiotics and the immune system. If the infection is not treated promptly, severe complications can arise, including implant failure, tissue trauma, chronic infections, or sepsis. Resent strategies have been developed to prevent medical implant infections. Here, we developed a bacteriophage conjugated liquid-infused surface (LIS) coating capable of repelling and killing bacteria. Furthermore, this coating contained a collagen layer, which promoted bone cell adhesion and proliferation. The fabricated coating was tested *in vivo*, in a sepsis mouse model using the highly pathogenic *Pseudomonas aeruginosa* bacteria. Mice containing the bacteriophage liquid-infused (Phage-LIS) coated implants had zero mortalities compared to groups containing untreated titanium implants (90% mortalities) or liquid-infused coated implants (70% mortalities). We envision a modular coating using therapeutic bacteriophages within a repellant LIS coating to prevent IAIs, along with biomolecules to promote tissue integration dependent on the application.

Keywords: Titanium implant, Liquid infused, LIS, AMR, Phage, Antibacterial, Coating, Sepsis, mouse model

5.2. Introduction

Titanium and titanium alloys continue to be some of the most sought-after materials for medical implants due to their unique material properties. Titanium provides high resistance to degradation, fatigue, and wear while providing high moduli and strength.[1,2] Furthermore, titanium alloys, especially grade 5 and grade 23, provide high corrosion resistance and display no cytotoxic characteristics.[3] For these reasons, titanium-based medical implants have been used in various applications, from orthopedic and dental implants to cardiovascular stents and mechanical heart valves.[4] Despite implant material or application, implant-associated infections (IAIs) remain one of the top medical complications in modern medicine. IAIs are the highest cause of implant failure in orthopedics,[5,6] and dental applications,[7] requiring lengthy hospital stays, prolonged antibiotic regimens, and multiple surgeries to eradicate the infection. Even when the probability for an IAI is low, as is with cardiac implants (1-6%), the risk for complications or mortality is substantial (27.5%),[8] accounting for a higher medical and financial burden to the individual and the medical institution. If an IAI is not diagnosed and treated promptly, severe complications can occur, including the possibility of sepsis. Sepsis is a clinical syndrome where an infection causes a dysregulated immune response.[9] Moreover, sepsis can quickly result in septic shock, which is characterized by failure of the circulatory system, which may result in multi-organ failure and mortality.[10]

Eradicating an established implant-associated infection can be complicated due to biofilm formation on the implant's surface. A biofilm is a self-secreted polymeric layer that protects surface-bound bacteria colonies.[11] The secreted extracellular matrix (ECM) is composed of extracellular DNA, polysaccharides, and glycoproteins, among other molecules, which promote cell adhesion, bacteria cell-to-cell communication (quorum sensing), and protects the bacterial cells from systemic antibiotics and the host's immune system.[11–14] In fact, it has been shown that bacteria in biofilms are 1000 times more resistant to antibiotics compared to planktonic bacteria.[15] **Figure 1a**. displays an oversimplified schematic of the evolution of biofilm formation. First, planktonic bacteria colonize the surface, where it proliferates, matures, and produces ECM. The ECM can then promote additional bacterial attachment, and in some cases, multi-species biofilms can be formed, increasing the

infection's complexity. Finally, bacteria can be expelled from the biofilm to create new colonies, thus repeating the cycle. Another complication caused by biofilms is that even if the infection is treated successfully, the leftover biofilm on a medical implant can facilitate the re-colonization of the surface by persisted cells causing an infection relapse.[13,16]

Implant-associated infection prevention continues to be a highly researched topic, leading scientists to formulate protective coatings on medical implants. There are two main methods for how these coatings operate. The first one kills the bacteria directly on the implant or in the peri-implant space, while the second category prevents bacterial attachment to the implant. Among the latter category, liquid-infused surface (LIS) research has become prominent due to its exceptional antifouling capabilities.[17–26] Liquid-infused surfaces, inspired by the *Nepenthes* pitcher plant, are surfaces containing a thin lubricating layer tethered through chemical and physical forces. The lubricating layer is chosen to be immiscible with the liquids that need repelling, thus creating a protective layer that prevents direct contact with the underlying substrate. Although LIS is a promising antifouling technology, LIS alone cannot indiscriminate between bacteria or the host cells, preventing important interactions required for proper host-implant integration. To circumvent this problem, our group has developed a plethora of multifunction LIS coatings, including LISs capable of preventing blood coagulation while promoting endothelialization in medical catheters;[21–23,25,27] LIS combined with antibiotics for a multi-stage protective layer;[28] and LIS conjugated with chitosan to enhance bone cell adhesion and proliferation on titanium implants.[29]

In this work, we set out to create a new generation of biofunctional liquid-infused coatings for medical implant materials. Here, we created a bacteriophage and collagen-conjugated LIS (Phage-LIS) coating on medical-grade titanium to promote cell attachment and proliferation while at the same time possessing the ability to repel and lyse bacteria. **Figure 1b**. displays the protective functions of the proposed coating. Here, the liquid-infused layer provides a non-adhesive film that prevents bacterial attachment, while the bacteriophage-collagen layer can kill the bacteria upon contact. Furthermore, the collagen layer increases the surface area for bacteriophage attachment and provides anchor points for proper adhesion and integration with the host's cells. Bacteriophages, also known as phages, were

chosen as the antibacterial agent due to their high stability, specificity, and self-dosing ability by reproducing themselves on site upon infecting bacterial pathogens.[30,31]

Even though phages were discovered in 1915,[32] their medical and research value has been greatly overshadowed by the discovery of antibiotics in the 1940s.[33,34] However, with the rise in antibiotic resistance and the creation of bacterial super-bugs,[35,36] bacteriophages have emerged as promising alternatives to antibiotics. Bacteriophages are mainly classified into two categories. The first is lytic or virulent phages due to their fast lytic action. Soon after a bacterium has been infected, the injected genome takes control of the bacteria's reproduction system to replicate itself, and newly formed phages lyse the bacteria from within, thus releasing the progeny phages into the environment. The second category of phages is known as temperate or lysogenic phages. Upon infection, lysogenic phages incorporate their genome into the bacterial genome, which stays dormant for a prolonged period. Upon an external trigger, the phage's genome awakens and transforms into the lytic life cycle to reproduce and release new progeny phages.[37] Because of this distinction, lytic phages are preferred for therapeutic applications, creating an immediate antibacterial effect and reducing the probability of horizontal gene transfer of virulence factor by temperate phages.[38]

The created Phage-LIS coating was optimized against *Pseudomonas aeruginosa*, the most common and hard to treat gram-negative bacterial pathogen in implant-associated infections.[39–41] The coating displayed an active liquid-infused layer through low sliding angles while promoting osteoblast-like cell adhesion and proliferation and showed no cytotoxicity. Moreover, the Phage-LIS coating reduced bacteria by 99.94% compared to infected untreated titanium surfaces *in vitro*. The Phage-LIS coatings were also tested *in vivo* in a sepsis mouse model. The treated samples prevented the mortality of mice with phage-treated implants. In contrast, the groups with untreated titanium implants or LIS implants displayed a 90% and 70% mortality rate after seven days, respectively.

We conceptualize a modular coating with the superior antifouling properties of LIS and the integration of cocktail bacteriophages to protect the implanted surface. Moreover, the multifunctional LIS can include modulatory molecules to promote proper biocompatibility

and integration with the host. These modular coatings can be adapted depending on the application and have the potential to be applied to other biomaterials where infection prevention is required.

5.3. Results and discussion

To create the phage-collagen liquid-infused coating (Phage-LIS), the titanium discs were first sanded, cleaned, and autoclaved, as discussed in the methods section. It is worth noting that after the sterilization process, the titanium samples were handled with sterile tools inside a biosafety cabinet (BSC) because phage-coated samples cannot be re-sterilized. Titanium discs were placed in sterile Petri dishes and oxygen-plasma treated to hydroxylate the surfaces. Immediately after, the samples were placed inside a vacuum chamber alongside Trichloro (1H,1H,2H,2H perfluorooctyl) silane (TPFS), and (3-Glycidyloxypropyl) trimethoxysilane (GPTMS) for the chemical vapor deposition (CVD) of the mixed silanes onto the surface (**Figure 1c**). In these silanes, the chlorine and methoxy groups are hydrolyzed into hydroxyl groups, which can covalently bond to hydroxylated surfaces via a condensation reaction.[42] The epoxy group of GPTMS is then capable of reacting with amine groups found on bacteriophages and collagen. On the other hand, the fluorine groups of the fluorosilane (FS) were used to render the surface hydrophobic and increase the affinity to the fluorinated lubricant Perfluoroperhydrophenanthrene (PFPP). After the CVD process, the silanized titanium discs were placed inside 48-well plates and submerged in a mixture containing the bacteriophages, collagen, and additional GPTMS linker molecules for 4 hours. Then, the samples were washed thoroughly with phosphate buffer saline (PBS) and stored at 4 ℃ in PBS until needed. A quality control step was implemented since the bacteriophage-coated surfaces cannot be re-sterilized. Here, the coated samples were submerged in antibiotic-free cell media and placed in a cell incubator for 24 hours. After 24 hours, the samples were checked under the microscope for microorganisms. After testing, the samples were allowed to air dry inside the BSC and then lubricated with PFPP to produce a liquid-infused interface.

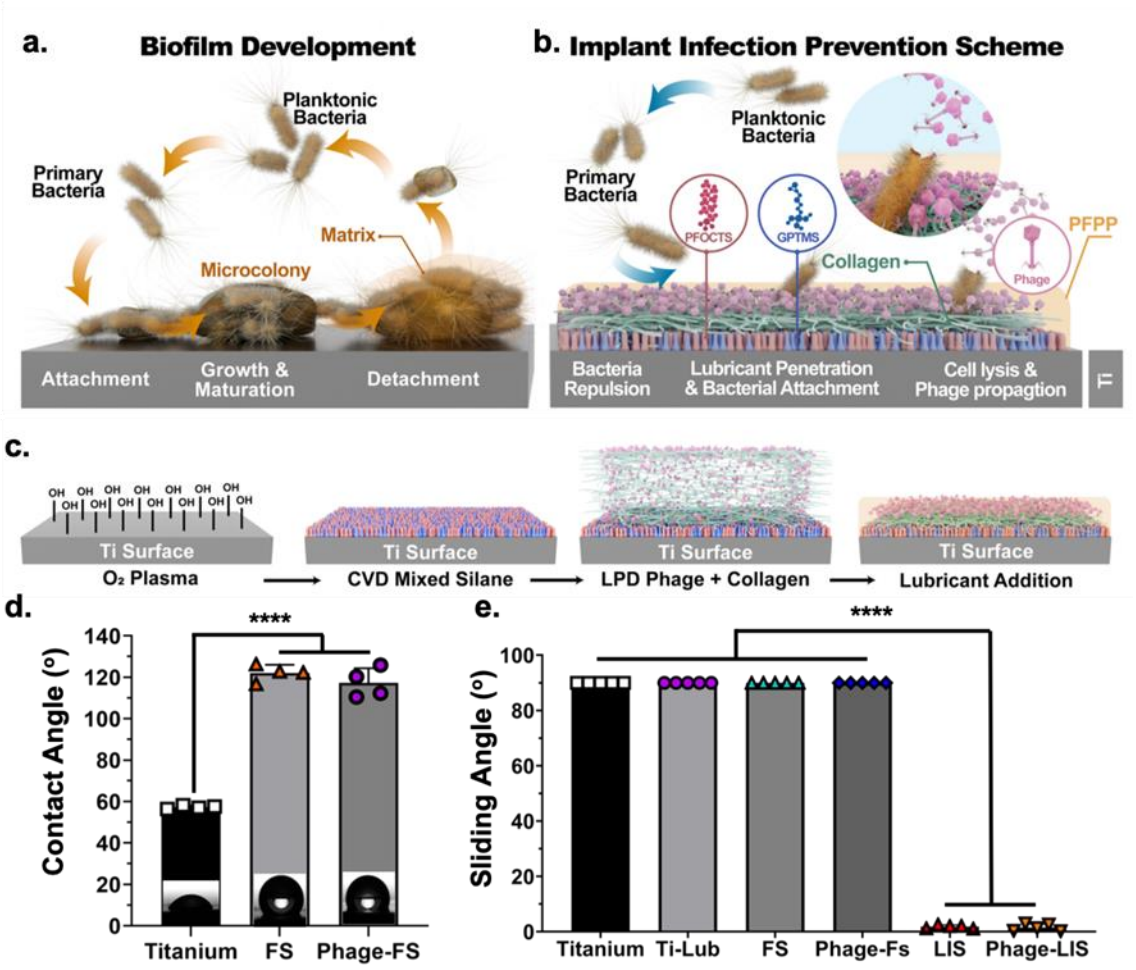

Figure 1. Implant Infection Prevention, Device Fabrication, and Wettability. a) Biofilm formation scheme. **b)** Infection Prevention scheme displaying bacterial cell repulsion, lubricant penetration, and cell lysis due to bacteriophage infection and propagation mechanism. **c)** The surface fabrication process displays the surface's hydroxylation, mixed silane deposition, and collagen-bacteriophage layer addition. Finally, the coated surfaces are lubricated with a fluorinated lubricant to form a liquid-infused layer. **d)** Water contact angle between pristine titanium (Ti), Ti after fluorosilanization (FS), and Ti with the addition of collagen, fluorosilane, and bacteriophages (Phage-FS). **e)** Water sliding angle for the coated titanium surfaces, both bare or lubricated with PFPP. Part d) and e) were analyzed using an ANOVA, n=4 for part d) and n=5 independent samples for part e). '***' represent a p-value of $P < 0.001$, and '*' represent a p-value of $P < 0.05$

5.3.1 Liquid-Infused Layer Testing

Contact angle and sliding angle experiments were conducted to test the integrity of the liquid-infused coating. The water contact angle was used as a rapid test to check if the fluorosilane layer rendered the coating hydrophobic. The results in **Figure 1d**. did align with our hypothesis. Here, untreated samples (Ti) had low contact angles that can be

characterized as being hydrophilic (less than 90 deg.).[43] On the other hand, fluorosilanized titanium (FS) obtained water contact angles of ~120 deg, reflecting a strong hydrophobic surface. Moreover, the optimized coating composed of the mixed silane layer and the collagen-phage layer (Phage-FS) remained hydrophobic despite collagen and phage being hydrophilic in nature.[44–47] Since the Phage-FS was hydrophobic, the water sliding angles were tested to evaluate the LIS characteristics (**Figure 1e**.). At first glance, water droplets on non-lubricated surfaces tend to pin on the surfaces and thus remain immobile even after reaching high tilting angles. Notably, droplets pinned on angles exceeding 90 degrees to the horizontal plane were given a maximum angle of 90 degrees. As expected, lubricated samples lacking the proper affinity to the lubricant caused the droplets to pin on the surface (Ti-lub). This predictable behavior is caused by the higher affinity between the Ti substrate and water, causing the droplet to displace the lubricant and reach the Ti surface.[43] Conversely, surfaces that were properly fluorosilanized and lubricated resulted in low sliding angles (< 5°), confirming a stable liquid-infused coating on the liquid-infused titanium (LIS) and the titanium coated with the phage-collagen liquid-infused layer (Phage-LIS). These results mirror the outcomes observed in our previous studies,[28,29,48] despite the differences in coating composition or variations in coating deposition methods.

To test the feasibility of a Phage-LIS, *P. aeruginosa* strains PAO1 and bioluminescent PAO1 (PAO1-lux) were screened to find strong lytic phages. **Figure S1a** shows that PAO1-lux was infected by JG004 and E79 phages, but was not infected by P32, P04, or PP7 phages. JG004 and E79 phages were tested independently and in combination at different Multiplicity of Infection (MOI) to evaluate their efficiency at impairing bacterial growth and to test if their combination had complementary antibacterial effects. The MOI represents the ratio between bacteriophage and bacteria, where a larger number indicates a higher phage concentration compared to bacterial concentration. **Figures S1d-f**. show that both JG004 and E79 were able to suppress bacterial growth for at least 12 hours, even at low MOIs, when used individually. However, the bacteria population increases thereafter, due to rise of resistant mutants. Furthermore, the combination of JG004 and E79 did not improve the outcome (**Figure S1f**), showing similar growth curves as when tested individually (**Figure S1d-e**), therefore implying a non-complementary bacteriophage set. Similar tests were performed on the non-bioluminescent PAO1 bacteria strain, which was

susceptible to five different phages (**Figure S1b**). The PAO1 bacteria strain and the P32 and E79 phage combination were chosen after extensive testing. The results in **Figure 2h** show that both P32 and E79 effectively reduced bacterial growth for at least 12 hours when tested individually at the very low MOI of 0.001. However, the P32-E79 combination showed exceptional bacterial growth suppression for at least 24 hours of incubation (**Figure 2h,** red line). These results infer complementary bacteriophage pair, reducing the bacteria's viability and the rise of resistant mutants. Notably, the phage pair (P32-E79) cannot be tested against PAO1-lux as this strain was not infected with P32. The high specificity shown by these phages demonstrated that even similar bacterial strains may have subtle genetic variations between strains from different labs. This limited our options in designing a phage cocktail against the bioluminescent strain. It is worth mentioning that in real life phage therapy cases, isolated pathogens are screened against a larger library of phages (phage banks) to find the suitable phages for the target pathogen. For the reasons stated above, even though PAO1-lux was initially used to optimize the bacterial load of the mouse sepsis model (described below), the PAO1-lux strain was not adopted for further testing due to the lack of synergistic phage pairing. Once the phages were chosen, the titanium discs were coated and tested *in vitro* against mammalian and bacteria cells.

The engineered Phage-LIS coating was tested against osteoblast-like SaOS-2 cells to assess the potential use in orthopedic and dental applications, where bone integration is essential.[29,49–51] **Figure 2a-b** shows a representative image of cells on the fabricated coatings. Here, untreated titanium showed the highest number of cells on the surface, followed by Phage-collagen (Phage-FS and Phage-LIS) coated surfaces. Lastly, fluorosilanized and LIS titanium contained the fewest cells (**Figure 2b**). When evaluating the cell morphology, LIS-coated titanium showed cells clumping on the surface, indicating poor cell adhesion.[29,52] Conversely, the cells growing on titanium or Phage-LIS coated samples were seen spreading and creating a monolayer, indicative of a healthy cell population. [29,52] Further testing was performed on LIS, Phage-LIS, and Ti (control) surfaces to evaluate if the coating had any cytotoxic effects or if it impaired the production of alkaline phosphatase (ALP). Alkaline phosphatase is an enzyme produced by osteoblasts cells in the process of bone mineralization.[53] **Figures 2c** and **2d** show that neither the LIS nor the Phage-LIS significantly affected cell viability or ALP production compared to

untreated titanium surfaces. Altogether, these results indicate that the Phage-LIS coating did not adversely affect mammalian cells. Moreover, the collagen-phage layer increased cell adhesion and proliferation compared to LIS-coated titanium, which aligns with the observations seen in our previous projects.[29]

Bacteriophage infectivity was tested on the coated titanium discs using a diffusion assay on PAO1 bacterial lawns (**Figure S1c**). The results showed that the phage-coated Ti samples had lytic activity in the presence and absence of the PFPP lubricant, indicating that the phage remained viable through the coating process and that phage-bacteria interactions were possible. Further testing was performed using a liquid assay to evaluate the bacteria colony forming units (CFU) and phage plaque forming units (PFU) after a 6 and 24-hour incubation. First, liquid-infused titanium, Phage-LIS coated, and untreated samples were placed in a 48-well plate and submerged in 400 µL of PAO1 (10^7 CFU/mL) containing solution. The well plate was set in a shaking incubator at 120 rpm and 37°C. After the incubation periods, the solution and the samples were tested for CFU and PFU, and the results are displayed in **Figure 2e-g**. The CFU found on the surfaces indicated that LIS and Phage-LIS coated samples reduced the bacterial burden on the surface compared to untreated Ti discs. After the 6-hour incubation, Phage-LIS had a 99.6% bacteria reduction compared to untreated Ti surfaces. After 24 hours, LIS had a 0.7 log reduction compared to untreated Ti samples, while Phage-LIS had a 3.2 log reduction on the surface of the samples. Not surprisingly, the bacteria's CFU was also reduced in the solutions containing the Phage-LIS samples (99.96% reduction compared to Ti), while no CFU reduction was seen in solutions containing LIS-treated when compared to untreated Ti controls. These results highlight the benefit of having a phage layer to protect the implant material and the nearby space. The plaque forming units were also quantified from the Phage-LIS treated discs and the solution. Interestingly, the phage availability increased from $10^{6.5}$ PFU on the surface of the treated Ti discs to ~10^{11} PFU of phage found in the solution after 6 hours. This drastic increase in antibacterial agents is one of the most remarkable characteristics seen with bacteriophages otherwise not found with conventional antibacterial agents. This means even a thin layer of phage coated on an implant surface could lead to replication and release of a large population of phages on site. In other words, antibiotic,[54–56] metallic,[57–59] or antimicrobial peptide[60,61] protective coatings are limited by the initial concentration,

while phages can increase in concentration if the phage successfully infects bacteria. Therefore, providing on demand bactericidal effect and having self-dosing properties. To further test the engineered Phage-LIS coating, an infectious murine model was created to assess the coating's ability to prevent severe morbidity or fatality in a sepsis model.

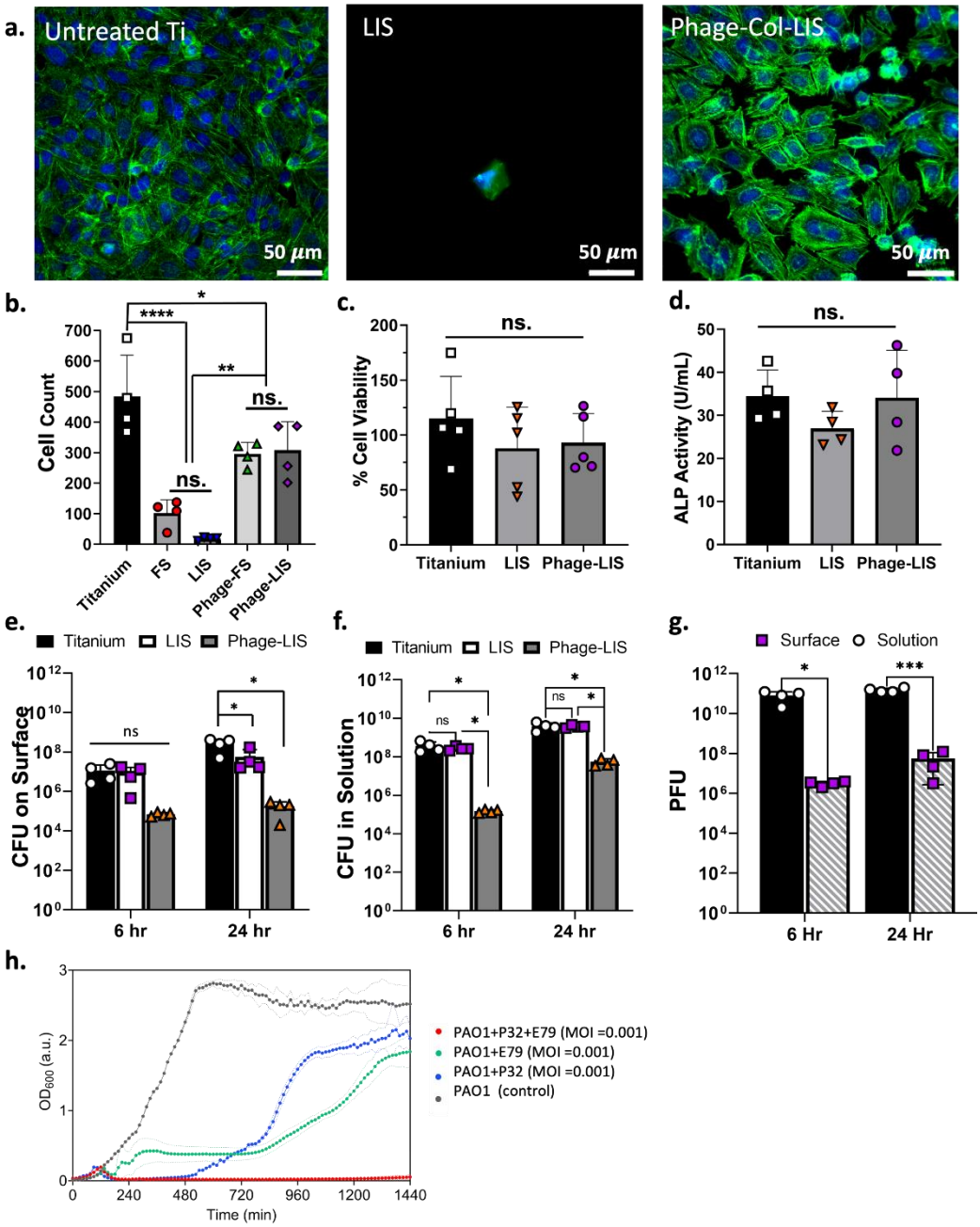

Figure 2. *In vitro* surface testing with mammalian and bacteria cells. a) Image representation of SaOS-2 cell population and morphology after a 3-day incubation period.

b) SaOS-2 Cell count after a 3-day incubation period. n=4 independent surface for all surfaces. **c)** Cell cytotoxicity assay after a 3-day incubation period of SaOS-2 cells. n= 5 independent surfaces. **d)** Alkaline phosphatase activity after a 3-day incubation of SaOS-2 cells. n= 4 independent surfaces n=4). **e)** Colony Forming Units (CFU) of P. aeruginosa on the surface of Ti and treated Ti samples. **f)** Planktonic CFU of P. aeruginosa left in a solution containing Ti and treated Ti samples (n=4). **g)** Plaque Forming Units (PFU) of phage-coated samples on the surface and in solution (n=4). **h)** Optical density growth curve of PAO1 bacteria with bacteriophages P32, E79 and synergistic combination of P32-E79. Parts b), c), d), e), and f) ANOVA were analyzed using an ANOVA, and part g) was analyzed using a student t-test. '****' represent a p-value of $P < 0.0001$, '***' represent a p-value of $P < 0.001$, '**' represent a p-value of $P < 0.01$, and '*' represent a p-value of $P < 0.05$, ns denotes a no statistical difference.

5.3.2 Establishing a Mouse Sepsis Model

A simple subcutaneous sepsis model was created before examining the engineered Phage-LIS coating *in vivo*. During the model development, 30 mice, 15 male (M) and 15 female (F), were infected with the bioluminescent PAO1-lux strain to monitor the infection progression. The mice were divided into six groups: PBS (control) and infected groups with bacterial loads ranging from 10^3 to 10^7 CFU. Furthermore, the groups were assorted such that each group had five mice (3M/2F or 2M/3F). During the surgery, the mice went under anesthesia, shaved, and their dorsal section was prepared for a surgical incision. The surgical incision was created roughly 2 cm below the scapulae, and then, a subcutaneous pocket was created through blunt dissection. A sterile and untreated titanium disc was inserted into the subcutaneous pocket, along with 10 µL of PBS or a predetermined bacterial concentration. Then, the wound was closed with autoclips, and the mice were set in a recovery cage before returning to their home cage. The mice were monitored daily for signs of sickness based on the categories displayed in Table S1. In addition, the mice were monitored every other day using an IVIS CT bioluminescent imaging equipment, which started the day after the surgery. **Figure 3** displays the observations seen between the tested groups. **Figure 3a** shows a representative bioluminescent image for the female mice infected with 10^6 and 10^7 CFU. Here, it can be seen that two mice (infected with 10^7 CFU) reached the endpoint before their second imaging on day three post-surgery. Furthermore, two of the remaining three mice (infected with 10^6 CFU) reached the endpoint by day eight

post-surgery. Interestingly, mice infected with 10^5 CFU or lower had a 100% survival rate. Conversely, mice infected with 10^6 and 10^7 CFU reached a 40% survival rate on days 8 and 2, respectively. It is worth noting that the symbol '#' in **Figures 3c-3f** represent the number of mortalities on each day, while **Figure 3b** shows the combined survival rates for each group. When analyzing the overall health differences between groups, some interesting trends appeared. First, mice infected with 10^5 CFU or lower displayed no physical or behavioral changes compared to control mice injected with PBS (**Figure 3f**). Second, mice infected with 10^4 CFU or lower did not have a significant drop in weight post-surgery, with most groups showing an increase in weight (**Figure 3d, 3e**). Furthermore, most mice groups recovered any weight loss within 2-3 days after surgery for groups infected with 10^5 CFU or lower. Contrariwise, mice infected with 10^6 and 10^7 had the largest weight loss, with most failing to recover to their original weight. When looking at the bioluminescent signal (**Figure 3c**), all groups showed a significantly higher signal on the first-day post-surgery than the PBS control group. Generally, the bacteria signal plateaued until days 5-7, when the signal started decreasing. This decrease in signal was likely caused by the activation of the adaptive immune response and overall decrease in bacteria. Apart from the mice infected with 10^6 and 10^7 CFU, all groups reached a bioluminescent signal comparable to the background noise by day 7-13. Based on these observations, we concluded that mice infected with 10^5 CFU or lower did not present any significant health issues, with all of these groups fully recovering nearly a week post-infection. In contrast, mice infected with 10^6 and 10^7 CFU showed relatively high bioluminescent signals throughout the 14-day experiment and reached a 60% mortality rate. The main difference between 10^6 and 10^7 CFU infected groups was in the onset of sickness and mortality, which was much sooner for the 10^7 CFU-infected group than the group infected with 10^6 CFU. Interestingly, the mortality rate was twice as high for female mice compared to male mice between 10^6 and 10^7 CFU-infected groups. Even though this mortality rate was significant, it could be explained by size difference, in other words, female mice might be more vulnerable to such high bacterial loads, since they weigh ~33% less than male mice. However, further testing should be performed to describe this phenomenon since sex hormones do have an impact on the regulation of the immune system. For example, a study performed by Sakr et al., concluded that even though the prevalence of severe sepsis was lower in females compared

to male patients, females had a higher mortality rate in the ICU.[62] Furthermore, multiple sclerosis studies have shown a direct link between sex hormones and the regulation of the immune system in the progressions of this disease,[63] therefore, there is a plausibility that sex hormones also impact the immune system in the progression of sepsis. Despite these sex difference, we chose to test our engineered coatings in both sexes, against a higher bacterial load (10^8 CFU) to have a higher mortality rate compared to the 60% mortality seen with 10^6 and 10^7 CFU bacterial loads.

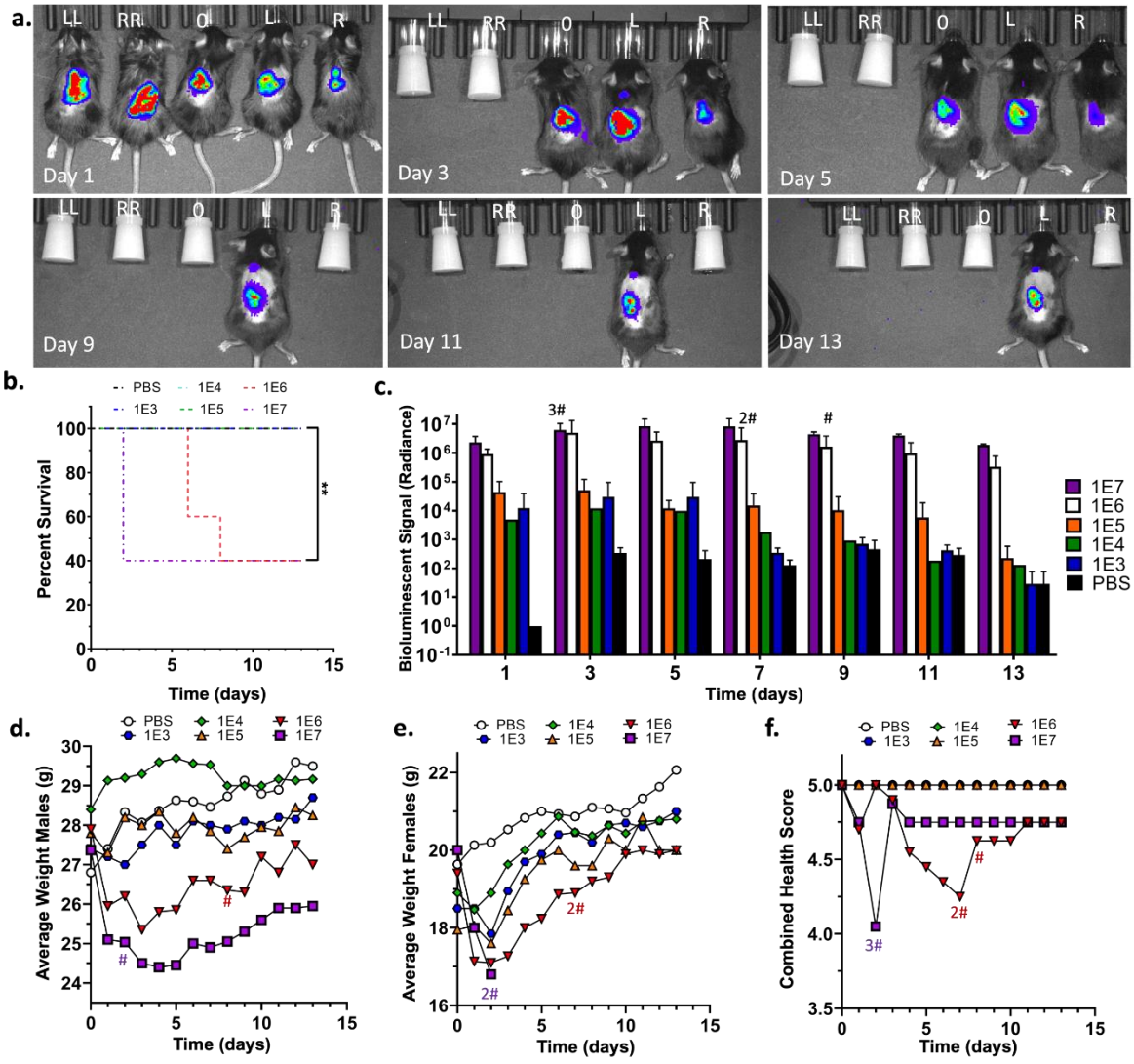

Figure 3. ***In vivo*** **Optimization of Bacterial Load for Sepsis Model.** Mice were implanted with a bare titanium surface, and bioluminescent PAO1-lux bacteria were introduced into the subcutaneous cavity with the following concentrations: $1x10^7$, $1x10^6$, $1x10^5$, $1x10^4$, $1x10^3$ CFU, and PBS as control. **a)** Representative bioluminescent imaging of female mice

with bacteria concentrations $1x10^7$ CFU for LL and RR and 1x106 CFU for mice labeled 0, L, and R. Missing mice represent mice that have reached the endpoint. **b)** Kaplan-Meier curve denoting the survival probabilities of each group of mice. **c)** Bioluminescent signal from mice with different bacterial loads. **d)** Average weight for male mice with different bacterial loads. **e)** Average weight for female mice with different bacterial loads. **f)** Average health score was given to mice for their appearance and attitude during their daily survey, as explained in Table S1, located in the supporting information section. Note: a score of 3 or lower in either category represented a mouse reaching the endpoint. The '#' symbol denotes the number of mice reaching the endpoint at different times. Part b) was analyzed using a Log-rank test. '**' represents a p-value of $P < 0.01$.

5.3.3 Bacteriophage-LIS Testing in Mouse Sepsis Model

With the mouse sepsis model established, the Phage-LIS coating was tested and compared against LIS and untreated titanium controls. For this experiment, 30 mice were divided equally between the 3 groups. In order to reduce the number of mice used, uninfected controls were not repeated in this experiment, therefore abiding by the 3Rs principles of animal studies.[64] The same surgical protocols were used for this experiment as in the previous section, where the mice were anesthetized, surgically prepared, and operated on to create a subcutaneous pocket. Titanium discs (either untreated or treated with either LIS or Phage-LIS coating) were then inserted in the subcutaneous space, and 10 µL of non-bioluminescent PAO1 bacteria (10^8 CFU) was pipetted into the subcutaneous cavity. Finally, the incision was closed with autoclips, and the mice were placed in a recovery cage for the anesthesia to wear off before returning to their home cage. The results from this experiment are summarized in **Figure 4**. The results demonstrated increased morbidity and higher mortality rates (**Figure 4e**) compared to those previously seen (**Figure 3b**). After seven days, the mortality rates for untreated Ti and LIS groups were 90% and 70%, respectively. Conversely, mice with Phage-LIS treated discs had a 100% survival rate (**Figure 4e**). When analyzing the data in more detail, most of the early mortalities occurred in female mice, which occurred on the first-day post-infection (purple '#' in **Figure 4** bi-cii). At the end of the seven days, the Ti group had a single male survivor, while the LIS group had three male survivors. Even though the survivor's weight and health scores did not recover fully for the Ti and LIS groups, these scores plateaued, indicating that their adaptive immune system was preventing the progression of the infection. The experiment was terminated after only seven days, mainly due to the creation of skin lesions, as seen in

Figure 4, column a. These wounds carried the risk of wound reopening, which would have resulted in implant loss and the introduction of other pathogens. Interestingly, none of the male mice containing the Phage-LIS implants exhibited these wounds. However, a few Phage-LIS treated female mice displayed similar but smaller necrotic wound patterns. The skin lesions differences between male and female mice (Phage-LIS group) may have occurred due to anatomical differences related to skin thickness and available immune cell within the skin tissue.[65,66] Although the male-female differences in wound healing were not further explored in this study, these differences should be further investigated to create more robust animal models or extract information relevant to human studies.

After reaching the endpoint, the mice were harvested, and their blood, liver, spleen, and titanium implants were collected for further analysis. Interestingly, the blood of Phage-LIS bacteria showed no bacteria on all collected samples, while some mice in the untreated Ti and LIS groups displayed active bacteria in the blood (**Figure 4f**). Furthermore, the blood samples collected from Phage-LIS samples had a bacteriophage concentration of ~ 10^3 PFU/mL, indicating that the phage was present at the implant site and circulating throughout the body. Not surprisingly, the bacteriophages were also present in other tissue, including the liver and spleen, although at lower concentrations than the phage on the titanium discs (**Figure S2d**). Scanning electron microscopy (SEM) images from the recovered titanium implants showed that Phage-LIS or LIS samples had little to no bacteria present on the implant compared to untreated Ti (**Figure 4 column d**). Moreover, the SEM images reveal low tissue deposition and traces of what once were live cells on the untreated Ti surfaces. On the other hand, both LIS and Phage-LIS titanium discs show the availability of tissue and cells on the surface of the recovered implants. When quantifying the bacteria found on the recovered titanium coupons or on the collected organs, it was discovered that there was no significant difference in bacteria quantity between groups (**Figure S2a-c**). However, the factors influencing these results must be discussed to weigh the CFU values fully. First, the difference in endpoints needs to be accounted for. While many of the mice in the Ti and LIS groups reached endpoint 1-3 days after infection, their bacteria population grew to the same level as those found on Phage-LIS samples after 7 days. This meant that the phage initially suppressed the bacteria growth, giving the adaptive immune system a fighting chance and preventing early mortality. Secondly, it must be understood that the

bacterial colonies retrieved from the phage samples (blood, liver, spleen, and Phage-LIS titanium) displayed phage-infected colonies, as seen in the plates in **Figure S3**. Even though the phage-infected colonies are being reported here, it must be noted that these colonies did not survive after a few days on the agar plates. This revelation highlighted a limitation in our quantification tools, and a different metric should have been chosen to compare bacteria virulence other than quantifying bacteria populations. Lastly, even though the reported CFUs might not be an accurate metric for cell population (due to the continuous lysis of bacterial cells), there also exists the possibility that bacteria mutations occurred, rendering both P32 and E79 phages ineffective. These mutations could account for an increased colony population, but these mutations may also change the virulence of the bacteria, as seen in other studies.[67,68] This point reiterates the need to use a more comprehensive testing set when comparing similar bacteria populations.

Another explanation for the high bacterial concentration in Phage-LIS group is the possibility that bacteria could diffuse to deeper parts of the tissue and not be exposed to phages circulating in the blood system. In other words, the phage could be obstructed by physical obstacles to reach to all the present bacteria in deeper tissue and organs in a sepsis model. Where failure in phage-bacteria interactions represent an obstacle in phage therapy,[69] as is with other bactericidal agents. It is worth mentioning that here we have developed a sepsis model to evaluate our phage-LIS coating performance at extreme conditions, and the presence of phage has led to decrease the mortality rate significantly, although there is still high concentration of bacteria present in the organs and on the coupons. There is a high chance that these bacteria have reduced virulence and produce lower amounts of toxins as reported in other phage therapy studies, which needs to be further evaluated. As is, this Phage-LIS coating is designed as preventative strategy, in real life cases, more phages can be administrated intravenously,[70] percutaneously, or via other administration routes such as intraperitoneal injection subcutaneous injection and intramuscular injection.[71] Moreover, adjunct antibiotic therapy can be used to complete the treatment as commonly reported in many cases.[72–75] Taking these point into account, there also exists the possibility that sepsis progression was nullified by the phage therapy, despite showing a high CFU numbers. This could be explained because phage, and phage proteins

have been shown to downregulate the immune response and reduce proinflammatory markers caused by bacterial endotoxins.[71]

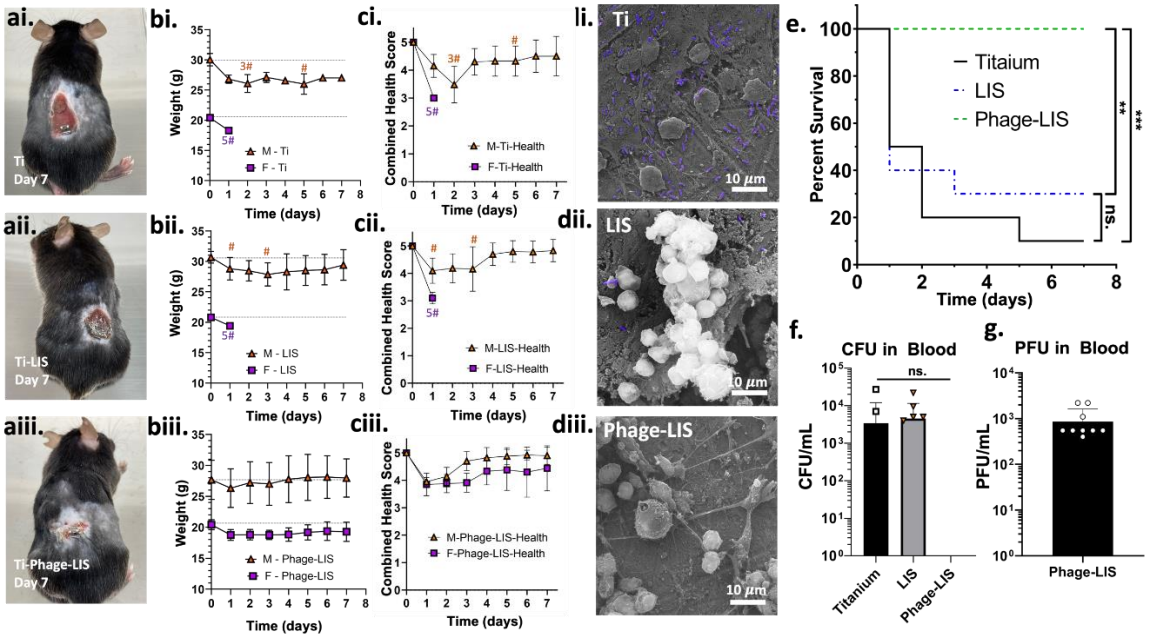

Figure 4. *In vivo* Results for Titanium and Coated Titanium Surfaces. Mice were implanted with either bare titanium, liquid infused (LIS), or Phage-LIS coated surface, and PAO1 bacteria was introduced into the subcutaneous cavity at a concentration of 1x108 CFU. **a)** Representative images of wounds created by the bacteria seven days post-infection. **b)** Average weight for male and female mice for Ti, LIS, and Phage-LIS groups. **c)** Average health scores given to mice for their appearance and attitude during their daily survey, as explained in Table S1, located in the supporting information section. Note: a score of 3 or lower in either category represented a mouse reaching the endpoint. **d)** Scanning Electron Microscopy images of excised titanium implants for Ti, LIS, and Phage-LIS groups. **e)** Kaplan-Meier curve denoting the survival probabilities of each group of mice. **f)** Colony Forming Units (CFU) found in blood samples of mice at the endpoint. g) Bacteriophage's Plaque Forming Units (PFU) found in blood samples of mice treated with phage-LIS coated implants at the endpoint. Note: the '#' symbol in figures b-c) denotes the number of mice reaching the endpoint at different time points. Part e) was analyzed using a Log-rank test, and part f) was analyzed using an ANOVA. '**' represents a p-value of $P < 0.01$ and n.s. for no statistical difference.

5.4. Conclusion

In this study we introduced a new generation of multifunctional liquid-infused coatings by adding bacteriophages and collagen into the LIS layer. The bacteriophages remained infective within the LIS coating, decreasing the bacteria's concentration on coated titanium

discs, as well as bacteria found in solution. The collagen layer on the Phage-LIS coated titanium enhanced bone cell deposition and proliferation compared to conventional LIS coated titanium samples. Which is an integral step for proper osseointegration in dental and orthopedic applications. Furthermore, the engineered coating was tested in a sepsis mouse model. The Phage-LIS coatings prevented the mortality of mice containing Phage-LIS implants. On the other hand, mice containing untreated Ti implants or LIS coated implants had 90% and 70% mortality rates, respectively. Overall, this study shows the potential use of phages-LIS coated implants as a prophylactic measure to reduce morbidity event in extreme infections. We envision this platform as a modular coating, where different phage cocktails and modulatory biomolecules can be interchanged based on the application.

5.5. Materials

Medical grade titanium alloy (grade 5, Ti6Al4V) sheets (12”x12”, 4 mm or 1 mm thick) were purchased from McMaster Carr (www.mcmaster.com) and laser cut into discs of 5 mm or 10 mm in diameter by CIM Metals Inc (www.cimmetals.com). Perfluoroperhydrophenanthrene (PFPP), Trichloro (1H,1H,2H,2H perfluorooctyl) silane (TPFS) 97%, (3-Glycidyloxypropyl) trimethoxysilane (GPTMS) 98%, Triton™ X-100, McCoy’s 5A modified medium, phosphate-buffered saline (PBS), bovine serum albumin (BSA), penicillin/streptomycin (pen/strep), and fetal bovine serum (FBS) were purchased from Sigma − Aldrich (Oakville, Canada). Phosphate-buffered saline (PBS) tablets and McConkey agar were purchased from VWR (Mississauga, ON, CA). Luria Broth (LB), agar powder Collagen I (rat tail), McCoy’s 5A modified medium, Trypsin–EDTA (0.25%), methanol-free formaldehyde, and Hoechst 33342 were purchased from Thermofisher Scientific (ON, CA). Phalloidin FITC Reagent, Cytotoxicity Assay (ab112118), and Alkaline Phosphatase Assay Kit (ab83369) were purchased from Abcam (abcam.com). Bacteriophages vB_Pae-Tbilisi32 (P32), JG004 (PO4). Pseudomonas aeruginosa (PAO1) strain was purchased from DSMZ (Germany) and PAO1-Lux from Dr. J. Goldberg's lab (Atlanta, GA, USA). Bacteriophages E79, PO4, and PP7 were purchased from Université Laval (QC, Canada).

5.6. Methods

Liquid-infused coatings were prepared similarly to our previous work.[28,29,48] Briefly, the titanium discs were sanded and polished using an orbital sander with grit papers ranging from 400 to 5000. Then, the discs were sonicated in acetone, 100% ethanol, and water for 5 min. to remove any debris. These washes were repeated until the final water wash was clear of debris. The samples were then autoclaved to sterilize the samples, and further manipulations were performed inside a biosafety cabinet (BSC) with sterile utensils as often as possible to maintain sterility. After autoclaving the samples, the titanium discs were placed in a plasma cleaner (Plasma Etch PE-100) for 5 min under medical-grade oxygen to hydroxylate the surfaces. Immediately after, the samples were placed in a vacuum chamber for the chemical vapor deposition (CVD) of TPFS (400 μL) for 3 h. at RT and -0.01 MPa vacuum pressure. Then, the samples were left on a hotplate at 60 ℃ overnight to finish the dehydration reaction. The samples were stored in sterile well plates at RT in the dark until needed. Before use, PFPP lubricant was added to each well, and excess was removed with a pipette to form the liquid-infused coating.

5.6.1 Preparation of combined Bacteriophage and Collagen Liquid-Infused Coating

The titanium discs were pretreated and sterilized, as discussed above. Then, the titanium discs were placed in an oxygen plasma cleaner at high power (150 W) using medical-grade oxygen at 480 mTorr for 5 min to hydroxylate the surfaces. Afterward, plasma-treated substrates were placed in a vacuum chamber alongside a petri dish with TPFS (400 μL) and GPTMS (20 μL). The chemical vapor deposition of TPFS and GPTMS was carried out for 3 h at room temperature under vacuum at -0.01 MPa. Immediately after the CVD process, the samples were placed in sterile well plates and submerged in a Phosphate Buffer Saline (PBS) solution containing collage (3 mg/mL) at a PBS to collagen 100:1 ratio. Furthermore, the PBS collagen solution also contained bacteriophages E79 [10^{11} PFU/mL], P32 [10^{8} PFU/mL], and GPTMS [10 μL/mL]. The samples were left in the solution for 4 h. at RT to allow for the deposition and binding of the collagen/phage layer (**Figure 1c**). Then, the samples were washed three times with sterile PBS, changing the samples to clean wells in between washes to reduce unbound bacteriophage redeposition. Then, the samples were

stored in the fridge at 4 °C while submerged in sterile PBS. Before use, the samples were removed from the fridge and placed in sterile well plates to dry inside the BSC. Finally, the samples were lubricated with PFPP by submerging them in the lubricant, followed by removing excess lubricant prior to use.

5.6.2 Contact Angle and Sliding Angle Measurements

Contact angle and sliding angle measurements were used to test the surfaces' wettability. Contact angle measurements were performed using a Kruss DSA30 optical goniometer (www.kruss-scientific.com) with Kruss Advanced software (v1.14.1). Contact angle measurements were taken using a 2 µL droplet of Milli-Q water at room temperature. A minimum of four independent samples were tested with four different droplets per sample. The sliding angles were measured using a digital angle level (ROK, Exeter, UK) on samples of untreated titanium (control), fluorosilanized titanium (Ti-FS), and phage-collagen-FS treated titanium (phage-FS). These samples were tested with or without PFPP lubricant, where FS-treated and lubricated samples created a liquid-infused interface. To obtain the sliding angles, the digital level was first calibrated to a horizontal leveled surface, and then samples were placed on the apparatus, followed by the addition of PFPP lubricant (if needed). The excess lubricant was removed by tilting the samples vertically for 30 seconds before testing. The digital level was reset to the horizontal position, and a 5 µL droplet of deionized water was placed on the samples. The tilting stage was raised gently, and the sliding angle was taken as the smallest inclination angle when the droplet started to slide. If the droplet failed to slide past the angle of 90 degrees, the sliding angle was recorded as a maximum of 90 degrees to the horizontal plane. The measurements were repeated four times on each sample, and a minimum of five samples were used in each group tested.

5.6.3 *In vitro* cell studies

5.6.3.1 Cell Morphology and Density Testing of Modified Titanium Surfaces

Samples were created as described above to test the cell morphology and cell density. The control groups were untreated titanium (Ti), fluorosilanized Ti (FS), liquid-infused Ti (LIS), and Ti coated with collagen, bacteriophages, and FS. The testing group was Ti coated

with collage, phage, and FS, with the addition of PPFP lubricant to create the Phage-LIS coating. Before starting the experiments, the samples were placed in 24-well plates and incubated in antibiotic-free cell media (McCoy's 5A, FBS) for 24 hours to ensure no samples were contaminated. Then, osteosarcoma SaOS-2 cells were seeded with 1x104 cells/well concentration with regular cell media (McCoy's 5A modified medium, 6% FBS, 1% Step/strep v/v). The cells were incubated for 3 days at 37 ℃ with 5% CO2. After the incubation period, the cell media were removed, and the samples were washed with PBS, fixed with 4% methanol-free formaldehyde solution, permeabilized with Triton X100, and surfaces were blocked with 4% BSA solution. Then, the cells were tagged with phalloidin FITC and Hoechst 33342 as per the vendor recommendations. The surfaces were imaged on a Nikon Ti2-U inverted microscope by sticking the surfaces upside down on a glass slide. A total of 4 images per sample were taken at random locations. A total of 4 independent samples per group were used for cell counting. To count the cells, the blue channel (containing the nuclear-stained images) was imported into ImageJ, converted into greyscale threshold to remove the background, and counted using the Analyze Particles feature.

5.6.3.2 Cell Cytotoxicity Assay

Per the manufacturer's protocols, the cell viability was tested using Abcam's colorimetric Cytotoxicity Assay (ab112118). Briefly, SaOS-2 cells were seeded onto wells containing treated and untreated titanium discs previously prepared. The control groups were untreated titanium (Ti) and LIS, while the experimental group was the phage-LIS coated titanium discs. The discs were placed in 48-well plates, checked for contamination, and the cells were seeded, as mentioned in the previous section. Seeded cells were incubated at 37 ℃ with 5% CO2 for 24 hours. The next day, the Assay solution was added (40 µL) to each well and incubated for 5 hours. Then, 100 µL of solution was transferred into a 96-well plate with black walls and clear bottom. The optical density was then measured at 570 and 605 nm, and the cell viability was calculated according to the following equation.

$$\%\ Cell\ Viability = 100\ x\ (R_{sample} - R_0)/(R_{ctrl} - R_0)$$

Where R_{sample} is the absorbance ratio of OD570/OD605 in the presence of samples. R_{ctrl} is the absorbance ratio of OD570/OD605 in the absence of the test compound (wells with cells). R_0 is the average background (wells with non-cell control) absorbance ratio of OD570/OD605. Five independent samples were used per group.

5.6.3.3 Alkaline Phosphatase Assay

To test for alkaline phosphatase activity, samples were prepared as described earlier. Untreated titanium (Ti) and liquid-infused titanium (LIS) were treated as the control group, while the bacteriophage-collagen-LIS (Phage-LIS) coated surfaces were treated as the experimental group. After sample preparation, the treated and untreated groups were placed in a sterile 48-well plate, submerged in 200 µL cell media, and seeded with $3x10^4$ SaOS-2 cells. The final media volume was adjusted to 400 µL per well. The cells were incubated for 5 days (without renewing cell media). The ALP activity was tested directly from the cell culture medium according to the manufacturer's protocols. Each sample was tested in duplicates, and four independent samples were used per group.

5.6.4 Bacterial culture and phage propagation

Bacterial cultures were prepared by streaking frozen glycerol stocks of *Pseudomonas aeruginosa* PAO1 strain and PAO1-P1-lux strain, stored at -80°C, and inoculating LB media in a culture tube. Culture tubes were incubated at 37°C for 14-16 hours while shaking at 180 rpm. In order to propagate *Pseudomonas aeruginosa* phages (JG004, vB_Pa2-Tbilisi32 (P32), PO4, PP7, and E79), a bacterial subculture of PAO1 was prepared by diluting overnight cultures of PAO1 in LB media (1:100) and growing it to mid-exponential phase (OD_{600} = 0.3) at 37°C under 180 rpm shaking. The bacterial subculture was then infected by introducing 10 µL from a concentrated stock phage, followed by incubation at 37°C at 180 rpm for 6 hours to allow phage propagation and phage concentration increase. The obtained phage lysate was then pelleted down at 7000 rcf at 4°C for 20 minutes. The top solution was decanted into a new tube, and the bacterial pellet formed at the bottom of the plate was discarded. The phage solution was sterile filtered using 0.45 µm and 0.22 µm syringe filters consecutively. Each phage was propagated on a separate day to avoid cross-contamination of phages. Bacterial and phage suspension concentrations were evaluated

using colony forming unit (CFU/mL) and plaque forming units (PFU/mL) assays. For CFU/mL counts, 10-fold dilutions of the bacterial suspension were prepared in PBS buffer and plated in triplicates on agar plates containing LB media and 1.5% agarose. Plates were incubated on a stationary incubator at 37°C overnight, and the colonies were counted the next day and used to calculate the CFU/mL. For obtaining PFU/mL numbers of phage suspensions, 10-fold dilutions of phage suspensions were prepared in PBS media and plated in triplicates on an agar plate (1.5% agarose) with a bacteria lawn on top. Bacteria lawn was prepared by mixing 100 µL of bacterial overnight cultures and 4 mL of melted soft agar (containing 0.6% agarose and LB media) at 50°C, poured on an agar plate, and cooled undisturbed at room temperature for at least 15 minutes. The plates were then incubated overnight at 37°C in a stationary incubator. Phage-mediated cleared zones, called phage plaques, were formed on the bacteria lawn and were counted to calculate PFU/mL.

5.6.4.1 Phage cocktail design

First, *Pseudomonas aeruginosa* PAO1 and PAO1-Lux strains were screened against five different bacteriophages using a diffusion assay. Briefly, bacterial lawns were grown on agar plates as previously described. Then, 10 µL of concentrated bacteriophages [10^9-10^{11} PFU/mL] were pipetted onto a bacterial lawn and incubated at 37°C overnight (**Figure S1a-b**). The next day, phages were picked from lysis zones, propagated, and filtered as described above. Finally, phage pairings were analyzed to find the phage pair with the most potent synergistic effects. This was achieved by monitoring the bacteria grown in a liquid assay. Bacteria PAO1 or PAO1-Lux growth was tested by monitoring the turbidity of the cultures infected with phage pairs using OD_{600} liquid assay. For this purpose, bacterial subcultures at OD_{600} = 0.1 were infected with each phage separately, and binary phage pairs at the multiplicity of infection (MOI) of 10 in a transparent flat bottom 96-well plate at a total assay volume of 200 µL per well. The turbidity of the culture was measured by incubating the plate at 37°C for 24 hours while shaking in a Synergy BioTek plate reader and recording the absorbance at 600 nm every 15 minutes. The phage performance was evaluated by comparing the absorbance of phage-infected bacteria to uninfected bacteria and media

control wells. Successful combinations were selected based on how close their absorbance was to wells containing sterile media only at the end of the 24 hours.

5.6.4.2 In vitro bacterial assays

The antibacterial performance of treated and untreated coupons was tested using a diffusion assay on a bacteria lawn and liquid infectivity assay as follows:

5.6.4.3 Diffusion assay

Bacteria lawns of *Pseudomonas aeruginosa* on agar plates were prepared as previously described. Treated and untreated Ti coupons were placed on top of bacteria lawns by their treated face down. Plates were then incubated at 37°C overnight in a stationary incubator, and the cleared zones surrounding each coupon were evaluated as their antibacterial activity in preventing bacterial growth.

5.6.4.4 Liquid infectivity assays

Ti coupons with LIS, fluorosilanized Phage-conjugated collagen titanium, and Phage-conjugated collagen-LIS were prepared under sterile conditions. Coated and uncoated Ti coupons were placed in 48 flat bottom well plate quadruplicates, and 400 µL of a bacterial suspension at a concentration of 10^7 CFU/mL was introduced to each well. Plates were incubated at 37°C in a shaking incubator at 120 rpm for 24 hours. Biofilm prevention ability was tested on the surface and in the solution containing each sample by preparing dilutions and plating on an agar plate to obtain CFU/mL numbers. The solution on top of each coupon sample was plated for CFU count numbers to test phage activity in the solution. To evaluate phage activity on the surface, coupons were removed from each well and immersed gently in wells containing sterile PBS 3 times to remove unadhered bacteria. Afterward, the coupons were placed in an Eppendorf tube containing 1 mL of sterile PBS and vortexed for 3 minutes to detach the adhered bacteria. The solution in each tube was then plated on agar plates to obtain CFU/mL counts for all samples and on a bacterial lawn (spread on top of an agar plate) for phage-containing groups to obtain PFU/mL values.

5.6.5 Mice Sepsis Model

5.6.5.1 Surgical procedures

McMaster's Animal Research Ethics Board (AREB) approved all protocols and procedures under the Animal Utilization Protocol (AUP) 21-10-32. The mouse surgical procedures were borrowed from Stravakis *et al*.,[76] with some modifications. For analgesia, the mice were administered 0.05 mL slow-release buprenorphine via a subcutaneous injection 45 minutes before the surgery. Then, the mice were anesthetized with inhalation of isoflurane (2%), shaved with peanut clippers, and prepped using three-step disinfecting solutions. Once the mice were anesthetized, a small incision was made in the mid-lower dorsal region, followed by gentle tissue undermining to create a subcutaneous pocket. Using a blunt dissection technique with flat iris scissors, the pocket was created going superior from the incision site towards the scapulae region. The 5 mm titanium disc was introduced and pushed into the pocket as far from the incision site as possible, the bacteria of a known concentration or PBS was pipetted into the pocket as discussed in the following section, and the incision site was then closed using autoclips.

5.6.5.2 Establishing a Sepsis Model

To establish a sepsis model, a total of 30 mice (15 male, 15 female) were tested against different *S. aureus* (PAO1-Lux) bacterial loads using untreated titanium implants. A total of 6 groups were tested; the control group had PBS without bacteria, and 5 experimental groups with bacterial loads ranging from $1x10^3$ – $1x10^7$ CFU and in the absence of antibiotic treatments post-surgery. The groups were distributed such that each group had 5 mice, but their sex was staggered so that each group would have either 2M and 3F or 3M and 2F. The infection progress was monitored using bioluminescent imaging using an IVIS CT scanner, and the mice's health was monitored daily for signs of sickness according to their endpoint monitoring protocol and the criteria defined in Table S1 in the supplementary section.

5.6.5.3 Bioluminescence Imaging

Bioluminescent imaging was performed using the IVIS CT scanner (perkinelmer.com) and software Living Image (v4.7.4. 64 bit) at the central animal facility. Mice were first

inoculated with the PAO1-Lux bacteria strain as discussed above and tracked at days 1, 3, 5, 7, 9, 11, and 13 post-surgeries to reduce the anesthesia burden on the mice as per the approved AUP. The mice were first anesthetized using an isoflurane induction chamber with oxygen (1.5 L/min) as the carrier gas. Mice were induced using 5% isoflurane and then maintained under anesthesia at around 2.5-3% for the scan duration. The field of view (FOV) was set at D (21.5 x 21.5 cm) to accommodate five mice per scan. To analyze the bioluminescent signal, a region of interest (ROI) was drawn to encompass the color map to obtain a total radiance (photo/sec/cm^2/sr) reading, and the value was subtracted from the ROI of the background.

5.6.5.4 Sepsis Mortality Mouse Model of Bacteriophage-LIS Titanium

After establishing the sepsis model with untreated titanium, a similar methodology was used to test the treated titanium discs; however, the initial bacterial load of 1x10^8 CFU was chosen to produce a more robust septic model with higher mortality rates. Notably, non-bioluminescent bacteria PAO1 was used instead of the previously tested PAO1-Lux because no strong synergistic bacteriophages were found (**Figure S1**). A total of 30 mice were divided into three groups: untreated titanium (Ti) discs as control, LIS titanium, and the bacteriophage-collagen LIS coated titanium (Phage-LIS). The group of mice without bacteria was not retested to reduce the number of animals used by following the 3Rs principles.[64] Three consecutive days of surgeries were performed, one per group, followed by a 7-day monitoring period. Mice were monitored for signs of sickness and signs of reaching the endpoint (**Table S1**). If a mouse reached the endpoint (EP) criteria, blood samples were taken, and then the mouse was euthanized, followed by the harvesting of the implant, the liver, and the spleen. The spleen, liver, blood, and implants were analyzed for CFU and PFU, with one implant being sent for SEM imaging.

5.6.5.5 *In vivo* bacterial assay

As described above, animal samples, including blood, retrieved coupons, liver, and spleen, were evaluated for the bacteria and phage presence after euthanizing each mouse. Blood samples were tested without further processing by 10-fold dilutions in PBS and plating on McConkey agar plates for CFU/mL and on agar plates containing bacteria lawns for

PFU/mL numbers as described above. To homogenize the livers and spleens, the organs were thawed, washed 3 times in sterile DPBS (ca/mg free), weighted and diluted in 100 mg/ml sterile DPBS (ca/mg free). Afterwards, the organs were run through the homogenizer for 5 min and 10 min for spleens and livers, respectively. Once the organs were homogenized, they were tested the same way as blood samples for PFU and CFU counts per gram. Retrieved coupons were placed in a sterile tube containing 1 mL of sterile PBS and vortexed for 3 minutes to detach adhered bacteria. Then, the solution in each tube was plated for CFU, and PFU counts on McConkey and bacteria lawn containing agar plates, respectively. PFU counts were only conducted for phage-containing coatings.

5.6.6 Scanning Electron Microscopy

Scanning Electron Microscopy (SEM), imaging was performed at the Electron Microscopy Facility in the Health Science Centre at McMaster University by the technician. The samples were tested in the same method as our previous work.[28]

5.6.7 Statistical analysis

Statistical analysis was performed using Prism 9 (v9.5.1). Parametric data were tested using either an ANOVA followed by a posthoc Tukey test or an unpaired student t-test. Survival curves were analyzed using a log-rank Mantel-Cox test. Significance levels were defined as significant '*' at p-values of <0.05, highly significant '**' at p-values < 0.01, and extremely significant '***' with p-values < 0.001.

5.7. References

1. Khorasani, A. M., Goldberg, M., Doeven, E. H. & Littlefair, G. Titanium in biomedical applications—properties and fabrication: A review. *Journal of Biomaterials and Tissue Engineering* vol. 5 593–619 Preprint at https://doi.org/10.1166/jbt.2015.1361 (2015).
2. Boehlert, C. J., Cowen, C. J., Quast, J. P., Akahori, T. & Niinomi, M. Fatigue and wear evaluation of Ti-Al-Nb alloys for biomedical applications. *Materials Science and Engineering C* **28**, 323–330 (2008).
3. Sidambe, A. T. Biocompatibility of advanced manufactured titanium implants-A review. *Materials* vol. 7 8168–8188 Preprint at https://doi.org/10.3390/ma7128168 (2014).

4. Blue, S. R., Wyatt, C. M. & Coffman, T. J. Endocarditis. in *Netter's Infectious Diseases* (eds. Elaine C. Jong & Dennis L. Stevens) 190–201 (W.B. Saunders, 2012).
5. *Early Revisions of Hip and Knee Replacements in Canada: A Quality, Productivity and Capacity Issue*. (2020).
6. D'Onofrio, K. Infection Most Common Culprit of Revision TKA Failure. https://www.aaos.org/aaosnow/2020/aaos-now-special-edition/research/557_knee/ (2020).
7. Kochar, S. P., Reche, A. & Paul, P. The Etiology and Management of Dental Implant Failure: A Review. *Cureus* **14**, (2022).
8. Malagù, M. *et al.* Risk Scores for Cardiac Implantable Electronic Device Infection: Which One to Believe In? *J Clin Med* **11**, 6556 (2022).
9. Sepsis. https://www.who.int/news-room/fact-sheets/detail/sepsis.
10. *In Focus: A National Look at Sepsis*. www.cihi.ca (2009).
11. Seth, A. K. *et al.* In vivo modeling of biofilm-infected wounds: A review. *Journal of Surgical Research* vol. 178 330–338 Preprint at https://doi.org/10.1016/j.jss.2012.06.048 (2012).
12. Zapotoczna, M., O'Neill, E. & O'Gara, J. P. Untangling the Diverse and Redundant Mechanisms of Staphylococcus aureus Biofilm Formation. *PLoS Pathogens* vol. 12 Preprint at https://doi.org/10.1371/journal.ppat.1005671 (2016).
13. Lewis, K. Persister Cells. *Annu Rev Microbiol* **64**, 357–372 (2010).
14. Roy, R., Tiwari, M., Donelli, G. & Tiwari, V. Strategies for combating bacterial biofilms: A focus on anti-biofilm agents and their mechanisms of action. *Virulence* **9**, 522–554 (2018).
15. Rasmussen, T. B. & Givskov, M. Quorum-sensing inhibitors as anti-pathogenic drugs. *International Journal of Medical Microbiology* **296**, 149–161 (2006).
16. Kumar, A., Alam, A., Rani, M., Ehtesham, N. Z. & Hasnain, S. E. Biofilms: Survival and defense strategy for pathogens. *International Journal of Medical Microbiology* **307**, 481–489 (2017).
17. Villegas, M., Zhang, Y., Abu Jarad, N., Soleymani, L. & Didar, T. F. Liquid-Infused Surfaces: A Review of Theory, Design, and Applications. *ACS Nano* **13**, (2019).
18. Howell, C., Grinthal, A., Sunny, S., Aizenberg, M. & Aizenberg, J. Designing Liquid-Infused Surfaces for Medical Applications: A Review. *Advanced Materials* 1802724 (2018) doi:10.1002/adma.201802724.
19. Sotiri, I., Overton, J. C., Waterhouse, A. & Howell, C. Immobilized liquid layers: A new approach to anti-adhesion surfaces for medical applications. *Exp Biol Med* **241**, 909–918 (2016).
20. Osborne, M., Aryasomayajula, A., Shakeri, A., Selvaganapathy, P. R. & Didar, T. F. Suppression of Biofouling on a Permeable Membrane for Dissolved Oxygen Sensing Using a Lubricant-Infused Coating. *ACS Sens* **4**, 687–693 (2019).
21. Badv, M., Weitz, J. I. & Didar, T. F. Lubricant-Infused PET Grafts with Built-In Biofunctional Nanoprobes Attenuate Thrombin Generation and Promote Targeted Binding of Cells. *Small* **15**, 1905562 (2019).
22. Badv, M., Imani, S. M., Weitz, J. I. & Didar, T. F. Lubricant-Infused Surfaces with Built-In Functional Biomolecules Exhibit Simultaneous Repellency and Tunable Cell Adhesion. *ACS Nano* **12**, 10890–10902 (2018).

23. Badv, M., Jaffer, I. H., Weitz, J. I. & Didar, T. F. An omniphobic lubricant-infused coating produced by chemical vapor deposition of hydrophobic organosilanes attenuates clotting on catheter surfaces. *Sci Rep* **7**, 11639 (2017).
24. Imani, S. M. *et al.* Micropatterned biofunctional lubricant-infused surfaces promote selective localized cell adhesion and patterning. *Lab Chip* **19**, 3228–3237 (2019).
25. Badv, M. *et al.* Biofunctional Lubricant-Infused Vascular Grafts Functionalized with Silanized Bio-Inks Suppress Thrombin Generation and Promote Endothelialization. *ACS Biomater Sci Eng* **5**, 6485–6496 (2019).
26. Kasapgil, E. *et al.* Polysiloxane Nanofilaments Infused with Silicone Oil Prevent Bacterial Adhesion and Suppress Thrombosis on Intranasal Splints. *ACS Biomater Sci Eng* **7**, 541–552 (2021).
27. Badv, M., Bayat, F., Weitz, J. I. & Didar, T. F. Single and multi-functional coating strategies for enhancing the biocompatibility and tissue integration of blood-contacting medical implants. *Biomaterials* vol. 258 120291 Preprint at https://doi.org/10.1016/j.biomaterials.2020.120291 (2020).
28. Villegas, M. *et al.* Antibiotic-Impregnated Liquid-Infused Coatings Suppress the Formation of Methicillin-Resistant Staphylococcus aureus Biofilms. *ACS Appl Mater Interfaces* **0**, null.
29. Villegas, M. *et al.* Enhancing osseointegration and mitigating bacterial biofilms on medical-grade titanium with chitosan-conjugated liquid-infused coatings. *Sci Rep* **12**, 1–11 (2022).
30. Green, S., Ma, L. & Maresso, A. Phage Therapy. *Encyclopedia of Microbiology* 485–495 (2019) doi:10.1016/B978-0-12-801238-3.66117-2.
31. Kortright, K. E., Chan, B. K., Koff, J. L. & Turner, P. E. Phage Therapy: A Renewed Approach to Combat Antibiotic-Resistant Bacteria. *Cell Host Microbe* **25**, 219–232 (2019).
32. Abedon, S. T., Kuhl, S. J., Blasdel, B. G. & Kutter, E. M. Phage treatment of human infections. *Bacteriophage* **1**, 66 (2011).
33. Merril, C. R., Scholl, D. & Adhya, S. L. The prospect for bacteriophage therapy in Western medicine. *Nat Rev Drug Discov* **2**, 489–497 (2003).
34. Kortright, K. E., Chan, B. K., Koff, J. L. & Turner, P. E. Phage Therapy: A Renewed Approach to Combat Antibiotic-Resistant Bacteria. *Cell Host Microbe* **25**, 219–232 (2019).
35. Gibb, B. P. & Hadjiargyrou, M. Bacteriophage therapy for bone and joint infections an instructional review. *Bone and Joint Journal* **103 B**, 234–244 (2021).
36. Li, B. & Webster, T. J. Bacteria antibiotic resistance: New challenges and opportunities for implant-associated orthopedic infections. *Journal of Orthopaedic Research* **36**, 22–32 (2018).
37. Bayat, F., Didar, T. F. & Hosseinidoust, Z. Emerging investigator series: bacteriophages as nano engineering tools for quality monitoring and pathogen detection in water and wastewater. *Environ Sci Nano* **8**, 367–389 (2021).
38. Melo, L. D. R., Oliveira, H., Pires, D. P., Dabrowska, K. & Azeredo, J. Phage therapy efficacy: a review of the last 10 years of preclinical studies. *Crit Rev Microbiol* **46**, 78–99 (2020).

39. Walker, J. N., Poppler, L. H., Pinkner, C. L., Hultgren, S. J. & Myckatyn, T. M. Establishment and Characterization of Bacterial Infection of Breast Implants in a Murine Model. *Aesthet Surg J* **40**, 516–528 (2020).
40. Cerioli, M. *et al.* Pseudomonas aeruginosa Implant-Associated Bone and Joint Infections: Experience in a Regional Reference Center in France. *Front Med (Lausanne)* **7**, 513242 (2020).
41. Fernandes, A. & Dias, M. The Microbiological Profiles of Infected Prosthetic Implants with an Emphasis on the Organisms which Form Biofilms. *J Clin Diagn Res* **7**, 219–223 (2013).
42. Treccani, L., Yvonne Klein, T., Meder, F., Pardun, K. & Rezwan, K. Functionalized ceramics for biomedical, biotechnological and environmental applications. *Acta Biomater* **9**, 7115–7150 (2013).
43. Villegas, M., Zhang, Y., Abu Jarad, N., Soleymani, L. & Didar, T. F. Liquid-Infused Surfaces: A Review of Theory, Design, and Applications. *ACS Nano* **13**, 8517–8536 (2019).
44. Chen, G. *et al.* Collagen fibers with tuned wetting properties for dual separation of oil-in-water and water-in-oil emulsion. *J Mater Chem A Mater* **8**, 24388–24392 (2020).
45. Shiue, S. J., Syu, F. S. & Lin, H. Y. Two types of bacteriophage-modified alginate hydrogels as antibacterial coatings for implants. *J Taiwan Inst Chem Eng* **134**, 104353 (2022).
46. Dang, H. T. T. & Tarabara, V. V. Virus deposition onto polyelectrolyte-coated surfaces: A study with bacteriophage MS2. *J Colloid Interface Sci* **540**, 155–166 (2019).
47. Hosseinidoust, Z., Van De Ven, T. G. M. & Tufenkji, N. Bacterial capture efficiency and antimicrobial activity of phage-functionalized model surfaces. *Langmuir* **27**, 5472–5480 (2011).
48. Hosseini, A. *et al.* Conductive Electrochemically Active Lubricant-Infused Nanostructured Surfaces Attenuate Coagulation and Enable Friction-Less Droplet Manipulation. *Adv Mater Interfaces* **5**, 1800617 (2018).
49. López-Valverde, N., Macedo-De-Sousa, B., López-Valverde, A. & Ramírez, J. M. Effectiveness of antibacterial surfaces in osseointegration of titanium dental implants: A systematic review. *Antibiotics* **10**, (2021).
50. Li, X. *et al.* Osseointegration of chitosan coated porous titanium alloy implant by reactive oxygen species-mediated activation of the PI3K/AKT pathway under diabetic conditions. *Biomaterials* **36**, 44–54 (2015).
51. Sobolev, A. *et al.* Bioactive Coating on Ti Alloy with High Osseointegration and Antibacterial Ag Nanoparticles. *ACS Appl Mater Interfaces* **11**, 39534–39544 (2019).
52. Rabel, K. *et al.* Controlling osteoblast morphology and proliferation via surface micro-topographies of implant biomaterials. *Scientific Reports 2020 10:1* **10**, 1–14 (2020).
53. Piattelli, A., Scarano, A., Corigliano, M. & Piattelli, M. Effects of alkaline phosphatase on bone healing around plasma-sprayed titanium implants: a pilot study in rabbits. *Biomaterials* **17**, 1443–1449 (1996).
54. Zhang, H. *et al.* Vancomycin-loaded titanium coatings with an interconnected micro-patterned structure for prophylaxis of infections: An: in vivo study. *RSC Adv* **8**, 9223–9231 (2018).

55. Chouirfa, H., Bouloussa, H., Migonney, V. & Falentin-Daudré, C. Review of titanium surface modification techniques and coatings for antibacterial applications. *Acta Biomater* **83**, 37–54 (2019).
56. He, S. *et al.* Antibiotic-decorated titanium with enhanced antibacterial activity through adhesive polydopamine for dental/bone implant. *J R Soc Interface* **11**, (2014).
57. Morimoto, T. *et al.* Development of Silver-Containing Hydroxyapatite-Coated Antimicrobial Implants for Orthopaedic and Spinal Surgery. *Medicina 2022, Vol. 58, Page 519* **58**, 519 (2022).
58. Zhang, Y. *et al.* Tantalum Nitride-Decorated Titanium with Enhanced Resistance to Microbiologically Induced Corrosion and Mechanical Property for Dental Application. *PLoS One* **10**, e0130774 (2015).
59. Zhou, J., Wang, X. & Zhao, L. Antibacterial, angiogenic, and osteogenic activities of Ca, P, Co, F, and Sr compound doped titania coatings with different Sr content. *Scientific Reports 2019 9:1* **9**, 1–11 (2019).
60. Rima, M. *et al.* Antimicrobial Peptides: A Potent Alternative to Antibiotics. *Antibiotics* **10**, 1095 (2021).
61. Huan, Y., Kong, Q., Mou, H. & Yi, H. Antimicrobial Peptides: Classification, Design, Application and Research Progress in Multiple Fields. *Front Microbiol* **11**, 582779 (2020).
62. Sakr, Y. *et al.* The influence of gender on the epidemiology of and outcome from severe sepsis. *Crit Care* **17**, 1–9 (2013).
63. Ryan, L. & Mills, K. H. G. Sex differences regulate immune responses in experimental autoimmune encephalomyelitis and multiple sclerosis. *Eur J Immunol* **52**, 24–33 (2022).
64. CCAC - Canadian Council on Animal Care: Three Rs. https://ccac.ca/en/three-rs/.
65. Azzi, L., El-Alfy, M., Martel, C. & Labrie, F. Gender differences in mouse skin morphology and specific effects of sex steroids and dehydroepiandrosterone. *Journal of Investigative Dermatology* **124**, 22–27 (2005).
66. Nguyen, A. V. & Soulika, A. M. The Dynamics of the Skin's Immune System. *Int J Mol Sci* **20**, (2019).
67. Chan, B. *et al.* Personalized Inhaled Bacteriophage Therapy Decreases Multidrug-Resistant Pseudomonas aeruginosa. *medRxiv* 2023.01.23.22283996 (2023) doi:10.1101/2023.01.23.22283996.
68. Markwitz, P. *et al.* Emerging phage resistance in pseudomonas aeruginosa PAO1 is accompanied by an enhanced heterogeneity and reduced virulence. *Viruses* **13**, 1332 (2021).
69. Dąbrowska, K. & Abedon, S. T. Pharmacologically Aware Phage Therapy: Pharmacodynamic and Pharmacokinetic Obstacles to Phage Antibacterial Action in Animal and Human Bodies. *Microbiology and Molecular Biology Reviews* **83**, (2019).
70. Petrovic Fabijan, A. *et al.* Safety of bacteriophage therapy in severe Staphylococcus aureus infection. *Nature Microbiology 2020 5:3* **5**, 465–472 (2020).
71. Górski, A. *et al.* The potential of phage therapy in sepsis. *Front Immunol* **8**, 317205 (2017).
72. Diallo, K. & Dublanchet, A. Benefits of Combined Phage–Antibiotic Therapy for the Control of Antibiotic-Resistant Bacteria: A Literature Review. *Antibiotics 2022, Vol. 11, Page 839* **11**, 839 (2022).

73. Łusiak-Szelachowska, M. *et al.* Bacteriophages and antibiotic interactions in clinical practice: what we have learned so far. *J Biomed Sci* **29**, 1–17 (2022).
74. Liu, C., Hong, Q., Chang, R. Y. K., Kwok, P. C. L. & Chan, H. K. Phage–Antibiotic Therapy as a Promising Strategy to Combat Multidrug-Resistant Infections and to Enhance Antimicrobial Efficiency. *Antibiotics 2022, Vol. 11, Page 570* **11**, 570 (2022).
75. Yilmaz, C. *et al.* Bacteriophage therapy in implant-related infections: An experimental study. *Journal of Bone and Joint Surgery* **95**, 117–125 (2013).
76. Stavrakis, A. I. *et al.* Combination prophylactic therapy with rifampin increases efficacy against an experimental staphylococcus epidermidis subcutaneous implant-related infection. *Antimicrob Agents Chemother* **58**, 2377–2386 (2014).

5.8. Supplementary Information

Table S1. Endpoint Monitoring Criteria.

Appearance Score (APR)	Attitude Score (ATT)	Body Conditioning (BC)
5-Normal; normal skin tent and posture	5-Normal; active in cage prior to & during handling	5-Obese
4-Skin tent present on dorsum	4-Decreased activity, but alert, responsive to handling	4-Over conditioned
3-Hunched posture, piloerection present, moderate skin tent	3-Lethargic, decreased resistance to handling, not grooming	3-Well Conditioned
2-Eyes sunken in, piloerection and skin tent severe	2-Non-responsive, mouse only moves when touched	2-Under conditioned
1-Failure to right itself-moribund	1-Failure to respond to hand in cage or touch	1-Emaciated

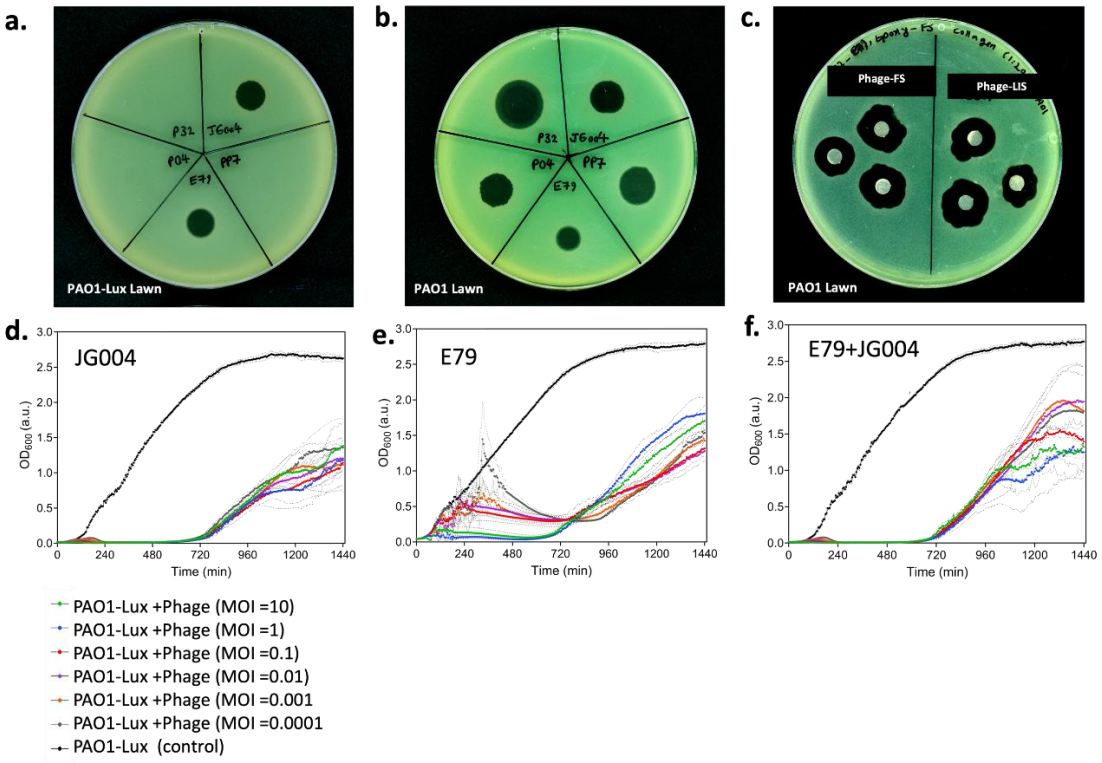

Figure S1. *In Vitro* Bacteriophage Screening. a) Screening of bioluminescent *P. aeruginosa* PAO1-Lux against five strong lytic bacteriophages showing phage activity from E79 and JG004. b) Screening of non-bioluminescence *P. aeruginosa* PAO1 against five strong lytic bacteriophages showing phage activity from P32, P04, PP7, E79 and JG004. c) Bacteriophage activity from the treated titanium samples against PAO1 bacteria. A strong lysis zone can be seen in the presence or absence of PFPP lubricant. d) Optical density kill curve between PAO1-Lux and JG004 bacteriophage. e) Optical density kill curve between PAO1-Lux and E79 bacteriophage. f) Optical density kill curve between PAO1-Lux and combined E79- JG004 bacteriophages. Note: the color legend in c-e) represents the Multiplicity of Infection (MOI) or the ratio between bacteriophage to bacteria. The color legend is denoted as black – No phage control, grey – MOI=0.0001, orange – MOI=0.001, magenta – MOI=0.01, red – MOI=0.1, blue – MOI=1, green – MOI=10.

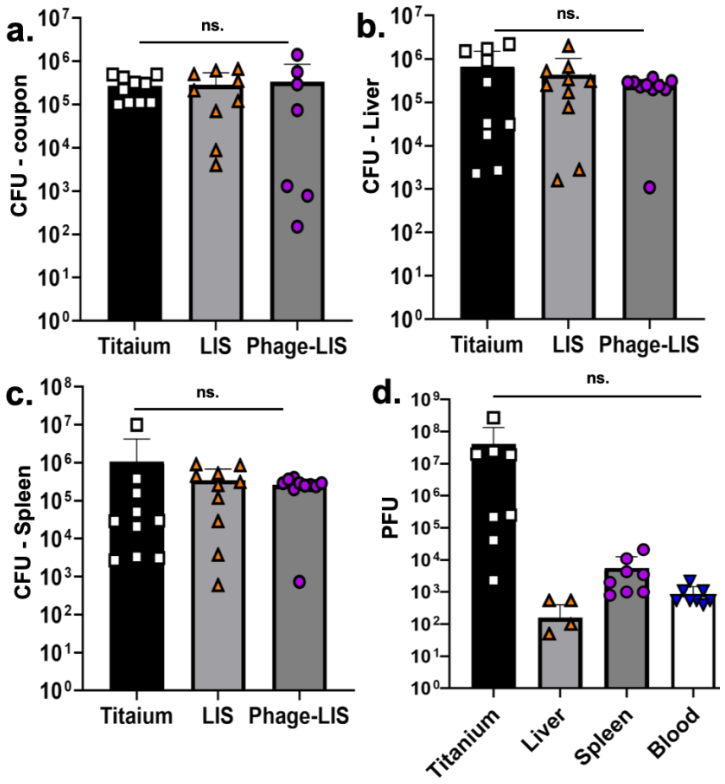

Figure S2. *Ex Vivo* Bacteria and Bacteriophage Quantification from Samples Taken at Endpoint. a) Bacteria Colony forming unit (CFU) from retrieved titanium implants at the endpoint. b) PAO1 bacteria CFU retrieved from liver samples at the endpoint. c) PAO1 bacteria CFU from retrieved spleen samples at the endpoint. d) Bacteriophage Plaque forming units (PFU) from titanium, liver, spleen, and blood samples obtained at the endpoint.

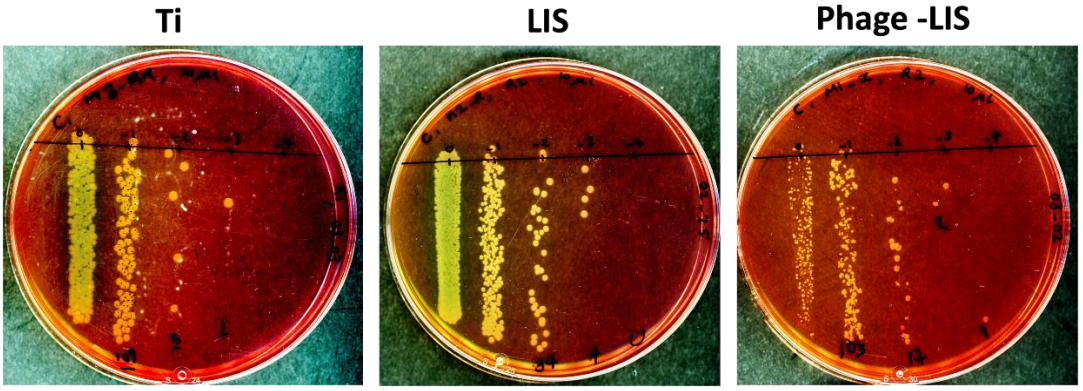

Figure S3. McConkey Agar Plates from Ex Vivo Titanium Samples. Representative images of McConkey agar plates with bacteria obtained from recovered titanium discs for untreated Ti, LIS-coated Ti, and Phage-LIS coated Ti. Notably, bacteria colonies obtained from Phage-LIS samples display phage activity, as noted by the dying colonies in the 0^{th} and 1^{st} dilutions. These colonies were lysed entirely within a few days.

Chapter 6: Regenerating Heavily Biofouled Dissolved Oxygen Sensors using Bacterial Viruses

Preface: This paper is focused on implementing phage to combat biofouling in marine environments. As a proof of concept, we demonstrated that treating the surface of a biofouled dissolved oxygen sensor with phages can effectively reduce biomass and restore the sensor's sensing capabilities. Our study highlights the versatile antibacterial properties of bacteriophages, extending their applicability beyond the realm of biomedical engineering to a broader spectrum of applications, such as environmental engineering.

Contribution: This work was an equal collaboration between me and Dhanyasri Maddiboina. I conducted all the DO measurements in water, characterized the biofilms by fluorescent microscopy, and contributed to phage treatment of the biofouled membranes. Dhanyasri cultured bacteria and prepared the phages, grew biofilm on the surface of the dissolved oxygen sensors. Dhanyasri and I prepared the samples and conducted the SEM imaging. We contributed equally to writing, data analysis and editing the manuscript. Dr. Zeinab Hosseinidoust and Dr. Tohid Didar conceptualized the project, supervised the experiments, and edited and approved the final manuscript.

Citation: This work is published in the Royal Society of Chemistry (RSC adv.).

Bayat, F., $^{\Psi}$ Maddiboina, D., $^{\Psi}$ Didar, T. F. & Hosseinidoust, Z. Regenerating heavily biofouled dissolved oxygen sensors using bacterial viruses. RSC Adv. 11, 8346–8355 (2021).

$^{\Psi}$ Equal contribution

6.1. Abstract

Bacterial biofilms are aggregates of bacterial cells embedded in a self-produced slimy extracellular polymeric matrix. Biofilm formation has always been considered as a major challenge for sensors used in underwater measurements, and is a primary source of measurement error, especially when it comes to long-term in situ monitoring. In this work, we demonstrate the utility of lytic bacteriophages (bacterial viruses) as a non-invasive strategy for removing bacterial biofilms formed on the gas permeable membrane of electrochemical dissolved oxygen sensors. Our results show that a 4-day Pseudomonas aeruginosa biofilm with a fully developed matrix significantly affected the sensor signal and response time, decreasing the signal by 32% and increasing the response time by 94%. In addition, measurements with the biofouled membrane had a very low signal to nose ratio compared to a clean sensor membrane. A single dose of overnight phage treatment effectively removed the biofilm (as indicated by scanning electron micrographs and fluorescence images of the membrane), without the need for repeated treatments. Furthermore, the sensor signal for de-ionized water that had plummeted by 32% for a fully biofouled membrane, was returned to the original value (7.96 ± 0.27 mg/L) after phage treatment and the signal to noise ratio (calculated as the ratio of mean to standard deviation) increased 8 fold for a phage-treated membrane compared to biofouled membrane. Our data indicate near complete regeneration and signal recovery for the dissolved oxygen sensor making the biofouled sensor reusable without the use of harsh chemicals that could destroy the fragile sensor membrane.

Keywords: bacterial fouling; sensor regeneration, membrane fouling; dissolved oxygen sensing, sensor fouling

6.2. Introduction

Biofouling, or biological fouling, is the unwanted deposition of microorganisms on biotic and abiotic surfaces[1]. Biofouling is troublesome and costly in fields as diverse as medical devices[2] and water transportation[3]. Bacteria are major contributors to biofouling events. Bacteria readily form surface-bound, 3-dimensional communities. These communities are known as bacterial biofilms and are usually encased in a slimy matrix of biopolymers, called the extracellular polymeric substance (EPS), which is secreted by the bacterial cells themselves [4]. From the point of view of a bacterial cell, biofilms are a means for survival and that is why bacterial biofilms are the most common form of bacterial existence in nature. Bacteria form biofilms on infected catheters and implants[2], on surfaces in the food industry[5] and membranes in water treatment plants[6], on ship hulls[7], and on marine sensors[8,9]. Biofouling has always been considered a major challenge for underwater measurements, especially when it comes to long-term *in situ* monitoring (*e.g.,* and environmental monitoring devices installed in lakes and rivers)[10]. Biofouling of sensor surfaces is a major concern in all physico-chemical sensors including pH and redox sensors, optical sensors, and electrochemical sensors and could result in unreliable measurements[11,12]. Biofilm starts to grow as soon as the sensor is immersed in water, and it has been reported that the quality of measurements decreases in less than a week[10]. Although many potential solutions have been proposed to combat biofouling in underwater measurements and monitoring, there is no single universally accepted method applicable to underwater environmental sensors.

Various methods and technologies have been used to prevent biofouling or remove biofilms from biofouled surfaces, such as mechanical treatment (wipers, water jetting, ultrasonic surface excitation)[11], chemical detergents and biocides[13], UV light exposure (which may kill bacteria but will not completely remove the biofilm)[14,15], chlorination[8], chemical modifications of surfaces (*e.g.,* using zwitterions, carboxylation, and charged hydrogels), and coating surfaces with antimicrobials[16], repellent coatings[17–19]. For sensing surfaces, however, cleaning methods should be chosen with care. Cleaning methods that involve harsh physical or chemical treatments could cause structural damage and harm the sensitive and sometimes delicate sensing surfaces[5]. It is noteworthy that antimicrobial

agents in general have limited activity against biofilms, because they could be neutralized or diluted to sublethal concentrations by bonding to the slimy matrix of biofilms before reaching all the individual bacterial cells within the biofilm[20]. In addition, improved intercellular interactions in biofilms leads to enhanced metabolic capacity of cells and antimicrobial resistance[21]. As a result, biofilms have been shown to be more resistant to chemical disinfectants and biocides compared to planktonic (free swimming) bacteria. Antimicrobial or repellent surface coatings, although not as invasive as mechanical scrubbing or chemical chlorination, require changing the sensing surface, which may interfere with measurements and sensor sensitivity, by changing the bio-interface properties. Besides, once the coating is depleted, the sensor will start to foul and will thus have to be removed and changed.

Bacteriophages are bacterial viruses that were discovered over a hundred years ago, well before penicillin, and almost immediately used to treat bacterial infections[22,23]. Bacteriophages (or phages, for short) are natural bacteria devourers, and their job in nature is to keep bacteria populations in check. They have been proposed and explored as potential biological tools to control or mitigate biofilm formation in different settings[24]. These human-friendly viruses are capable of infecting bacteria very specifically, thus not harming the delicate microbial balance in the surrounding environment, a characteristic that has made them attractive for different applications as therapeutics, biocontrol agents, prophylactics and even sensing agents[25–27]. After binding to host cell surface receptors, phages insert their genome into the host bacterium. A class of phages known as lytic or virulent phages immediately take control of the host cell machinery and turn the bacteria cell into a phage factory. At the end of this replication process, known as the lytic cycle, the bacterial cell is lysed, and hundreds of new phages are released to infect other bacteria. Temperate or mild phages are another class of phage. Those integrate their genome with that of the host bacteria and lay dormant until activated by an external stimulus such as UV light, temperature change, or a sub-lethal concentration of a toxic chemical, which in turn activate the lytic cycle and ultimately lyse the bacterial cell[28,29]. Lytic phages are the group of phages that are recommended and mostly explored for controlling bacterial populations, because they offer an immediate antibacterial action. Although phages are being heavily investigated for their use as therapeutics[30], they have remained obscure to

most environmental engineers. With only a few reports published on mitigation of membrane fouling[31,32] and no prior report on cleaning fouled sensors, there is a gap in knowledge regarding the performance of phage for engineering applications, which calls for more investigations in this field.

In this work, we use a lytic bacteriophage cocktail to remove a fully developed biofilm of *Pseudomonas aeruginosa* PAO1 (PA) from the membrane of a dissolved oxygen (DO) sensor. *Pseudomonas aeruginosa* is one of the most prevalent opportunistic microorganisms, inhabiting soil, seawater, freshwater, sewage, plants, and animals.[1] This microorganism is a strong biofilm former and is responsible for difficult to treat hospital acquired infections,[2] persistent food contamination,[2] and marine biofouling,[3,4] due to its high capacity to colonize and form biofilms on surfaces submerged in aquatic environments.[5] It has been shown that other microorganisms are stimulated to settle and colonize the submerged surfaces in marine environments in the presence of the EPS secreted by biofilm forming species such as *Pseudomonas aeruginosa*.[6] In addition, studying the biofilms formed on nanofiltration membranes in water treatment plants has confirmed that *P. aeruginosa* is one of the important species dominating the biofilm communities.[7] As a result, in this study, *P. aeruginosa* is used for biofilm formation on the surface of DO sensor membranes as a representative for biofilm forming species in aquatic environment for this proof of concept study. We demonstrate the effectiveness of a single dose of lytic phage treatment on the fouled sensor membrane in recovering DO sensor signal to the original level, increasing the signal to noise ratio and decreasing the response time.

6.3. Results and discussion

In this study, PA biofilms were grown on DO sensor membranes following baseline measurements (**Figure 1A**). Biofouled membranes were then subjected to overnight incubation in a phage suspension consisting of a 1:1 mixture of phages vB_Pae-Kakheti25 and vB_Pae-Tbilisi32 in LB media. The choice of phage was based on previous experience in our lab with a library of PA phages and their performance against PA

biofilms in a stationary microtiter plate model. We chose two phages for treating the biofilm instead of one phage, because it has been shown that using more than one phage decreases the frequency of evolution of phage-resistant bacteria[38–40], thus increasing the efficiency of phage treatment. **Figure 1B** shows a simplified schematic of the phage lytic cycle that leads to the destruction of bacterial cells in a biofilm as a result of phage action. Control biofilms were incubated overnight in fresh LB media without any phage.

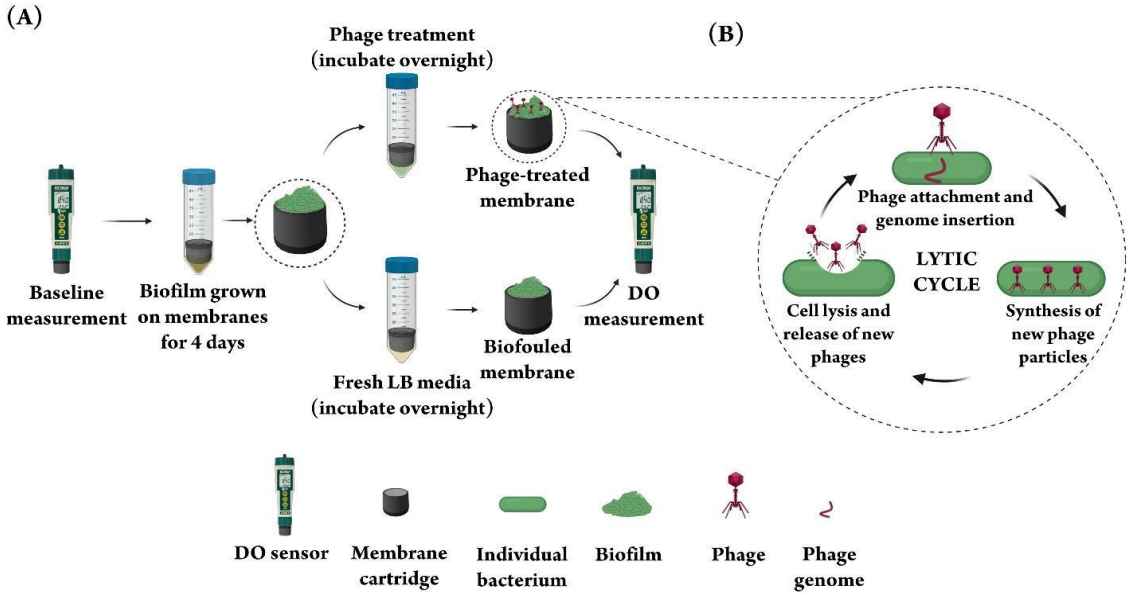

Figure 1. (A) Schematic diagram showing the workflow for artificially fouling the membranes of DO sensors and subsequent phage treatment. After baseline measurement with the DO sensor, the membranes were incubated with a PA culture for 4 days to form a thick bacterial biofilm, then treated with phage overnight before subsequent DO measurements. **(B)** A simplified diagram of the phage lytic cycle that leads to lysis and destruction of the bacterial cells comprising the biofilm on the sensor membrane. First, phage attaches to specific receptors on the bacteria cell surface and injects its genome into the bacterium, thus taking over the cell reproduction machinery. Hundreds of phage particles are synthesized and assembled in each bacterium and the bacterium is subsequently lysed to release the new phages into the environment to infect more bacterial cells.

6.3.1 Biofilm removal with phage

To ensure a thick biofilm form on the sensor membranes, we first assessed the appropriate length of time needed to allow for biofilm formation on the membrane by quantifying biofilm growth in a 96-well plate for the duration of four days. The biofilm level was quantified using crystal violet, a commonly used dye that binds and stains both bacteria and the surrounding matrix[37]. As shown in **Figure 2A**, the level of total biomass steadily increased over the four-day period. The SEM images of PA biofilm grown on DO sensor membranes in **Figure 2B** confirm the trend shown in **Figure 2A** and correlate with the well-documented stages of a PA biofilm lifecycle[41–43]. As depicted in **Figure 2C**, the biofilm developmental process begins with (i) attachment of PA cells to a surface. This is followed by (ii) the cells spreading across the surface instead of upward, as can be seen in our 1-day and 2-day biofilm SEM images by visibility of the membrane underneath the cells, and the beginning of EPS production. A consistent increase in cell clustering and matrix production can be seen between day 1-3 images as the biofilm matures. The next stage of growth (iii) is the development of water channel structures and an increase in biofilm height, exhibited in the 3-day and 4-day SEM images where the membrane surface is not visible anymore (**Figure 2B**). The 4-day biofilm SEM image shows full maturation (this is stage *iv* in **Figure 2C**) as evidenced by encasement of the cells in EPS, which appears as the glue-like substance between the bacterial cells (**Figure 2B**). Mature biofilms are very difficult to eradicate, even with harsh chemical and/or mechanical treatments[44,45]. Additionally, clusters from a mature biofilm commonly detach[46], allowing the bacterial cells to spread and establish biofilms elsewhere (this is stage *v* in **Figure 2C**). Based on these results, we chose 4 days of incubation as the time point that would result in a strong, well-developed biofilm and a thick matrix for all subsequent experiments, in an effort to properly demonstrate the biofilm-fighting ability of our phage treatment.

Next, we determined the required length of time for phage treatment to reduce biofilm levels. We chose 6 hrs and overnight (16-18 hrs) as these reflect timepoints commonly found to be effective in our lab for various phage-host pairs. The amount of biofilm remaining on the sensor membranes was quantified before and after phage treatment by staining the biofilm with Hoechst, a Deoxyribonucleic acid (DNA)-binding fluorescent

dye that can penetrate the bacterial cell wall and stain the bacterial genome[47]. As shown in **Figure 3A**, a 6-hr phage treatment was capable of diminishing the fluorescence signal from stained bacteria, but an overnight treatment was the most effective at reducing the amount of biofilm on the DO membrane.

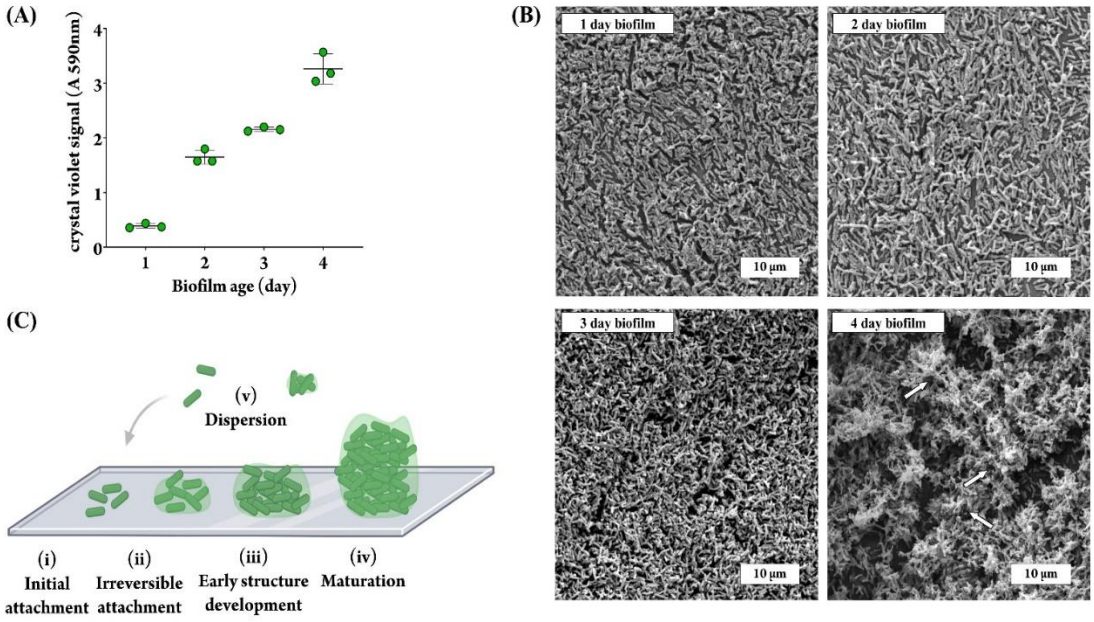

Figure 2. (**A)** Amount of PA biofilm grown in a microtiter plate for the duration of one to four days, quantified as absorbance of re-solubilized crystal violet stain at 590 nm. Each data point represents an average of 20 technical replicates (n=3). **(B)** SEM images of PA biofilm grown on DO sensor membranes for one, two, three, and four days. White arrows indicate some of the water channels visible in the matrix structure. **(C)** Schematic of a PA biofilm lifecycle: (i) initial attachment of cells to the surface; (ii) lateral spreading of cells and production of EPS, leading to irreversible attachment; (iii) early development of biofilm structure; (iv) mature biofilm architecture; (v) dispersion of cells from the biofilm and continuation of the cycle.

The fluorescence images from treated and non-treated membranes reflect the quantitative measurements, with an overnight phage treatment resulting in the least amount of staining on the membrane (**Figure 3B**). It should be noted that the biofilm EPS is composed of exopolysaccharides, proteins, and extracellular DNA (eDNA)[4], and therefore the DNA-binding fluorescent dye can bind to both the eDNA and the DNA inside the bacterial cells. To confirm the trends observed with fluorescence imaging of the membranes, SEM was used to visualize a biofouled membrane following phage treatment. The SEM images

show that the phages were able to clear the dense matrix structure and no intact bacterial cells were visible (**Figure 3C)**. As shown in **Figure 1B**, lytic phages self-propagate by lysing bacterial cells and propagating themselves in the process, on site, which results in biofilm reduction over time. There is, however, traces of what appears to be cellular debris on the phage-treated membrane, which is expected to be a result of phage-mediated bacterial lysis. The full removal of the biofilm matrix is an interesting observation because it suggests the involvement of matrix-degrading enzymes. Phages coevolved with bacteria over millions of years and have developed specific strategies to combat biofilms. Some phages carry or express enzymes to degrade extracellular proteins and polysaccharides, key components of a biofilm matrix, and reach the bacterial cells embedded inside.[48] Alternatively, some phages can induce such enzymes from within the bacterial genome.[48]

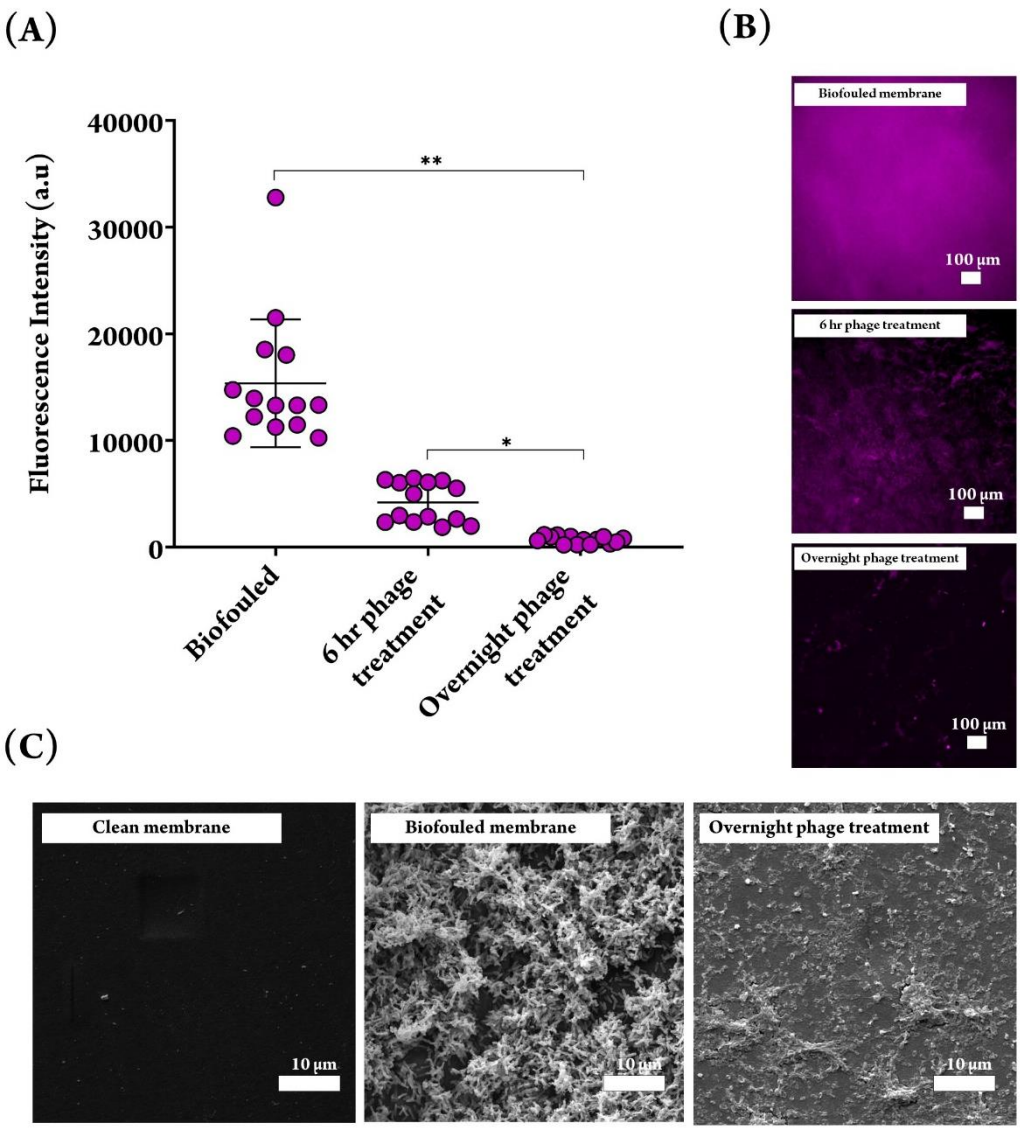

Figure 3. (A) Fluorescence intensity of biofouled and phage treated membranes for 6 hr and overnight phage treatments, stained with Hoechst dye and quantified with ImageJ software. Significant difference in fluorescence intensity was observed between biofouled and phage treated membranes. Overnight phage treatment resulted in a significantly lower fluorescence signal, compared to 6 hr treated phage. Significant difference when comparing biofouled membranes with 6 hr and overnight phage treated membranes (* $P<0.05$, ** $P<0.001$). (B) Fluorescence micrographs of biofouled, 6 hr- and overnight phage treated membranes. The fluorescence signal does not differentiate between intracellular and extracellular DNA. (C) SEM images depicting a clean DO sensor membrane, a biofouled membrane with a 4-day PA biofilm, and a biofouled membrane subjected to an overnight phage treatment.

6.3.2 Sensor signal recovery

As is evident from the fluorescence microscopy images of phage treated samples, overnight phage treatment led to a significant decrease in amount of biomass, and successfully removed biofilms from the surface of DO sensor membrane. As a result, these membranes were used for further analysis to measure DO concentrations in DI water, and the resulting sensor signals were compared with clean and biofouled membranes. The sensor used in this study is an electrochemical sensor that contains an electrode, electrolyte and a selectively permeable membrane. This Polytetrafluoroethylene (PTFE)-based membrane allows dissolved oxygen in water to pass through and hinders the diffusion of water and other large components, thus playing a central role in the generation of an accurate electrochemical DO signal[49]. Once passed through the membrane, diffused oxygen undergoes an electrochemical reaction within the electrolyte solution, producing an electrical signal which is shown in the sensor display.

DO sensor signal decreased from 7.96 ± 0.27 mg/L for a clean membrane to 5.39 ± 1.63 mg/L after growing biofilms for four days on membranes (32% decrease in signal after biofouling). Biofilm blocks the pores on the membrane surface and prevents proper oxygen diffusion through the small pores on the surface of permeable membranes, therefore significantly decreasing the signal and increasing the noise (note the increase in standard deviation). After incubating the biofouled membranes in the phage suspension overnight, which removed the biofilm from the surface of the membranes, the signal to noise ratio increased significantly (8-fold increase) and phage treatment was able to successfully recover the absolute DO sensor measurement by (7.75 ± 0.30 mg/L, **Figure 4A**). Although some cellular and matrix debris still remained on the surface, results from DO measurement indicate that this did not affect the measurements, and the drastic decrease in amount of biomass following phage treatment worked well to enhance oxygen diffusion through the permeable membrane. In addition, the sensor response time that had increased following the biofilm formation on the membrane was also recovered after phage treatment, decreasing from 282.7± 47.12 sec for a biofouled membrane to 158.3±19.41sec for a phage treated membrane, which was comparable to the response time of a clean sensor 145.7±21.27 sec (**Figure 4B**). On the other hand, when a 10%

bleach solution, a common bactericidal chemical, was used to remove biofilms from the surface of DO sensor membranes, a high variability in DO measurement and response time were observed. Although the results do not show significant difference from phage treated membranes, it is not a hidden fact that using chemicals such as bleach have adverse consequences including but not limited to, metals and painted surfaces corrosion, reaction with other chemicals and release of toxic products which can be extremely harmful to the environment. [8]

Dissolved oxygen is one of the pivotal parameters defining the health of water bodies and marine environments. Aquatic creatures rely on dissolved oxygen, and they require at least 5 mg/L to survive[49]. Electrochemical DO sensors, such as the one used for our investigation, are known for accuracy and fast response time, both of which have been significantly affected by biofouling of the sensor membrane, as indicated by our data, clearly demonstrating how biofouling could pose a major challenge for the use of DO sensors in marine environment monitoring. A single phage treatment, however, regenerated the sensor surface and completely recovered the signal to its original value, as well as lowering the response time to that of a clean sensor. This demonstrates the utility of phage for non-invasive cleaning of DO sensors and suggests potential for cleaning of other sensor surfaces that have been subjected to biofouling.

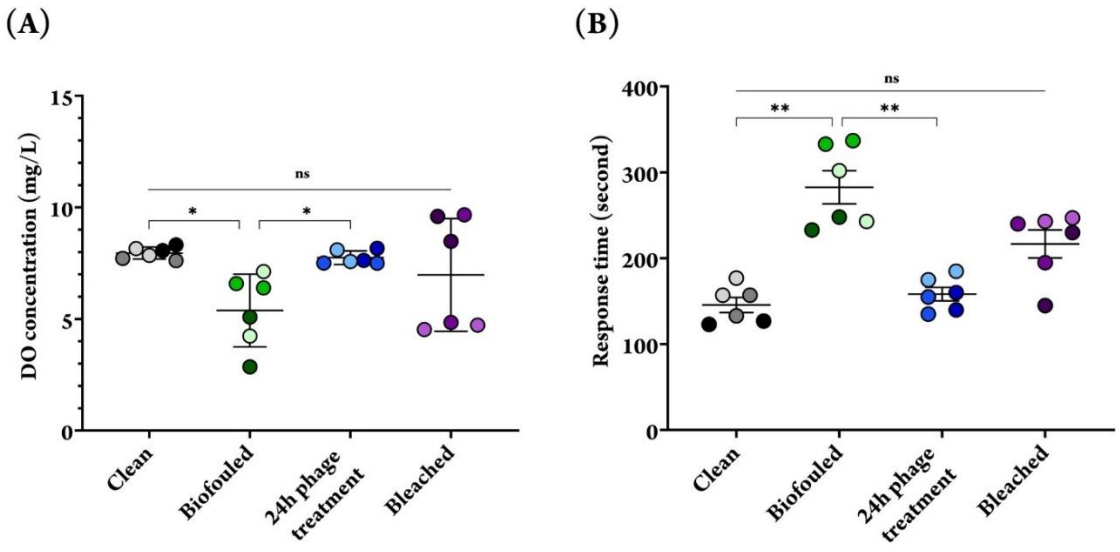

Figure 4. (A) DO measurement for clean, biofouled, phage treated, and bleached sensor membranes in DI water. **(B)** Response time of DO sensor measured with clean, biofouled, phage treated and bleached membranes. The data points show the average of three measurements with each membrane. Experiments were performed in triplicates, and for each replicate, 2 membranes were used, bringing the total number of membranes used for each condition to six. Different color shades have been used to differentiate the data points for each biological replicate. Significant difference when comparing phage treated membranes with biofouled and clean membranes (* $P<0.05$, ** $P<0.01$).

6.4. Conclusion

We present an effective method for cleaning biofouled sensors and completely restoring the sensor signal to its original value with no harsh chemicals or mechanical treatments required, which is beneficial for use on delicate membranes and sensitive sensing surfaces. We achieved these results with only a single phage treatment, and without the need for repeated treatments, owing to the self-propagating nature of bacteriophages[50]. Phages can replicate on the sensor membrane, as long as they have access to viable host bacteria, allowing for a continuous cycle of infection until the biofilm is cleared and resulting in recovery of the DO sensor function. Aside from being polymicrobial, environmental biofilms typically develop a strong matrix, which would require the use of phage with matrix degrading enzymes.

The specificity of phages in being able to only infect a few closely related strains of bacteria means they are non-destructive towards beneficial microbes present in the

environment in which the sensor is installed,[51] unlike harsh cleaning agents. The lack of environmental toxicity means phage treatments could be readily applied on site, without the need to remove the sensor from the point at which it was installed. In that case, the phage treatment can be applied by submerging the sensor in a closed container with phage.

It is worth noting that phage-host specificity would require the real-life application of our proposed method to involve a pre-screening for specific lytic phages that can infect the bacteria comprising the biofilm. In this study, we grew mono-species biofilms using a lab strain of bacteria known to be a strong biofilm-former as a demonstration of the effectiveness of phage treatment against sensor biofouling. Environmental biofilms are typically a mixture of multiple species[52], which would require the use of more than one type of phage. Finding phages that infect the multispecies environmental biofilm is usually as easy as screening the same aquatic environment for phage, because phages reside in the same niche as their host. In fact, even for therapeutic use in humans, phages are routinely isolated from environmental reservoirs such as ponds, lakes, streams, or even sewage[18]. This means that with seasonal changes in the composition of environmental biofilms formed in aquatic environments, we have access to an endless supply of phages that change and evolve with changes in the host population. With time, this would lead to a library of phages that can be used for a certain niche to tackle environmental biofilms on sensors and can be easily screened against new target bacteria. Generating phage preparations for environmental applications is relatively low cost because, unlike therapeutic applications, extensive purification may not be required.

In summary, with the correct selection of phage, bacteriophage treatment could find broad utility in regenerating not only DO or membrane-based sensors, but any sensor surface that is subject to extensive biofouling.

6.5. Materials

The ExStik II DO600 dissolved oxygen meter and DO603 membrane kits were purchased from Extech Instruments (Nashua, USA). Phosphate buffered saline (PBS) (0.1 M, pH 7.4) was prepared using tablets from VWR (Mississauga, Canada). Clear, flat-bottom, sterilized, 96-well tissue culture plates and crystal violet were also purchased from VWR. LB Broth, Miller, sterile 50mL conical centrifuge tubes, and glutaraldehyde (50%) were purchased from Fisher Scientific (Mississauga, Canada). Hoechst 33342 nucleic acid stain (ex/em 350/461 nm) was purchased from Thermofisher Scientific (Massachusetts, USA). Formaldehyde was purchased from Caledon Laboratories (Georgetown, Canada).

6.6. Methods

6.6.1 Bacterial strain, phage, and culture conditions

The bacterial strain used in this study was *Pseudomonas aeruginosa* PAO1 (PA) and the phages used were vB_Pae-Kakheti25 and vB_Pae-Tbilisi32 (DSMZ, Germany). Bacterial overnights of PA were prepared by inoculating LB broth with a frozen glycerol stock and incubating at 37°C and 180 rpm for 16-18 hrs. Phage suspensions were propagated by diluting the overnight culture 1:1000 into 50mL of LB media in a baffled Erlenmeyer flask and incubating at 37°C and 180 rpm. When the optical density of the culture at 600 nm (OD_{600}) reached 0.5, 10µL of either phage vB_Pae-Kakheti25 or vB_Pae-Tbilisi32 was added and the culture and incubated for 6 hrs, or overnight. The resulting phage lysate was centrifuged for 10 min at 7000×g, then the supernatant was filtered through a 0.2µm syringe filter and stored in the fridge. The concentration of the phage suspension (number of plaque forming units per mL, PFU/mL) was determined using the agar overlay technique[36].

6.6.2 Biofilm formation and quantification

Biofilms were formed on the membranes by placing the DO membrane cassette face down in a 50mL conical tube containing 2mL of an overnight PA culture, diluted 1:1000 in LB broth. The membranes were incubated at 37°C and 80 rpm for 1-4 days. Biofilm was then quantified through fluorescence microscopy followed by image analysis. For biofilms

formed in 96-well plates, we diluted an overnight culture 1:1000 in LB broth, added 200µL of diluted suspension to each well, and incubated the plate at 37°C and 80 rpm for 1-4 days. Biofilms were then quantified using the crystal violet method, as described elsewhere[37]. Briefly, biofilms were washed three times with PBS buffer, stained with crystal violet, and then quantified by dissolving the crystal violet in acetone and reading the absorbance at 590 nm with a BioTek plate reader.

6.6.3 Phage treatment

Membranes with biofilm were rinsed in PBS three times and then incubated in 2mL of a 1:1 mixture of vB_Pae-Kakheti25 and vB_Pae-Tbilisi32 (10^9 PFU/mL each) in a 50mL conical tube at 37°C and 80 rpm for 6 hrs or overnight. The control fouled membranes were treated the same way but incubated in LB broth instead of a phage suspension.

6.6.4 Bleach treatment

Same as phage treatment, membranes with biofilm were rinsed in PBS three times, and then incubated in 2 mL of a 10% bleach solution in a 50 mL conical tube at 37°C and 80 rpm overnight.

6.6.5 Sensitivity readings

DO concentration of stirred deionized (DI) water was measured using the DO sensor with clean, biofouled, phage-treated and bleached membranes installed. Two membranes were used per condition and the measurements were repeated three times with each membrane. Each experiment was performed in triplicates. The response time for each membrane was recorded as the time the sensor readings showed fluctuations $< \pm 0.01$ mg/L for 30 seconds.

6.6.6 Fluorescence microscopy

Biofouled and phage-treated membranes were fixed with 4% formaldehyde in PBS for 30 min and rinsed with DI water. Fixed samples were stained with 400 µL of 25 µg/mL Hoechst 33342 in DI water for 1 hr and rinsed lightly with DI water afterwards to remove unbound fluorescence dye. Images were recorded using Nikon Eclipse Ti2-E motorized

inverted fluorescence microscope, and the results were quantified using ImageJ image processing software. For quantification, two membranes and seven frames of each membrane were used.

6.6.7 Scanning electron microscopy (SEM)

Membranes were cut out of their cassette and rinsed with PBS three times. Following fixation with 30% glutaraldehyde for 30 min at 4°C, the membranes were dehydrated in a gradient of ethanol solutions (10%, 30%, 50%, 70%, 90%, 100%) for 10 mins each, then dried using a Leica EM CPD300 critical point dryer (Leica Mikrosysteme GmbH, Austria). Those were then coated with 20nm of gold using a Polaron Model E5100 sputter coater (Polaron Equipment Ltd., UK). SEM images were obtained using a Tecan VEGA II LSU SEM (Tecan USA, PA, USA) at 10 kV and 4700x magnification.

6.6.8 Statistical analysis

Data are presented as means ± standard deviation. Statistical significance was assessed using analysis of variance and post-hoc analysis with Tukey's test, where significant difference was considered as $P < 0.05$. All experiments were performed in triplicates unless otherwise specified.

6.7. References

(1) Flemming, H. Biofouling and Me: My Stockholm Syndrome with Biofilms. *Water Res.* **2020**, *173*, 115576. https://doi.org/10.1016/j.watres.2020.115576.
(2) Malheiro, J.; Simões, M. *Antimicrobial Resistance of Biofilms in Medical Devices*; Elsevier Ltd, 2016. https://doi.org/10.1016/B978-0-08-100382-4.00004-6.
(3) Salta, M.; Wharton, J. A.; Blache, Y.; Stokes, K. R.; Briand, J. F. Marine Biofilms on Artificial Surfaces: Structure and Dynamics. *Environ. Microbiol.* **2013**, *15* (11), 2879–2893. https://doi.org/10.1111/1462-2920.12186.
(4) Rabin, N.; Zheng, Y.; Opoku-Temeng, C.; Du, Y.; Bonsu, E.; Sintim, H. O. Biofilm Formation Mechanisms and Targets for Developing Antibiofilm Agents. *Future Med. Chem.* **2015**, *7* (4), 493–512. https://doi.org/10.4155/fmc.15.6.
(5) Moreira, J. M. R.; Fulgêncio, R.; Alves, P.; Machado, I.; Bialuch, I.; Melo, L. F.; Simões, M.; Mergulhão, F. J. Evaluation of SICAN Performance for Biofouling Mitigation in the Food Industry. *Food Control* **2016**, *62*, 201–207. https://doi.org/10.1016/j.foodcont.2015.10.023.
(6) Nguyen, T.; Roddick, F. A.; Fan, L. Biofouling of Water Treatment Membranes: A Review of the Underlying Causes, Monitoring Techniques and Control

Measures. *Membranes (Basel).* **2012**, *2* (4), 804–840. https://doi.org/10.3390/membranes2040804.

(7) Cao, S.; Wang, J. D.; Chen, H. S.; Chen, D. R. Progress of Marine Biofouling and Antifouling Technologies. *Chinese Sci. Bull.* **2011**, *56* (7), 598–612. https://doi.org/10.1007/s11434-010-4158-4.

(8) Whelan, A.; Regan, F. Antifouling Strategies for Marine and Riverine Sensors. *J. Environ. Monit.* **2006**, *8* (9), 880–886. https://doi.org/10.1039/b603289c.

(9) Henderson, P. Fouling and Antifouling in Other Industries- Power Stations, Desalination Plants- Drinking Water Supplies and Sensors. In *Biofouling*; Wiley-Blackwell: Oxford, UK, 2010; pp 288–305. https://doi.org/10.1002/9781444315462.ch20.

(10) Delauney, L.; Compare, C.; Lehaitre, M. Biofouling Protection for Marine Environmental Sensors. *Ocean Sci.* **2010**, *6* (2), 503–511. https://doi.org/10.5194/os-6-503-2010.

(11) Lehaitre, M.; Compère, C. Biofouling and Underwater Measurements. *Real-Time Coast. Obs. Syst. Mar. Ecosyst. Dyn. Harmful Algal Bloom. Theory, Instrum. Model.* **2008**, 463–493.

(12) Grzegorczyk, M.; Pogorzelski, S. J.; Pospiech, A.; Boniewicz-Szmyt, K. Monitoring of Marine Biofilm Formation Dynamics at Submerged Solid Surfaces with Multitechnique Sensors. *Front. Mar. Sci.* **2018**, *5* (OCT), 1–16. https://doi.org/10.3389/fmars.2018.00363.

(13) Whittaker, C.; Ridgway, H.; Olson, B. H. Evaluation of Cleaning Strategies for Removal of Biofilms from Reverse-Osmosis Membranes. *Appl. Environ. Microbiol.* **1984**, *48* (2), 395–403. https://doi.org/10.1128/aem.48.2.395-403.1984.

(14) Li, J.; Hirota, K.; Yumoto, H.; Matsuo, T.; Miyake, Y.; Ichikawa, T. Enhanced Germicidal Effects of Pulsed UV-LED Irradiation on Biofilms. *J. Appl. Microbiol.* **2010**, *109* (6), 2183–2190. https://doi.org/10.1111/j.1365-2672.2010.04850.x.

(15) Gora, S.; Rauch, K.; Ontiveros, C.; Gagnon, G. Ultraviolet Light Emitting Diodes (UV LEDs) for Biofilm Control. *16th Int. Environ. Spec. Conf. 2018, Held as Part Can. Soc. Civ. Eng. Annu. Conf. 2018* **2019**, No. 2017, 226–232.

(16) Pichardo-Romero, D.; Garcia-Arce, Z. P.; Zavala-Ramírez, A.; Castro-Muñoz, R. Current Advances in Biofouling Mitigation in Membranes for Water Treatment: An Overview. *Processes* **2020**, *8* (2), 1–22. https://doi.org/10.3390/pr8020182.

(17) Osborne, M.; Aryasomayajula, A.; Shakeri, A.; Selvaganapathy, P. R.; Didar, T. F. Suppression of Biofouling on a Permeable Membrane for Dissolved Oxygen Sensing Using a Lubricant-Infused Coating. *ACS Sensors* **2019**, *4* (3), 687–693. https://doi.org/10.1021/acssensors.8b01541.

(18) Schooley, R. T.; Biswas, B.; Gill, J. J.; Hernandez-Morales, A.; Lancaster, J.; Lessor, L.; Barr, J. J.; Reed, S. L.; Rohwer, F.; Benler, S.; Segall, A. M.; Taplitz, R.; Smith, D. M.; Kerr, K.; Kumaraswamy, M.; Nizet, V.; Lin, L.; McCauley, M. D.; Strathdee, S. A.; Benson, C. A.; Pope, R. K.; Leroux, B. M.; Picel, A. C.; Mateczun, A. J.; Cilwa, K. E.; Regeimbal, J. M.; Estrella, L. A.; Wolfe, D. M.; Henry, M. S.; Quinones, J.; Salka, S.; Bishop-Lilly, K. A.; Young, R.; Hamilton, T. Development and Use of Personalized Bacteriophage-Based Therapeutic Cocktails to Treat a Patient with a Disseminated Resistant Acinetobacter Baumannii Infection. *Antimicrob. Agents Chemother.* **2017**, *61* (10).

https://doi.org/10.1128/AAC.00954-17.

(19) Badv, M.; Jaffer, I. H.; Weitz, J. I.; Didar, T. F. An Omniphobic Lubricant-Infused Coating Produced by Chemical Vapor Deposition of Hydrophobic Organosilanes Attenuates Clotting on Catheter Surfaces. *Sci. Rep.* **2017**, *7* (1), 1–10. https://doi.org/10.1038/s41598-017-12149-1.

(20) Hall-Stoodley, L.; Costerton, J. W.; Stoodley, P. Bacterial Biofilms: From the Natural Environment to Infectious Diseases. *Nat. Rev. Microbiol.* **2004**, *2* (2), 95–108. https://doi.org/10.1038/nrmicro821.

(21) Flemming, H. C.; Wingender, J.; Szewzyk, U.; Steinberg, P.; Rice, S. A.; Kjelleberg, S. Biofilms: An Emergent Form of Bacterial Life. *Nat. Rev. Microbiol.* **2016**, *14* (9), 563–575. https://doi.org/10.1038/nrmicro.2016.94.

(22) D'Hérelle, F. Sur Un Microbe Invisible Antagoniste Des Bacilles Dysentériques. *Comptes rendus Acad Sci Paris* **1917**, No. 165, 373–375.

(23) D'Hérelle, F. *The Bacteriophage, Its Role in Immunity*; Baltimore, Williams & Wilkins, 1922.

(24) Ferriol-González, C.; Domingo-Calap, P. Phages for Biofilm Removal. *Antibiotics* **2020**, *9* (5), 1–16. https://doi.org/10.3390/antibiotics9050268.

(25) Ma, W.; Panecka, M.; Tufenkji, N.; Rahaman, M. S. Bacteriophage-Based Strategies for Biofouling Control in Ultrafiltration: In Situ Biofouling Mitigation, Biocidal Additives and Biofilm Cleanser. *J. Colloid Interface Sci.* **2018**, *523*, 254–265. https://doi.org/10.1016/j.jcis.2018.03.105.

(26) Kortright, K. E.; Chan, B. K.; Koff, J. L.; Turner, P. E. Phage Therapy: A Renewed Approach to Combat Antibiotic-Resistant Bacteria. *Cell Host Microbe* **2019**, *25* (2), 219–232. https://doi.org/10.1016/j.chom.2019.01.014.

(27) Richter, Ł.; Janczuk-Richter, M.; Niedziółka-Jönsson, J.; Paczesny, J.; Hołyst, R. Recent Advances in Bacteriophage-Based Methods for Bacteria Detection. *Drug Discov. Today* **2018**, *23* (2), 448–455. https://doi.org/10.1016/j.drudis.2017.11.007.

(28) Salmond, G. P. C.; Fineran, P. C. A Century of the Phage: Past, Present and Future. *Nat. Rev. Microbiol.* **2015**, *13* (12), 777–786. https://doi.org/10.1038/nrmicro3564.

(29) Harada, L. K.; Silva, E. C.; Campos, W. F.; Del Fiol, F. S.; Vila, M.; Dąbrowska, K.; Krylov, V. N.; Balcão, V. M. Biotechnological Applications of Bacteriophages: State of the Art. *Microbiol. Res.* **2018**, *212–213* (February), 38–58. https://doi.org/10.1016/j.micres.2018.04.007.

(30) Gordillo Altamirano, F. L.; Barr, J. J. Phage Therapy in the Postantibiotic Era. *Clin. Microbiol. Rev.* **2019**, *32* (2), 1–25. https://doi.org/10.1128/CMR.00066-18.

(31) Bhattacharjee, A. S.; Choi, J.; Motlagh, A. M.; Mukherji, S. T.; Goel, R. Bacteriophage Therapy for Membrane Biofouling in Membrane Bioreactors and Antibiotic-Resistant Bacterial Biofilms. *Biotechnol. Bioeng.* **2015**, *112* (8), 1644–1654. https://doi.org/10.1002/bit.25574.

(32) Ayyaru, S.; Choi, J.; Ahn, Y. H. Biofouling Reduction in a MBR by the Application of a Lytic Phage on a Modified Nanocomposite Membrane. *Environ. Sci. Water Res. Technol.* **2018**, *4* (10), 1624–1638. https://doi.org/10.1039/c8ew00316e.

(33) Sivri, N.; Jones, M.; Allen, M. J. Pseudomonas Aeruginosa Isolated From the Marine Environments in the Istanbul Coastal Area (Turkey). *Fresenius Environ. Bull.* **2014**, *23* (12B), 1.

(34) Holban, A. M.; Chifiriuc, M. C.; Cotar, A. I.; Bleotu, C.; Grumezescu, A. M.; Banu, O.; Lazar, V. Virulence Markers in Pseudomonas Aeruginosa Isolates from Hospitalacquired Infections Occurred in Patients with Underlying Cardiovascular Disease. *Rom. Biotechnol. Lett.* **2013**, *18* (6), 7243–7254.

(35) Wu, S.; Liu, G.; Jin, W.; Xiu, P.; Sun, C. Antibiofilm and Anti-Infection of a Marine Bacterial Exopolysaccharide against Pseudomonas Aeruginosa. *Front. Microbiol.* **2016**, *7* (FEB), 1–15. https://doi.org/10.3389/fmicb.2016.00102.

(36) Green, M. R.; Sambrook, J. *Molecular Cloning: A Laboratory Manual (Fourth Edition)*; 2012; Vol. 1. https://doi.org/10.3724/SP.J.1141.2012.01075.

(37) O'Toole, G. A. Microtiter Dish Biofilm Formation Assay. *J. Vis. Exp.* **2010**, No. 47, 10–11. https://doi.org/10.3791/2437.

(38) Hosseinidoust, Z.; Tufenkji, N.; van de Ven, T. G. M. Predation in Homogeneous and Heterogeneous Phage Environments Affects Virulence Determinants of Pseudomonas Aeruginosa. *Appl. Environ. Microbiol.* **2013**, *79* (9), 2862–2871. https://doi.org/10.1128/AEM.03817-12.

(39) Hosseinidoust, Z.; Tufenkji, N.; van de Ven, T. G. M. Formation of Biofilms under Phage Predation: Considerations Concerning a Biofilm Increase. *Biofouling* **2013**, *29* (4), 457–468. https://doi.org/10.1080/08927014.2013.779370.

(40) Hosseinidoust, Z.; van de Ven, T. G. M.; Tufenkji, N. Evolution of Pseudomonas Aeruginosa Virulence as a Result of Phage Predation. *Appl. Environ. Microbiol.* **2013**, *79* (19), 6110–6116. https://doi.org/10.1128/AEM.01421-13.

(41) Stoodley, P.; Sauer, K.; Davies, D. G.; Costerton, J. W. Biofilms as Complex Differentiated Communities. *Annu. Rev. Microbiol.* **2002**, *56* (1), 187–209. https://doi.org/10.1146/annurev.micro.56.012302.160705.

(42) Rasamiravaka, T.; Labtani, Q.; Duez, P.; El Jaziri, M. The Formation of Biofilms by Pseudomonas Aeruginosa : A Review of the Natural and Synthetic Compounds Interfering with Control Mechanisms. *Biomed Res. Int.* **2015**, *2015*, 1–17. https://doi.org/10.1155/2015/759348.

(43) Southey-Pillig, C. J.; Davies, D. G.; Sauer, K. Characterization of Temporal Protein Production in Pseudomonas Aeruginosa Biofilms. *J. Bacteriol.* **2005**, *187* (23), 8114–8126. https://doi.org/10.1128/JB.187.23.8114-8126.2005.

(44) Simões, M.; Pereira, M. O.; Vieira, M. J. Effect of Mechanical Stress on Biofilms Challenged by Different Chemicals. *Water Res.* **2005**, *39* (20), 5142–5152. https://doi.org/10.1016/j.watres.2005.09.028.

(45) Chen, X.; Stewart, P. S. Biofilm Removal Caused by Chemical Treatments. *Water Res.* **2000**, *34* (17), 4229–4233. https://doi.org/10.1016/S0043-1354(00)00187-1.

(46) Guilhen, C.; Forestier, C.; Balestrino, D. Biofilm Dispersal: Multiple Elaborate Strategies for Dissemination of Bacteria with Unique Properties. *Mol. Microbiol.* **2017**, *105* (2), 188–210. https://doi.org/10.1111/mmi.13698.

(47) Simmons, W. L.; Dybvig, K. Biofilms Protect Mycoplasma Pulmonis Cells from Lytic Effects of Complement and Gramicidin. *Infect. Immun.* **2007**, *75* (8), 3696–3699. https://doi.org/10.1128/IAI.00440-07.

(48) Motlagh, A. M.; Bhattacharjee, A. S.; Goel, R. Biofilm Control with Natural and Genetically-Modified Phages. *World J. Microbiol. Biotechnol.* **2016**, *32* (4), 1–10. https://doi.org/10.1007/s11274-016-2009-4.

(49) Hsu, L.; Selvaganapathy, P. R.; Brash, J.; Fang, Q.; Xu, C. Q.; Deen, M. J.; Chen,

H. Development of a Low-Cost Hemin-Based Dissolved Oxygen Sensor with Anti-Biofouling Coating for Water Monitoring. *IEEE Sens. J.* **2014**, *14* (10), 3400–3407. https://doi.org/10.1109/JSEN.2014.2332513.

(50) Loc-Carrillo, C.; Abedon, S. T. Pros and Cons of Phage Therapy. *Bacteriophage* **2011**, *1* (2), 111–114. https://doi.org/10.4161/bact.1.2.14590.

(51) Salmond, G. P. C.; Fineran, P. C. A Century of the Phage: Past, Present and Future. *Nat. Rev. Microbiol.* **2015**, *13* (12), 777–786. https://doi.org/10.1038/nrmicro3564.

(52) Balcázar, J. L.; Subirats, J.; Borrego, C. M. The Role of Biofilms as Environmental Reservoirs of Antibiotic Resistance. *Front. Microbiol.* **2015**, *6* (OCT), 1–9. https://doi.org/10.3389/fmicb.2015.01216.

6.8. Supplementary Information

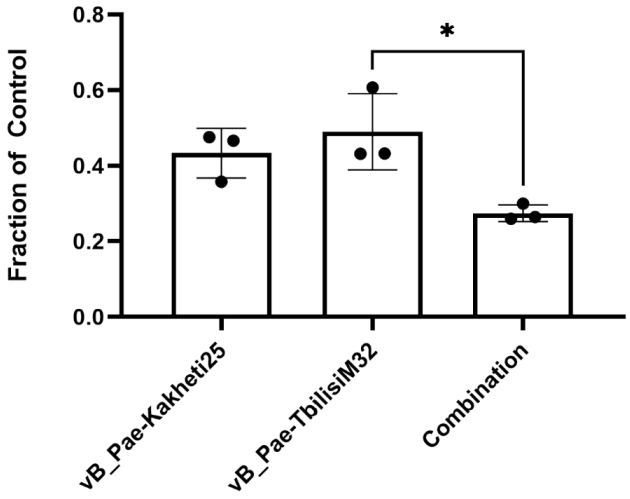

Figure S1. PA biofilm removal (compared to the no-phage control) in a microtiter plate after treating a 4-day PA biofilm with single phages or a phage mixture, quantified as absorbance of re-solubilized crystal violet stain at 590 nm. Shown are the data point (the average of 10 technical replicates) for three independent biological replicates.

Chapter 7. Concluding remarks and Future Direction

7.1. Conclusions

The global challenge of antibiotic resistance has been rapidly spreading around the world, posing a significant threat to public health. The process of discovering new antibiotics has proven to be very slow and extremely expensive. In response to this crisis, bacteriophages have emerged as a promising alternative for combating antibiotic resistance. Their unique attributes make them a powerful tool in the fight against bacterial resistance, with the potential to make a substantial impact on the health and well-being of both humans and animals.

This thesis delves into the various applications of bacteriophages, aiming to bridge the gap between theoretical knowledge and practical solutions. I have explored a range of applications from developing assays to selecting phages for personalized phage therapy, and utilizing them in eradication and prevention of biofilms in both biomedical and environmental contexts.

I have developed a thermally stable ATP bioluminescent assay within sugar polymer matrices, enabling real-time monitoring of phage-mediated bacterial cell lysis. This approach involves creating all-inclusive dried tablets containing ATP assay reagents, a library of different phages, and sugar polymers such as pullulan and trehalose. These tablets have demonstrated remarkable efficacy in rapidly detecting strongly lytic phages, with results available in as little as 30 minutes. However, it is essential to note that the phage-bacteria dynamics may vary based on the bacterial species. This method serves as an initial screening tool for identifying lytic phages against specific bacterial isolates. For a more comprehensive assessment of long-term infectivity and the design of phage cocktails, additional liquid growth curve assays, such as turbidity measurements and tracking cellular respiration, can be implemented over extended timeframes. Optimizing the ATP bioluminescence assay for use in a 384-well plate format can also offer a distinct advantage over time-consuming and labor-intensive spot test assays. Moreover, the shelf

stability of phages preserved in sugar matrices facilitates their transport between phage therapy centers worldwide.

Next, I explored the feasibility of loading phages into physically cross-linked hydrogels based on nanoclay and CMC. The development of binary phage cocktails demonstrated improved efficacy compared to single-phage treatments, particularly in addressing the rise of phage-resistant mutants. *In vitro* bacterial assays validated the activity of loaded phages in eradicating established biofilms and preventing their formation. Beyond their antibacterial behavior, these hydrogels have been shown to promote bone formation by inducing ALP enzyme secretion, known as an early osteogenic marker. Altogether, the injectable phage-loaded hydrogel based on laponite, and CMC was identified as a simple, phage friendly, and osteogenic promoter suitable for bone healing, enhancing orthopedic implant osteointegration, and fighting recalcitrant bacterial infections.

To improve the performance of repellent coatings on medical implants based on liquid infused, we introduced phage into these coatings. Both *in vitro* and *in vivo* results demonstrated improved outcomes compared to coatings without phage, confirming the effectiveness of phages as natural self-dosing antibacterial agents. A thin layer of phage on the surface of Titanium coupons found its way to the surrounding tissue, blood, and organs such as spleen and liver in a sepsis mouse model. Specifically, the survival rate of animals receiving phage-conjugated coatings was 100% at the end of the 7-day study. Although there was no bacterial cell detected in blood samples of the group receiving phage containing coating, the bacterial load in coupon and its surrounding tissue was similar to controls. The extremely high survival rates could potentially be related to decreased virulence and pathogenicity of bacterial cells following exposure to phage.

Finally, we showed how the applications of phage can be extended to other areas, such as environmental engineering by effectively eradicating stablished biofilms from surfaces like dissolved oxygen sensors to restore their functionality. This was simply possible by immersing the biofouled surface into the phage solution overnight. I also reviewed the applications of phages in designing biosensors for quality monitoring in water and wastewater.

Overall, we hope the research presented in this thesis offers valuable contributions to the broadening landscape of phage applications in addressing current global challenges. The versatility and potential of phages offers promising solutions to enhance the health and well-being of our communities and the environment.

7.2. Recommendations for future work

There are various aspects in each project, detailed below, that can be further explored.

Project 1. All-inclusive sugar-based tablets comprising ATP bioluminescence assay components and phage

- Conducting extended stability testing for dried tablets under varying storage conditions.
- Streamlining the assay for smaller volumes to enable its execution in a 384-well plate format.
- Assessing the assay's performance with diverse bacterial species, including *E. coli*, *S. aureus*, and others.

Project 2. Phage-loaded injectable hydrogel for bone and implant associated infections

- Evaluating the developed hydrogels with additional bacterial species, including *E. coli*, *S. aureus*, and others.
- Conducting *in vivo* animal studies to assess the performance of phage-loaded hydrogels.
- Designing and testing more complex phage cocktails in hydrogels to monitor potential resistance development over longer durations.
- Investigating the pathogenicity of bacteria following exposure to single phages or phage cocktails (both single and multiple species).
- Comparing the immune cell response to phage solutions and phage-loaded hydrogels.
- Developing and conducting *in vivo* testing of hydrogels loaded with both phages and antibiotics after confirming their synergistic behavior *in vitro*.

Project 3. Phage-conjugated LIS coatings on titanium implants

- Employing large animal models such as rabbits, to assess the coating’s effectiveness in both implant infection and infected fractured bone models.

- Conducting extended-duration animal studies for more comprehensive insights.
- Investigating the phenotypes and genotypes of bacteria cells retrieved from mice to identify possible mutations, alterations in virulence and pathogenicity, and reduced fitness.
- Assessing the immune response to coatings conjugated with phages.
- Developing more intricate phage cocktails to enhance the efficacy of phage-LIS coatings against multi-species infections.
- Conjugating a combination of phages and antibiotics into these coatings.

Project 4. Recovering heavily biofouled DO sensor membranes

- Growing biofilms involving multiple species and assessing the anti-biofouling efficacy of a specifically designed phage cocktail.
- Continuously measuring dissolved oxygen (DO) in real-time during phage treatment to monitor the signal alteration as the phages degrade the biofilm matrix.

APPENDIX I: Bacteriophages as Engineering Nano Tools for Monitoring and Detection of Pathogen in Water and Wastewater

Preface: In this chapter, we explore the utilization of bacteriophages as a unique tool for designing detection and monitoring system for environmental applications. While bacteriophages are undergoing substantial research for their applications in the biomedical sector, encompassing therapeutics, diagnostics, and biosensing, they remain relatively obscure to scientists from other fields, particularly environmental researchers. Furthermore, a notable gap exists in translating the insights provided by phage microbiologists into practical real-world applications, a gap that we have endeavored to bridge in our comprehensive review paper. The information presented here offers utility to a broad audience interested in developing detection and monitoring methods involving phages, as well as viruses in a broader context. Additionally, it provides valuable insights for researchers engaged in the exploration of nanoscience and nanotechnology with a focus on virus-based nanomaterials. We have not only highlighted the existing challenges in this field but have also pointed out knowledge gaps that require further research and investigation.

Contribution: I performed the literature review and prepared the original draft. The manuscript was revised and approved by Dr. Hosseinidoust and Dr. Didar.

Citation: F. Bayat, T. F. Didar & Z. Hosseinidoust, Emerging investigator series: bacteriophages as nano engineering tools for quality monitoring and pathogen detection in water and wastewater. **Environ. Sci. Nano 8, 367–389** (**2021**).

Significance: *This paper was selected for the Journal cover in recognition of the quality and significance of our research.*

1. Abstract

Waterborne bacterial pathogens are a major public health concern worldwide, taking many lives and imposing huge economic burden. Rapid and specific detection of pathogens and proper water quality monitoring is an urgent need for preventing the spread of bacterial pathogens and disease outbreaks. Bacteriophages, or phages for short, are the most abundant and ubiquitous biological entities on our planet. These bacterial viruses play a pivotal role in ecosystems as diverse as oceans, soil and the human gut. Phage bio-probes have high specificity, are able to differentiate between viable and non-viable bacteria, and can be easily mass produced, attributes that renders them promising candidates for pathogen detection applications. However, translation of phage-based biosensors to commercial products has been slow. In this comprehensive review, we discuss the current status of phage-based biosensors/bioassays for detection of waterborne bacterial pathogens, and important design parameters for bacteriophage-based detection platforms. We also discuss the challenges and promises of using phage-based detection methods in water and wastewater samples, as well as the future outlook for use of bacteriophages as a powerful tool in environmental engineering.

2. Introduction

Bacteria are present in every niche in the biosphere and play an important role in maintaining the balance in our ecosystem. Pathogenic bacteria, however, are a source of disease in humans, animals, and plants, leading to serious health risks and economical burden[1], prompting us to fight back with biocides and antimicrobials, not only to eradicate contamination, but also to prevent it. Prophylactic use, however, has led to overuse of these antimicrobials (antivirals, antifungals, and antiparasitic), and biocides (disinfectants and surfactants) that has in turn led to serious environmental pollution and contamination of our drinking water and food, as well as the emergence and spread of multi-drug resistant superbugs in the environment, endangering our health and the health of our environment.[2] The spread of antimicrobial resistance (AMR) in the environment has

reached an alarming level and is now considered one of the major challenges globally, taking more than 700,000 lives per year, with an estimated death toll of 10 million people by 2050.[3] Effluents released to the environment from different sources such as livestock farms, municipal sewage, agricultural activities, and wastewater treatment plants all promote AMR in the environment and continuously contaminate soil, water, and sediments.[4] Continuous monitoring and sensitive detection of bacterial pathogens could help to identify contamination at the source and prevent or at least mitigate the risks associated with their spread in the surrounding environment. Detection platforms that allow for real-time, on-site detection/monitoring further have the benefit of finding the contamination early on, leading to effective prevention of disease outbreaks, lower usage of biocides and thus lower contribution to the spread of AMR microorganisms.

Bacteriophages, or phages for short, are the most abundant and ubiquitous biological entities on our planet. Their population is estimated to be 10-fold that of the bacterial population and they have a pivotal role in different ecosystems as diverse as oceans, soil and the human microbiome.[5] The role of these friendly viruses in nature is to keep bacterial populations in check; so, they could be considered as natural antibacterial agents. Bacteriophages were discovered over 100 years ago (years before antibiotics took over) and have been used since as antimicrobials, bacteria typing agents for detecting unknown bacterial strains, as well as unique tools to understand the origins of life.[6] Phages are best known for their high specificity, meaning they are capable of targeting a specific strain of bacteria while leaving other microorganisms inhabiting the same niche intact[7], which makes them promising agents for bacteria detection and contamination monitoring. Genetic material of phage (DNA or RNA) is enclosed in a protein coat called capsid. Different families and genera of phages have been recognized so far, and they are mainly categorized by the nature of their nucleic acid (genetic material) and capsid morphology.[8] **Figure 1** shows a few of phages from different families. Tailed phages such as T4 and T7 and filamentous phages such as M13 are the two most commonly studied groups of phages for biosensing applications.[9–11]

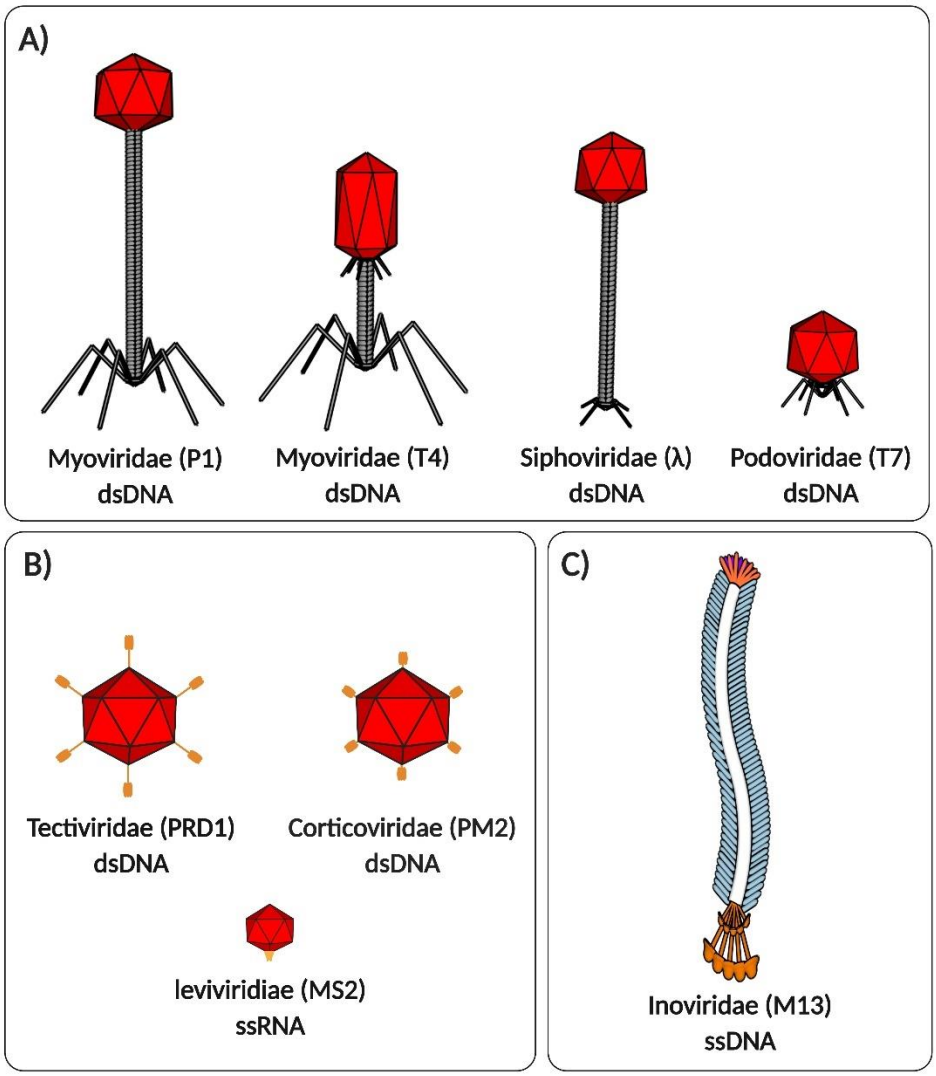

Figure 1. Phages classified based on morphology and genetic material (double stranded DNA: dsDNA, single stranded RNA: ssRNA, and single stranded DNA: ssDNA). **(A)** tailed phages, **(B)** icosahedral phage, (C) filamentous phage.

Phages, similar to all viruses, are obligate parasites and they need to take advantage of the bacterial host replication machinery to reproduce. Phages replicate by infecting host bacterial cells in a four-steps process including adsorption (phage binding to specific receptors on bacterial cells), genome insertion (phage inserting its genome into bacterial cells), synthesis of progeny phages (newly synthesized virions as a result hijacking bacterial replication machinery), and release of progeny phages. Phages can have different life cycles, namely the lytic cycle (**Figure 2A)**, which ultimately leads to lysis and destruction of the host cell (lytic or non-temperate phages), the lysogenic cycle (**Figure**

2B), which leads to the phage genome being incorporated into the bacterial genome and laying dormant until induced through various environmental triggers to the lytic cycle (temperate phages).[7] Although release of progeny phages is a destructive process in most cases and leads to bacterial cell death, filamentous phages secrete progeny phages without causing any major disruption to the bacterial cell wall, and this generally non-bactericidal phage infection is called chronic infection/cycle[12,13] (**Figure 2C**).

Regardless of the replication cycle, phages have the inherent ability to replicate within the bacterial cell; thus, they replicate on site as long as bacterial host is present and can therefore amplify a small signal for detection purposes. They are easy to produce and, in theory, we have access to a tremendous diversity of phage in the environment to target emerging phage-resistant bacteria.[14] Phages are ubiquitous in every niche of the environment and to date, no toxicity towards humans, animals, and plants has been reported.[15,16] Having a genome, phages can also mutate to acquire the ability to infect the bacterial strains that may have acquired phage resistance, leading to what is hypothesized to be a continuous arms race between bacteria and their phage predators. Phages and phage-derived enzymes and proteins could also be used to target bacteria in biofilm mode, the most common mode of existence for bacteria in nature.[17] Because of these unique characteristics, phages are strong tools not only for controlling opportunistic bacteria in different environmental settings, but also for detection and monitoring of contaminations; thus, fighting against the spread of multi-drug resistant superbugs.

In this systemic review, we discuss the important aspects of bacteriophage-based methods for detection of environmental pollution and monitoring of potential outbreaks in drinking water and wastewater. We also discuss the challenges and future outlook for use of bacteriophages as a powerful tool in environmental engineering. We will not cover application of bacteriophages for environmental cleanup and for treating infections in agriculture, animal husbandry and factory farming (including aquaculture). The interested reader in referred to existing comprehensive reviews on the aforementioned subjects.[18–23] **Figure 3** presents an overview of the reported and anticipated use of phage in pathogen detection and monitoring of water and wastewater.

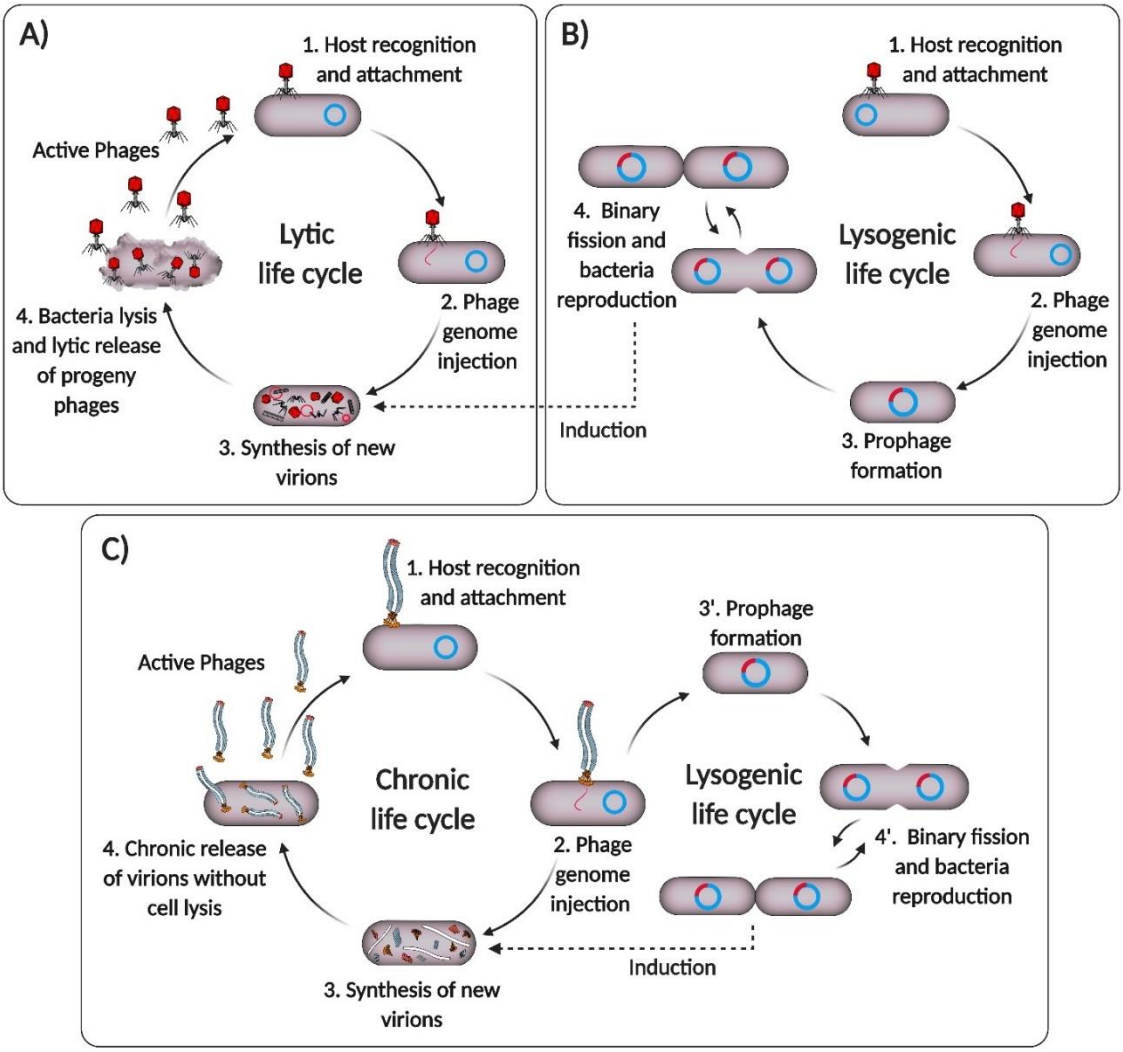

Figure 2. Different phage replication cycles. **(A)** The lytic cycle starts by (1) phage adsorption, (2) phage genome insertion into bacterial cell, (3) synthesis of new virions (progeny phages), and 4) bacterial lysis (5) and release of new phage into the surrounding environment. **(B)** Lysogenic cycle starts with phage adsorption (1) and genome insertion (2); however, the phage genome is incorporated into the bacterial genome, forming a prophage (3) that is replicated through the bacterial reproduction cycle (4). The lysogenic cycle could be induced to start the lytic cycle which ultimately leads to cell lysis (shown by the dashed arrow). **(C)** The phage chronic lifestyle starts with phage adsorption (1) and genome insertion (2). After new virions (progeny phages) are synthesized inside the bacterial cell (3), they are released without lysing bacterial cells (4). Some chronic phages can also adopt a lysogenic lifestyle, in which the phage genome is incorporated into the bacterial genome forming a prophage (3′) and is replicated through the bacterial reproduction cycle (4′) until the chronic cycle is induced (shown by the dashed arrow).

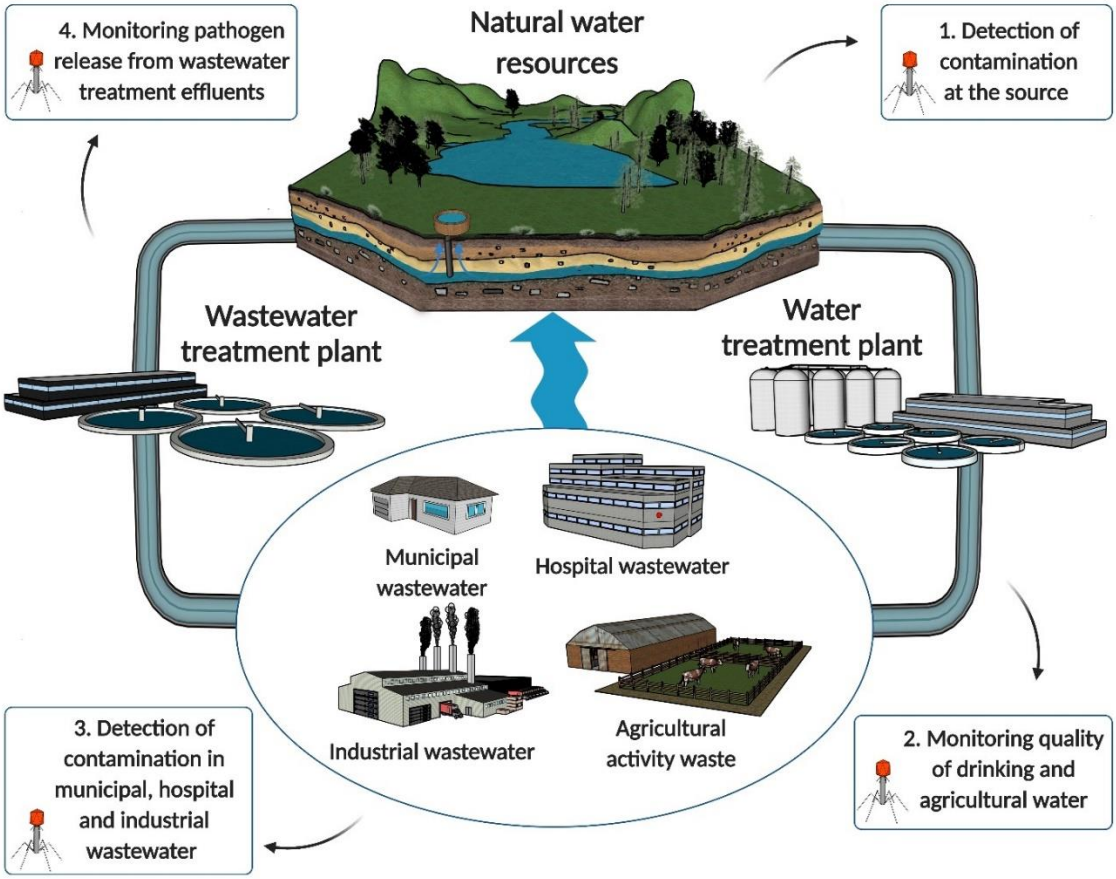

Figure 3. Overview of areas of application of phages in detection and/or monitoring of bacterial contamination in water and wastewater. (1) Natural water resources such as rivers and lakes and ground water can become contaminated through environmental factors such as heavy rainfalls or flooding or with waste from municipal wastewater, waste from industrial plants or factory farms due to treatment deficiencies. Bacteriophages can be used to monitor the health of natural water resources. (2) Water treatment plants deliver clean water to houses and industry, the quality of treated drinking water delivered from water treatment plants can be monitored using phage. (3) Wastewater from manufacturing plants, agricultural activities, and households could enter ground water and natural water resources. Using phages, we can monitor wastewater to catch contamination at the source. (4) The efficiency of wastewater treatment process in wastewater treatment plants can be monitored to prevent the release and spread of pathogenic bacteria through plant effluents.

3. Bacteriophages as sensing probes

Worldwide, 144 million people are reliant on untreated surface water from rivers, lakes, ponds, and streams for sustenance,[24,25] and every year, 3.4 million, mostly children under

the age of 5, die as a result of water-associated diseases.[24] It is estimated that by 2050, 1.8 billion people worldwide will have very limited access to clean water, and some countries will face a severe water shortage.[26] Waterborne pathogens are also among the main causes of severe illnesses in developed countries,[27] and waterborne disease outbreaks occur continuously. At least, 24 disease outbreaks have happened in developed countries during 2001-2016 that have been reported in the scientific literature.[24] Contaminated drinking water could originate from groundwater and surface water contamination (*e.g.*, environmental factors such as heavy rainfalls or flooding could enter contaminants into water supplies by runoffs), treatment deficiencies at the water treatment plants, and water distribution systems failure.[28] In addition, a change in temperature can change the life cycle of microbes and lead to biofilm formation in water pipes.[27,28] Recreational water-based centers such as pools and spray pads were also reported to cause disease outbreaks, with the leading bacterial pathogens being *Escherichia coli* O157:H7, *Shigella sonei*, *Pseudomonas spp.*, and *Legionella spp.*[27] Irrigation of agricultural products with contaminated water from various sources including environmental water, or wastewater, has led to disease outbreak, and it has already cost many lives around the world.[29] The use of phage in monitoring and early detection of outbreaks can therefore be focused on both the water resource and the source of contamination (**Figure 3**).

3.1. Waterborne bacterial pathogens and their significance in quality monitoring

According to WHO regulations, no detectable bacteria and coliforms should be present in 100 mL of drinking and crop rinsing water.[30] *E. coli* concentration in recreational and irrigation water must be less than 100 cells per 100 mL of water.[31] Minimal infectious dose (MID) of pathogenic bacteria is an important factor that should be considered in monitoring environmental sources for outbreaks.[27] **Table 1** presents the common waterborne bacterial pathogens in water supplies, according to WHO,[27,32] along with MID's. *E. coli* O157 and other coliforms are a major source of waterborne infections, and they may cause severe symptoms such as haemolytic uraemia and hemorrhagic colitis.[30] Toxigenic *Vibrio cholerae* and *Campylobacter* are the common cause of diarrhoea, and several waterborne outbreaks have been recorded by these two bacteria.[32] They have an

infectious dose of 10^8 and 10^3 respectively.[28,33] *Shigella* is another dangerous waterborne bacterial pathogen with low infective dose (10-100 organisms) that infects more than 2 million people every year with about 60,000 death, mostly in developing countries.[32] MID does not show a threshold above which infection occurs and every single pathogen could initiate infection upon digestion. In fact, MID characterizes the probability of infection caused by pathogenic microorganisms[34] and in theory, it is the minimum required sensitivity of any adopted detection and monitoring method.

Table 1. Major bacterial pathogens in drinking-water and associated diseases*

Pathogen	Associated disease[27]	Health significance	Persistence in water supplies [a]	Resistance to chlorine	Relative infectivity [b]	MID (# organisms)[31–33,35]
Burkholderia pseudomallei	Melioidosis	High	May multiply	Low	Low	NA
Campylobacter jejuni, C. coli	Diarrhea, reactive arthritis	High	Moderate	Low	Moderate	10^3
Escherichia coli (E. coli)	Acute diarrhea, bloody diarrhea, and gastroenteritis	High	Moderate	Low	Low to High	<100
Legionella spp.	Acute respiratory illness, pneumonia (legionellosis)	High	May multiply	Low	Moderate	NA
Non-tuberculous mycobacteria	Pulmonary disease, skin infection	Low	May multiply	High	Low	NA
Salmonella typhi	Typhoid fever, paratyphoid fever, fever, and other serious salmonellosis	High	Moderate	Low	Low	10^5

Shigella spp.	Bacillary dysentery or shigellosis	High	Short	Low	High	10-100
Vibrio cholerae	Gastroenteritis, cholera	High	Short to long	Low	Low	10^8

*Reproduced with permission from WHO Guidelines for drinking water quality[32]

[a] Detection period for infective stage in water at 20 °C: short, up to 1 week; moderate, 1 week to 1 month; long, over 1 month.

[b] Infective dose from epidemiological evidence and experiments with human volunteers and animal studies: High means 1-10^2 organisms or particles, moderate 10^2-10^4, and low >10^4

3.2. Phage-based biosensors and bioassays for water-borne pathogens

Different biosensors and bioassays have been developed to detect pathogenic bacteria in water.[30,36] The most common pathogen detection techniques in water include culture-based methods,[37] Polymerase Chain Reaction (PCR),[38] Mass Spectroscopy (MS),[39] and a range of assays such as antibody-based assays or immunoassays (*e.g.*, Enzyme-linked Immunosorbent Assay (ELISA)[40] and Lateral Flow Immunoassay (LFIA)[41]) that are based on the specific interaction between antibody and its antigen. It is important to note that each detection technique has outstanding limitations in addition to distinct advantages, for instance, nucleic acid, MS-based techniques, and ELISA are not capable of distinguishing between live and dead bacteria and could give false positive results. Culture methods are the gold standard for bacteria monitoring and detection but are time consuming and biased by growth rate. ELISA, MS, and immunoassays need skilled operators and specialized equipment, substantial sample preparation and purification and can be costly.[42,43]

Bacteriophages have three distinctive properties that makes them suitable candidates for use as specific recognition elements in bioassays and biosensors. One of most powerful characteristics of phages is their ability to distinguish between live and dead bacteria because they are only able to infect live bacteria.[44] This property, along with long shelf life, and relatively cheaper production, sets phage apart from the two other specific recognition elements commonly used in biosensors, specifically aptamers and antibodies.[45] They can be very specific to their host and can bind/infect a single species

or even a single strain of bacteria with high specificity. The phage lytic/chronic cycle produces hundreds of progeny phages, a characteristic that can be used to amplify the signal *in situ* for low concentration of contaminant. Furthermore, having functional groups on their surface, phages can easily be immobilized on a sensor surface.[46] In addition, although different phages can have different characteristic, but the tremendous diversity in the phage community means it is possible to find phages that tolerate harsh environments such as high temperatures up to 76°C, organic solvents, and a wide range of pH (compared to antibodies).[43,47,48]

Phages have been successfully used as a specific recognition element to target bacterial pathogens in foods,[49,50] environmental settings,[51] and human infections.[52] **Table 2** summarizes different phage-based detection methods that have been investigated for waterborne bacterial pathogen detection. Interestingly, most of the research in this field has been focused on *E. coli* detection (mostly non-pathogenic lab strains) as a model organism, and several other bacterial pathogens that have high health significance and could give rise to deadly waterborne infectious disease outbreaks such as *Legionella spp., Shigella spp., Vibrio cholerae,* and *Yersinia enterocolitica* (**Table 1**) have been largely neglected. What is clear from **Table 2** is that regardless of the different signal transduction methods employed, phage-based pathogen detection could achieve a very low detection limit, sometimes down to 10 colony forming units (CFU's) and in most cases the detection time is significantly less than that needed for culture-based techniques.

Table 2. Phage-based biosensor and bioassays to detect waterborne bacterial pathogens

Target pathogen	Sample	Transduction platform	Phage	Detection time	Detection scheme	Stability	LOD	Ref.
E. coli XL1-Blue, *E. coli K12*	Artificial river water	Electrochemical impedance spectroscopy (EIS)	M13 (wild-type)	30 min	Immobilization of M13 phage on electrodeposited gold nanoparticles (AuNPs) on glassy carbon electrode	16 days at 45 °C, very good to high stability in pH 3–10	~14 CFU mL^{-1}	46
E. coli (ECOR-13)	Drinking water	Electrochemical	T7 reporter phage	4–12 hours	Reporter phage conjugated with magnetic beads are used to separate and detect target cells	The NRGp7-MBs were stable at 4 °C for 2 weeks	10^5 CFU mL^{-1} within 4 hours, 1 CFU per 100 mL in 12 hours	53
E. coli ER2738, *P. aeruginosa*, *V. cholerae*, *Xanthomonas campestris*	Seawater and tap water	Colorimetric	Engineered M13	Less than an hour	Engineered M13 phages express RBP[a] with thiolated capsid that allows AuNP attachment, resulting in color change	NA	100 cells	54
E. coli BL21	Drinking water	Colorimetric and luminescent assay	Engineered reporter T7 phage	10–12 hours	Visualization of released reporter enzyme (NanoLuc-CMB[a]) trapped on a cellulose filter upon phage infection	NA	1 CFU mL^{-1}	55
E. coli	LB media	Colorimetric	Engineered reporter T7 phage	≤8 hours	Magnetic cellulose-based particles are used to separate and concentrate the overexpressed ALP[a]-CMB enzyme, followed by colorimetric detection	NA	1.2×10^3 CFU mL^{-1} in 3.5 hours (without enrichment) 10^1 CFU mL^{-1} in 8 hours (with enrichment)	56
E. coli BL21	Lake water	Bioluminescent assay	Engineered reporter phage T7	3 hours	Collection of expressed reporter enzyme (Nanoluc-CMB) with microcrystalline cellulose and detection with suitable substrate	NA	<10 CFU mL^{-1}	57
E. coli BL21	Drinking water	Electrochemical	Engineered T7 phages	3–7 hours	Electrochemical detection of released native and overexpressed enzyme β-gal upon phage infection	NA	10^5 CFU mL^{-1} in 3 hours 10^2 CFU mL^{-1} in 7 hours	58
E. coli BL21	LB broth	Colorimetric	Engineered T7	7 hours	Colorimetric detection of released native and overexpressed enzyme (β-gal) upon phage infection in solution	NA	10 CFU mL^{-1}	59
Bacillus anthracis spores	Pond and lake water	Bioluminescent assay	*B. anthracis* reporter phage (Wβ::luxAB-2)	8–12 hours	Detection of reporter enzyme in solution	NA	10 and 10^2 CFU mL^{-1}	60

Table 2. Continued

B strain of *E. coli* (ATCC 11303)	PBS buffer	Electrochemical impedance spectroscopy (EIS)	T2 phage (wild type)	NA	Immobilization of phage on carbon nanotube modified electrode surface using charge directed orientation technique	NA	10^3 CFU mL^{-1}	61
E. coli O157: H7	Municipal and agricultural water	NA	Coliphage ECML-117	2 hours	Separation of target cells using phage conjugated magnetic beads and detection of released bacterial DNA using q-PCR	NA	10^2 CFU mL^{-1}	62
E. coli BL21	Broth and river water	NA	Engineered T7 phage	7 hours (10^3 CFU mL^{-1}), 9 hours (10^2 CFU mL^{-1})	Phage amplification-based lateral flow assay (LFA)	NA	10^2–10^3 CFU mL^{-1}	63
E. coli TD2158 and *Salmonella enterica* typhimurium 14028S	Sea water	Fluorescent	Phage HK620:: PrrnB-gfp and P22:: PrrnB-gfp	1 hour	Detection of target cells with expressed fluorescent protein (GFP[a]) upon phage infection using flow cytometer	NA	10 cells per mL	64
E. coli BL21	Drinking water	Colorimetric	T7 phage	2.5 h	Separation of target cells with phage conjugated magnetic beads and detection of released reporter enzyme (β-gal)	NA	10^4 CFU mL^{-1} and 10 CFU mL^{-1} (6 hour of pre-enrichment)	65
E. coli ER2738	Drinking water	Fluorescent	Tetracysteine tagged M13 (M13KE-TC phage)	N/A	Detection of labeled progeny phages (TC-phage-FlAsH[a]) using flow cytometer and fluorescence microscope	NA	1 CFU mL^{-1} in 40 mL of drinking water	66
E. coli	Water	Luminescent and colorimetric	Wild-type and engineered T4	8 hours	Sample filtration (capturing bacterial cells), addition of phage and detection of released reporter enzyme (β-gal) upon phage infection	NA	40 or <10 CFU mL^{-1}	31
E. coli	Drinking water	Bioluminescent	Engineered T7	5 hours	Sample filtration (capturing bacterial cells), addition of phage, and detection of reporter enzyme (NanoLuc-CBM)	NA	<20 CFU mL^{-1} in 100 mL water	67
E. coli K12 (*ER2378*)	Drinking water	Colorimetric	Engineered M13KE phage	<4 hours	Sample filtration (capturing bacterial cells), addition of phage, collection and detection of reporter enzyme (β-gal)	NA	50 CFU L^{-1}	68

*RBP: receptor binding protein, CBM: carbohydrate binding module (with specificity to cellulose), ALP: alkaline phosphatase, GFP: green fluorescent protein, FlAsH: fluorescein arsenical helix binder

3.3. Different categories of phage-based sensors

Phage affinity towards specific host cells is the key feature of phage-based detection of bacterial cells. Host range could be narrow or wide depending on the ability of phage to uniquely identify the bacterial surface receptors including pili, flagella, external polysaccharides, or a wide range of membrane-bond proteins. As a result, phage can target bacterial strains, species, genera, or even a single bacterial serotype.[69] Lytic phages including T4, T7 and MS2, and lysogenic filamentous phages such as M13 have been widely investigated so far to be used in phage-based detection of pathogens.[9,70] Filamentous phages like M13 are non-lytic chronic phages which secrete progeny phages

without lysing bacterial cells.[13] Thus, most of the common filamentous phage-based detection methods are based on phage binding to target bacterial cells.[9] On the other hand, lytic phages also have the ability to lyse the bacterial cells and release the intracellular components as a biomarker.

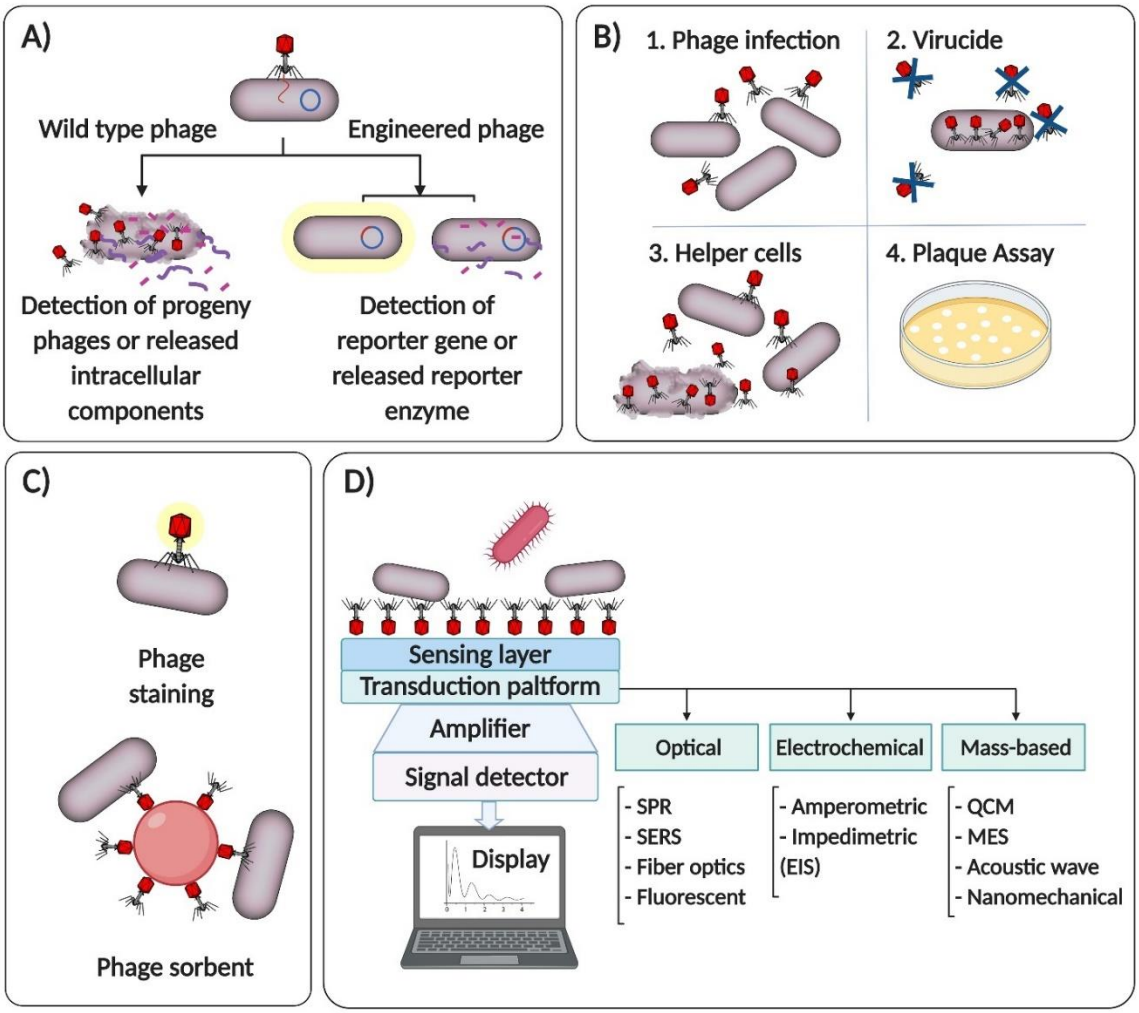

Figure 4. Phages used as bio-probes in different bioassays and biosensors. **(A)** Phage infection assays. These assays can use wild type or engineered phage. With wild type phage, progeny phages (by phage typing or through phage amplification assays) or the intracellular components released from the bacterial cell during cell lysis can be detected using different detection platforms. With engineered phage, the expressed reporter gene or released reporter enzyme is detected using optical, electrochemical, etc. detection platforms. **(B)** Phage amplification assay used in conjunction with infection-based assays consists of four steps. (1) Phage is added to sample, and if the target host cell is present, phage infection occurs. (2) The remaining phages are destroyed before release of progeny phages by adding a viricide which is then neutralized. (3) Helper cells (healthy host cells) are then introduced to the solution to provide the chance for progeny phages to amplify,

(4) which could be simply detected by top agar plaque assay. **(C)** Phage binding assays. These assays use the process of phage binding (usually without the use of an extra transduction platform) for bacteria detection. Common approaches are staining phage with nucleic acid dye (detecting with flow cytometer or microscopy) or conjugating phage with micro/nanoparticles to separate/detect host cells coupled with PCR or optical, electrochemical detection platforms. **(D)** Phages can be immobilized on a substrate to form a bioactive surface that can be used as the sensing layer in biosensors. Binding phages to target host cells causes a change in conductivity, optical properties, or mass. In this case, the electrical, fluorescent, colorimetric, or luminescent signal generated by phage-host binding or host lysis is transduced using the sensor platform.

There are different strategies for detecting bacterial pathogens using both wild-type and engineered phages. **Figure 4** shows different approaches that can be employed to use phages as bio-probes in biosensing applications. Phage infection assays rely on the process of infection and/or lysis for bacteria detection (**Figure 4A**). Once phages infect their host, they release progeny phages and intracellular components, either of which can be used to detect bacterial pathogens. The release of progeny phage can be simply detected by phage typing and phage amplification assays. Phage typing that takes advantage of the ability of phage to specifically infect and lyse its host. In this method, small droplets of phage solution are added to a lawn of bacteria. If the bacteria are within the host range of phage, the lawn spots overlaid by phage will be lysed and cleared zones called plaques appear.[71] This method is time consuming, and only detects culturable bacteria. Phage amplification assay is used to quantify the progeny phages as a result of phage infecting bacterial host cells (**Figure 4B**). In this assay, phage is added to bacteria containing sample to amplify. Afterwards, any phages not infecting the cells are destroyed so that only progeny phages remain in the mix, which are then amplified further by addition of healthy host cells and subsequently detected by a standard plaque assay.[72] Other than progeny phages, intracellular components released as a result of phage lysis have also been used for detection purposes. Adenosine triphosphate (ATP),[73] adenylate kinase (AK),[74] β-D-galactosidase,[31] α-glucosidase and β-glucosidase[75] are different intracellular components that can be considered as cell markers and detected using suitable substrates and different optical (fluorescent, bioluminescence, or colorimetric) or electrochemical detection platforms.

Phages have also the unique potential of being genetically modified to carry a reporter gene that can be transferred to live host cells upon phage infection (reporter phage). The introduced reporter gene is then expressed and enables the detection of target bacterial cells. The reporter gene will only be expressed when phage inserts the gene into live host cells since phage is not able to reproduce independently. Luciferase expressing gene (*lux* and *luc*),[76,77] E. coli β-galactosidase (*lacZ*),[31,59] bacterial ice nucleation (*inaW*),[78] and green fluorescent protein expressing gene (*gfp*)[64,79] are among the most frequently used reporter genes for biosensing applications.[52,80]

Phage can bind to surface bacterial receptors and act as a capture element. Phage-based detection methods based on host capture can be used with free phage[66] or phage conjugated with micro/nano particles to separate/detect pathogens in liquid[56,62] (**Figure 4C**). Phages can also be immobilized on a surface to form a bioactive surface that can be used as a sensing layer in biosensors (**Figure 4D**) or in some cases interact with intracellular components. The interaction can be used to generate electrical,[81] fluorescent,[64,82] colorimetric,[56] and luminescent[44] signals using different transduction platforms.[43,83] Recently, nanomechanical biosensors based on micro/nano cantilever platform have attracted attention for being able to detect different biological entities (DNA, RNA, proteins, viruses, and bacteria) with high sensitivity and fast response.[84,85] In these biosensors, biological interactions on a cantilever surface leads to deflection in a nanometer scale (static mode) or change in resonance frequency (dynamic mode).[86] Interaction between phage T7 and *E. coli* using cantilever based nanomechanical sensor has been investigated. Phage infection with concentration as low as 10^3 PFU/mL led to reduced fluctuation and bending of the cantilever, which shows successful analysis of the dynamics of interactions between phage and bacterial cells that can be applied to develop label free, highly sensitive, fast response and cost-effective phage-based biosensors.[87]

It is noteworthy that the large size of phage compared to other biological elements such as aptamers and antibodies could be restrictive in some transduction platforms. For example, in surface plasmon resonance (SPR), surface enhanced Raman Spectroscopy (SERS), and quartz crystal microbalance (QCM) transduction platforms, where the signal is strongly dependent on distance from the sensor surface and decreases significantly with

increasing the distance, the large size of phage could negatively affect the sensitivity.[88] Using large biological probes on the surface means lower density of capturing elements on the surface, an important factor affecting biosensor sensitivity. Drying of phage is another challenge in phage-based biosensors that could lead to loss of binding affinity, although some phages are more resilient to desiccation. Various methods have been reported in the literature to preserve phages that are sensitive to desiccation.[89,90]

3.4. Sensor design using phage display technology

M13 phages have an outstanding ability to undergo genetic modifications easily to express target specific affinity molecules on the surface using phage display technology,[91] a technique introduced by George Smith in 1985.[92] Incorporation of a foreign gene to express receptor binding peptides on the surface of filamentous bacteriophages that are capable of binding to cell receptors on the outer membrane of bacterial cells provides an exceptional opportunity for expanding the usage of phage-based biosensors and bioassays.[93] Phage display technology provided the opportunity to go beyond whole bacterial cells' detection. Modified filamentous phages to display specific peptides, antibodies, reporter genes, and fluorescent dyes have been developed to target organisms (bacteria, virus, spores), biomolecules (proteins, enzymes, DNA) and specific contaminants for an efficient biomonitoring system in the environment.[94] For example, recognition elements discovered by phage display have been reported to be able to detect cholera toxins,[95] *Bacillus anthracis* spores,[95] 2,4,6-trinitrotoluene (TNT),[96], mercury (Hg^{2+}),[97] lead (Pb^{2+}).[98] These filamentous phage probes can be immobilized on a substrate to develop biosensors, and the signal is detected using different transduction platforms including piezoelectric (acoustic wave biosensor),[99,100] magnetoelastic,[101,102] SPR,[103] and SERS,[91] producing an electrical or optical signal.

3.5. Design parameters for phage-based biosensors

Limit of detection. Detection of low concentration of pathogens in a large volume of water usually requires enrichment of the samples prior to detection.[27] An enrichment step increases the initial bacteria concentration to a higher level matching the detection limit

of the subsequent assay. By incubating the bacterial culture in LB media for 4 hours as an enrichment step, T7 reporter phage have been able to detect less than 10 CFU/mL of *E. coli* from 100 mL sample within 8 hours using a colorimetric assay compared to LOD equal to 1.2×10^3 CFU/mL in 3.5 hrs with no enrichment step.[56] In a similar study, having applied a pre-enrichment step of 6 hrs to allow further bacterial growth in a colorimetric assay, LOD decreased from 10^4 CFU/mL to 10 CFU/mL using T7 phage conjugated magnetic beads to detect *E. coli* BL21 in drinking water, sacrificing the assay time (**Figure 5A**).[65] Filtration is another approach that could be applied to increase the limit of detection without using an enrichment step. A single CFU/100 mL of *E. coli* has been detected using a T7 phage-based membrane filtration process that used 8 hours of pre-enrichment step to increase the density of bacterial cells on a filter before adding phage in order to achieve a detectable visual signal (**Figure 5B**).[55] Similarly, concentrating bacterial sample by a syringe filter to capture bacterial cells helped to decrease the limit of detection from ~100 CFU/mL to less than 20 CFU/100 mL while maintaining a shorter assay time (5h) in comparison with traditional culture-based detection methods (**Figure 5C**).[67]

Magnetic separation is another fast method that can improve the limit of detection without requiring an enrichment step. This method is also able to capture and separate bacterial cells from complex samples, thereby reducing the interference of the sample matrix during signal detection.[43]Engineered T7 Phage conjugated to magnetic beads (MBs) were used to capture and separate *E. coli* BL21 from water sample (**Figure 5A-(1)**). The captured bacterial cells with phage-MBs were collected using a magnet prior to bacterial cell lysis and resuspended in buffer afterwards. As a result of cell lysis, β-gal was released and detected using a suitable colorimetric substrate.[65] Phage-functionalized MBs were also used to capture and separate bacterial cells (*E. coli* O147:H7) that were quantified using q-PCR.[62] In another study, engineered T7 reporter phage with carbohydrate binding module (CBM) tagged alkaline phosphatase (ALP) gene was used as a bio-probe. After phage infection and cell lysis, the released reporter enzyme ALP-CMB, which has binding affinity to cellulose, was collected using magnetic cellulose particles. The separated reporter enzyme was detected and quantified using a colorimetric assay afterwards.[56]

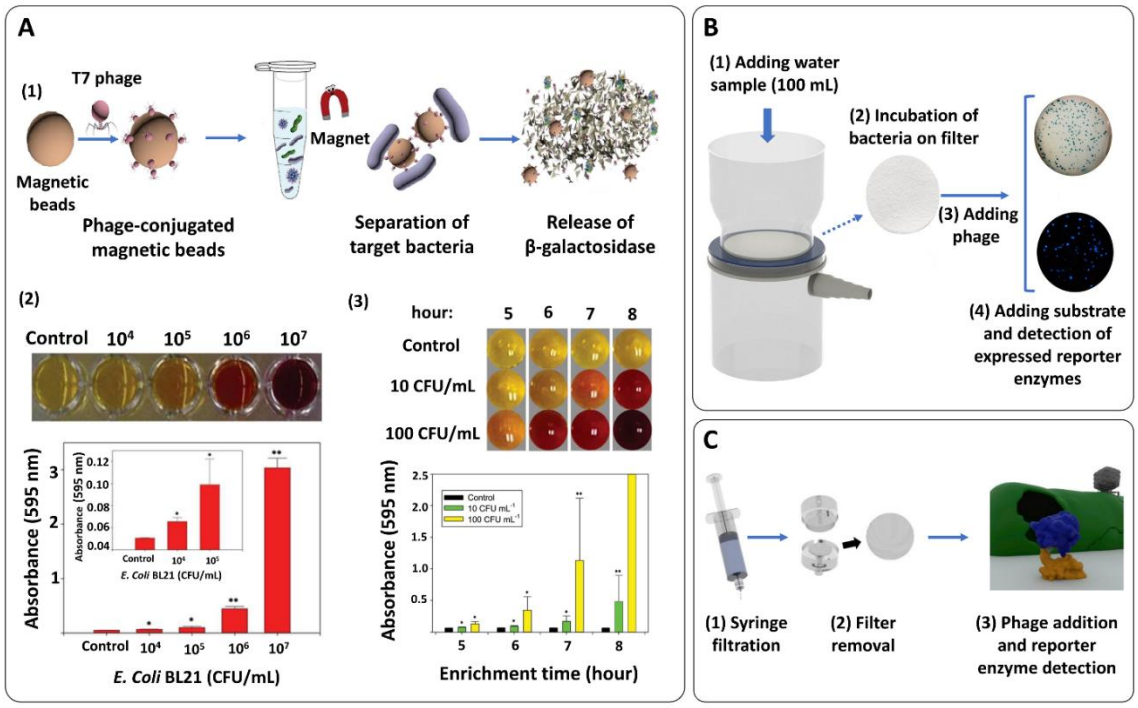

Figure 5. Approaches to improve the limit of the detection of phage-based bioassays. **(A)** Example of enrichment effect on phage-based colorimetric assay to detect *E. coli* BL21 in drinking water. (1) T7 reporter conjugated magnetic beads used for phage-mediated lysis and release of β-galactosidase enzyme, which was then detected using a substrate to produce a colorimetric readout. (2) Image and colorimetric readout for samples, which gives LOD qual to 10^4 CFU/mL. (3) Photographs and colorimetric readout for samples containing 10 and 100 CFU/mL of *E. coli* after enrichment for 5-8 hours, leading to decrease the LOD form 10^4 CFU/mL to 10 CFU/mL. Reprinted with permission from J. Chen et al.,[65] copy right (2015) American chemical society. **(B)** Example of phage-based colorimetric and bioluminescence assay combined with filtration and enrichment. (1) 100 mL of water sample is filtered using a filter membrane (47 mm diameter with a 0.22 µm pore size), (2) the filter was then removed and incubated on an absorbent pad allow further bacteria growth. (3) Engineered phages were added to infect target bacterial cells (*E. coli*) to express desired reporter enzymes genetically fused to a protein capable of binding to cellulose filter upon release (CMB), that (4) can be detected with a suitable substrate to provide colorimetric or luminescent signal. Reprinted with permission from T. Hinkley et al.,[55] copy right (2018) Springer Nature **(C)** Example of filter-based detection of *E. coli* in drinking water using engineered phage. (1) 100 mL of water sample is filtered using 0.22 µm cellulose filter to separate the bacteria, (2) the filter is removed and placed on LB media, and (3) engineered phages (grey) are added to infect target bacterial cells and result in subsequent release of reporter enzyme NanoLuc (blue) fused to CMB (orange) with specificity to cellulose that is detected with a luminescence assay. Reprinted with permission from T. Hinkley et al.,[67] copy right (2020) MDPI.

Detection time. Microbial contaminants can rapidly grow and infect water supplies. Rapid investigative monitoring of drinking water resources to identify the number and types of

pathogens before drinking water reaches the consumers is key to prevent water-associated disease outbreaks and improve public health. Some phage-based bioassays have been reported to have significantly shorter assay time compared to the conventional detection methods, *i.e.*, culture methods.[46,64] Reporter phage technology accompanied with flow cytometry as a rapid and real time detection device has been implemented to develop a fast and sensitive detection assay. Detecting reporter proteins overexpressed within target bacterial cells after phage genome insertion successfully enabled detection of 10 bacterial cells.mL^{-1} in around 1 hr without any enrichment or concentration step. In this assay, a recombinant phage expressing a fluorescent gene is used as a detection probe that produces fluorescence signal after phage inserts its genome into metabolically active target cells which are able to produce GFP (Green fluorescent protein).[64]

Combining phage-based bio-probes with micro/nanoparticles and use of fast optical detection platforms is one of the promising ways to reduce the detection time, while maintaining the low limit of detection. For example, use of gold nanoparticles in combination with phage has led to fast and sensitive detection (~ 100 cells) of bacterial pathogens in sea and tap water in less than an hour. In this assay, a thiolated engineered M13 phage with a receptor binding protein fused to the minor coat protein pIII (chimeric M13) is added to the bacteria containing sample. Thiolated phage attaches to target cells, and the bacteria-phage complex is then separated from free phages with centrifugation and resuspended in a solution containing gold nanoparticles. Thiolation allows binding and aggregation of gold nanoparticles on the phages, and this aggregation results in a visible color change as a result of change in surface plasmon resonance properties.[54]

Phage-based magnetic separation of bacterial pathogens in combination with fluorescent detection using flow-cytometry has been shown to decrease the detection time significantly. For this purpose, wild-type T4 phages were covalently bound to the surface of magnetic-fluorescent particles to develop a multifunctional bio-probe that is able to absorb, separate and detect target bacterial cells using flow cytometry. The capture efficiency of the phage bioconjugate was high (90-100%) and it was able to detect ~ 10^4 CFU/mL of bacterial in 15 minutes.[104]

Non-culturable cells. When exposed to physical or chemical stress (*e.g.* unfavorable temperature, loss of nutrients, and chlorine exposure), many bacteria respond by entering

a latent state of growth, an atypical state of growth known as viable but non-culturable (VBNC).[105] Bacteria in this state pose a serious health risk because the damaged cells are not detectable by conventional culture-based methods, but are able to repair themselves, re-grow and return to the active state with the potential of disease initiation.[106] *E. coli*, *H. pylori*, and *V. cholerae* are examples of bacterial pathogens that are able to exist in VBNC state, leading to false negative results using culture-dependent analysis methods.[27] It has also been shown that *E. coli* could enter the water distribution system as a result of water treatment discrepancies or damaged pipes to form biofilms inside drinking water networks. The bacteria trapped in the form of biofilm inside pipes are often not detected because of culture-based microbial analysis limitations and also due to the fact that only water samples are tested and culture based and enzymatic methods are not able to detect metabolically active but non-culturable bacteria, putting human health at risk.[107] Lytic *P. aeruginosa*-specific phage was shown to have the ability to interact with injured cells that were in a VBNC state, and they successfully detected *P. aeruginosa* in water.[106] Thus, using specific lytic phage could be useful to monitor the treated water to ensure there is no potential active bacteria in VBNC state and verify the water quality after water treatment and purification, avoiding possible false negative response of pathogenic bacteria detection. It is important to note that not all phages are expected to have the ability to propagate/bind effectively in VBNC or biofilm cells and therefore careful selection of phage is very important.

Viable versus non-viable cells. Discrimination between viable and non-viable cells is an important aspect of a reliable waterborne pathogen detection method that cannot be addressed with most of the common detection methods including nucleic acid-based methods such as PCR, microarrays, and pyrosequencing, and this lack of specificity could lead to false positive results.[108] Given the fact that phages take control of the host genetic machinery to replicate, phage-based biosensors and bioassays are capable of successfully detecting viable bacterial cells. In order to determine the ability of phages to discriminate between live and dead bacteria, *E. coli* ECOR13 cells were treated with 70% ethanol and a luminescent phage-based assay was used to detect ethanol and non-ethanol treated samples. Results showed that only non-ethanol treated samples were able to produce luminescent signal following phage and substrate addition.[67] The immune-based lateral

flow assay (LFA) have been widely used to detect some strains of *E. coli* bacteria using antibodies, e.g. polyclonal antibodies (Poly Abs) against *E. coli* O111 used in LFA to detect *E. coli* O111 antigen.[109] As it is evident, this detection approach is also not able to distinctively detect live bacterial pathogens. However, when combined with bioengineered bacteriophage, LFA could discriminate in favor of live cells detection using a phage amplification stage and resulted in a sensitive detection of *E. coli* with LOD of 100 CFU/100mL in a river water sample.[63] In addition, tetracysteine (TC)-tagged M13 in conjunction with highly sensitive fluorescence labeling of biarsenical dye called fluorescein arsenical helix binder (FlAsH) was able to successfully detect trace amount of viable bacteria (1 CFU/mL of *E. coli* ER2738) in artificially contaminated drinking water with high background of dead cells and other bacteria using flow cytometry and fluorescence microscope.[66]

Use of whole phage versus phage components. In addition to whole phage (wild type or genetically modified), phage components including receptor-binding proteins (RBPs),[110] lysins protein, and long tail fibers[42] can be used in biosensors and bioassays. RBPs are the phage proteins located either on fibrous, extended tail fibers or on short tail spikes, responsible for determining the phage specificity towards bacterial cells and are considered as capturing elements of bacteriophages. They can bind to specific structures present on outer bacterial cell membranes such as polysaccharides, proteins, pili or flagella.[111] RBPs have several advantages that makes them intriguing bio-probes in detection application. For example, RBPs can bind to bacterial cells but do not lyse them which is beneficial for mass-based sensing platforms since cell lysis leads to signal loss. Not being able to cause cell lysis also prevents virulence gene transfer or release of toxic components of bacterial cells.[112]

Free vs surface-bound phage. Phage-based bio-probes can be immobilized on various substrates and have the potential to be implemented in different biosensor platforms. The successful immobilization of phage on a surface means phages should remain active (able to infect or capture target elements), and have high surface density.[113] Moreover, orientation of phages on the surface has a tremendous effect on its functionality which should be considered in sensor design. For example, lytic tailed phages should be oriented

with their heads on the surface and their tail directed away to be able to capture target cells by the receptors located on their tail fibers. Filamentous phages should also have their bacterial capture proteins exposed to be able to bind to bacteria, unless there are peptides expressed on their envelope that requires their parallel alignment to the surface. Various methods have also been developed to align phages on the surface in a way that its capture efficiency is less compromised.[114] An area that has remained unexplored for surface-bound phage is the effect of non-specific binding in complex matrices (such as wastewater) on the sensing signal. This is a challenge that is not specific to phage-based detection platforms and affects all biosensors that are expected to operate in complex fluids. Technologies such as repellent coatings could be explored for overcoming this challenge.[115–119]

Interference with colloidal matter or disinfectants in water samples. The functionality of phage-based detection probes is also affected by the presence of environmental interferants present in real water and wastewater samples that can significantly affect the phage functionality in practice, regardless of using suspended or immobilized phage on a surface. These interferants include colloidal matter, dead bacterial cells, extracellular polymeric matrix of biofilms, natural organic materials and disinfectants that can significantly affect phage functionality by blocking phage receptors which prevents phage binding/infecting live bacterial cells. Thus, the functionality of developed phage-based biosensors and bioassays should also be evaluated under conditions close to the final application.[120] Moreover, purity of phage used in biosensor applications is important since the amplification of phage in bacterial culture involves the release of cellular debris such as proteins, lipids, and carbohydrates that could block phage receptors and affect phage binding ability to target cells and the efficiency of immobilization of phages on a surface.[83]

Point-of-use detection. On-site rapid analysis of bacterial pathogens without the need for highly trained personnel and high-tech equipment could be greatly beneficial in analyzing the natural water resources such as lakes, rivers, and springs, and for the testing of irrigation and recreational water.[31] The ability to detect bacterial pathogens on the field to have real-time data is beneficial to provide early warnings and effective prevention of

water-associated disease outbreak, especially when there is insufficient resources.[36] Phage-based colorimetric, luminescent, and fluorescent assays are suitable for resource-limited areas because they produce data visually or by simple portable light detection tools.[31,64] Despite the fact that colorimetric detection techniques do not have the highest sensitivity, they have drawn attention because of simplicity and the potential for being implemented for on-site detection. Cell phones with digital cameras have made it possible to detect visible and luminescent signals with high sensitivity on the field.

Multiplex detection. The ability to detect multiple bacteria at the same time is beneficial in different fields including environmental monitoring.[45] Although possible in principal, to date, there has been no report for a phage-based biosensor platform to detect multiple bacterial cells. In principal, effective phage biosensors will have to be designed for each pathogen of interest with the specific phage, or a multiplex sensor must be employed to cast a wide net for pathogens of interest, and therefore multiplex phage-based biosensors/bioassay designs are long overdue. As an example, optical phage-based bioassays with fluorescent, bioluminescent, and colorimetric output signals have the potential to detect multiple target pathogens. For this purpose, by having different phage-based bio-probes coated on a surface or in a microtiter plate format, each capable of binding/infecting a different bacterial pathogen and release of intracellular components, or reporter enzymes/genes (in case of using engineered reporter phage), multiple bacterial pathogens could be possible. In addition, it is also important to note that we do not necessarily expect a water sample to be contaminated with only one bacterial strain. If only one type of phage is used for contaminant detection, specificity of bacteriophages towards their host could result in false negative results and miss detecting the other strains of the pathogenic bacteria and other species of pathogens. As a result, phage host range must be determined by evaluating its binding/infectivity against different strains of target bacterial pathogens, and sometimes a mixture of phages might be required to be able to detect all common strains of the target bacteria. For this purpose, host range of three wild-type *P. aeruginosa* phages have been evaluated to ensure that the isolated phage mixture is able to detect as many *P. aeruginosa* strains as possible in water samples[121], an

important aspect that must be considered in all the phage-based bioassays and biosensors developed for detecting waterborne bacterial pathogens.

4. Specific considerations for phage-based detection/monitoring in wastewater

With the rise of water scarcity and environmental pollution, proper collection, treatment and disposal and reuse of wastewater is getting more and more attention as an urgent necessity.[122] One of the main potential applications of treated wastewater is in agricultural irrigation because agricultural sector uses around 70-80% of the global water.[123] However, wastewater treatment and reuse should be monitored with great care since inadequate treatment could contaminate the environment and deteriorate the quality of existing freshwater resources, and could also lead to contaminated crops.[122,124,125] Moreover, wastewater treatment plants have drawn attention as being a very large source of antibacterial resistant genes/bacteria (ARG/ARB) that has the potential to spread in the environment through sludge and effluent water.[126,127]

The literature on use of phage for detection of bacteria in wastewater is scarce and most of the reported use of bacteriophages related to wastewater has been for biocontrol. We have chosen to compile the biocontrol literature in **Table 3**, because most of the phages used for biocontrol can be used for monitoring and detection, and furthermore, most of the challenges that are discussed below apply to both biocontrol and detection. Phages targeting ARB can be isolated from swage and wastewater treatment plants, and they have the potential to be utilized as bio-recognition elements to detect and monitor the presence of ARB in treated water and wastewater to prevent the release of ARB to the environment and contamination of natural and artificial water resources.

4.1. Sewage as a source of phage

Most cases of phage use for wastewater/sludge treatment used phages isolated from natural aquatic environments and wastewater plants.[128] Phages are abundant in wastewater and sewage and have been used as indicators for pathogenic bacteria.[129,130] There are up to 268 different bacterial species in wastewater and every wastewater plant

has its own specific sludge properties and its unique microbial community.[128,131] The concentration of viruses in activated sludge from both laboratory-scale reactor and full-scale wastewater treatment plants is predicted to be around 10^8-10^9 mL^{-1}.[132] It has been reported that phage population fluctuates in wastewater treatment plants, probably in response to changes in their bacterial host abundance; however, convoluted phage-host interactions makes it hard to fully understand the microbial ecology in sludge and wastewater treatment plants.[133] Several studies have shown that phages obtained from diverse microbial communities such as sludge and wastewater are polyvalent and display a wider host range in comparison with phages obtained from other environment.[133,134] Therefore, wastewater and wastewater treatment plans are very rich sources for phages that can be isolated and used for designing biosensors, bioassays and monitoring strategies for both natural aquatic environments and wastewater.

Table 3. Summary of studies that have used phage as a pathogen and operational biocontrol for wastewater and sludge

Sample	Phage function	Comments	Phage source	Host	Ref.
Hospital wastewater	Pathogen biocontrol	Antibiotic resistant pathogens were observed in all samples	Swage	*E. coli*, *Pseudomonas* sp. *Streptococcus* sp. and *Bacillus* spp.	135
Lab culture of environmental salmonella strains	Pathogen biocontrol	A cocktail of three salmonella specific phages isolated and used as biocontrol	Wastewater	Environmental salmonella strains	136
Wastewater containing sewage, agricultural and industrial wastes	Pathogen biocontrol	A phage cocktail as biocontrol, and fine powder of banana leaves as bio-adsorbent were used to improve wastewater recycling	Wastewater	*E. coli*, *P. aeruginosa* and *S. typhi*	137
Bacteria cultures from clinical and environmental origins	Pathogen biocontrol	Phage in combination with solar radiation was used to inactivate highly antibiotic resistant *E. coli PI-7*	Wastewater	*E. coli PI-7*	138
Activated sludge from aeration tank (for phage isolation and microcosm studies)	Pathogen biocontrol	Polyvalent phage cocktails were used to suppress a model ARB (β-lactam-resistant *Escherichia coli* NDM-1) in activated sludge microcosm	Sludge	β-Lactam-resistant *Escherichia coli* NDM-1	139
Lab cultures of bacteria	Pathogen biocontrol	Isolated virulent pSs-1 was used as a potential biocontrol for *Shigellosis*	Environmental water	*S. flexneri* and *S. sonnei*	140
Activated sludge	Foaming biocontrol	Four isolated phages successfully reduced the *Gordonia* concentration by 10 fold (9 days after treatment)	Wastewater treatment plant	*Gordonia* species	141
Biomass acclimatized with *S. natans*	Bulking biocontrol	Lytic phage (SN-phage) successfully decreased sludge bulking and turbidity of biomass containing *S. natans* No cross infectivity with other bacteria including *E. coli*, *P. aeruginosa*, *N. multiformis* and *N. europaea* was observed	Mixed liquor of local municipal wastewater treatment plan	*Sphaerotilus natans*	142
Biomass acclimatized with *H. hydrossis*	Bulking biocontrol	HHŸ-phage specifically attacked *H. hydrossis*, with no cross infectivity, and improved sludge settling properties	Mixed liquor of a wastewater treatment plant	*H. hydrossis*	143
Laboratory scale foaming test	Foaming biocontrol	Bacteriophage GTE7 was used to fight against foaming and successfully reduced the foam stability	Wastewater treatment plant	*Gordonia* and *Nocardia* species	144
Lab cultured *Skermania piniformis* collected from activated sludge samples	Foaming biocontrol	Isolated and characterized phage SPI1 is the first reported lytic phage targeting *S. piniformis*	Activated sludge	*Skermania piniformis*	145
Laboratory scale foaming test	Foaming biocontrol	Isolated NOC1, NOC2 and NOC3 phages successfully reduced foaming in lab scale reactor (phages were stable at pH 6–10 and non-tolerant to extremely acidic or basic environment)	Wastewater	*Nocardioforms*	146, 147
Lab cultured *Nocardia* strains	Foaming biocontrol	Lytic NTR1 phage isolated and used as foaming biocontrol	Activated sludge	*Nocardia transvalensis*, *Nocardia brasiliensis* and *Nocardia farcinica*	148
Lab cultured bacteria	Foaming biocontrol	Nine *Gordonia* phages (most of them targeting more than one *Gordonia* species) isolated; three of them were potential candidates for phage cocktail design for activated sludge foaming control	Wastewater and natural water environment	*Gordonia* species	149

4.2. Deactivation and interference

Deactivation and the presence of interferants in the samples are perhaps the most important challenges for using phage probes with wastewater samples. Inactivation of phage could happen as a result of phage attaching to colloidal particles present in wastewater and becoming part of the settled sludge. Poor penetration of phages into sludge flocs, inactivation or loss of phages as a result of environmental stress or insufficient host concentration (reapplying phage could be a possible solution),[134] and low infectivity rate of phages in activated sludge are challenges that could hinder the use of

phage probes.[150] The same challenge exists for phage biocontrol in wastewater and sludge, and phage to host ratio is an important parameter that should be optimized for each case in phage treatment of sludge.[143] This ratio will likely have to be optimized for use of phage as a biorecognition element to counter the deactivation/interference effects outlined above.

4.3. Horizontal gene transfer

It has been reported that phages contribute to antibiotic resistance spread in wastewater treatment plants as a genetic exchange mediator.[151,152] Phages could contribute to horizontal gene transfer between bacterial cells through transduction process. This could give rise to the emergence of extremely pathogenic antimicrobial resistant genes. For phages used in wastewater/sludge treatment, a suitable phage candidate should not be temperate or carry toxic genes, which may spread undesired toxic genes in the environment and increase of virulence of natural bacterial populations. For instance, among nine Gordonia phages isolated from activated sludge plants on the east coast of Australia, only three of them were acceptable for sludge treatment. Four of the isolated phages were lysogenic, and the other two appeared to contain a putative VIP2 family actin-ADP-ribosylating toxin gene which targets eukaryotic proteins.[149] Avoiding the use of lysogenic phages could reduce the chance of incorporation of phage DNA into host chromosome.[134] Of course, this is less of a concern if phage is to be used on aliquots of wastewater or sludge for detection/monitoring of contaminants.

4.4. Detection and monitoring of bacteria in biofilm mode

Bacterial biofilms are complex dynamic bacterial communities that live on surfaces. Active bacteria can transform from swimmers to stickers rapidly by change in gene expression and attaching to and colonizing biotic and abiotic surfaces. Biofilm formation helps bacteria to survive in harsh conditions by facilitating cell-cell interaction, concentrating nutrients, providing protection against environmental challenges such as UV and acid exposure, dehydration, salinity, and several antibiotics and antimicrobial agents.[153] In biofilms, aggregates of bacterial cells are embedded in a self-produced

polymeric extracellular matrix (ECM) composed of exopolysaccharides, extracellular DNA, and proteins.[154]

Biofilm formation on pipe surfaces in drinking water distribution system is a major problem that leads to changes in water quality and increase of corrosion rate at surfaces. It is estimated that in water distribution system, 95% of all microbial cells form biofilms and just 5% are free floating bacteria. Although drinking water biofilms are predominately formed by non-pathogenic microorganism, biofilms give home to microbial pathogens that could be released as a result of perturbation or active detachment and cause health threats to humans. Moreover, pathogens could be present in VBNC state in biofilms of drinking water system, and get back to culturable state and initiate infections.[155] In addition, in membrane-based water and wastewater treatments, biofilm formation leads to membrane biofouling and significantly decreases the filtration efficiency and increases the operational costs.[156,157] In fact, biofouling is considered "Achilles heel" of membrane technology. Therefore, real life application of phage-based detection and monitoring methods would most likely encounter bacteria in the biofilm mode, which is an important parameter to be taken into consideration when designing bacteria detection or monitoring systems. This aspect has remained entirely unexplored in the literature on phage-based detection and monitoring.

Bacteriophages have been explored as a means to control or mitigate biofilm formation in water distribution network.[158] Reports on biofilm challenge with phage suggest that even though bacteria are encased in an ECM, some phages still have the ability to penetrate through and bind their host bacteria, a property that allows for most detection methods discussed above to be applicable to bacterial biofilms, albeit maybe with a lower efficiency. Amplification-based techniques might be especially challenged by host bacteria in biofilm mode, because, although this cannot be generalized, it is believed that amplification of phage in bacterial biofilms, which may be functioning at a reduced metabolic rate, may not be as efficient as in actively growing bacterial cells. Some phages have the potential to degrade the ECM of the biofilms. Proteolytic enzymes and polysaccharase enzymes are the two enzymes that phages can synthesize to degrade extracellular proteins and polysaccharides, the two main components of biofilm ECM,

and reach to bacterial cells embedded inside them.[159] To increase the efficiency of phage-based detection, phages can be used that express these ECM degrading enzymes, or purified enzymes can be supplied along with the phage of choice to help degrade the biofilm matrix, in situations where the bacterial contamination is expected to be in biofilm mode. This is an area that deserves more attention from the scientific community.

5. Outlook and future directions

Phages offer several unique properties, namely specificity and unparalleled diversity, that renders them attractive candidates for use as sensing probes for monitoring microbial quality of water.,. With increased understanding of phages in the environmental engineering community, more application of phage is expected in not only biocontrol, but also detection and monitoring of contaminations in environmental resources. In order to meet the needs of water quality monitoring and prevention of waterborne disease outbreaks, focus on developing phage-based bioassays and biosensors with lower limit of detection and shorter sample analysis time is of great importance. To achieve this goal, there are some areas in this field that needs further attention to speed up the process of developing fast, highly sensitive and efficient phage-based biosensing platforms that are discussed in the following paragraphs.

In most phage-based biosensing approaches, enrichment of the sample has been widely used as a way to improve the limit of detection which is time-consuming, and there are very few reports of studies that have been able to detect a single or small number of bacterial pathogens in water. This is also of great importance when it comes to monitoring the quality of drinking water in order to prevent the occurrence of waterborne disease outbreaks. Although there are tremendous amounts of natural phages in the environment that can be isolated and used for capturing/infecting pathogenic bacteria for both biocontrol and detection/biosensing applications, genetic engineering of phage has grabbed attention due to offering unique opportunity to modify phage genome in order to address some of the limitations of natural phages[160] and offer additional phage-based detection tools such as reporter phage technology that is currently being investigated to improve phage-based bioassays and biosensors and provide rapid, sensitive and reliable

detection probes.[161] However, many of known phages have not been characterized yet, and their genetic modification is not feasible, and there is still no fast, efficient and highly reliable strategy that can be generalized to do genetic modification of a wide range of phages.[162] Moreover, phage genes are not fully characterized and functions of the majority of their genome are still unknown.[163] Advances in high-throughput sequencing, genome editing, and synthetic biology pave the way towards design and engineering of new phage-based detection tools using high throughput reliable genetic modification that can be used in real-world applications for detecting bacterial pathogens in environmental samples in a sensitive, fast, and enrichment-free way.[164,165] CRISPR-Cas-assisted phage genome engineering is one of the promising techniques that has been applied to improve the efficiency and speed of phage genome editing,[160,163,166] and can open up new opportunities for developing phage-based bio-recognition elements with elevated performance.

As is the case with applications of phages in the medical sector, building large libraries of phages, and developing methods for fast screening of the phage library to choose the best phage to target a specific bacteria of interest will make phage applications in the environmental sector easier. Another restricting factor in phage research is the limited availability of phage genomes in the common public databases, which are important for comparing phage genomes with each other and also with bacterial cells.[143]Looking at most of the research conducted in developing phage-based bioassays and biosensors for bacterial pathogen detection in water, it seems that there is gap between choosing target pathogens and the real-world applications of monitoring microbial quality of water samples. Recently, with emergence and prevalence of antibiotic resistance bacteria/genes (ARB/ARG), measures should be taken to specifically monitor and detect the presence of trace amounts of antibiotic resistance in natural water and wastewater treatment plants. There have been reports of detecting the presence of ARB/ARG in drinking water,[167–169] and recreational water[170] underlining the fact the spread of ARB through water could be a major health challenge. WHO has published a list of bacterial pathogens that have developed antibiotic resistance and there is an urgent need of finding alternatives to antibiotics for fighting against them. *Acinetobacter baumannii*, *Pseudomonas aeruginosa*, *Enterobacteriaceae*, *Enterococcus faecium*, and *Staphylococcus aureus* are on top of this

list[171] that could expose public health in extreme danger if they find their ways to natural water resources and water distribution systems. Phages are investigated heavily to tackle the antibiotic resistance as one of the promising alternative treatments in multidrug resistance bacterial infections.[172–174] However, the potential of phage as a tool to detect these deadly superbugs in water and wastewater has been neglected, which could be useful as a prophylactic measure to stop the spread of the infectious disease at the source. Application of phage bio-probe as a detection tool for monitoring and diagnosis of antibiotic resistant has been mainly focused food, and clinical samples.[175] There is pressing need of developing fast, effective, and sensitive detection tools to monitor the effluents released from wastewater treatment plants focusing specifically on detecting multidrug resistance superbugs, especially when it comes to usage of treated wastewater in agricultural settings.

Increasing phage stability for long term storage and preservation (preparing stable liquid or powder formulation for phages of interest) is another important aspect of using phage for detection purposes. Phages are usually isolated from the natural environments, enriched, and purified to be applied in environmental settings. Having been isolated, phages need to be protected to preserve their infectivity and stability. Different stabilizing methods of phage in liquid or powder form have been suggested so far;[89,90] however, more work is needed to develop environmentally friendly, applicable and cost-effective method to preserve phage titer and store phage (possibly on the sensor platforms) for environmental applications.

Phage efficacy in binding/infecting bacterial cells can be altered due to different reasons. For example, while phages are believed to be robust and resist harsh environments, environmental factors such as temperature, pH and water salinity could affect the infection efficacy of phages (inactivation of phages in the environment)[176]. Moreover, implementation of phage probes to detect pathogens in complex fluids such as wastewater is challenging and needs more investigation. The presence of interferants including colloidal matter, dead bacterial cells, natural organic materials, and disinfectants can block phage receptors and prevent phage binding/infecting live bacterial cells. Non-specific attachment is also another challenge in real samples that can affect the

performance of phage probes in biosensors. The effect of phage purity on performance of phage-based bioassays/biosensors should also be investigated since the release of cellular debris such as proteins, lipids, and carbohydrates during phage propagation process could block phage receptors and affect phage binding/infecting target cells.

Phages are often specific to only a few strains of bacteria,[177] and this can lead to false negative results by missing other strains of the same bacterial species which are out of their host range. As a result, phages with ability to infect as many strains of the same bacteria species as possible is beneficial for detection and sensing application, and sometimes, using a mixture of phages or a phage cocktail could be used to broaden the phage host range so that they can infect more strains of the same bacteria species.[121] While many phages are specific to a single bacterial species, there some phages that can infect more than one species or genera (polyvalent phages).[178] In conclusion, phage host range is an important parameter that should be evaluated before implementing bacteriophages as bio-probes in bioassays and biosensors to prevent false positive or negative results. Phages contribute significantly to regulation of ecology, diversity, and virulence of microbial community. Phage predation controls bacteria population, activity, and community composition.[179] Phages can change the environmental microbiome through different strategies such as killing a competing bacteria, changing the pathogenicity of bacteria by encoding toxins or virulence factors, acting as a genetic vector to transfer genetic information between bacterial cell through HGT (introduction of foreign genes into a bacterial genome).[180] Phages could function as genetic vectors to exchange genetic information through generalized or specialized transduction.[179,181] Although applications of phage for detection and monitoring are not expected to release large concentrations of phage into the environment that may disrupt the ecosystem, care should be taken to use phages that are sequenced and known to be free of toxin coding genes.

Finally, phage-based detection of bacteria in environmental biofilms has remained relatively unexplored. Keeping in mind that biofilms are the most common state of bacteria in nature, care should be taken when designing phage-based detection and monitoring solutions that are expected to detect bacteria in the biofilm mode because both the presence of ECM and the reduced metabolic activity of bacteria in the biofilm mode may affect the efficacy of detection.

Conflicts of interest

The authors have no conflict of interest to report.

Acknowledgement

The authors acknowledge and thank Pooya Torab Ahmadi for helping with preparing illustrations. The illustrations were created using Sketchup software and Biorender (BioRender.com).

6. References

1 F. Balloux and L. van Dorp, Q&A: What are pathogens, and what have they done to and for us?, *BMC Biol.*, 2017, **15**, 4–9.

2 A. C. Singer, H. Shaw, V. Rhodes and A. Hart, Review of antimicrobial resistance in the environment and its relevance to environmental regulators, *Front. Microbiol.*, 2016, **7**, 1–22.

3 J. E. M. Watts, H. J. Schreier, L. Lanska and M. S. Hale, The rising tide of antimicrobial resistance in aquaculture: Sources, sinks and solutions, *Mar. Drugs*, 2017, **15**, 1–16.

4 C. P. Henriot, D. Martak, Q. Cuenot, C. Loup, H. Masclaux, F. Gillet, X. Bertrand, D. Hocquet and G. Bornette, Occurrence and ecological determinants of the contamination of floodplain wetlands with Klebsiella pneumoniae and pathogenic or antibiotic-resistant Escherichia coli., *FEMS Microbiol. Ecol.*, 2019, **95**, 1–12.

5 S. Batinovic, F. Wassef, S. A. Knowler, D. T. F. Rice, C. R. Stanton, J. Rose, J. Tucci, T. Nittami, A. Vinh, G. R. Drummond, C. G. Sobey, H. T. Chan, R. J. Seviour, S. Petrovski and A. E. Franks, Bacteriophages in natural and artificial environments, *Pathogens*, 2019, **8**, 1–19.

6 K. E. Kortright, B. K. Chan, J. L. Koff and P. E. Turner, Phage Therapy: A Renewed Approach to Combat Antibiotic-Resistant Bacteria, *Cell Host Microbe*, 2019, **25**, 219–232.

7 G. P. C. Salmond and P. C. Fineran, A century of the phage: Past, present and future, *Nat. Rev. Microbiol.*, 2015, **13**, 777–786.

8 H.-W. Ackermann, in *Bacteriophages : methods and protocols*, eds. M. R. J. Clokie and A. M. Kropinski, Humana Press, Totowa, NJ, 2009, vol. 501, pp. 127–140.

9 J. W. Lee, J. Song, M. P. Hwang and K. H. Lee, Nanoscale bacteriophage biosensors beyond phage display, *Int. J. Nanomedicine*, 2013, **8**, 3917–3925.

10 Moon, Choi, Jeong, Sohn, Han and Oh, Research Progress of M13 Bacteriophage-Based Biosensors, *Nanomaterials*, 2019, **9**, 1448.

11 R. Peltomaa, E. Benito-Peña, R. Barderas and M. C. Moreno-Bondi, Phage Display in the Quest for New Selective Recognition Elements for Biosensors, *ACS Omega*, 2019, **4**, 11569–11580.

12 C. Howard-Varona, K. R. Hargreaves, S. T. Abedon and M. B. Sullivan, Lysogeny in nature: Mechanisms, impact and ecology of temperate phages, *ISME J.*, 2017, **11**, 1511–1520.

13 Z. Hobbs and S. T. Abedon, Diversity of phage infection types and associated terminology: the problem with 'Lytic or lysogenic', *FEMS Microbiol. Lett.*, 2016, **363**, 1–8.
14 M. Jamal, S. M. A. U. S. Bukhari, S. Andleeb, M. Ali, S. Raza, M. A. Nawaz, T. Hussain, S. u. Rahman and S. S. A. Shah, Bacteriophages: an overview of the control strategies against multiple bacterial infections in different fields, *J. Basic Microbiol.*, 2019, **59**, 123–133.
15 D. M. Lin, B. Koskella and H. C. Lin, Phage therapy: An alternative to antibiotics in the age of multi-drug resistance, *World J. Gastrointest. Pharmacol. Ther.*, 2017, **8**, 162.
16 R. A. Frampton, A. R. Pitman and P. C. Fineran, Advances in Bacteriophage-Mediated Control of Plant Pathogens, *Int. J. Microbiol.*, 2012, **2012**, 1–11.
17 L. K. Harada, E. C. Silva, W. F. Campos, F. S. Del Fiol, M. Vila, K. Dąbrowska, V. N. Krylov and V. M. Balcão, Biotechnological applications of bacteriophages: State of the art, *Microbiol. Res.*, 2018, **212**–**213**, 38–58.
18 J. Mathieu, P. Yu, P. Zuo, M. L. B. Da Silva and P. J. J. Alvarez, Going Viral: Emerging Opportunities for Phage-Based Bacterial Control in Water Treatment and Reuse, *Acc. Chem. Res.*, 2019, **52**, 849–857.
19 M. Ye, M. Sun, D. Huang, Z. Zhang, H. Zhang, S. Zhang, F. Hu, X. Jiang and W. Jiao, A review of bacteriophage therapy for pathogenic bacteria inactivation in the soil environment, *Environ. Int.*, 2019, **129**, 488–496.
20 A. Svircev, D. Roach and A. Castle, Framing the future with bacteriophages in agriculture, *Viruses*, 2018, **10**, 1–13.
21 R. L. Dy, L. A. Rigano and P. C. Fineran, Phage-based biocontrol strategies and their application in agriculture and aquaculture, *Biochem. Soc. Trans.*, 2018, **46**, 1605–1613.
22 A. Gigante and R. J. Atterbury, Veterinary use of bacteriophage therapy in intensively-reared livestock, *Virol. J.*, 2019, **16**, 155.
23 A. Culot, N. Grosset and M. Gautier, Overcoming the challenges of phage therapy for industrial aquaculture: A review, *Aquaculture*, 2019, **513**, 734423.
24 M. M. Osiemo, G. M. Ogendi and C. M'Erimba, Microbial Quality of Drinking Water and Prevalence of Water-Related Diseases in Marigat Urban Centre, Kenya, *Environ. Health Insights*, 2019, **13**, 1–7.
25 World Health Organization (WHO), Drinking water fact sheets, https://www.who.int/en/news-room/fact-sheets/detail/drinking-water, (accessed 14 June 2019).
26 A. K. Biswas and C. Tortajada, Water crisis and water wars : myths and realities, *Int. J. Water Resour. Dev.*, 2019, **35**, 727–731.
27 F. Y. Ramírez-Castillo, A. Loera-Muro, M. Jacques, P. Garneau, F. J. Avelar-González, J. Harel and A. L. Guerrero-Barrera, Waterborne pathogens: Detection methods and challenges, *Pathogens*, 2015, **4**, 307–334.
28 N. A. Moreira and M. Bondelind, Safe drinking water and waterborne outbreaks, *J. Water Health*, 2017, 83–96.
29 R. J. Gelting and M. Baloch, A systems analysis of irrigation water quality in environmental assessments related to foodborne outbreaks, *Aquat Procedia*, 2018, **2**, 130–137.

30 S. Kumar, M. Nehra, J. Mehta, N. Dilbaghi, G. Marrazza and A. Kaushik, Point-of-Care Strategies for Detection of Waterborne Pathogens, *Sensors*, 2019, **19**, 4476.

31 S. Burnham, J. Hu, H. Anany, L. Brovko, F. Deiss, R. Derda and M. W. Griffiths, Towards rapid on-site phage-mediated detection of generic Escherichia coli in water using luminescent and visual readout, *Anal. Bioanal. Chem.*, 2014, **406**, 5685–5693.

32 World Health Oraganization (WHO), *Guidelines for Drinking-water Quality: fourth edition incorporating the first addendum.*, Geneva, 2017.

33 H. Bridle, K. Gilbride and J. Green, in *Waterborne Pathogens: Detection Methods and Applications*, Elsevier, 2014, pp. 41–64.

34 H. Bridle, in *Waterborne Pathogens: Detection Methods and Applications*, Elsevier, 2014, pp. 9–40.

35 A. L. Harding and K. B. Byers, in *Biological Safety, principles and practices*, eds. D. O. Fleming and D. L. Hunt, American Society Microbiolgy, Washington, DC, 4th edn., 2006, vol. 42, p. 680.

36 S. M. Z. Hossain and N. Mansour, Biosensors for on-line water quality monitoring – a review, *Arab J. Basic Appl. Sci.*, 2019, **26**, 502–518.

37 H. Tavakoli, M. Bayat, A. Kousha and P. Panahi, The Application of Chromogenic Culture Media for Rapid Detection of Food and Water Borne Pathogen, *Agric. Environ. Sci*, 2008, **4**, 693–698.

38 A. F. Maheux, L. Bissonnette and M. G. Bergeron, in *PCR Detection of Microbial Pathogens: Second Edition, Methods in Molecular Biology*, 2013, vol. 943, pp. 289–305.

39 N. Singhal, M. Kumar, P. K. Kanaujia and J. S. Virdi, MALDI-TOF mass spectrometry: An emerging technology for microbial identification and diagnosis, *Front. Microbiol.*, 2015, **6**, 1–16.

40 I. Hubner, I. Steinmetz, U. Obst, D. Giebel and D. Bitter-Suermann, Rapid determination of members of the family Enterobacteriaceae in drinking water by an immunological assay using a monoclonal antibody against enterobacterial common antigen, *Appl. Environ. Microbiol.*, 1992, **58**, 3187–3191.

41 E. Morales-Narváez, T. Naghdi, E. Zor and A. Merkoçi, Photoluminescent Lateral-Flow Immunoassay Revealed by Graphene Oxide: Highly Sensitive Paper-Based Pathogen Detection, *Anal. Chem.*, 2015, **87**, 8573–8577.

42 U. Farooq, Q. Yang, M. W. Ullah and S. Wang, Bacterial biosensing: Recent advances in phage-based bioassays and biosensors, *Biosens. Bioelectron.*, 2018, **118**, 204–216.

43 Ł. Richter, M. Janczuk-Richter, J. Niedziółka-Jönsson, J. Paczesny and R. Hołyst, Recent advances in bacteriophage-based methods for bacteria detection, *Drug Discov. Today*, 2018, **23**, 448–455.

44 N. Franche, M. Vinay and M. Ansaldi, Substrate-independent luminescent phage-based biosensor to specifically detect enteric bacteria such as E. coli, *Environ. Sci. Pollut. Res.*, 2017, **24**, 42–51.

45 J. Chen, S. M. Andler, J. M. Goddard, S. R. Nugen and V. M. Rotello, Integrating recognition elements with nanomaterials for bacteria sensing, *Chem. Soc. Rev.*, 2017, **46**, 1272–1283.

46 M. Sedki, X. Chen, C. Chen, X. Ge and A. Mulchandani, Non-lytic M13 phage-based highly sensitive impedimetric cytosensor for detection of coliforms, *Biosens. Bioelectron.*, 2020, **148**, 111794.
47 A. E. Smartt, T. Xu, P. Jegier, J. J. Carswell, S. A. Blount, G. S. Sayler and S. Ripp, Pathogen detection using engineered bacteriophages, *Anal. Bioanal. Chem.*, 2012, **402**, 3127–3146.
48 G. Ertürk and R. Lood, Bacteriophages as biorecognition elements in capacitive biosensors: Phage and host bacteria detection, *Sensors Actuators, B Chem.*, 2018, **258**, 535–543.
49 T. Y. Thung, E. Lee, N. A. Mahyudin, K. Anuradha, N. Mazlan, C. H. Kuan, C. F. Pui, F. M. Ghazali, N.-K. Mahmud Ab Rashid, W. D. Rollon, C. W. Tan and S. Radu, Evaluation of a lytic bacteriophage for bio-control of Salmonella Typhimurium in different food matrices, *LWT*, 2019, **105**, 211–214.
50 M. Schmelcher and M. J. Loessner, Application of bacteriophages for detection of foodborne pathogens, *Bacteriophage*, 2014, **4**, e28137.
51 U. Farooq, M. Wajid Ullah, Q. Yang and S. Wang, in *Molecular Electronics [Working Title]*, IntechOpen, 2019, p. 13.
52 I. Sorokulova, E. Olsen and V. Vodyanoy, Bacteriophage biosensors for antibiotic-resistant bacteria, *Expert Rev. Med. Devices*, 2014, **11**, 175–186.
53 D. Wang, T. Hinkley, J. Chen, J. N. Talbert and S. R. Nugen, Phage based electrochemical detection of: Escherichia coli in drinking water using affinity reporter probes, *Analyst*, 2019, **144**, 1345–1352.
54 H. Peng and I. A. Chen, Rapid Colorimetric Detection of Bacterial Species through the Capture of Gold Nanoparticles by Chimeric Phages, *ACS Nano*, 2019, **13**, 1244–1252.
55 T. C. Hinkley, S. Singh, S. Garing, A. L. M. Le Ny, K. P. Nichols, J. E. Peters, J. N. Talbert and S. R. Nugen, A phage-based assay for the rapid, quantitative, and single CFU visualization of E. coli (ECOR #13) in drinking water, *Sci. Rep.*, 2018, **8**, 14630.
56 S. Singh, T. Hinkley, S. R. Nugen and J. N. Talbert, Colorimetric detection of Escherichia coli using engineered bacteriophage and an affinity reporter system, *Anal. Bioanal. Chem.*, 2019, **411**, 7273–7279.
57 T. C. Hinkley, S. Garing, S. Singh, A. L. M. Le Ny, K. P. Nichols, J. E. Peters, J. N. Talbert and S. R. Nugen, Reporter bacteriophage T7NLC utilizes a novel NanoLuc::CBM fusion for the ultrasensitive detection of: Escherichia coli in water, *Analyst*, 2018, **143**, 4074–4082.
58 D. Wang, J. Chen and S. R. Nugen, Electrochemical Detection of Escherichia coli from Aqueous Samples Using Engineered Phages, *Anal. Chem.*, 2017, **89**, 1650–1657.
59 J. Chen, S. D. Alcaine, A. A. Jackson, V. M. Rotello and S. R. Nugen, Development of Engineered Bacteriophages for Escherichia coli Detection and High-Throughput Antibiotic Resistance Determination, *ACS Sensors*, 2017, **2**, 484–489.
60 C. Nguyen, R. Makkar, N. J. Sharp, M. A. Page, I. J. Molineux and D. A. Schofield, Detection of Bacillus anthracis spores from environmental water using bioluminescent reporter phage, *J. Appl. Microbiol.*, 2017, **123**, 1184–1193.
61 Y. Zhou, A. Marar, P. Kner and R. P. Ramasamy, Charge-Directed Immobilization

of Bacteriophage on Nanostructured Electrode for Whole-Cell Electrochemical Biosensors, *Anal. Chem.*, 2017, **89**, 5734–5741.

62 Z. Wang, D. Wang, A. J. Kinchla, D. A. Sela and S. R. Nugen, Rapid screening of waterborne pathogens using phage-mediated separation coupled with real-time PCR detection, *Anal. Bioanal. Chem.*, 2016, **408**, 4169–4178.

63 S. D. Alcaine, K. Law, S. Ho, A. J. Kinchla, D. A. Sela and S. R. Nugen, Bioengineering bacteriophages to enhance the sensitivity of phage amplification-based paper fluidic detection of bacteria, *Biosens. Bioelectron.*, 2016, **82**, 14–19.

64 M. Vinay, N. Franche, G. Grégori, J. R. Fantino, F. Pouillot and M. Ansaldi, Phage-based fluorescent biosensor prototypes to specifically detect enteric bacteria such as E. coli and Salmonella enterica Typhimurium, *PLoS One*, 2015, **10**, 1–17.

65 J. Chen, S. D. Alcaine, Z. Jiang, V. M. Rotello and S. R. Nugen, Detection of Escherichia coli in Drinking Water Using T7 Bacteriophage-Conjugated Magnetic Probe, *Anal. Chem.*, 2015, **87**, 8977–8984.

66 L. Wu, T. Luan, X. Yang, S. Wang, Y. Zheng, T. Huang, S. Zhu and X. Yan, Trace detection of specific viable bacteria using tetracysteine-tagged bacteriophages, *Anal. Chem.*, 2014, **86**, 907–912.

67 T. C. Hinkley, S. Garing, P. Jain, J. Williford, A.-L. M. Le Ny, K. P. Nichols, J. E. Peters, J. N. Talbert and S. R. Nugen, A Syringe-Based Biosensor to Rapidly Detect Low Levels of Escherichia Coli (ECOR13) in Drinking Water Using Engineered Bacteriophages, *Sensors*, 2020, **20**, 1953.

68 R. Derda, M. R. Lockett, S. K. Y. Tang, R. C. Fuller, E. J. Maxwell, B. Breiten, C. A. Cuddemi, A. Ozdogan and G. M. Whitesides, Filter-based assay for Escherichia coli in aqueous samples using bacteriophage-based amplification, *Anal. Chem.*, 2013, **85**, 7213–7220.

69 A. E. Smartt and S. Ripp, Bacteriophage reporter technology for sensing and detecting microbial targets, *Anal. Bioanal. Chem.*, 2011, **400**, 991–1007.

70 R. Peltomaa, I. López-Perolio, E. Benito-Peña, R. Barderas and M. C. Moreno-Bondi, Application of bacteriophages in sensor development, *Anal. Bioanal. Chem.*, 2016, **408**, 1805–1828.

71 C. Kirchhelle, The forgotten typers: The rise and fall of Weimar bacteriophage-typing (1921–1935), *Notes Rec. R. Soc. J. Hist. Sci.*, 2019, **32**, 20190020.

72 M. Zourob and S. Ripp, in *Recognition Receptors in Biosensors*, Springer, New York, 2010, pp. 415–448.

73 V. Gupta and H. M. Saxena, A new bacteriophage based luminescence assay for diagnosis of brucellosis, *Indian J. Exp. Biol.*, 2017, **55**, 296–302.

74 R. Blasco, M. J. Murphy, M. F. Sanders and D. J. Squirrell, Specific assays for bacteria using phage mediated release of adenylate kinase, *J. Appl. Microbiol.*, 1998, **84**, 661–666.

75 M. Yemini, Y. Levi, E. Yagil and J. Rishpon, Specific electrochemical phage sensing for Bacillus cereus and Mycobacterium smegmatis, *Bioelectrochemistry*, 2007, **70**, 180–184.

76 S. Kim, M. Kim and S. Ryu, Development of an engineered bioluminescent reporter phage for the sensitive detection of viable salmonella typhimurium, *Anal. Chem.*, 2014, **86**, 5858–5864.

77 D. Zhang, C. P. Coronel-Aguilera, P. L. Romero, L. Perry, U. Minocha, C.

Rosenfield, A. G. Gehring, G. C. Paoli, A. K. Bhunia and B. Applegate, The Use of a Novel NanoLuc-Based Reporter Phage for the Detection of Escherichia coli O157:H7, *Sci. Rep.*, 2016, **6**, 6–13.

78 P. K. Wolber and R. L. Green, Detection of bacteria by transduction of ice nucleation genes, *Trends Biotechnol.*, 1990, **8**, 276–279.

79 M. Oda, M. Morita, H. Unno and Y. Tanji, Rapid Detection of Escherichia coli O157:H7 by Using Green Fluorescent Protein-Labeled PP01 Bacteriophage, *Appl. Environ. Microbiol.*, 2004, **70**, 527–534.

80 S. Ripp, in *Whole Cell Sensing System II*, Springer, Berlin, Heidelberg, 2009, vol. 123, pp. 65–83.

81 A. Shabani, M. Zourob, B. Allain, C. A. Marquette, M. F. Lawrence and R. Mandeville, Bacteriophage-modified microarrays for the direct impedimetric detection of bacteria, *Anal. Chem.*, 2008, **80**, 9475–9482.

82 M. Namura, T. Hijikata, K. Miyanaga and Y. Tanji, Detection of Escherichia coli with Fluorescent Labeled Phages That Have a Broad Host Range to E. coli in Sewage Water, *Biotechnol. Prog.*, 2008, **24**, 481–486.

83 A. Singh, S. Poshtiban and S. Evoy, Recent advances in bacteriophage based biosensors for food-borne pathogen detection, *Sensors (Switzerland)*, 2013, **13**, 1763–1786.

84 A. K. Basu, A. Basu and S. Bhattacharya, Micro/Nano fabricated cantilever based biosensor platform: A review and recent progress, *Enzyme Microb. Technol.*, 2020, **139**, 109558.

85 F. Pujol-Vila, R. Villa and M. Alvarez, Nanomechanical Sensors as a Tool for Bacteria Detection and Antibiotic Susceptibility Testing, *Front. Mech. Eng.*, 2020, **6**, 1–18.

86 J. Tamayo, P. M. Kosaka, J. J. Ruz, Á. S. Paulo and M. Calleja, Biosensors based on nanomechanical systems, *Chem. Soc. Rev.*, 2013, **42**, 1287–1311.

87 J. Mertens, A. Cuervo and J. L. Carrascosa, Nanomechanical detection of: Escherichia coli infection by bacteriophage T7 using cantilever sensors, *Nanoscale*, 2019, **11**, 17689–17698.

88 D. C. Vanegas, C. L. Gomes, N. D. Cavallaro, D. Giraldo-Escobar and E. S. McLamore, Emerging Biorecognition and Transduction Schemes for Rapid Detection of Pathogenic Bacteria in Food, *Compr. Rev. Food Sci. Food Saf.*, 2017, **16**, 1188–1205.

89 V. Leung, A. Szewczyk, J. Chau, Z. Hosseinidoust, L. Groves, H. Hawsawi, H. Anany, M. W. Griffiths, M. M. Ali and C. D. M. Filipe, Long-Term Preservation of Bacteriophage Antimicrobials Using Sugar Glasses, *ACS Biomater. Sci. Eng.*, 2018, **4**, 3802–3808.

90 V. Leung, L. Groves, A. Szewczyk, Z. Hosseinidoust and C. D. M. Filipe, Long-Term Antimicrobial Activity of Phage-Sugar Glasses is Closely Tied to the Processing Conditions, *ACS Omega*, 2018, **3**, 18295–18303.

91 I. Kim, J.-S. Moon and J.-W. Oh, Recent advances in M13 bacteriophage-based optical sensing applications, *Nano Converg.*, 2016, **3**, 1–17.

92 G. Smith, Filamentous fusion phage: novel expression vectors that display cloned antigens on the virion surface, *Science (80-.).*, 1985, **228**, 1315–1317.

93 R. Peltomaa, E. Benito-Peña, R. Barderas and M. C. Moreno-Bondi, Phage display

in the quest for new selective recognition elements for biosensors, *ACS Omega*, 2019, **4**, 11569–11580.

94 R. S. Sharma, S. Karmakar, P. Kumar and V. Mishra, Application of filamentous phages in environment: A tectonic shift in the science and practice of ecorestoration, *Ecol. Evol.*, 2019, **9**, 2263–2304.

95 J. M. Lim, N. S. Heo, S. Y. Oh, M. Y. Ryu, J. H. Seo, T. J. Park, Y. S. Huh and J. P. Park, Selection of affinity peptides for interference-free detection of cholera toxin, *Biosens. Bioelectron.*, 2018, **99**, 289–295.

96 E. R. Goldman, M. P. Pazirandeh, P. T. Charles, E. D. Balighian and G. P. Anderson, Selection of phage displayed peptides for the detection of 2,4,6-trinitrotoluene in seawater, *Anal. Chim. Acta*, 2002, **457**, 13–19.

97 X. Wang, T. Yang, X. Zhang, M. Chen and J. Wang, In situ growth of gold nanoparticles on Hg2+-binding M13 phages for mercury sensing, *Nanoscale*, 2017, **9**, 16728–16734.

98 R. Nian, D. S. Kim, T. Nguyen, L. Tan, C. W. Kim, I. K. Yoo and W. S. Choe, Chromatographic biopanning for the selection of peptides with high specificity to Pb2+ from phage displayed peptide library, *J. Chromatogr. A*, 2010, **1217**, 5940–5949.

99 E. V. Olsen, I. B. Sorokulova, V. A. Petrenko, I. H. Chen, J. M. Barbaree and V. J. Vodyanoy, Affinity-selected filamentous bacteriophage as a probe for acoustic wave biodetectors of Salmonella typhimurium, *Biosens. Bioelectron.*, 2006, **21**, 1434–1442.

100 E. V. Olsen, J. Sykora, I. Sorokulova, W. Neely, V. Petrenko, I.-H. Chen, J. Barbaree and V. Vodyanoy, Phage Fusion Proteins As Bioselective Receptors For Piezoelectric Sensors, *ECS Trans.*, 2019, **2**, 9–25.

101 S. Huang, H. Yang, R. S. Lakshmanan, M. L. Johnson, J. Wan, I. H. Chen, H. C. Wikle, V. A. Petrenko, J. M. Barbaree and B. A. Chin, Sequential detection of Salmonella typhimurium and Bacillus anthracis spores using magnetoelastic biosensors, *Biosens. Bioelectron.*, 2009, **24**, 1730–1736.

102 R. S. Lakshmanan, R. Guntupalli, J. Hu, D. J. Kim, V. A. Petrenko, J. M. Barbaree and B. A. Chin, Phage immobilized magnetoelastic sensor for the detection of Salmonella typhimurium, *J. Microbiol. Methods*, 2007, **71**, 55–60.

103 N. Karoonuthaisiri, R. Charlermroj, M. J. Morton, M. Oplatowska-Stachowiak, I. R. Grant and C. T. Elliott, Development of a M13 bacteriophage-based SPR detection using Salmonella as a case study, *Sensors Actuators, B Chem.*, 2014, **190**, 214–220.

104 M. Janczuk, Ł. Richter, G. Hoser, J. Kawiak, M. Łoś, J. Niedziółka-Jönsson, J. Paczesny and R. Hołyst, Bacteriophage-Based Bioconjugates as a Flow Cytometry Probe for Fast Bacteria Detection, *Bioconjug. Chem.*, 2017, **28**, 419–425.

105 World Health Organization (WHO), *Assessing Microbial Safety of Drinking Water - Improving Approaches and Methods*, OECD Publishing, 2003.

106 M. Ben Said, M. Ben Saad, F. Achouri, L. Bousselmi and A. Ghrabi, The application of phage reactivation capacity to sens bacterial viability and activity after photocatalytic treatment, *Environ. Technol. (United Kingdom)*, 2020, **0**, 1–9.

107 T. Juhna, D. Birzniece, S. Larsson, D. Zulenkovs, A. Sharipo, N. F. Azevedo, F. Ménard-Szczebara, S. Castagnet, C. Féliers and C. W. Keevil, Detection of

Escherichia coli in biofilms from pipe samples and coupons in drinking water distribution networks, *Appl. Environ. Microbiol.*, 2007, **73**, 7456–7464.

108 R. A. Deshmukh, K. Joshi, S. Bhand and U. Roy, Recent developments in detection and enumeration of waterborne bacteria: a retrospective minireview, *Microbiologyopen*, 2016, **5**, 901–922.

109 Y. Terao, T. Yonekita, N. Morishita, T. Fujimura, T. Matsumoto and F. Morimatsu, Potential rapid and simple lateral flow assay for Escherichia coli O111, *J. Food Prot.*, 2013, **76**, 755–761.

110 F. Born, P. Braun, H. C. Scholz and G. Grass, Specific detection of yersinia pestis based on receptor binding proteins of phages, *Pathogens*, 2020, **9**, 1–19.

111 D. Dams, L. Brøndsted, Z. Drulis-Kawa and Y. Briers, Engineering of receptor-binding proteins in bacteriophages and phage tail-like bacteriocins, *Biochem. Soc. Trans.*, 2019, **47**, 449–460.

112 A. Singh, D. Arutyunov, C. M. Szymanski and S. Evoy, Bacteriophage based probes for pathogen detection, *Analyst*, 2012, **137**, 3405–3421.

113 Z. Hosseinidoust, T. G. M. Van De Ven and N. Tufenkji, Bacterial capture efficiency and antimicrobial activity of phage-functionalized model surfaces, *Langmuir*, 2011, **27**, 5472–5480.

114 Z. Hosseinidoust, A. L. J. Olsson and N. Tufenkji, Going viral: Designing bioactive surfaces with bacteriophage, *Colloids Surfaces B Biointerfaces*, 2014, **124**, 2–16.

115 M. Badv, J. I. Weitz and T. F. Didar, Lubricant-Infused PET Grafts with Built-In Biofunctional Nanoprobes Attenuate Thrombin Generation and Promote Targeted Binding of Cells, *Small*, 2019, **15**, 1905562.

116 M. Osborne, A. Aryasomayajula, A. Shakeri, P. R. Selvaganapathy and T. F. Didar, Suppression of Biofouling on a Permeable Membrane for Dissolved Oxygen Sensing Using a Lubricant-Infused Coating, *ACS Sensors*, 2019, **4**, 687–693.

117 M. Villegas, Y. Zhang, N. Abu Jarad, L. Soleymani and T. F. Didar, Liquid-Infused Surfaces: A Review of Theory, Design, and Applications, *ACS Nano*, 2019, **13**, 8517–8536.

118 S. M. Imani, M. Badv, A. Shakeri, H. Yousefi, D. Yip, C. Fine and T. F. Didar, Micropatterned biofunctional lubricant-infused surfaces promote selective localized cell adhesion and patterning, *Lab Chip*, 2019, **19**, 3228–3237.

119 M. Badv, C. Alonso-Cantu, A. Shakeri, Z. Hosseinidoust, J. I. Weitz and T. F. Didar, Biofunctional Lubricant-Infused Vascular Grafts Functionalized with Silanized Bio-Inks Suppress Thrombin Generation and Promote Endothelialization, *ACS Biomater. Sci. Eng.*, 2019, **5**, 6485–6496.

120 D. V. Dixon, Z. Hosseinidoust and N. Tufenkji, Effects of environmental and clinical interferents on the host capture efficiency of immobilized bacteriophages, *Langmuir*, 2014, **30**, 3184–3190.

121 S. M. Ezzat and M. I. Azzam, An approach using a novel phage mix for detecting Pseudomonas aeruginosa in water, *Water Environ. J.*, 2020, **34**, 189–202.

122 J. Fito and S. W. H. Van Hulle, Wastewater reclamation and reuse potentials in agriculture: towards environmental sustainability, *Environ. Dev. Sustain.*, 2020, 1–24.

123 H. Hettiarachchi and R. Ardakanian, *Safe Use of Wastewater in Agriculture*, 2018.

124 I. Al Baz, R. Otterpohl and C. Wendland, Eds., *Efficient Management of*

wastewater: Its Treatment and Reuse in Water-Scarce Countries, Springer Berlin Heidelberg, 2008.

125 L. Rizzo, W. Gernjak, P. Krzeminski, S. Malato, C. S. McArdell, J. A. S. Perez, H. Schaar and D. Fatta-Kassinos, Best available technologies and treatment trains to address current challenges in urban wastewater reuse for irrigation of crops in EU countries, *Sci. Total Environ.*, 2020, **710**, 136312.

126 A. Novo, S. André, P. Viana, O. C. Nunes and C. M. Manaia, Antibiotic resistance, Antimicrobial residues and bacterial community composition in urban wastewater, *Water Res.*, 2013, **47**, 1875–1887.

127 M. Munir, K. Wong and I. Xagoraraki, Release of antibiotic resistant bacteria and genes in the effluent and biosolids of five wastewater utilities in Michigan, *Water Res.*, 2011, **45**, 681–693.

128 S. A. A. Jassim, R. G. Limoges and H. El-Cheikh, Bacteriophage biocontrol in wastewater treatment, *World J. Microbiol. Biotechnol.*, 2016, **32**, 1–10.

129 G. Saxena, R. N. Bharagava, G. Kaithwas and A. Raj, Microbial indicators, pathogens and methods for their monitoring in water environment, *J. Water Health*, 2015, **13**, 319–339.

130 M. M.F. Mesquita and M. B. Emelko, in *Bacteriophages*, ed. I. Kurtboke, InTech, 2012, pp. 57–80.

131 G. Bitton, in *Wastewater Microbiology*, John Wiley & Sons, Inc., Hoboken, NJ, USA, 2005, pp. 259–290.

132 K. Otawa, S. Hyon Lee, A. Yamazoe, M. Onuki, H. Satoh and T. Mino, Abundance, Diversity, and Dynamics of Viruses on Microorganisms in Activated Sludge Processes, *Microb. Ecol.*, 2007, **53**, 143–152.

133 O. H. Shapiro and A. Kushmaro, Bacteriophage ecology in environmental biotechnology processes, *Curr. Opin. Biotechnol.*, 2011, **22**, 449–455.

134 S. Ahiwale, P. Koparde, P. Deore, V. Gunale and B. P. Kapadnis, in *Microorganisms in Environmental Management*, Springer Netherlands, Dordrecht, 2012, pp. 289–313.

135 D. Periasamy and A. Sundaram, A novel approach for pathogen reduction in wastewater treatment, *J. Environ. Heal. Sci. Eng.*, 2013, **11**, 1–9.

136 Y. Turki, H. Ouzari, I. Mehri, A. Ben Ammar and A. Hassen, Evaluation of a cocktail of three bacteriophages for the biocontrol of Salmonella of wastewater, *Food Res. Int.*, 2012, **45**, 1099–1105.

137 N. El-Dougdoug, M. Nasr-Eldin, M. Azzam, A. Mohamed and M. Hazaa, Improving Wastewater Treatment Using Dried Banana Leaves and Bacteriophage Cocktail, *Egypt. J. Bot.*, 2020, **60**, 199–212.

138 N. Al-Jassim, D. Mantilla-Calderon, G. Scarascia and P. Y. Hong, Bacteriophages to Sensitize a Pathogenic New Delhi Metallo β-Lactamase-Positive Escherichia coli to Solar Disinfection, *Environ. Sci. Technol.*, 2018, **52**, 14331–14341.

139 P. Yu, J. Mathieu, G. W. Lu, N. Gabiatti and P. J. Alvarez, Control of Antibiotic-Resistant Bacteria in Activated Sludge Using Polyvalent Phages in Conjunction with a Production Host, *Environ. Sci. Technol. Lett.*, 2017, **4**, 137–142.

140 J. W. Jun, S. S. Giri, H. J. Kim, S. K. Yun, C. Chi, J. Y. Chai, B. C. Lee and S. C. Park, Bacteriophage application to control the contaminated water with Shigella, *Sci. Rep.*, 2016, **6**, 1–7.

141 M. Liu, J. J. Gill, R. Young and E. J. Summer, Bacteriophages of wastewater foaming-associated filamentous Gordonia reduce host levels in raw activated sludge, *Nat. Publ. Gr.*, 2015, 1–13.
142 J. Choi, S. M. Kotay and R. Goel, Bacteriophage-based biocontrol of biological sludge bulking in wastewater, *Bioeng. Bugs*, 2011, **2**, 214–217.
143 S. M. Kotay, T. Datta, J. Choi and R. Goel, Biocontrol of biomass bulking caused by Haliscomenobacter hydrossis using a newly isolated lytic bacteriophage, *Water Res.*, 2010, **45**, 694–704.
144 S. Petrovski, R. J. Seviour and D. Tillett, Prevention of Gordonia and Nocardia stabilized foam formation by using bacteriophage GTE7, *Appl. Environ. Microbiol.*, 2011, **77**, 7864–7867.
145 Z. A. Dyson, J. Tucci, R. J. Seviour and S. Petrovski, Isolation and characterization of bacteriophage SPI1, which infects the activated-sludge-foaming bacterium Skermania piniformis, *Arch. Virol.*, 2016, **161**, 149–158.
146 K. Khairnar, P. Pal, R. H. Chandekar and W. N. Paunikar, Isolation and Characterization of Bacteriophages Infecting Nocardioforms in Wastewater Treatment Plant, *Biotechnol. Res. Int.*, 2014, **2014**, 1–5.
147 K. Khairnar, R. Chandekar, A. Nair, P. Pal and W. N. Paunikar, Novel application of bacteriophage for controlling foaming in wastewater treatment plant- an eco-friendly approach, *Bioengineered*, 2016, **7**, 46–49.
148 S. Taylor, T. L. Brown, J. Tucci, P. Lock, R. J. Seviour and S. Petrovski, Isolation and characterization of bacteriophage NTR1 infectious for Nocardia transvalensis and other Nocardia species, *Virus Genes*, 2019, **55**, 257–265.
149 Z. A. Dyson, J. Tucci, R. J. Seviour and S. Petrovski, Lysis to kill: Evaluation of the lytic abilities, and genomics of Nine bacteriophages infective for Gordonia spp. and their potential use in activated sludge foam biocontrol, *PLoS One*, 2015, **10**, 1–16.
150 S. Withey, E. Cartmell, L. M. Avery and T. Stephenson, Bacteriophages - Potential for application in wastewater treatment processes, *Sci. Total Environ.*, 2005, **339**, 1–18.
151 R. Lood, G. Ertürk and B. Mattiasson, Revisiting antibiotic resistance spreading in wastewater treatment plants - Bacteriophages as a much neglected potential transmission vehicle, *Front. Microbiol.*, 2017, **8**, 1–7.
152 G. U. Gunathilaka, V. Tahlan, A. I. Mafiz, M. Polur and Y. Zhang, Phages in urban wastewater have the potential to disseminate antibiotic resistance, *Int. J. Antimicrob. Agents*, 2017, **50**, 678–683.
153 L. Hall-Stoodley, J. W. Costerton and P. Stoodley, Bacterial biofilms: From the natural environment to infectious diseases, *Nat. Rev. Microbiol.*, 2004, **2**, 95–108.
154 N. Rabin, Y. Zheng, C. Opoku-Temeng, Y. Du, E. Bonsu and H. O. Sintim, Biofilm formation mechanisms and targets for developing antibiofilm agents, *Future Med. Chem.*, 2015, **7**, 493–512.
155 H.-C. Flemming, B. Bendinger, M. Exner, J. Gebel, Kistemann, T., G. Schaule, U. Szewzyk and J. Wingender, in *Microbial Growth in Drinking-Water Supplies: Problems, Causes, Control and Research Needs*, eds. D. van der Kooij and P. W.J.J. van der Wielen, IWA publishing, 2013, vol. 12, pp. 207–238.
156 B. Wu, R. Wang and A. G. Fane, The roles of bacteriophages in membrane-based

water and wastewater treatment processes: A review, *Water Res.*, 2017, **110**, 120–132.

157 W. Ma, M. Panecka, N. Tufenkji and M. S. Rahaman, Bacteriophage-based strategies for biofouling control in ultrafiltration: In situ biofouling mitigation, biocidal additives and biofilm cleanser, *J. Colloid Interface Sci.*, 2018, **523**, 254–265.

158 S. Liu, C. Gunawan, N. Barraud, S. A. Rice, E. J. Harry and R. Amal, Understanding, monitoring, and controlling biofilm growth in drinking water distribution systems, *Environ. Sci. Technol.*, 2016, **50**, 8954–8976.

159 A. M. Motlagh, A. S. Bhattacharjee and R. Goel, Biofilm control with natural and genetically-modified phages, *World J. Microbiol. Biotechnol.*, 2016, **32**, 1–10.

160 S. Kilcher and M. J. Loessner, Engineering Bacteriophages as Versatile Biologics, *Trends Microbiol.*, 2019, **27**, 355–367.

161 S. Meile, S. Kilcher, M. J. Loessner and M. Dunne, Reporter Phage-Based Detection of Bacterial Pathogens: Design Guidelines and Recent Developments, *Viruses*, , DOI:10.3390/v12090944.

162 D. P. Pires, S. Cleto, S. Sillankorva, J. Azeredo and T. K. Lu, Genetically Engineered Phages: a Review of Advances over the Last Decade, *Microbiol. Mol. Biol. Rev.*, 2016, **80**, 523–543.

163 A. Hatoum-Aslan, Phage genetic engineering using CRISPR–Cas systems, *Viruses*, , DOI:10.3390/v10060335.

164 T. K. Lu, J. Bowers and M. S. Koeris, Advancing bacteriophage-based microbial diagnostics with synthetic biology, *Trends Biotechnol.*, 2013, **31**, 325–327.

165 Y. Chen, H. Batra, J. Dong, C. Chen, V. B. Rao and P. Tao, Genetic engineering of bacteriophages against infectious diseases, *Front. Microbiol.*, 2019, **10**, 1–12.

166 S. R. Duong, M. M., Carmody, C. M., Qinqin, M., Peters, J. E., Nugen, Optimization of T4 Phage Engineering via CRISPR/Cas9, *Sci. Rep.*, 2020, submitted.

167 R. Destiani and M. R. Templeton, The antibiotic resistance of heterotrophic bacteria in tap waters in london, *Water Sci. Technol. Water Supply*, 2019, **19**, 179–190.

168 S. Bergeron, R. Boopathy, R. Nathaniel, A. Corbin and G. LaFleur, Presence of antibiotic resistant bacteria and antibiotic resistance genes in raw source water and treated drinking water, *Int. Biodeterior. Biodegrad.*, 2015, **102**, 370–374.

169 E. Sanganyado and W. Gwenzi, Antibiotic resistance in drinking water systems: Occurrence, removal, and human health risks, *Sci. Total Environ.*, 2019, **669**, 785–797.

170 C. Belding and R. Boopathy, Presence of antibiotic-resistant bacteria and antibiotic resistance genes in coastal recreational waters of southeast Louisiana, USA, *J. Water Supply Res. Technol. - AQUA*, 2018, **67**, 800–809.

171 E. Tacconelli, E. Carrara, A. Savoldi, D. Kattula and F. Burkert, *Global priority list of antibiotic-resistant bacteria to guide research, discovery, and development of new antibiotics*, .

172 A. Petrovic Fabijan, A. Khalid, S. Maddocks, J. Ho, T. Gilbey, I. Sandaradura, R. C. Y. Lin, N. Ben Zakour, C. Venturini, B. Bowring and J. R. Iredell, Phage therapy for severe bacterial infections: a narrative review, *Med. J. Aust.*, 2020, **212**, 279–

285.
173 F. L. Gordillo Altamirano and J. J. Barr, Phage therapy in the postantibiotic era, *Clin. Microbiol. Rev.*, 2019, **32**, 1–25.
174 D. J. Malik, I. J. Sokolov, G. K. Vinner, F. Mancuso, S. Cinquerrui, G. T. Vladisavljevic, M. R. J. Clokie, N. J. Garton, A. G. F. Stapley and A. Kirpichnikova, Formulation, stabilisation and encapsulation of bacteriophage for phage therapy, *Adv. Colloid Interface Sci.*, 2017, **249**, 100–133.
175 I. Sorokulova, E. Olsen and V. Vodyanoy, Bacteriophage biosensors for antibiotic-resistant bacteria, *Expert Rev. Med. Devices*, 2014, **11**, 175–186.
176 E. Jo, M. K, R. Mi and A. Górski, The influence of external factors on bacteriophages — review, 2011, 191–200.
177 B. Koskella and S. Meaden, Understanding bacteriophage specificity in natural microbial communities, *Viruses*, 2013, **5**, 806–823.
178 A. Ross, S. Ward and P. Hyman, More is better: Selecting for broad host range bacteriophages, *Front. Microbiol.*, 2016, **7**, 1–6.
179 J. L. Balcázar, How do bacteriophages promote antibiotic resistance in the environment?, *Clin. Microbiol. Infect.*, 2018, **24**, 447–449.
180 J. R. Penadés, J. Chen, N. Quiles-Puchalt, N. Carpena and R. P. Novick, Bacteriophage-mediated spread of bacterial virulence genes, *Curr. Opin. Microbiol.*, 2015, **23**, 171–178.
181 D. Debroas and C. Siguret, Viruses as key reservoirs of antibiotic resistance genes in the environment, *ISME J.*, 2019, **13**, 2856–2867.

APPENDIX II: Strategies to Prevent Bacterial Infections on Titanium-BASED Orthopedic and Dental Implants

Preface: In this chapter, we reviewed various antibacterial strategies for the prevention of biofilm formation on titanium-based orthopedic and dental implants. Two primary categories of coatings can be applied on titanium-based implants including anti-adhesion and bactericidal coatings to combat biofouling and bacterial inactions. Chemical and physical surface modification techniques and polymer-based coatings have been utilized to create repellent surface to prevent bacterial adhesion and colonization. In addition, various types of bactericidal agents including metallic coatings based on Ag, Zinc, copper, etc., antibiotics, bactericidal chemicals and polymers, and bacteriophages have been incorporated into different coating strategies to eradicate the bacteria and reduce the bacteria load and virulency. Lastly, we have examined the in vivo models employed to assess the effectiveness of these strategies and delved into the commercialization prospects of antibacterial coatings.

Contribution: I contributed to Collecting relevant research papers, articles, and other sources, figure design, and writing. Notably, I authored the entire "3.3. Bacteriophages" section.

Citation:

M. Villegas M, **F. Bayat**, T. Kramer, E. Schwarz, D. Wilson, Z. Hosseinidoust, T. F. Didar, Strategies to Prevent Bacterial Infections on Titanium-Based Orthopedic and Dental Implants. ChemRxiv. Cambridge: Cambridge Open Engage; 2023; This content is a preprint and has not been peer reviewed.

1. Abstract

Titanium and titanium alloys remain the gold standard for dental and orthopedic implants. These materials are heavily used because they are bioinert, have strong mechanical properties, and promote integration with bone. However, implant-associated infections (IAIs) remain one of the leading causes of implant failure. Eradicating an IAI can be difficult since bacteria can form biofilms on the medical implant, protecting the bacterial cells against systemic antibiotics and the host's immune system. If the infection is not treated promptly and aggressively, device failure is inevitable, leading to costly multi-step revision surgeries. To circumvent this dire situation, scientists and engineers continue to fabricate novel strategies to protect the surface of medical implants from bacteria. In this review, we report on emerging strategies to prevent infection in titanium implants. These strategies include anti-adhesion properties provided by polymers, superhydrophobic, superhydrophilic, and liquid-infused surface coatings, as well as strategies and coatings employed to lyse the bacteria. We also explore commercially available technologies or under clinical trials and discuss future trends.

2. Introduction

Titanium and titanium alloys remain one of the most widely used materials for medical implants. Titanium alloys, especially medical grade titanium (Ti6Al4V), are commonly used in orthopedic and dental applications due to their high moduli, strength, and bioinert properties. The titanium oxide passivation layer protects the implant from corrosion and allows for direct fusion with bone to provide mechanical stability.[1] The process of osseointegration, or the direct structural and functional connection between implant and bone, is paramount for the long-term stability of a load-bearing implant.[1] Failure of orthopedic and dental implant can occur shortly after implantation (weeks post-surgery) or even years after implantation.[2] Among the causes of device failure, implant-associated infections (IAI) remain the top cause for revision surgeries in orthopedic and dental implants in North America, primarily because bacterial infections cause bone resorption and device loosening.[2–5] Eradication of IAI is particularly challenging because surface-dwelling bacteria are protected by a self-secreted biofilm, making them 1000 times less

susceptible to antibiotics than planktonic bacteria and also reduces the effectivity of the host's immune cells.[6] A bacterial biofilm can be defined as a surface-associated bacterial community embedded in an extracellular matrix (ECM).[7] The ECM is composed of polysaccharides, extracellular DNA, and glycoproteins, which create a polymeric habitat for the bacteria. Furthermore, the ECM enhances cell-to-cell communication among bacteria (quorum sensing) and provides an optimal surface for bacteria recolonization if needed.[6,8–11] In Canada alone, the cost of orthopedic revision surgeries involving an IAI costs 2.3 times that of the initial implantation surgery at a cost of $25,000, while in the US, the cost for a revision arthroplasty surgery costs around $49,000.[3,12] The higher costs come from the surgical treatments, requiring single- or multi-stage procedures.[13] In the revision arthroplasty, the infected implant is removed, the necrotic tissue is debrided, and the patient is treated with systemic antibiotics for an extended period of time to eradicate the infection.[13] Once the bone has healed and there are no signs of infection, a secondary surgery is required to introduce new long-term prosthetic.[13]

In the past, the main strategy to prevent IAI revolved around rapidly integrating the biomaterial with the host body and "win the race to the surface".[14] This is because any surface that has already been occupied by a connective (bone) or soft tissue, would not be available for bacteria colonization. This strategy focuses on coating the biomaterial with functional biomolecules, which enhance cell adhesion,[15] promote bone cells chemotaxis,[16–19] induce differentiation of immature cells into bone cells,[18–21] increase vascularization and healing of the peri-implant space,[22] or use immunomodulator molecules that promotes the hosts' anti-inflammatory response and tissue healing.[23,24] Review papers on osseointegration through these strategies can be found elsewhere.[20,23,25–28]

It is important to understand how bacteria can infect a medical device and how a biofilm can form. **Figure 1** illustrates the process of biofilm formation and bacteria colonization. First, planktonic bacteria attach to the surface and proliferate into a microcolony. Then, the colony grows in mass and secretes the ECM. Different bacteria stains may attach and form a symbiotic multi-strain colony at this stage. Finally, some bacteria are expelled into the planktonic phase to colonize new surfaces. It is noteworthy that an infected medical

implant can occur prior to insertion of the device, as well as post-operation. In some cases, device infection can occur years after implantation, which are considered a 'late infection'.[29] In this review, we will highlight the current state of surface coating technologies to prevent bacterial biofilms. These coatings, also highlighted in Table 1, can be divided into bacteria repulsive coatings, which prevent bacterial colonization, or bactericidal coatings, which lyses bacteria that come in contact with the coating or in the peri-implant space as shown in **Figure 1b**.

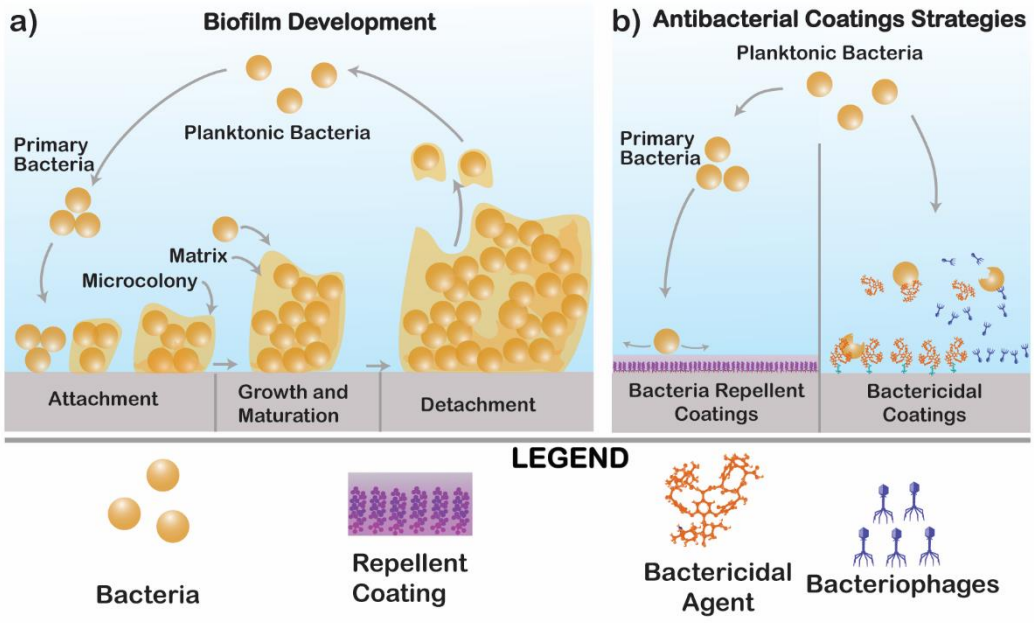

Figure 1. Schematic representation of antibacterial coatings. a) Schematic representation of biofilm formation and development. b) Schematic representation of different antibacterial coating strategies. Figure adapted with permission.[30] Copyright 2019 American Chemical Society.

Table 1. Different categories of antibacterial coatings.

Category	Components	Special Notes	Reference
Superhydrophobic	Nanostructure via anodic oxidation Coated with fluorosilane	Surfaces showed low bacteria after 4-hour incubation	31
	Plasma etched with Ar, O_2, hexamethyldisiloxane	Used a one-step fabrication process. Low bacteria adhesion after 24-hour incubation	32
	Hydrothermal synthesis of nanoflower topographies	Superior hemocompatibility, low bacterial adhesion after 24-hours	33
	Titania nanotubes followed by silanization	Low biofilm formation after 24-hour bacterial incubation on superhydrophobic, compared to superhydrophilic coatings	34
	Femtosecond laser ablation	*S. aureus* colonized the surface to a greater extent than *P. aeruginosa* showing a geometry dependency	35
Liquid Infused Surfaces	Surface roughened with ultrashort laser ablation coated with a fluorinated polymer	Tested different combinations of surface roughness and different lubricants. Spike like nano/micro textures showed the highest bacterial reduction	36
	Spiked roughness through laser ablation and GPL 104 lubricant	Tested against different bacteria found in the oral cavity and displayed a 60% reduction in bacteria compared to Ti.	37
	Ti coated with Chitosan and fluorosilane Lubricated with perfluoroperhydro phenanthrene	Chitosan – LIS showed good biofilm reduction and osteoblast-like cell adhesion while traditional LIS did not support cell adhesion.	7
Polymeric Coatings	Silk-sericin and PMAA	Promoted osseointegration and reduced bacterial adhesion	38
	Silk-sericin and tannic acid	Reduction in *E. coli* and *S. aureus* adhesion	39
	PLL-*g*-PEG	Up to 93% reduction in *S. aureus after 24-hours*	40
	Multivalent PEGylated peptides	Tetravalent titanium-binding peptides (TBP) reduced *S. aureus* biofilm formation after 5-hours.	41
	Citral and thymol and PEG	No biofilm was formed on the coating and bacteria was sparse compared to uncoated Ti	42
	Tannic acid and PEG	Compared one-step vs. two-step deposition processes. One-step procedure was 12-14% more efficient at repelling bacteria.	43
	Electrospinning of polyethylene oxide (PEO)	Hydrophilic nano fibers reduced *S. epidermidis* biofilm formation after a 24-hours incubation	44

	Electrospun chitosan mixed with PEO and bioactive glass particles	Coating showed reduced *S. epidermidis* attachment after a 48-hour incubation period.	45
	Hyperbranched poly-L-lysiene polymer	Antibacterial osteoconductive properties in an in vivo model	46
Metallic Coatings	Tantalum-nitride (TaN) vs. titanium nitride (TiN) coating	TaN showed lower biofilm formation and thickness after 14 days compared to the TiN coating	47
	Microporous coating composed of cobalt, fluorine, calcium, oxygen, phosphorus and different concentrations of strontium (0%, 6%, 11%,18%) wt.	90% decrease in bacteria compared with Ti after 28-days. Coatings that had 11% strontium content provided the best osteogenic properties.	48
	Calcium phosphate and zinc	89% reduction in *P. gingivalis* bacteria compared to CaP coated titanium.	49
	Strontium, calcium phosphate, and zinc	Increasing the concentration of zinc in the coating increased the bactericidal effects of the coating. Coatings showed no cytotoxic effects against MC3T3-E1 cells.	50
	Silver strontium	*S. aureus* reduction was proportional to silver concentration. Large silver concentrations had cytotoxic effects toward osteoblast.	51
	Silver and hydroxy apatite	Inhibited *S. aureus*, *E. coli*, and MRSA	52
	Silver nanocomposite on an amorphous hydrocarbon layer.	Reduced *E. coli* and *S. aureus* dependent on silver concentration. Coating was cytotoxic at high silver concentrations	53
Antibiotic Coatings	Vancomycin via AEEA linker	Covalent attachment of AEEA linker provided higher interactions and effectiveness of vancomycin. Reducing bacteria by 88% after 2-hour incubation.	54
	Cefotaxime sodium antibiotic via Polydopamine	Surface was hemocompatibility, biocompatible and broad spectrum against gram-negative and gram-positive bacteria	55
	Vancomycin and SRP-1 peptide linker	Coating would degrade and antibiotic was released in the presence of enzyme produced by *S. aureus.*	56
	Gentamycin and bone morphogenetic protein in a biodegradable polymer	Coating prevented infection and had osteoinductive properties.	57
	Rifampicin was embedded into hydroxyapatite and poly-caprolactone polymer	Polymer provided osteoblast cell attachment and proliferation. 3-log reduction in bacteria after 24-hour incubation	58
	Chitosan-bioglass with tetracycline and melittin	3-log reduction of MRSA after 6-hours	59

	Levofloxacin into PDEGMA polymer brushes	Drug release was temperature dependent. Brushes provided an anti-adhesion surface which reduced biofilm formation after 7-days	[60]
	Vancomycin on ethylene glycol PEG7 brushes	Reduced *S. aureus* 20-fold after 21-days in an animal model.	[61]
	Doxycycline on TiZr	Coatings were tested *in vivo*. The coated samples showed less cytotoxicity, and upregulated bone healing	[62]
	Bacitracin bonded via dopamine	Coating was tested in a rat model and prevented osteolysis caused be *S. aureus* (2.2-log reduction in CFU)	[63]
	Polyetheretherketone coating with BMP-2 and gentamicin	The coating had different release profiles for gentamicin and BMP-2. The coating was tested *in vivo* and showed increased bone deposition.	[57]
Bacteriophage	HPMC gel with linezolid and *S. aureus* specific bacteriophage	Combined coating showed the highest bacterial reduction in an *in vivo* model.	[64,65]
Misc.	Photosensitizer Indocyanine Green and RGD peptide on mesoporous polydopanine nanorparticle polymer	Coating provided photothermal and photodynamic therapy upon laser irradiation, decreasing bacteria by 99.7% in an animal model. Some cytotoxicity was seen.	[66]

3. Anti-adhesion Coatings

Anti-adhesion surfaces mitigate bacterial infections by preventing the unwanted accumulation of microbes on the implant's surface, which typically leads to bacterial build-up and the formation of biofilms. In order to give a surface anti-adhesive property, a specialized coating must be added, or the surface must be physically or chemically altered. Many strategies have been used throughout the literature to create the desired anti-adhesion property of the surface. For one, superhydrophobic surfaces have proved to be short-term inhibitors of bacterial adhesion due to their low surface free energy.[67] Next, liquid-infused surfaces, which involve creating a smooth interface on a surface through infusion with a layer of viscous liquid, have been shown to prevent bacterial adhesion and biofouling.[30] Polymeric coatings, including PEG and silk, have also shown a promising solution to prevent bacterial adhesion.[38,41] Finally, UV treatment prior to implantation has been shown to impair the accumulation of bacteria without compromising the biocompatibility of the surface [68] These methods and corresponding experimental results will be discussed in more detail

3.1. Superhydrophobic coatings

Surface wettability is a simple method to measure the free energy of a surface and has become an increasingly popular research topic. Two primary states of wetting on a rough solid surface have been identified based on Young's model. Wenzel's theory describes that liquid will follow the surface roughness and fully penetrate the surface. In contrast, Cassie-Baxter's theory says liquid will be suspended due to trapped air in crevices on the rough surface.[69,70] With recent advances in micro/nanotechnology, scientists and engineers have produced superhydrophobic surfaces by increasing the surface roughness and changing the surface chemistry. Superhydrophobic surfaces have low surface energy and are defined by a water contact angle greater than 150^{o}.[67,71] This large contact angle is explained by the Cassie-Baxter theory, stating that the contact angle increases when microstructures are present on the surface.[70] Superhydrophobic surfaces have enhanced corrosion resistance, improved hemocompatibility, and the ability to self-clean.[32,33,71] However, these surfaces have been distinguished as a viable inhibitor of bacterial adhesion and biofilm formation.

In recent years, various methods have been used to fabricate superhydrophobic surfaces on titanium. Furthermore, the produced superhydrophobic coatings have been effective at preventing bacterial adhesion. Generally, superhydrophobic surfaces are known to be created in a complex two-step fashion. The first step is to modify the surface roughness, and the second is to lower the surface free energy by adding a surface coating, increasing the surface's hydrophobicity.[32] Although many methods exist to create a roughened surface topography in the first step; the second step normally involves adding hydrocarbon or fluorocarbon groups to render the surface superhydrophobic. While the two-step process is facile, there have also been attempts to simplify the process of making the superhydrophobic surface by employing a one-step technique. In a study performed by Lin *et al.*, the authors aimed to determine how the adhesion of *S. aureus* would vary on hydrophilic, hydrophobic, and superhydrophobic titanium surfaces.[31] Lin *et al.* created a superhydrophobic nanotube structure via anodic oxidation followed by PTES (1H, 1H, 2H, 2H-perfluorooctyltriethoxysilane) in a self-assembled technique [31] SEM images showed that fewer bacteria had adhered to the superhydrophobic surface compared to the other surfaces at the 4-hour mark.[31] The bacterial cells on the superhydrophobic surface were also scattered and did not tend to gather, making them easier to be removed.[31] In a different study, Souza *et al.* created a unique one-step superhydrophobic coating on titanium by glow discharge plasma. The process used Ar, O2, and hexamethyldisiloxane gases, which etched the surface of titanium and made it superhydrophobic.[32] The authors compared the bacterial adhesion on a superhydrophobic coating to a non-coated titanium surface that served as the control.[32] An *in vitro* assay was performed using saliva as the microbial inoculum to evaluate the anti-biofilm property of the surfaces against bacterial and fungal adhesion.[32] The results for the superhydrophobic surface at the 2-hour mark showed an 8-fold reduction in total microbial adhesion compared to the control.[32] After 24 hours, scanning electron microscopy (SEM) images showed a robust biofilm developed on control surfaces, while the superhydrophobic surface had small and sparsely distributed colonies. Although a bacterial infection was mitigated in the short-term, longer periods need to be tested to see if the surface colony does not develop into a mature biofilm.[32] Montgomerie *et al.* created a superhydrophobic Titania coating through hydrothermal synthesis and vapor-phase silanization.[33] The produced coating contained a fractal geometry that

resembled a nanoflower (**Figure 2ai**). The nanoflower coating had superior hemocompatibility compared to flat Ti, showing fewer platelets and leukocyte adhesion.[33] Additionally, the surfaces were tested against the adhesion of *S. aureus* and *E.coli.* Images of the surface topography before bacterial incubation and after a 24-hs bacterial incubation show that a biofilm layer was forming on the control Titania for both *S. aureus* and *E. coli*. At the same time, there was no biofilm formation on the superhydrophobic surface, and very few bacteria were visible on the surface (**Figure 2ai**).[33] The biofilm formation on the surfaces was also quantified via fluorescent staining after 6 and 24-hour incubation periods. The results show that the superhydrophobic surface consistently had the lowest amount of live bacterial adhesion for both *S. aureus* and *E. coli* in comparison to all other surfaces ($p \leq 0.05$) (**Figure 2a,ii-iii**).[33] Barlet *et al.* conducted a comparable study, testing the adhesion of gram-positive and gram-negative bacteria on superhydrophobic and superhydrophilic titania nanotubes.[34] The superhydrophobic surface in this study was created by anodizing and chemically etching titanium to form titania nanotube arrays. Then the titania nanotube arrays were silanized to modify the surface chemistry and introduce superhydrophobicity.[34] Similar results were yielded from this study, as the number of adhered bacteria (for both *S. aureus* and *P. aeruginosa*) on the superhydrophobic surface was significantly lower than on all other surfaces ($p < 0.05$), and no biofilm formation was observed within 24 hours.[34] In contrast, Fadeeva *et al.* used a femtosecond laser ablation technique to fabricate superhydrophobic structures on titanium. In this study, *S. aureus* cells could colonize the superhydrophobic titanium surface after 18 hrs; however, the *P. aeruginosa* cells did not adhere.[35] The authors hypothesized that the *S. aureus* cells adhered more easily to the surface because of their spherical shape, allowing them to stick to the surface without requiring a large surface area. In contrast, *P. aeruginosa* cells containing an elongated rod shape may require more surface contact to adhere.[35] Overall, it is evident from all these studies that the superhydrophobic surfaces mitigated bacterial adhesion, showing fewer and more dispersed bacteria compared to the controls.

A negative aspect of superhydrophobic coatings is that the effectiveness of the surface to prevent bacterial adhesion seems to diminish as time passes. A study by Hwang *et al.* identified that the superhydrophobic surface might even encourage bacterial adhesion during long-term exposure. This increase in bacteria can be due to the high surface area

typically created on the superhydrophobic surface and the addition of proteins from the complex solution.[72,73] Although there is encouraging evidence that superhydrophobic surfaces mitigate bacterial adhesion in the short-term, further research should focus on long-term studies to investigate their effectiveness for medical implants.

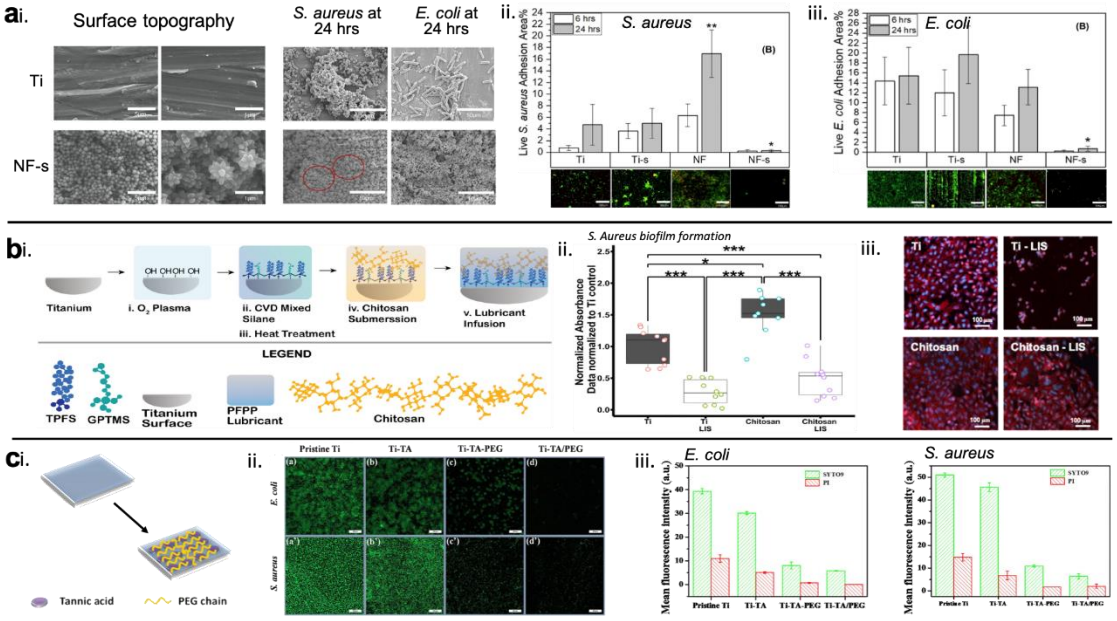

Figure 2. Anti-adhesion coatings. **ai**) SEM images of control (Ti) and superhydrophobic titania nanoflower (NF-s) surfaces before bacterial incubation and 24 hours after bacterial incubation. Bacterial cell adhesion area percentage for live **aii)** S. aureus and **aiii)** E. coli. Figure 2a was adapted with permission.[33] **bi)** Schematic representation of chitosan-conjugated liquid-infused coatings on titanium. **bii**) Crystal violet evaluation of *S. aureus* biofilm formation. **biii)** Fluorescent microscopy images of SaOS-2 cell proliferation after seven-day cell cultures (nuclei: blue; microfilaments: red). Figure 2b was adapted with permission.[7] **ci)** Schematic representation of substrate coated with tannic acid and PEG. **cii)** Fluorescent images of bacteria adhesion for *E. coli* and *S. aureus*. **ciii)** Mean fluorescent intensity values of adherent bacteria for *E. coli* and *S. aureus.* Figure 2c was adapted with permissions.[43]

3.2. Liquid infused coatings

Inspired by the Nepenthes pitcher plant, liquid-infused surfaces (LISs) are a class of functional materials with a tethered layer of liquid, creating a smooth interface.[74–82] LISs are recognized for their stable liquid-repelling behavior under low sliding angles.[83] For the LIS to be stable and repellant, the substrate must have a high affinity to the lubricant, and the lubricant must be immiscible with the liquid that needs repelling.[74,83,84] The lubricant

should be selected for the specific application. For example, for medical implants, the lubricant must be biocompatible and immiscible with complex liquids, such as plasma or blood. For a LIS to have clinical applications, many factors must be considered, including cytotoxicity toward human cells, environmental toxicity, the effect of leached products or byproducts, and the stability and longevity of the liquid inside the body.[85] Throughout the literature, LISs have been documented to effectively reduce bacterial adhesion and biofilm formation.[78–81,86,87]

LISs exist in one- (1D), two- (2D), and three-dimensional (3D) forms, with 2D being the most popular.[74] In a 1D LIS, the surface structure retaining the lubricant exists in a single plane on the order of one to multiple monolayers.[74] The thin lubricant layer is adhered to the substrate through intermolecular interactions or is directly grafted to the substrate.[74] In a 2D LIS, the surface structure is roughened, and the lubricant is encased by capillary action through nano-topographical features.[74] Finally, 3D LISs trap lubricant through a 3D pore network that also stores lubricant.[74] This review will primarily discuss 2D LISs, as they are the most prevalent type of LIS reported in the literature. Two primary methods exist to prepare 2D LISs: (i) modify an existing rough surface with an adequate chemical coating to match the lubricant chemistry, or (ii) roughen the surface of a substrate with low-surface-energy.[83] Many methods exist to create nanostructures on the substrate surface, including emulsion and phase separation, chemical and physical etching, mold transcribing, spin-coating, spraying, electrochemical decomposition, and more.[83] It should be noted that although the textured surface improves the LIS interface and promotes lubricant retention, the most critical step in creating a LIS is obtaining compatible surface chemistry between the substrate and the lubricant.[83] Scientific literature has proven that many efficient LIS substrates exist, including metals, non-metals, and polymers. However, titanium (Ti) is this review's primary substrate of interest.

Titanium LIS have been created through various methods by scientists and engineers to repel liquid and solid materials. A recent study by Doll et al. created LIS and performed surface structuring using ultrashort laser ablation.[36] Doll et al. tested titanium SLIPS with four structures (hierarchical, micro-, and nanosized spikes, micro-sized grooves, nanosized ripples, and unstructured surfaces) and five infusing perfluoropolyether lubricants of

different viscosities.[36] The SLIPS were fabricated by initially creating a rough surface, followed by dip coating the titanium with a fluorinated polymer.[36] Each lubricant was spin-coated onto each surface, creating a thin, homogenous liquid film.[36] Before the experiments, the LIS and uncoated Ti, were sterilized using UV irradiation.[36] Samples were tested against gram-positive *Streptococcus oralis* (*S. oralis*) bacterium. This study aimed to investigate biofilm formation and initial bacterial adhesion. For biofilm formation, samples were incubated in an inoculum of 4×10^{10} CFU/mL *S. oralis* for 18 hours under static conditions, and a maximum concentration of 0.3% lubricant in solution was used.[36] All SLIPS surface structures experienced reduced biofilm formation compared to their corresponding uncoated surfaces.[36] Spike SLIPS exhibited the highest reduction in biofilm formation of all tested surface structures. Each spike/lubricant combination was further investigated for biofilm volume and live/dead distribution of cells.[36] The biofilm volume on all spike SLIPS was 100-fold decreased compared to unstructured, uncoated Ti control.[36] For evaluating initial bacterial adhesion, samples were incubated in an inoculum of 3×10^{11} CFU/mL *S. oralis* for 5 hours under constant agitation at 150 rpm.[36] Spike slips coated with Krytox 143 AZ (143 AZ), and Krytox GPL 104 (GPL 104) lubricants demonstrated the highest effects on limiting bacterial adhesion, as quantified by dividing the total surface area covered with bacteria by the mean surface area of a single bacterium in ImageJ.[36] These surfaces were further investigated to determine their long-term stability. Both samples could resist gravitational forces and ambient conditions for up to 15 days while maintaining biofilm repellant properties.[36] Cellular viability was quantified to determine cytocompatibility of 143 AZ and GPL 104 lubricants against human gingival fibroblasts. It was determined that metabolic activity was not significantly different from that of the control cells.[36] When lubricant concentration increased to greater than 5%, metabolic activity decreased.[36] Therefore, the authors concluded that the lubricant is not cytotoxic up to 5% concentration. Contrastingly, it should be noted that the LIS tested with a 0.3% concentration of lubricant exhibited no growth of fibroblasts or osteoblasts. Since the 0.3% lubricant was not proven to be toxic to fibroblasts, making these surfaces more appealing for biomedical applications where soft tissue sealing and osseointegration are not critical.[36] A later study by Doll et al. investigated antiadhesive mechanisms to repel *S. oralis* biofilms using LIS.[37] The LIS were fabricated similar to the previous study, except only spike

structures were created on the surface using laser ablation, and only GPL 104 was used as the lubricant.[37] The LIS were tested against *S. oralis* and an oral multispecies composed of *S. oralis*, *Actinomyces naelundii* (*A. naelundii*), *Veillonella dispar* (*V. dispar*), and *Porphyromonas gingivalis* (*P. gingivalis*).[37] Biofilms were allowed to grow in a flow chamber system, and when tested against *S. oralis*, biofilm volume was reduced in the experimental Titanium LIS (biofilm volume = 2.9 x 106 μm^3 ± 1.9 x 106 μm^3) as opposed to the uncoated, unstructured Ti (biofilm volume = 3.8 x 107 μm^3 ± 2.3 x 107 μm^3).[37] Doll et al. furthered their research by testing SLIPS against multispecies communities that would be found in the oral cavity. The dominant species in the community was *S. oralis*, followed by *V. dispar*, while *A. naelundii* and *P. gingivalis* made up smaller portions.[37] The LIS samples experienced a biofilm reduction of approximately 60% when tested against the multispecies community compared to the Ti control group.[37] Bacterial adhesion forces were also reduced in LIS, as quantified by single bacterial cell force spectroscopy.[37] It should be noted that this study by Doll et al. did not further investigate coating cytocompatibility or toxicity. Therefore, it is still probable that the produced LISs are not appropriate for applications where osseointegration is critical. Conversely, recent literature has suggested that including chitosan in LISs can be beneficial in mitigating the lack of osseointegration promotion. A study by Villegas et al. created chitosan impregnated slippery LISs designed to facilitate cell adhesion and prevent biofilm formation.[7] Chitosan is a natural, biodegradable biopolymer found in shellfish, which has been reported to promote the proliferation of osteoblasts and mesenchymal cells.[7] To create the coatings, titanium alloys (Ti6Al4V) were initially treated with oxygen-plasma to hydroxylate and sterilize the surface.[7] To create a stable interface in the coating, fluorinated silane Trichloro(1H,1H,2H,2H-perfluorooctyl) (TPFS) was selected, as it has a high affinity for perfluoroperhydro phenanthrene (PFPP) lubricant.[7] After disinfection, titanium samples were conjugated with chitosan in aseptic conditions to create covalent bonds between the biopolymer and the surface. This process, in further detail, is outlined schematically in **Figure 2bi**. The functional coatings were tested against MRSA (methicillin-resistant staphylococcus aureus) MW2 strain to determine their bacteria repellent properties.[7] Untreated titanium, conventional liquid-infused titanium (Ti-LIS), and chitosan-coasted titanium (Chitosan) were selected as control samples.[7] The experimental combined chitosan

and liquid-infused coatings (Chitosan-LIS). Biofilm formation was quantized by crystal violet evaluation, where crystal violet values are proportional to biomass found on the surface.[7] A high value of normalized absorbance indicates large biomass; likewise, a low value indicates low biomass. Chitosan LIS reduced biofilm formation of MRSA up to 50% and 75% compared to untreated Ti and Chitosan Ti control groups. These results are summarized in **Figure 2bii**, and all data were normalized to the untreated Ti control group. Osteoblast-like SaOS-2 osteosarcoma cells were used to test cell adhesion and viability.[7] The control groups were untreated Ti, Ti-LIS, and Chitosan; the experimental group was Chitosan-LIS. As seen in **Figure 2biii**, after three- and seven-day cell cultures, Chitosan-LIS samples experienced high cell densities, superior to those of untreated Ti. This proves that the chitosan biopolymer increases mammalian cell adhesion and significantly promotes cell proliferation.[7] This study suggests that chitosan conjugated infused LISs have the potential to be beneficial in applications where bone ingrowth and tissue integration are critical.

Altogether, liquid-infused surfaces have great potential in the field of anti-adhesion coatings. Their simple fabrication steps and low sliding angles make them an efficient and inexpensive method to repel harmful bacteria and mitigate biofilm formation. Nevertheless, in the field of orthopedic and dental applications, it remains crucial for bioactive titania to present osteoconductive properties, and further research should be conducted into the cytocompatibility of liquid-infused surfaces. Although LISs have shown promise as antibacterial coatings, substantial progress must be made before these coatings can be applied clinically. Polymeric coatings are another alternative for anti-adhesion coatings. Like LISs, polymeric anti-adhesion coatings work to repel the surface attachment of bacteria. However, in place of a slippery surface, polymeric coatings repel bacterial attachment through polymer brushes adhered to the surface. Polymeric coatings have demonstrated their efficiency in preventing biofouling and will be further investigated in this review.

3.3. Polymeric coatings

Polymeric coatings have been discovered to have anti-biofilm properties and have been increasingly used in orthopedic applications to prevent the build-up of bacteria. A polymer

is commonly known as a material that consists of large molecules, where each molecule is comprised of repeating subunits. In general, polymers are suitable candidates to be involved with titanium coatings because of their stability, biocompatibility, and ability to prevent corrosion.[42,88] Polymeric coatings are usually characterized by the term polymer brush, which refers to a surface coating that contains polymers tethered to a surface.[88] This 'brushing' effect is created as the polymer molecules tend to repel the attachment surface due to steric repulsion and osmotic pressure, elongating the molecules near the attachment site and stretching them away from the surface.[88] The brushes are typically characterized by a high density of grafted polymer chains. They may either be in a solvated state, where the polymer layer consists of both solvent and polymer, or a melt state, where the polymer chains occupy the free space entirely.[88] These polymer brushes tend to have antifouling properties, but their effectiveness depends on the type of polymer and the bacteria strain present.[88] There are two main kinds of polymers, naturally occurring and synthetic. Researchers have taken a particular interest in the viability of silk-functionalized surfaces for natural polymers. For synthetic polymers, coatings on titanium comprised of polyethylene glycol (PEG) or polyethylene oxide (PEO) are the most common throughout the literature. Both categories of polymers and their efficacy will be addressed.

Silk is a natural polymer used as a component in titanium coatings to reduce bacterial adhesion. Raw silk is known to be produced in fiber form by various insects and spiders [38] Silk contains two different proteins: sericin and fibroin.[38] Sericin is preferred over fibroin because it is water soluble and easier to process. Furthermore, sericin is highly hydrophilic and is biocompatibile.[38,39] Zhang *et al.* produced a polymer using silk-sericin (SS) and polymethacrylic acid (PMAA) to promote osseointegration and inhibit bacterial adhesion on titanium implants.[38] The titanium surfaces were modified using surface-initiated atom transfer radical polymerization, allowing vastly different functions to be imparted on the same titanium surface.[38] The results from the study determined that the surface modified with PMAA and SS was effective at preventing the adhesion of bacteria, with this surface having significantly fewer *S. aureus* and *S. epidermidis* cells adhered compared to the control.[38] Additionally, the surface was still adhesive to osteoblast cells, and the coating did not prevent osseointegration, which was considered unique and advantageous.[38] Next, Cheng *et al.* attempted to create an antifouling titanium surface through the co-deposition

of natural tannic acid (TA) and SS.[39] The authors deposited the conjugated TA and SS on titanium surfaces via surface adhesive trihydroxyphenyl groups in TA, demonstrating a safe and environmentally friendly way of fabricating anti-adhesive coatings on a metallic surface. The titanium surfaces with co-deposited TA and SS showed a reduction in both *E. coli* and *S. aureus* compared to the controls, which had many viable bacterial cells adhered to the surface.[39] Most bacteria that had adhered to the modified surface were alive, and only a few were dead, confirming that the surface mainly had anti-adhesion abilities and negligible bactericidal properties.[39] Overall, it is clear that employing silk in titanium coatings is a promising approach to inhibit the attachment of bacteria. However, resources on this topic are limited and more research should be carried out with sericin, fibroin, and various derivatives to construct effective anti-adhesive surfaces.

Synthetic polymers are advantageous in tissue engineering applications because they have low toxicity and degradation rates.[44] Coatings comprised of PEG or PEO are characterized by flexible, highly hydrated chains of biocompatible polymers that hinder the attachment of bacteria through the water layer that covers the titanium surface and introduces a high activation barrier against bacterial adhesion.[44] PEG, in particular, has been used in polymer coatings for a plethora of reasons. PEG, specifically dense PEG brushes, are frequently involved in the preparation of coatings as they effectively decrease the number of proteins adsorbed on implant surfaces.[40] Furthermore, PEG can improve ductility and stop the coating from being brittle and fragile.[41] A unique PEG-based coating was used in a study by Harris *et al.*, where a poly(L-lysine)-*grafted*-poly(ethylene glycol) (PLL-*g*-PEG) coating was synthesized on titanium oxide surfaces, and the attachment of *S. aureus* was investigated.[89] Results of the study show that at the 24-hour mark, the PLL-*g*-PEG-coated surface reduced the amount of adherent *S. aureus* by 89–93% compared to the uncoated titanium control.[40] It was found that the bacteria-to-bacteria interactions were more substantial than the bacteria-to-surface interactions, as the small number of bacteria stuck on the polyethylene glycolated surface tended to clump together.[40] Next, Khoo *et al.* also tested the *S. aureus* resistance, but instead on titanium that was coated with multivalent PEGylated-peptides.[41] This study examined the ability of mono, di, and tetravalent titanium-binding peptides (TBPs) to resist bacterial adhesion.[41] Khoo *et al.* determined that all the PEGylated-peptide treated surfaces had considerably lower biofilm density than the

uncoated titanium surfaces.[41] Furthermore, it was concluded that the performance of the coating improved with more TBP repeats, with the tetravalent coating showing a 90% reduction in *S. aureus* biofilm formation after 5 hours of incubation, while there was a 32% and 47% reduction, respectively with the monomer and dimer.[41] In addition, Valliammai *et al.* evaluated the effectiveness of the synergistic combination of citral and thymol in a polymeric coating to inhibit the biofilm formation of methicillin-resistant *S. aureus* (MRSA).[42] PEG was used in the formulation of this coating to aid antibiofilm agents citral and thymol and to increase the plasticity of the coating, allowing the coating's outer surface to be smooth so that there were no ridges or crevices for the bacteria could adhere to.[42] After 24 hours of incubation, a robust MSRA biofilm was seen on the uncoated titanium, while on the coated specimen, there was no biofilm formation and the bacterial cells were sparse.[42] Similarly, Guo *et al.* investigated an antifouling polymeric coating created by mixing and co-depositing TA and PEG onto the titanium surface.[43] This study compared the effectiveness of a one-step simultaneous deposition process (**Figure 2ci**) against a two-step one at preventing adhesion of *S. aureus* and *E. coli*.[43] The anti-adhesion properties of the coating after 24 hours were observed through CLSM images, where green fluorescence highlighted the live bacteria with intact membranes and red fluorescence showed the bacteria that have damaged membranes.[43] Biofilm formation was evident on the pristine Ti surface, and on the TA-modified surface as a strong green fluorescence was present on both (**Figure 2cii**).[43] There was a low green fluorescence signal, implicating a minuscule bacteria presence seen on the surfaces that had the co-deposited polymer, both by the one-step (Ti-TA/PEG) and two-step (Ti-TA-PEG) deposition processes (**Figure 2cii**).[43] The same trend was observed for both *S. aureus* and *E. coli*.[43] The authors determined the mean fluorescent intensities of each image, confirming the antifouling properties of the Ti-TA/PEG surface. The results indicate that Ti-TA/PEG surfaces were 14.6% more effective at repelling bacteria than Ti-TA-PEG for *E. coli* and 12.4% for *S. aureus* (**Figure 2ciii**).[43] The effectiveness of PEG-based coatings is evident, but polymeric coatings consisting of PEO, particularly PEO nanofibers, have had promising anti-microbial effects. For one, Şimşek *et al.* examined a PEO coating created with sequential electrospinning and crosslinking processes.[44] Electrospinning involves utilizing electrical forces to make tiny polymeric fibers, which has been identified as a simple and cost-effective technique to

create polymeric nanofiber coatings on metallic surfaces.[44] Moreover, electrospinning polymers do not require chemicals or high temperatures to coat a substrate, providing a highly functional and biocompatible coating.[44] It was determined that the PEO nanofiber coating significantly reduced the attachment of *S. epidermidis* after 24 hours of incubation, as a robust biofilm layer had formed on the bare titanium. However, the modified surfaces by the PEO nanofibers had a minimal amount of bacterial attachment and no proliferation or colonization.[44] The authors attributed this outcome to the PEO chains, which were very hydrophilic and flexible and could exert osmotic repulsion.[44] In a similar study, Boschetto *et al.* tested the performance of a distinctive coating for titanium that involved electrospun chitosan mixed with PEO-based nanofibers and incorporated with bioactive glass particles.[45] Their analyses showed that substantially fewer *S. epidermidis* cells were found on the coated surfaces compared to the uncoated controls after 48 hours of incubation.[45] The coating showed a more effective action against bacteria than the uncoated titanium surfaces, likely because of the chitosan nanofibers that were a component in the coating.[45] Chitosan is a natural agent generally known to have bactericidal abilities.[45] Bactericidal coatings differ from anti-adhesion coatings as they represent a category of therapeutics that can kill any bacteria that populate on the surface instead of just decreasing and inhibiting the initial attachment of bacteria. This could provide a distinct advantage in orthopedic and dental applications as bactericidal coatings could continuously lyse bacteria on the implant and the peri-implant space. In contrast, anti-adhesion coatings have no bactericidal effects. Therefore, bacterial cells may eventually colonize the surface and form a biofilm. Bactericidal coatings, seen in various types and forms, will be discussed in the next section.

4. Bactericidal Coatings

Many antibacterial mechanisms exist to prevent bacterial adhesion, proliferation, and subsequent biofilm formation. Bactericidal coatings are active or passive coatings that can be applied onto a surface to kill bacteria.[90] In passive coatings, bactericidal surfaces disturb bacterial cells upon surface contact with the coating, which leads to cell death.[91] Conversely, active coatings represent bactericidal agents that are released from the surface coating to kill surface adhered bacteria and bacteria in the surrounding space.[90] There are many advantages and disadvantages to using passive and active coatings. A strong passive

coating will inhibit bacterial adhesion to the surface and prevent biofilm formation without the release of antibacterial agents that could be toxic to the host.[90] Since antibacterial agents are not released, implant integration and osteogenic differentiation are not altered, and there is no cause for the development of bacterial resistance.[90] However, there is some risk for *in vivo* applications, as passive coatings can recruit plasma proteins from biological fluids that will enhance the colonization of bacteria.[90] Unlike passive coatings, active coatings have the ability to target bacteria in the peri-implant space, which can protect the implant effectively post implantation. However, active coatings must maintain a minimum inhibitory concentration (MIC) in order to be effective, and since the bactericide is released continuously, the long-term effectivity of the coating will eventually be compromised. Another consideration that needs to be addressed with active bactericidal coatings is the release dynamics. For example, large burst concentrations can be cytotoxic to the surrounding tissue, therefore preventing proper healing. In contrast, slow release over a long period of time of bactericides such as antibiotics has the potential to cause bacterial resistance, which would promote additional infection.[90] For these reasons, bactericidal coatings continue to be heavily researched due to their great potential in combatting implant-associated infections (IAI). There are a plethora of bactericidal coatings include polymeric coatings,[92–94] antibacterial coatings,[17,62,63,95–100] bacteriophage containing coatings,[101] metallic coatings,[47,48,50,51,53,102,103] and more. Here, we will delineate the current state of these technologies.

4.1. Metallic coatings

Among the many classes of bactericidal coatings, metal-based coatings exert their antibacterial effects through several metal-dependent methods. Silver (Ag) destroys the cell wall and cytoplasmic membrane to release silver ions which degenerate ribosomes and inhibit protein synthesis.[102] Silver ions are able to deactivate respiratory enzymes on the cytoplasmic membrane, which terminates ATP synthesis.[102] Reactive oxygen species (ROS) are produced as a cellular response to bacterial invasion in some habitats by abiotic processes.[104,105] ROS will cause membrane disruption and work alongside silver ions to bind to deoxyribonucleic acid (DNA) and prevent replication.[102] The silver nanoparticles will accumulate in the cell wall and migrate across the cytoplasmic membrane, causing

perforation and degeneration, leading to organelle release and overall bacterial death. Similarly, the antimicrobial mechanism of copper (Cu) involves ROS generation and DNA degradation.[102] To exert antibacterial effects, zinc (Zn) aids in ROS generation and Zn^{2+} ion release, and strontium (Sr) works to inhibit bacterial cytoplasmic membrane permeability and cell metabolism.[102] Many different metals have been researched for their antibacterial effects as bactericides; including tantalum,[47] strontium,[48,50,51] copper,[103] silver,[51–53,102,103,106,107] and zinc[49,50,103] These metals have all been found to provide some degree of protection against various strains of bacteria as discussed below.

Metal-based coatings can be created through many different methods. Common methods include the use of metallic nanoparticles striking the surface, coating the surface using metal-infused thermal spraying techniques, micro-arc oxidation (MAO), magnetron sputtering, and complete surface incubation in calcifying solutions. A study conducted by Zhang *et al.* deposited tantalum-nitride (TaN) and titanium nitride (TiN) coatings onto commercial pure Ti through magnetron sputtering in a multi-functional coating rig.[47] Prior to coating, titanium was polished with a series of silicon carbide (SiC) abrasive papers and cleaned ultrasonically in acetone, anhydrous ethanol, and de-ionized (DI) water.[47] Magnetron sputtering was used to deposit a thin metallic film onto the Ti base. Ta and Ti of 99.99% purity were used as sputtering targets for deposition of TaN and TiN thin films onto the Ti substrate.[47] A significant reduction of biofilm formation ($p < 0.05$) against gram-positive (*A. viscosus and S. mutans*) and gram-negative (*P. gingivalis*) bacteria was observed.[47] The titanium nitride (TiN) sample had a biofilm thickness of 17 µm after 14 days of incubation with mixed bacteria, in comparison to the TaN sample which had a reduction of 8 µm, proving that the addition of metallic tantalum was beneficial in reducing biofilm thickness. Nonetheless, although the biofilm thickness was reduced in the TaN sample, low levels of biofilm still pose a risk for future adverse events related to bacterial infection. Additionally, tantalum was not explicitly tested against mammalian cells, so there is some concern for cytotoxicity.

Single step micro-arc oxidation (MAO) is a common technique used to adhere metallic coatings to titanium, including strontium,[48] copper,[103] and strontium-silver bactericidal coatings.[51] MAO is an effective method of including metal substrates into porous coatings.

Strontium is often chosen as an active agent for its osteogenic effects through the activation of calcium-sensing receptors and inhibition of bone resorption by increasing osteoprotegerin.[102] In addition, strontium can also inhibit bacterial cell metabolism by interfering with cytoplasmic membrane permeability.[102] In a study by Zhou *et al.*, MAO was used to create a microporous coating where strontium (Sr) was combined with cobalt (Co), fluorine (F), calcium (Ca), oxygen (O_2), and phosphorus (P).[48] The formulated coatings varied in strontium concentration and were tested *in vitro* for their osteogenic effects against mesenchymal stem cells (MSC).[48] The results indicated that the coatings including titanium, cobalt, phosphorus, calcium, and fluorine with varying percent weights of strontium (TiCPCF, TiCPCF-S6, TiCPCF-S11, and TiCPCF-S18) improved cell attachment and differentiation substantially in comparison to the Ti control group.[48] It was found that a Sr content of 11% weight in the TiO_2-based doped coating provided the best osteogenic activity *in vitro* as it was best able to stimulate MSC osteogenic differentiation.[48] After a 28-day incubation period with bacteria, all coatings had similar antibacterial removal rates of up to 92%, compared to the Ti control group (antibacterial rate of less than 10%).[48] The high antibacterial removal rate in the TiCPCF, TiCPCF-S6, TiCPCF-S11, and TiCPCF-S18 groups after 28 days indicates the potential for long-term antibacterial activity. Furthermore, the coatings tested by Zhou *et al.* showed no cytotoxic effects when tested against immature osteoblasts derived from mice (MC3T3-E1 cells). However, it is worth noting that other literature has proven that excessive concentrations of strontium can inhibit osteogenic differentiation and proliferation in osteoblasts.[108] This likely because at high concentrations Sr presents cytotoxic effects. Current evidence suggests that strontium is more efficient as a bone implant material than a bactericidal agent in terms of its abilities to promote osteogenic differentiation.[48,50,51,102] It is noteworthy that the TiCPCF coating without strontium experienced similar antibacterial removal rates to the optimized TiCPCF-S11 coating, indicating that the strontium addition likely had negligible bactericidal effects.

Zinc has been proven to provide low cytotoxic risk, while also reducing biofilm formation against gram-positive (*S. aureus*) and gram-negative (*P. gingivalis and E. coli*) bacteria.[49,50,103] A 2017 study conducted by Aranya *et al.* created calcium phosphate (CaP) based zinc coatings to observe the antibacterial efficiency of zinc as a metallic bactericide.[49]

Titanium alloy (Ti-6AL-4V, ASTM alloy standard Grade 5) disks were polished, rinsed with DI water, and air dried before applying the Zn-CaP coating. The Zn-CaP coating was tested against gram-negative bacteria (*P. gingivalis*) for three days. The results displayed a biofilm reduction of 89% compared to CaP coated Ti (55% reduction), indicating that the presence of zinc provided some degree of antibacterial protection.[49] When pairing zinc with strontium and calcium phosphate (SrCaP), the killing rates for SrCaPZn1 against *S. aureus* and *E. coli* reached 61.25% and 55.38%, respectively.[50] Increasing the concentration of zinc 4-fold (SrCaPZn4) had increased killing rates of 83.01% and 71.28% for *S. aureus* and *E. coli*, respectively.[50] The antibacterial results indicated a zinc-dependent relationship.[50] When testing the coatings with MC3T3-E1 cells *in vitro* and evaluating cell viability, the coatings displayed strong cytocompatibility for all zinc concentrations, indicating there was no excessive release of Zn^{2+}ions.[50]

The half maximal inhibitory concentration (IC_{50}) of a substance is the concentration of a substance that is required to inhibit a biological process by half.[109] A 2020 review conducted by Shimabukuro stated that the IC_{50} of silver, copper, and zinc for MC3T3-E1 cells, are 2.77 µM, 15.9 µM and 90 µM, respectively. These values indicate that silver is the most toxic element against osteoblast cells.[103] Silver has high cytotoxic activity because of its rapid burst releases of Ag^+ ions into the surrounding fluid.[51] This rapid release also leads to dramatically low silver content left in the coating, posing a risk for subsequent bacterial infections. A study conducted by Zhang *et al.* formulated silver strontium coatings and tested them using a bacterial inhibition zone (BIZ) assay against *S. aureus*.[51] The BIZ displayed a direct proportionality with Ag content (SrAg0.08 – 2.1 +/- 0.3mm vs. SrAg0.34 – 6.45 +/- 0.1mm, $p < 0.05$).[51] However, larger silver content also resulted in cytotoxic effects against MC3T3-E1 cells.[51] Silver has also been combined with calcium phosphates (CaP) to produce strong bactericidal effects against *S. aureus*, *E. coli*, and *Methicillin Resistant S. aureus* (MRSA) while providing an osteogenic effect .[52,106,107] For example, Ando *et al.'s* thermal spraying technique for Ag-CaP coated titanium completely inhibited MRSA adhesion (<10 colony forming units (CFU) after 10^2 CFU MRSA inoculation).[52] The thermal spraying powder was prepared by mixing 3 wt% of silver oxide and 97 wt% of hydroxyapatite (HA) and shaking them together to mix.[52] The coating was applied on the sand-blasted surface of the disk using a flame spraying system.[52] This coating was

proven to have strong antibacterial effects against *S. aureus*, *E. coli*, and MRSA in fetal bovine serum (FBS) and was not found to be cytotoxic against V79 Chinese hamster lung cells. Thukkaram *et al.* created a thin film amorphous hydrocarbon coating (a-C:H) with varying silver concentrations on medical grade Ti using a combination of gas aggregation source (GAS) and plasma-enhanced chemical vapor deposition (PE-CVD).[53] Coatings were bonded to the surface using the GAS system which lasted only 2.5 minutes. **Figure 3ai** highlights the fabrication process of the coating using the GAS PE-CVD system to create the Ag nanocomposite coating. The GAS system produced silver nanoparticles (AgNPs) with an average diameter of 24 +/- 6 nanometers (nm) embedded in a hydrocarbon matrix to prevent unwanted high burst release of silver ions into the body.[53] As seen in **Figure 3ai**, the matrix served as a reservoir for the continuous out-diffusion of silver ions.[53] Additional evidence by Thukkaram *et al*. demonstrated that coatings with a greater amount of AgNPs had a 6-log reduction in *E. coli* and a 4-log reduction in *S. aureus* after 24 hours of incubation.[53] Coatings with less AgNPs also provided strong antibacterial effects, however bactericidal efficacy was found to increase with silver content.[53] The a-C:H matrix was not found to induce any significant antibacterial activity in the absence of silver (Fig 3aii). Cytocompatibility testing with MC3T3 osteoblast cells was performed for a period of 7 days. The results indicated that the coated titania experienced a cell viability greater than 90% +/- 10%, in comparison, the uncoated Ti experienced a cell viability of about 70% +/- 10% (Fig 3aiii). It should be noted that lower Ag concentrations provided better MC3T3 cell viability, as increasing the silver content produced some cytotoxicity effects.[53]

The combined evidence suggests that the use of metallic elements in surface coatings have strong bactericidal activity against gram-positive and gram-negative bacteria. A critical strength that metallic coatings possess over other bactericidal coatings, such as bacteriophage or antibiotic coatings, is that they can be sterilized using standard procedures such as gamma irradiation,[110] alcohol disinfection,[110] and autoclave.[111,112] It should be noted that when many sterilization steps are used, the metal ion concentration may decrease. A study by DeVasConCellos *et al.* performed a rigorous sterilization process of their silver coatings, including autoclave, passivation, and ultrasonic cleaning.[113] The coating survived the sterilization process with fewer particles present on the surface, as observed by scanning electron microscopy (SEM).[113] The ability to ensure that the coating is sterile is beneficial

in the prevention of bacteria formation. Nevertheless, it remains extremely important to optimize metal concentration to prevent metallic bactericidal coatings from becoming cytotoxic. Metallic coatings display several advantages, first, they are effective against a broad-range of bacteria. Secondly, metallic coatings are easily manufactured and easily tuned and combined with other components. Lastly, metallic coatings can be sterilized through traditional means. One of the biggest disadvantages metallic coatings have is their lack of specificity, which can result in metallosis, or cytotoxicity toward the host's body. For this reason, the most common antibacterial coatings use molecules that can specifically target bacteria. In the next sections, we will review some common antibiotic coatings used for medical implants.

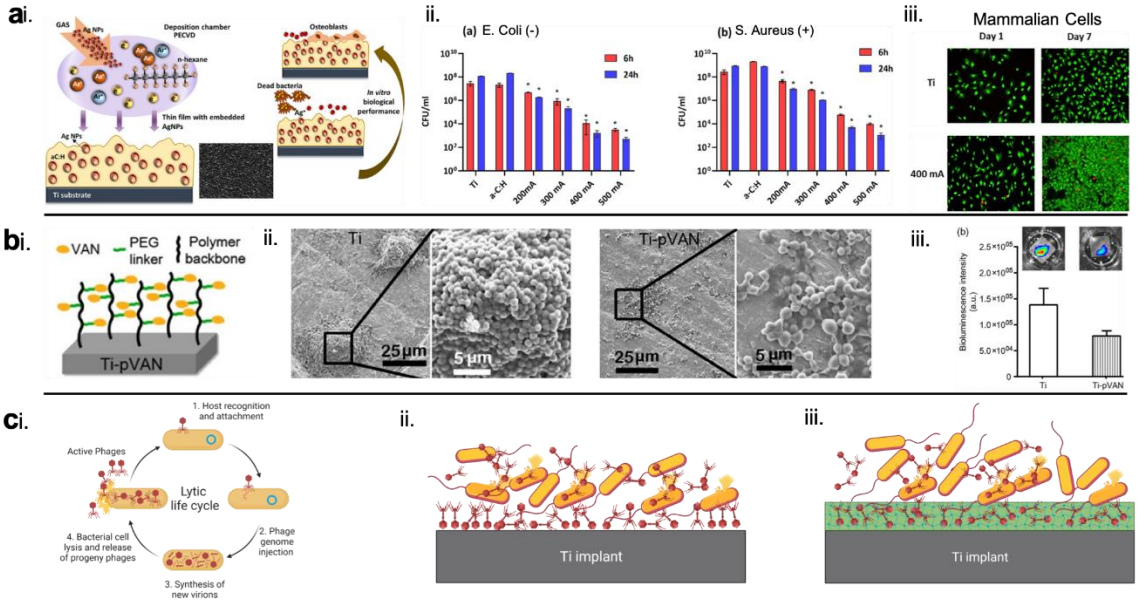

Figure 3. Bactericidal coatings. **ai**) Schematic representation of silver imbedded in a polymer coated on Ti. **aii)** Colony forming units (CFU) assay for *E. coli* and *S. aureus*. **aiii)** Fluorescent live/dead assay of osteoblast cells. Figure 3a was adapted with permission.[53]. **bi)** Schematic representation of vancomycin binded to polymer brush linker. **bii**) SEM images of *S. aureus* on Ti control and antibiotic coated surface. **biii)** Bioluminescent quantification of live bacteria. Figure 3b was adapted with permission. [114] **ci)** Schematic representation of the bacteriophage's lytic life cycle. **cii)** Bacteriophages physically or covalently bonded to Ti. **ciii)** Bacteriophages loaded into polymeric coating. Figure 3c was created in biorender.com.

4.2. Antibiotic coatings

Antibiotics remain the most common prophylactic agents studied. Antibiotics delivered locally at the implant site could have an integral role post-surgery, since the periprosthetic tissue might be damaged, avascular or necrotic, limiting any systemic antibiotic and the immune system from reaching the implant zone,[115] which could lead to an increased risk of implant infection and biofilm formation.[26] The antibiotic for local delivery should be chosen properly based on target agents, and ideally should be broad-spectrum as the infections are usually polymicrobial.[115] To decrease the chance of antibiotic resistance occurrence, the use of at least two antibiotics from different families has been recommended.[115] In recent years, several antibiotic coatings have been created using polymers,[92–94] ceramics,[58,116,117] polymer-ceramic composites,[58,118] and hydrogel coatings[119] to mitigate bacterial infections. Different methods have been implemented to apply antibiotic-loaded coating on Titanium-based dental/orthopedic implants, including electrospinning,[58,120] dip coating,[93] electrophoretic deposition,[118,121,122] plasma spray coating,[123] and sol-gel solutions.[124–126]

Antibiotics are applied onto an implant's surface in two general ways. The first one involves chemical immobilization on the surface, while the second one comprises of loading the antibiotics into the implant or into a porous sacrificial coating bonded on the implant's surface. The former method usually provides protection only at the surface of the implant since diffusion of the antibiotic is limited. On the other hand, loading the antibiotics provides the opportunity to have a controlled release of the antibiotics by fine-tuning the properties of the sacrificial layer (pore size and dissolvability). Another advantage of loading the antibiotics into a sacrificial layer is that the loading capacity is increased compared to coating the antibiotics directly onto the implant's surface.[115] The initial burst release of antibiotics is of great importance and should be higher than the minimum inhibition concentration (MIC) to protect the implant site against a bacterial infections. The subsequent release of antibiotic is relatively slow which is controlled by degradation rate of the coating or the elution of the antibiotics. The ideal long-term release of drug spans from several months to years post-surgery to prevent late infections.[127] It is worth noting the consequences of poorly designing the coating. If the initial burst release is too high, the

coating could become depleted from antibiotics prematurely. Furthermore, high release of antibiotics could also cause negative effects toward the host's tissue.[128] If the coating releases the antibiotic is low, below the MIC, this could give bacteria the opportunity to create resistance to the antibiotics.

Physical adsorption of antibiotics directly onto the surface might not be suitable for long-term implantation due to the fast kinetics of drug release into the environment. Moreover, this approach is also limited by the amount of antibiotics being loaded, however, increasing the surface area through micro/nano structuring can improve the drug loading capacity. For example, the interconnected micropatterned Ti surface was shown to enhance the vancomycin loading through hole pattern structure.[129] To prevent antibiotic loss, covalent bonding onto the surfaces is preferred. This can be achieved through surface functionalization of titanium implants using linker such as silanes, catechol, and phosphor-based molecules.[130] For example, the covalent attachment of vancomycin to Ti surface was reported to reduce Staphylococcus aureus colony-forming units (CFU) by 88% ± 16% over 2 hours.[54] This was achieved by creating by coating Ti with 3-aminopropyltriethoxysilane (APTS; $NH_2PrSi(OEt)_3$), a hydrophilic flexible linker 8-amino-3,6-dioxaoctanoate (aminoethoxyethoxy-acetate; AEEA) to extend the Vancomycin away from Ti surface to increase interactions with to the bacterial cell wall.[54] Covalent attachment of vancomycin to the surface of aminopropylated Ti alloy with aminopropyl-triethoxysilane and sequential coupling with two Fmoc-[2-(2-amino-ethoxy)-ethoxy]-acetic acid (AEEA) linkers has also shown to prevent *Staphylococcus epidermidis* biofilm formation.[131] In a different study, polydopamine (PD), a mussel-inspired molecule with excellent adhesive properties was used to graft Cefotaxime sodium (CS), to the surface of Ti implant. The interaction between the amino groups in CS and the catechol/quinone groups in PD through Michael addition and Schiff-base reactions provides the covalent grafting of the antibiotic to the surface.[55] The coating showed good hemocompatibility, no cytotoxicity and reduced gram-positive and gram-negative bacteria after 3 days.[55] In a different study, Zhang *et al*., formulated an infection-dependent drug-releasing surface.[56] In this method, vancomycin was covalently attached to the Ti surface through a tailor-made peptide which can be cleaved by a serine protease-like protease (SplB) secreted by S. aureus, providing an on-demand antibacterial response upon infection.[56]

Synergistic effect of antibacterial properties offered by both the loaded antibiotics and antibacterial properties of other coating components can enhance the coating performance. Drug-loaded biodegradable coatings can also provide the opportunity for dual functionality by promoting both antibacterial effect and osseointegration.[121,132] Min et al. reported a dual therapy nanolayered biodegradable polymeric coating on titanium implant using a layer-by-layer (L-b-L) deposition method containing gentamycin sulfate with bone morphogenetic protein (BMP-2), a prominent osteoinductive growth factor, to provide a bacteria killing and bone inducing microenvironment.[57] Rifampicin-loaded electrospun nanofibrous coating on titanium composed of hydroxyapatite (HA), a biocompatible osteoinductive ceramic and poly-caprolactone (PCL) polymer has shown an improved cell proliferation/adhesion and an effective antibacterial performance. This combination showed a 3-log reduction of *S. aureus* and *S. epidermidis*, and 2-log reduction of *P. aeruginosa* after a 24-hour incubation period. However, the long-term performance of these coating was not evaluated.[58] A composite chitosan-bioglass coating on titanium implant loaded with tetracycline and melittin, an antimicrobial peptide with a synergistic effect with antibiotics in killing drug resistant bacteria and prevent biofilm formation has been developed. A bacterial population decrease of >3-log has been reported after 6 hours for planktonic and adherent MRSA, confirming the synergistic effect of tetracycline and Melittin.[59] Choi et al. reported the development of a levofloxacin-loaded thermo-responsive poly (di(ethylene glycol) methyl ether methacrylate) (PDEGMA) brushes on titanium implants to disrupt bacterial colonization and biofilm formation. These polymeric brushes were synthesized via surface-initiated activator regeneration by electron transfer atom transfer radical polymerization on the surface of titanium, followed by immersion in a levofloxacin solution, to load the polymer brushes with antibiotics. Increasing the temperature to 37°C and 45°C led to faster drug release rate up to 6 hours, confirming a controlled thermo-responsive drug release behaviour. These levofloxacin loaded polymeric brushes showed a 90% reduction of living bacteria after a 24-hour incubation *in vitro*, which was further tested *in vivo* in rats, showing an excellent antibiofouling properties with significantly lower amount of S. aureus after 7-days post innoculation.[60] A vancomycin-bearing polymer brushes on the surface of titanium alloy-based pins has also been prepared using surface-initiated atom transfer radical polymerization and copper-catalyzed azide-

alkyne cycloaddition followed by vancomycin conjugation to azido-functionalized side chains of polymethacrylates. A flexible hydrophilic oligo (ethylene glycol) linker (PEG7) was also used to maintain the antibiotic activity of the covalently anchored vancomycin (**Figure 3b-i**). The treated titanium pins were able to successfully reduce the adherent bacteria by 20-fold compared to untreated control samples after 21 days post implantation in *S. aureus* infected mouse femoral canal.[61] **Figure 3b-ii** and **iii** shows the s. aureus adhesion to untreated and vancomycin treated surfaces *in vitro* after 5 hour incubation with 1.2×10^5 CFU/mL and quantification of bioluminescent signal after a 7-hour incubation with 2.3×10^6 CFU/mL.[61]

A lipid-based coating loaded with amikacin and/or vancomycin has been applied on titanium and successfully inhibited biofilm formation when exposed to S. aureus and P. aeruginosa for 24-hours, displaying a 5-log and 3-log bacterial reduction respectively. In this coating, the unloaded phosphatidylcholine-based material showed some antibacterial effect *in vitro*, although this inhibitory effect was not observed during the *in vivo* testing. This observation was interpreted to happen as a result of competing effects of protein and cell adhesion which shows the importance of *in vivo* studies in evaluating the coating's performance.[133]

Antibiotic coatings continue to be researched extensively as a prophylactic measure for medical implants. These technologies are of great value in dental and orthopedic applications as their use can reduce systemic dosing of antibiotics, protecting the medical surface from bacterial adhesion and biofilm formation and in some cases improve osseointegration. There are several limitations which need to be addressed before these coatings can be adapted in clinical settings. First, the long-term stability of the coating needs to be optimized. Although several studies show the efficacy of the coatings after 24-hours, with a few studies spanning 1-week to 1-month periods, ideally these coatings must be effective for longer periods (3 – months to several years). Secondly, the antibiotic coatings need to be design with a dose profile which maintains the MIC, but doesn't cause any cytotoxicity. This Goldilocks' concentration can be challenging to maintain over the long-term, since the loading capacity is limited and the antibiotic concentration will be depleted with time. Lastly, with the use of antibiotics, especially when at low concentration,

carry the risk of creating novel antibiotic resistant bacteria which could will be detrimental to the patient and could limit the efficacy of additional antibiotic treatments. Perhaps all of these downfalls can be circumvented though the novel use of bacteriophages, as discussed in the next section.

4.3. Bacteriophages

With high rates of antibiotic resistance among Gram-positive *S. aureus* and *S. epidermidis*, and increasing resistance among gram-negative bacteria such as *Enterobacter*, *Acinetobacter*, *Klebsiella*, and *Pseudomonas*, treating implant-associated infections are turning into a major challenge worldwide leading to increased rates of implanted device failure.[134,135] Bacteriophages, or phages for short, are bacterial viruses which have been around as antibacterial agents to treat bacterial infections for almost 100 years.[136] With increased prevalence of chronic bacterial infections due to spread of antimicrobial resistance as a global threat, phages have regained attention after being overshadowed for a long time by antibiotics' discovery in 1940s.[137,138] Phages are the most widespread entities on the planet earth with approximate population of 10^{31}, 10 times larger than bacterial population,[139] and they have different shapes and sizes. Morphologically, phages belong to two major categories including tailed (head-tail) and PFP (polyhedral, filamentous, or pleomorphic) and their size ranges from about 23 nm to filamentous phages with up to 2 μm length.[140] Phages are classified into two main categories including lytic or virulent, and lysogenic or temperate. In the lytic life cycle, having identified the host, phage inserts its genome into bacterial cell and takes control of the bacterial reproduction system and replicates itself. Newly formed phages, called progeny phages, are then released to the environment by lysis the bacterial cell. In the other hand, temperate phages incorporated its genome into the bacterial genome, a process known as prophage formation, and stays dormant until triggered by external factors such as UV exposure, heat, or chemicals, and as a result of this, the lysogenic life cycle is converted into lytic cycle.[141] For therapeutic applications, lytic phages are mostly preferred because of their immediate antibacterial effect as well as preventing the spread of horizontal gene transfer of virulence factor by temperate phages.[142]

Phages can attack bacterial cells and replicate themselves on-site by taking advantage of bacterial reproduction machinery.[143,144] This unique characteristic sets phage apart from the rest of antibacterial agents as phages can be implemented as self-sustained antibacterial agents. Another intriguing aspect of bacteriophages is their high specificity in attacking bacterial species down to the strain level. Phage's specificity mitigates damage to the human microflora as opposed to antibiotics which can affect the good bacteria along with the troublesome ones.[145,146] In addition, phages can be potent biofilm eradicators due to their ability to produce endolysins and EPS depolymerases that can disrupt the biofilm matrix. This provides the opportunity for having access to biofilm depth and attacking the hidden bacteria.[147]

Although promising results have been obtained showing the success of phage therapy in treating bacterial infections, there are some challenges associated with its application in clinical settings. Bacteria can develop resistance against phage infections similar to resistance developed against antibiotics. On the other hand, unlike antibiotics, phages are smart antibacterial agents containing genomic materials enclosed in a proteinous capsid that enables them to fight against phage resistance by genetic mutations to circumvent bacteria defense mechanisms.[148] Phage resistance mechanism include preventing phage adsorption to bacterial cell receptors, preventing the phage DNA entrance, cutting phage nucleic acids and abortive phage infection. Preventing phage adsorption is the most common resistant mechanism which occurs by point mutations and changes in the expression of surface receptors.[149] However, there are reports that show phage resistance can lower fitness and/or reduce virulence which can lead to enhanced performance of the immune system in eradicating the invading bacteria.[150–152] Another limitation could arise from narrow host range of bacteriophages. Although the narrow spectrum is an important characteristic of phages which helps preserving the natural human microflora as opposed to antibiotics, this sometimes requires the application of phage cocktails which are designed to have synergistic effects in removing various strains of the same bacterial species or looking for phages with broad spectrum-strain lytic activity.[153] Application of phage cocktails, or combination therapy with phage and other antimicrobial agents such as antibiotics, antimicrobial peptides, biofilm disrupting enzymes could enhance the efficacy of phage therapy in treating bacterial infections.[154]

The ability of phage in bacterial biofilm eradication can be a game changer when it comes to treating chronic bacterial infections as biofilms are the most challenging forms of bacterial infections and they are very hard to treat. However, almost all of the studies included only a monomicrobial infection model to assess the ability of phage in biofilm eradication. Another area which requires more exploration is assessing the efficacy of phage therapy in treating polymicrobial biofilm infections.

There are several reports *in vitro* and *in vivo* studies supporting the application of phage therapy for treating patients with implant associated infections (IAI). Injectable phage delivering hydrogel based on poly(ethylene glycol)-4-maleimide (PEG-4-MAL) hydrogel[155] have shown highly effective in reducing the P. aeruginosa population in both planktonic and biofilm states with a 4.7 fold less live bacteria in a mouse radial defect model. Alginate-based hydrogel systems[156,157] have been investigated for IAI treatment. Phage host range can be narrow down to strain levels, however, CRISPR-Cas9 technology can be implemented to modify the phage to have wider host range.[158] Moreover, this technology has been used to remove the staphylococcal cytotoxin and enterotoxin genes which can significantly enhance the safety of phage therapy.[159]

The use of phage as adjunct therapy for treating peri-prosthetic joint infections has been tested *in vivo* by implementing a combination of a phage cocktail with vancomycin against *S. aureus*. Titanium implants infected with *S. aureus* was press fit into a defect created in the distal femur of rats, and phage cocktail and/or vancomycin were administrated via the intraperitoneal (i.p.) route on day 21 to 27 post-surgery. Dual phage cocktail/antibiotic therapy showed the best results in treating infections and a 22.5-fold reduction was observed within joint tissue of animals with decreased swelling in the implanted knee. This supports the potential of phage therapy in combination with antibiotics to treat periprosthetic joint infections.[160] Local injection of *P. aeruginosa* and MRSA phages have been shown to successfully decrease the implant-related infections in a rat model, and when accompanied by appropriate antibiotic regimen, the biofilm of both bacteria was effectively eradicated.[161] Injection of a cocktail of highly lytic phages isolated form environmental sources, into the joint after replacement and joint closure accompanied with antibiotic

treatment led to promising results and eradication of infection among patients with relapsing S. aureus prosthetic knee infection.[162]

Kaur et al. proposed a dual antibacterial using hydroxypropyl methylcellulose (HPMC) gel coating containing a broad-spectrum lytic phage against *S. aureus* strains, and linezolid (a bacteriostatic agent which inhibits the bacterial protein synthesis and creation of initiation complex in gram positive cocci including streptococci, enterococci, staphylococci) on K-wires which are commonly used in orthopedic implant for pin fixation. The results confirmed a significant reduction in the adhered viable bacteria on implants and the surrounding tissue with no sign of resistant mutants arising in the phage and/or linezolid coated implants *in vivo*. The maximum bacterial reduction was observed when dual coated K-wires were used with a maximum decrease in associated inflammation. This result has been interpreted to happen due to the synergistic effect of phage and linezolid. Linezolid as a protein synthesis inhibitor prevents bacterial growth while boosting the phage assembly, production, lysis, and overall enhanced lytic activity of phage.[64,65]

In addition to use of whole phage as a bacteria devourer virus in treating bacterial infections, phage endolysins, or simply lysins, have been proposed as one of the interesting antibacterial agents. Phage-derived endolysins are peptidoglycan hydrolases used by bacteriophages towards the end of lytic cycle to rupture the peptidoglycan layer of the bacterial cell wall.[163] Currently, one endolysin (CF-301) has been used to treat bacteremia patients; however, there are no reports of antibacterial phage lysins for treating musculoskeletal infections.[152]

Overall, several successful cases of human clinical studies with phage monotherapy and phage-antibiotic combined therapy have been reported so far which along with several *in vivo* and *in vitro* studies demonstrates the significant potential application of phage therapy in treating orthopedic device-associated infections.[152] Similar to all pros and cons associated with use of other bactericidal agents, there are advantages and disadvantages to use of phages in treating bacterial infections which needs to be considered in designing phage-based coatings. This includes preserving phage infectivity (long term stability), narrow host range, phage resistance, and complicated interaction between phage-bacteria

and human immune system. There are immediate needs of exploring phage pharmacodynamic and pharmacokinetics to shed more light on the efficacy of phage therapy in clinical settings by conducting more *in vivo* studies. Phage can be embedded into hydrogels and polymeric coatings or applied directly onto the implant surface, with or without other antibacterial strategies, to prevent implant-associated infections. Although there are no reports of incorporating phage coatings on titanium-based orthopedic and dental implants, there are evidence showing their potential applications in these applications, especially with alarming rates of global antibiotic.

5. Animal Studies

In vivo testing is a crucial step to promote these coatings along the commercialization pipeline and to translate these technologies from research to clinical use. Here, we will delineate some of the recent titanium-treated antibacterial coatings that have been tested under *in vivo* conditions.

When designing coatings for orthopedic and dental implants, osseointegration is a key factor to be considered, as proper integration is essential to produce a strong mechanical interlocking between the bone and the prosthetic device. This is especially important in load bearing prosthetics, as poor integration can cause loosening and failure of the device. As mentioned earlier, titanium surfaces are bioinert, and therefore provide a non-toxic and favorable surface for bone cells to grow onto. However, having a bioinert surface does not represent a surface with optimal conditions for bone to grow. For this reason, coatings have been developed with osteogenic molecules to enhance bone cell adhesion and differentiation to enhance bone integration. Among the osteogenic factors, the most used are hydroxyapatite (HA) and calcium phosphate (CaP) coatings which have been shown to have osteoinductive and osteoconductive properties. It is worth noting that osteoinduction refers to the ability to stimulate immature host cells to develop into osteogenic cells, while osteoconduction refers to the ability to induce bone cell ingrowth and osteoid deposition.[164] Walter *et al*. coated titanium zirconium (TiZr) alloy discs with doxycycline using electrochemical deposition.[62] The coated samples were introduced onto rabbits near the bone marrow region of the tibia in the absence of bacteria. The samples were collected after 4 or 8 weeks of bone healing and the results demonstrated some positive trends. First, the

doxy-coated titanium samples showed less cytotoxicity compared to TiZr control. Secondly, doxy-coated samples expressed upregulated genes for alkaline phosphatase (ALP), osteocalcin, and bone morphogenic protein-2 (BMP-2).[62] Lastly, an increased bone mineral density (BMD) and total bone volume was seen doxy-coated samples compared to uncoated devices.[62] All of these results put together indicate a positive osteoinductive effect for the doxycycline coating. A similarly coating was used by Rahmati *et al*. on TiZr alloy.[97] The antibiotic coating release profile was tested *in vitro* under acidic conditions to represent a bacterial infection.[97] The results indicated a neglegible antibiotic releaser for the first 24-hours, followed by an increased burst release concentration. Although physiological condtions were not tested, the researchers alluded that the coating should be more resistant at higher pH. The antibiotic coating was tested with two animal models (rabbit and dog). In the animal studies mirco-CT scans indicated a significat bone in-growth after an 8-week period. The researchers also performed histological studies, however, there was no statistical difference between uncoated and coated TiZr. Although doxycyclene did not show a great improvement in osseointegration, this data still proved that adding a layer of doxycyclene did not hinder any bone growth onto antibiotic coated devices. Although doxycyclene is a known antibiotic, no bacteria studies were performed *in vivo* or *in vitro*. Nie *et al*. also formulated an antibacterial coating using antibiotics (bacitracin).[63] The bacitracin was covalently bonded to dopamine-conjugated titanium rods via EDC/NHS chemistry and imbedded into the femur of Sprague-Dawley rats, in the presence or absense of *s. aureus*. After a 3-week period, the rats were tested using X-ray radiographic imaging which showed no signs of infection in the Ti-bacitracin (with s. aureus) group, or the Ti rod incubated in PBS. In contrast, the Ti sample imbeded with *s. aureus* did show signs of osteolysis. These results were also validated with micro-CT scans which showed a reduced bone volume in the infected device, while no bone loss was seen in the antibiotic coated implant.[63] Further testing was performed *ex vivo* using a spread plate assay, showing a 2.16 log CFU reduction compared to the infected Ti control. *In vivo* osseointegration studies were also performed using micro-CT testing in the absense of bacterial. Here, bone volume was enhanced on the antibiotic coated Ti samples, compared to Ti, or dopanine coated Ti samples, therefore proving that bacitracin has an osteoconductive effect.[63] This study showed promising results regarding osseointegration and the antibacterial activity of their

coating, however, neither this, nor their previous study[99] tested the longevity of their coating which is another important aspect to consider. Another commonly borad-spectrum antibiotic is gentamicin. In a study perfromed by Min *et al*., gentamicin and osteoconductive growth factor (BMP-2) were coated in a layer-by-layer (LbL) fashion onto Polyetheretherketone (PEEK) substrates.[57] The LbL approach provides the advantage of independently tune of multidrug release kinetics (**Figure 4ai**).[57] Therefore, these researchers envisioned a coating that releases antibiotics early on post-surgical implantation, followed by a slow release of BMP-2 to prommote osseointegration and to "win the race to the surface".[57] Their rat animal model consited of drilling small incision on the tibia into the medullary cavity, introducing an uncoated implants and then inoculating them with *s. aureus* ($5x10^5$ CFU) to produce an osteomyeletus model.[57] After a 7-day period, a revision surgery was perfromed and the infected implant was replaced with either coated implants or uncoated control.[57] The BMP-2 and gentamicin (BG) coated samples reduced the bacterial CFU by 2-3 orders of magnitude compared to uncoated control (**Figure 4aii-4aiii**).[57] Furthermore, when comparing for newly bone formation, uncoated samples showed significat bone destructuion due to long-term inflamation caused by the bacteria. On the other hand, gentamicin coated samples showed some bone growth, but samples containing gentamicin and BMP-2 displated increased bone formation.[57] In terms of the mechanical stability of the implant, the BG coated sample displayed 10-15 times shear strenght compared to uncoated control. This study demonstrated a novel coating with a unique osteomyletitis animal model. Although this study was not performed on titanium substrates, similar methods could be applied to create a layer-by-layer deposition of different bioactive drugs with independent release control on titanium, or other substrates.

Antibiotics are not the only methods to treat infected prosthetics. For example, Yuan *et al*. created a mesoporous polydopanine nanorparticle (MPDA) mesh loaded with photosensitizer Indocyanine Green (ICG) as shown in **Figure 4b**.[66] This coating provided photothermal (PTT) and photodynamic (PDT) therapeutic actions to lyse bacteria under near infrared (NIR) light. The MPDA were coated onto amino-modified titania, loaded with ICG, and further modified with RGD peptide to provide osteoconductive properties. *In vivo* testing was performed on a rat mode, where Ti rods were coated incubated with an *s. aureus*

biofilm and then implanted into the femulr of the rats.[66] One day post-surgery, the rods were irradiated with an 808 nm laser to activate the PTT and PDT effects. After two weeks the rods were removed and the teste ex-vivo against bacteria. The results showed a reduction of bacteria up to 99.7% and the disruption of the biofilm compared to irradiate Ti (only 15% bacteria reduction). **Figure 4bii** and **5biii**, clearly disply the a difference is CFU on a spread plate assay, as well as a disrupted biofilm (SEM ismages). The produced coating was also tested for cytocompatibily *in vitro*, which showed a greater mesenchymal stem cell (MSC) population compared to Ti samples due to the osteoconductive RGD proteins. Nevertheless, upon irradiating the samples containing MSCs with NIR light, the cell viability was reduced due to cytotoxic effects produced by PTT and PDT. All together, this technology can be proved to be beneficial in a medical prosthetic. Although the photothermal and photodynamic therapies can be cytotoxic towards the bone cells, these effects will only be seen upon NIR irradiation, which will be likely be administered through a controlled regiment in a clinical setting. On the other hand, this technology could treat established bacterial infections without requiring surgical precedure. One of the caveats for this technology is the possibility of overexposing the coating to NIR light with natural light. IR sources, such as the sun, could potentially create device losening due to PTT and PTD activation, therefore, extensive research into this technology is required. Yang *et al*., coated titanium with a hyperbranched poly-L-lysiene polymer (HBPL) which proved to have osseocoductive properties and excelent antibacteria properties *in vitro* against gram-positive and gram-negative bacteria (**Figure 4ci-iv**).[46] The HBPL was tested in an *in vivo* in a rat model by drilling holes into the tibia of the rat and introducing titanium screws in the presense of bacteria (*S. aureus*). After 3 days, the rats were euthanized and the screws and surrounding tissues were collected. Samples from the implant and the mdullary cavity were sonnicated then streak plated onto brain heart infusion agar paltes. As seen in **Figure 4civ**, the Ti-HBPL coated samples significantly reduced bacterial colonies compared with the control groups. Histological staining also showed inflamation near the Ti-bone interface for the Ti and Ti-GPTMS groups but not on the HBPL coated samples. The HBPL coating was also tested against bone formation using micro-CT scanning and histological staining in the presence or absence of bacteria 4 weeks after implantation. In both tests, the Ti-HBPL samples showed increased bone formation compared to Ti control. **Figures 5cii** and

5ciii show the new bone formation on all three groups, and shows further proof that new bone formation was possible, even when the implant was infected with *s. aureus*. Although the bone volume / total volume (BV/TV) percentage growth is smaller in the noninfected rat model (**Figure 4ciii**.), the absolute BV/TV did indicate that the infection did reduce bone formation.[46] This type of polymer is beneficial as an antibacterial coating, since it is not cytotoxic, had no proinflamatory response, enhanced osseointegration and reduced bacterial viability with *in vivo* and *in vitro*. This polymer's main antibacterial mode of action is through the production of ROS.

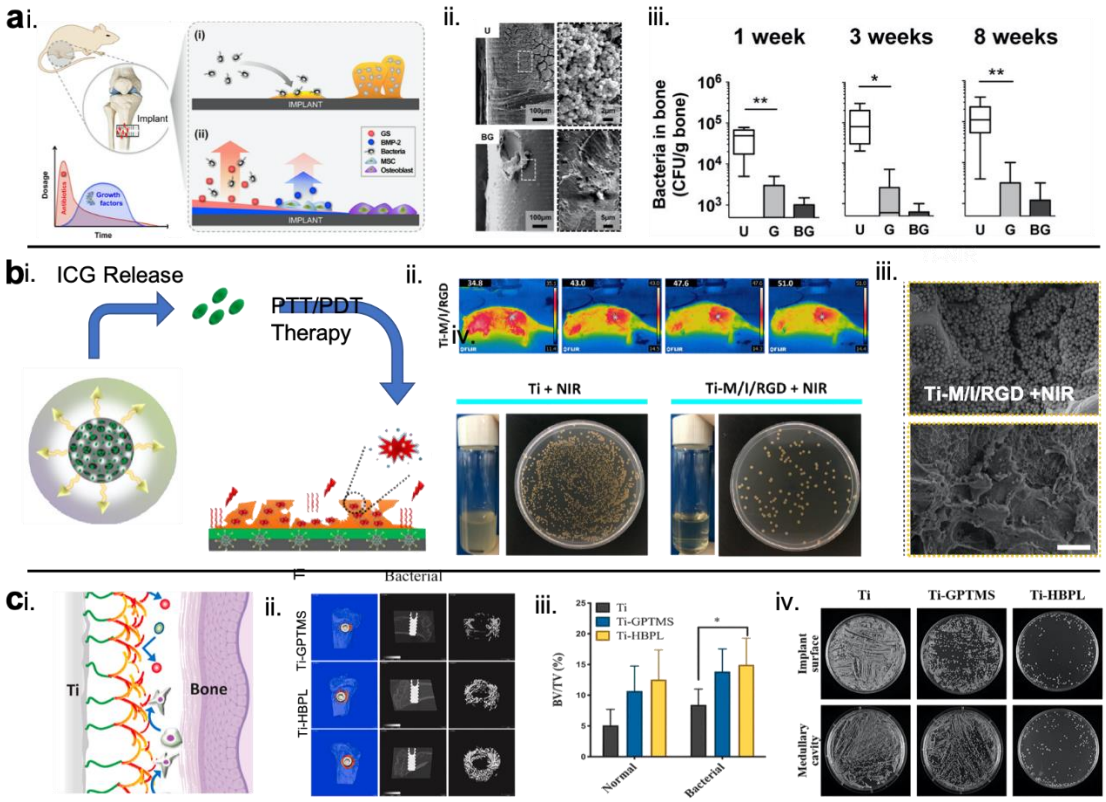

Figure 4. In vivo studies for antibacterial coatings. a) Doxycycline coating titanium was implanted into the tibia of a rabbit model and showed an increased bone formation toward the titanium screw using a 3D micro-CT technique. Figures 4a. were modified with permissions.[57] **b)** Mesoporous polydopamine nanoparticles were loaded with osteogenic peptide RGD and indocyanine green (ICG) to enhance osseointegration and eradicated biofilms upon near infrared (NIR) stimulus, respectively. When exposed to NIR, the ICG in the nanoparticles produced photothermal and photodynamic therapies to destroy biofilms and kill S. aureus with 99.7% efficiency. Scale bar in 5biii. represents 5 µm. Figures 4b. were modified with permissions.[66] **c)** Titanium coated with a hyperbranched poly-L-lysine

promoted osseointegration (ii, iii) and lysed bacteria (iv) in a rat animal model. Figures 4c. were modified with permissions.[46]

6. Commercialization of antibacterial coatings

Although several antibacterial coatings have been presented thus far, only a handful have been adopted in commercial and clinical settings. For example, the Defensive Antibacterial Coating (DAC) is a hydrogel composed of hyaluronic acid and poly-lactic acid, components which are naturally produced by the body.[165] This coating is meant to be applied onto the medical device at the time of operation, providing a hydrophilic physical barrier which prevents bacteria adhesion. Furthermore, this coating is resorbed by the body within 72 hours, detaching any bacteria into the planktonic phase in the process. The DAC coating can also be combined with active antibiotics, which would be released as the hydrogel dissociates. Although this coating provides an easy solution in the short-term, it is evident that such coating would not provide protection days after the surgery. An antibiotic-tethered coating has also been approved for intermedullary nails for tibia injuries in Switzerland.[166] The current coating is designed with gentamicin, but this technology could be implemented with other antibiotics. As discussed earlier, antibiotic coatings can be cytotoxic in large concentrations or could lead to drug-resistant bacteria, therefore making this coating more difficult to be adopted worldwide. Moreover, antibiotics require a minimum inhibitory concentration (MIC) to be efficient against a pathogen, which limits the long-term results of such coating as these molecules tend to degrade over time. A different coating which has been approved in some European countries is Bactiguard.[167] This metal coating is composed of a gold, silver, and palladium, which created a small current through a galvanic effect to prevent bacterial adhesion.[167,168] Metallic coatings have the potential to prevent bacteria adhesion long-term, as the coating does not dissociate. Furthermore, these noble metals will not impede ossiointegration, so long as the concentrations of any ions produced remains low. Silver-containing hydroxy apatite has also been developed for use in orthopedic applications and for spinal surgeries.[102] These coatings have been shown to prevent bacteria postoperatively, and also provide exceptional osteoconductive properties due to the HA layer. Although these metallic coatings are becoming popular due to the low risk of bacterial resistance, there is still some skepticism

behind metallic coatings, mainly, the potential toxicity of metal ions' release, or that the antibacterial pathways are still not clear.[169]

7. Conclusion

Implant-associated infections remain one of the major causes for medical device failure, especially in dental and orthopedic settings. This review highlights several strategies employed on titanium to prevent implant infections. These strategies include anti-adhesion coatings to repel bacteria or bactericidal coatings that lyse bacteria. In the later strategy, surfaces are typically modified to create a non-stick coating using polymers, superhydrophobic, liquid-infused or other strategies. Care must be employed when designing these coatings since they can also prevent host cell interaction which can impede new bone formation and lead to aseptic loosening. However, through the combination of these surface coatings with osteogenic factors, proper osseointegration is possible. If the goal is to use these coatings in orthopedic or dental settings, these surfaces must be tested against bacteria attachment, but also proper bone integration. Furthermore, these coatings need to be tested for their long-term stability, as several studies showed these coatings to be effective after 24- or 48-hours, with few experiments spanning more than two weeks. Nevertheless, the multifunctional coatings do show a promising steppingstone to develop these technologies to prevent IAI long-term. The second major category of antibacterial coatings were composed of bactericidal agents. Metallic coatings have been shown to have some of the greatest longevity because these coatings do not rely on molecules that degrade or elude from the surface to properly fend off against bacteria. However, metallic coatings have poor specificity, which increases the probability of cytotoxic interactions with the host and promote inflammation and prosthetic loosening. For this reason, these coatings must be further optimized to prevent these negative effects. Other bactericidal coating includes antibiotics and lytic proteins that have been shown to be effective against bacteria with higher specificity. These molecules are either covalently attached onto the surface or are loaded into the structure, allowing it to elute from the surface. In some coatings, the structure material is biodegradable which allows for different dosing kinetics from the bactericidal agents. The advantages from the covalently bonded molecules, is that their availability is not depleted and lost systematically, while protecting the surface upon

bacterial contact. The downside is that this strategy limits the interactions between these molecules and nearby bacteria.

Moreover, their long-term stability needs to be better understood, as lysed bacterial components could adhere to the surface, essentially blocking the interactions between the bactericidal agents and newly attached bacteria. The advantages of loading the structure with the bactericidal coatings include a higher loading capacity, and controlled dosing kinetics. Care must be employed, since large initial burst of the bactericidal molecules can be cytotoxic or could deplete the coating from the bactericidal molecules. Moreover, unlike metallic coatings, antibiotics might not be effective long-term and methods to prolong their stability needs to be investigated. A new strategy that could circumvent the issue discussed with antibiotics or metallic coatings can arise from the use of bacteriophages. Bacteriophages have been shown to be highly specific to a bacteria family, therefore reducing the chance for cytotoxicity. Furthermore, because bacteriophages reproduce after infecting the host bacteria, their availability is more abundant, and not limited by what was loaded onto the surface. Although this strategy is still in its infancy, it shows promising results for future study and for future commercial products.

8. References

1. López-Valverde, N., Macedo-De-Sousa, B., López-Valverde, A. & Ramírez, J. M. Effectiveness of antibacterial surfaces in osseointegration of titanium dental implants: A systematic review. *Antibiotics* **10**, (2021).
2. Sakka, S., Baroudi, K. & Nassani, M. Z. Factors associated with early and late failure of dental implants. *J Investig Clin Dent* **3**, 258–261 (2012).
3. *Early Revisions of Hip and Knee Replacements in Canada: A Quality, Productivity and Capacity Issue*. (2020).
4. D'Onofrio, K. Infection Most Common Culprit of Revision TKA Failure. https://www.aaos.org/aaosnow/2020/aaos-now-special-edition/research/557_knee/ (2020).
5. Trouillet-Assant, S. *et al.* Dual Impact of Live Staphylococcus aureus on the Osteoclast Lineage, Leading to Increased Bone Resorption. *J Infect Dis* **211**, 571–581 (2015).
6. Rasmussen, T. B. & Givskov, M. Quorum-sensing inhibitors as anti-pathogenic drugs. *International Journal of Medical Microbiology* **296**, 149–161 (2006).
7. Villegas, M. *et al.* Enhancing osseointegration and mitigating bacterial biofilms on medical-grade titanium with chitosan-conjugated liquid-infused coatings. *Sci Rep* **12**, 1–11 (2022).

8. Seth, A. K. *et al.* In vivo modeling of biofilm-infected wounds: A review. *Journal of Surgical Research* vol. 178 330–338 Preprint at https://doi.org/10.1016/j.jss.2012.06.048 (2012).
9. Zapotoczna, M., O'Neill, E. & O'Gara, J. P. Untangling the Diverse and Redundant Mechanisms of Staphylococcus aureus Biofilm Formation. *PLoS Pathogens* vol. 12 Preprint at https://doi.org/10.1371/journal.ppat.1005671 (2016).
10. Roy, R., Tiwari, M., Donelli, G. & Tiwari, V. Strategies for combating bacterial biofilms: A focus on anti-biofilm agents and their mechanisms of action. *Virulence* **9**, 522–554 (2018).
11. Lewis, K. Persister Cells. *Annu Rev Microbiol* **64**, 357–372 (2010).
12. Bhandari, M., Smith, J., Miller, L. E. & Block, J. E. Clinical and Economic Burden of Revision Knee Arthroplasty. *Clin Med Insights Arthritis Musculoskelet Disord* **5**, 89 (2012).
13. Zimmerli, W. Clinical presentation and treatment of orthopaedic implant-associated infection. *J Intern Med* **276**, 111–119 (2014).
14. Shi, Z., Neoh, K. G., Kang, E. T., Poh, C. & Wang, W. Bacterial adhesion and osteoblast function on titanium with surface-grafted chitosan and immobilized RGD peptide. *J Biomed Mater Res A* **86A**, 865–872 (2008).
15. Petrie, T. A., Reyes, C. D., Burns, K. L. & García, A. J. Simple application of fibronectin–mimetic coating enhances osseointegration of titanium implants. *J Cell Mol Med* **13**, 2602 (2009).
16. Vertesich, K. *et al.* Alendronate enhances osseointegration in a murine implant model. *J Orthop Res* **39**, 719 (2021).
17. Lee, D. W., Yun, Y. P., Park, K. & Kim, S. E. Gentamicin and bone morphogenic protein-2 (BMP-2)-delivering heparinized-titanium implant with enhanced antibacterial activity and osteointegration. *Bone* **50**, 974–982 (2012).
18. Saithna, A. The influence of hydroxyapatite coating of external fixator pins on pin loosening and pin track infection: A systematic review. *Injury* **41**, 128–132 (2010).
19. Chen, C., Li, H., Kong, X., Zhang, S. M. & Lee, I. S. Immobilizing osteogenic growth peptide with and without fibronectin on a titanium surface: effects of loading methods on mesenchymal stem cell differentiation. *Int J Nanomedicine* **10**, 283 (2015).
20. Eliaz, N. & Metoki, N. Calcium Phosphate Bioceramics: A Review of Their History, Structure, Properties, Coating Technologies and Biomedical Applications. *Materials* **10**, 334 (2017).
21. Wildemann, B., Lübberstedt, M., Haas, N. P., Raschke, M. & Schmidmaier, G. IGF-I and TGF-beta 1 incorporated in a poly(d,l-lactide) implant coating maintain their activity over long-term storage—cell culture studies on primary human osteoblast-like cells. *Biomaterials* **25**, 3639–3644 (2004).
22. Raines, A. L. *et al.* VEGF-A Regulates Angiogenesis during Osseointegration of Ti Implants via Paracrine/Autocrine Regulation of Osteoblast Response to Hierarchical Microstructure of the Surface. *J Biomed Mater Res A* **107**, 423 (2019).
23. Tan, G. *et al.* Antibacterial and Anti-Inflammatory Coating Materials for Orthopedic Implants: A Review. *Coatings 2021, Vol. 11, Page 1401* **11**, 1401 (2021).
24. Li, Q., Liang, B., Wang, F. & Wang, Z. Delivery of Interleukin 4 from a Titanium Substrate Coated with Graphene Oxide for Enhanced Osseointegration by Regulating Macrophage Polarization. *ACS Biomater Sci Eng* **6**, 5215–5229 (2020).

25. Vaidya, P., Mahale, S., Kale, S. & Patil, A. Osseointegration-A Review. *IOSR Journal of Dental and Medical Sciences (IOSR-JDMS) e-ISSN* **16**, 45–48 (2017).
26. Lu, X. *et al.* Multifunctional Coatings of Titanium Implants Toward Promoting Osseointegration and Preventing Infection: Recent Developments. *Front Bioeng Biotechnol* **9**, (2021).
27. Agarwal, R. & García, A. J. Biomaterial strategies for engineering implants for enhanced osseointegration and bone repair. *Advanced Drug Delivery Reviews* vol. 94 53–62 Preprint at https://doi.org/10.1016/j.addr.2015.03.013 (2015).
28. Zhao, T., Chu, Z., Ma, J. & Ouyang, L. Immunomodulation Effect of Biomaterials on Bone Formation. *Journal of Functional Biomaterials 2022, Vol. 13, Page 103* **13**, 103 (2022).
29. Kaufman, M. G., Meaike, J. D. & Izaddoost, S. A. Orthopedic Prosthetic Infections: Diagnosis and Orthopedic Salvage. *Semin Plast Surg* **30**, 66 (2016).
30. Villegas, M. *et al.* Antibiotic-Impregnated Liquid-Infused Coatings Suppress the Formation of Methicillin-Resistant Staphylococcus aureus Biofilms. *ACS Appl Mater Interfaces* **13**, 27774–27783 (2021).
31. Lin, C. *et al.* Effect of superhydrophobic surface of titanium on staphylococcus aureus adhesion. *J Nanomater* **2011**, (2011).
32. Souza, J. G. S. *et al.* Targeting Pathogenic Biofilms: Newly Developed Superhydrophobic Coating Favors a Host-Compatible Microbial Profile on the Titanium Surface. *ACS Appl Mater Interfaces* **12**, 10118–10129 (2020).
33. Montgomerie, Z. & Popat, K. C. Improved hemocompatibility and reduced bacterial adhesion on superhydrophobic titania nanoflower surfaces. *Materials Science and Engineering: C* **119**, 111503 (2021).
34. Bartlet, K., Movafaghi, S., Dasi, L. P., Kota, A. K. & Popat, K. C. Antibacterial activity on superhydrophobic titania nanotube arrays. *Colloids Surf B Biointerfaces* **166**, 179–186 (2018).
35. Fadeeva, E. *et al.* Bacterial retention on superhydrophobic titanium surfaces fabricated by femtosecond laser ablation. *Langmuir* **27**, 3012–3019 (2011).
36. Doll, K. *et al.* Development of Laser-Structured Liquid-Infused Titanium with Strong Biofilm-Repellent Properties. *ACS Appl Mater Interfaces* **9**, 9359–9368 (2017).
37. Doll, K. *et al.* Liquid-Infused Structured Titanium Surfaces: Antiadhesive Mechanism to Repel Streptococcus oralis Biofilms. *ACS Appl Mater Interfaces* **11**, 23026–23038 (2019).
38. Zhang, F., Zhang, Z., Zhu, X., Kang, E. T. & Neoh, K. G. Silk-functionalized titanium surfaces for enhancing osteoblast functions and reducing bacterial adhesion. *Biomaterials* **29**, 4751–4759 (2008).
39. Cheng, Y. F. *et al.* Tannic acid-assisted deposition of silk sericin on the titanium surfaces for antifouling application. *Colloids and Interface Science Communications* **35**, (2020).
40. Harris, L. G., Tosatti, S., Wieland, M., Textor, M. & Richards, R. G. Staphylococcus aureus adhesion to titanium oxide surfaces coated with non-functionalized and peptide-functionalized poly(L-lysine)-grafted- poly(ethylene glycol) copolymers. *Biomaterials* **25**, (2004).
41. Khoo, X. *et al.* Staphylococcus aureus resistance on titanium coated with multivalent PEGylated-peptides. *Biomaterials* **31**, 9285–9292 (2010).

42. Valliammai, A., Selvaraj, A., Mathumitha, P., Aravindraja, C. & Pandian, S. K. Polymeric antibiofilm coating comprising synergistic combination of citral and thymol prevents methicillin-resistant Staphylococcus aureus biofilm formation on titanium. *Materials Science and Engineering C* **121**, (2021).
43. Guo, L. L. *et al.* Simultaneous deposition of tannic acid and poly(ethylene glycol) to construct the antifouling polymeric coating on Titanium surface. *Colloids Surf B Biointerfaces* **200**, 111592 (2021).
44. Şimşek, M., Aldemir, S. D. & Gümüşderelioğlu, M. Anticellular PEO coatings on titanium surfaces by sequential electrospinning and crosslinking processes. *Emergent Mater* **2**, (2019).
45. Boschetto, F. *et al.* Antibacterial and osteoconductive effects of chitosan/polyethylene oxide (PEO)/bioactive glass nanofibers for orthopedic applications. *Applied Sciences (Switzerland)* **10**, (2020).
46. Yang, Z. *et al.* Covalent grafting of hyperbranched poly-L-lysine on Ti-based implants achieves dual functions of antibacteria and promoted osteointegration in vivo. *Biomaterials* **269**, 120534 (2021).
47. Zhang, Y. *et al.* Tantalum Nitride-Decorated Titanium with Enhanced Resistance to Microbiologically Induced Corrosion and Mechanical Property for Dental Application. *PLoS One* **10**, e0130774 (2015).
48. Zhou, J., Wang, X. & Zhao, L. Antibacterial, angiogenic, and osteogenic activities of Ca, P, Co, F, and Sr compound doped titania coatings with different Sr content. *Scientific Reports 2019 9:1* **9**, 1–11 (2019).
49. Kulkarni Aranya, A. *et al.* Antibacterial and bioactive coatings on titanium implant surfaces. *J Biomed Mater Res A* **105**, 2218–2227 (2017).
50. Zuo, K. *et al.* Zinc-Doping Induces Evolution of Biocompatible Strontium-Calcium-Phosphate Conversion Coating on Titanium to Improve Antibacterial Property. *ACS Appl Mater Interfaces* **14**, 7690–7705 (2022).
51. Zhang, Y. Y. *et al.* Evaluation of osteogenic and antibacterial properties of strontium/silver-containing porous TiO2 coatings prepared by micro-arc oxidation. *J Biomed Mater Res B Appl Biomater* **109**, 505–516 (2021).
52. Ando, Y. *et al.* Calcium phosphate coating containing silver shows high antibacterial activity and low cytotoxicity and inhibits bacterial adhesion. *Materials Science and Engineering: C* **30**, 175–180 (2010).
53. Thukkaram, M. *et al.* Investigation of Ag/a-C:H Nanocomposite Coatings on Titanium for Orthopedic Applications. *ACS Appl Mater Interfaces* **12**, 23655–23666 (2020).
54. Jose, B., Antoci, V., Zeiger, A. R., Wickstrom, E. & Hickok, N. J. Vancomycin covalently bonded to titanium beads kills Staphylococcus aureus. *Chem Biol* **12**, 1041–1048 (2005).
55. He, S. *et al.* Antibiotic-decorated titanium with enhanced antibacterial activity through adhesive polydopamine for dental/bone implant. *J R Soc Interface* **11**, (2014).
56. Zhang, Y. *et al.* Smart Titanium Coating Composed of Antibiotic Conjugated Peptides as an Infection-Responsive Antibacterial Agent. *Macromol Biosci* **21**, 1–8 (2021).
57. Min, J. *et al.* Designer Dual Therapy Nanolayered Implant Coatings Eradicate Biofilms and Accelerate Bone Tissue Repair. *ACS Nano* **10**, 4441–4450 (2016).
58. Kranthi Kiran, A. S. *et al.* Drug loaded electrospun polymer/ceramic composite nanofibrous coatings on titanium for implant related infections. *Ceram Int* **45**, 18710–18720 (2019).

59. Zarghami, V., Ghorbani, M., Bagheri, K. P. & Shokrgozar, M. A. Improving bactericidal performance of implant composite coatings by synergism between Melittin and tetracycline. *J Mater Sci Mater Med* **33**, (2022).
60. Choi, H. *et al.* Drug Release from Thermo-Responsive Polymer Brush Coatings to Control Bacterial Colonization and Biofilm Growth on Titanium Implants. *Adv Healthc Mater* **10**, 1–12 (2021).
61. Zhang, B., Braun, B. M., Skelly, J. D., Ayers, D. C. & Song, J. Significant Suppression of Staphylococcus aureus Colonization on Intramedullary Ti6Al4V Implants Surface-Grafted with Vancomycin-Bearing Polymer Brushes. *ACS Appl Mater Interfaces* **11**, 28641–28647 (2019).
62. Walter, M. S. *et al.* Bioactive implant surface with electrochemically bound doxycycline promotes bone formation markers in vitro and in vivo. *Dental Materials* **30**, 200–214 (2014).
63. Nie, B. *et al.* Immobilizing bacitracin on titanium for prophylaxis of infections and for improving osteoinductivity: An in vivo study. *Colloids Surf B Biointerfaces* **150**, 183–191 (2017).
64. Kaur, S., Harjai, K. & Chhibber, S. In Vivo Assessment of Phage and Linezolid Based Implant Coatings for Treatment of Methicillin Resistant S. aureus (MRSA) mediated orthopaedic device related infections. *PLoS One* **11**, 1–23 (2016).
65. Kaur, S., Harjai, K. & Chhibber, S. Bacteriophage Mediated Killing of Staphylococcus aureus In Vitro on Orthopaedic K Wires in Presence of Linezolid Prevents Implant Colonization. *PLoS One* **9**, (2014).
66. Yuan, Z. *et al.* Remote eradication of biofilm on titanium implant via near-infrared light triggered photothermal/photodynamic therapy strategy. *Biomaterials* **223**, 119479 (2019).
67. Zhang, X., Wang, L. & Levänen, E. Superhydrophobic surfaces for the reduction of bacterial adhesion. *RSC Adv* **3**, 12003–12020 (2013).
68. Gallardo-Moreno, A. M. *et al.* In vitro biocompatibility and bacterial adhesion of physico-chemically modified Ti6Al4V surface by means of UV irradiation. *Acta Biomater* **5**, 181–192 (2009).
69. Wenzel, R. N. Resistance of Solid Surfaces to Wetting by Water. *Ind Eng Chem* **28**, 988–994 (1936).
70. Cassie, A. B. D. & Baxter, S. Wettability of porous surfaces. *Transactions of the Faraday Society* **40**, 546 (1944).
71. Wang, Z. & Ren, B. Preparation of superhydrophobic titanium surface via the combined modification of hierarchical micro/nanopatterning and fluorination. *J Coat Technol Res* **19**, 967–975 (2022).
72. Hwang, G. B. *et al.* The Anti-Biofouling Properties of Superhydrophobic Surfaces are Short-Lived. *ACS Nano* **12**, 6050–6058 (2018).
73. Saulacic, N. & Schaller, B. Prevalence of Peri-Implantitis in Implants with Turned and Rough Surfaces: a Systematic Review. *J Oral Maxillofac Res* **10**, e1 (2019).
74. Peppou-Chapman, S., Hong, J. K., Waterhouse, A. & Neto, C. Life and death of liquid-infused surfaces: a review on the choice, analysis and fate of the infused liquid layer. *Chem Soc Rev* **49**, 3688 (2020).
75. Badv, M., Jaffer, I. H., Weitz, J. I. & Didar, T. F. An omniphobic lubricant-infused coating produced by chemical vapor deposition of hydrophobic organosilanes attenuates clotting on catheter surfaces. *Sci Rep* **7**, 11639 (2017).

76. Villegas, M., Cetinic, Z., Shakeri, A. & Didar, T. F. Fabricating smooth PDMS microfluidic channels from low-resolution 3D printed molds using an omniphobic lubricant-infused coating. *Anal Chim Acta* **1000**, 248–255 (2018).
77. Hosseini, A. *et al.* Conductive Electrochemically Active Lubricant-Infused Nanostructured Surfaces Attenuate Coagulation and Enable Friction-Less Droplet Manipulation. *Adv Mater Interfaces* **5**, 1800617 (2018).
78. Badv, M., Imani, S. M., Weitz, J. I. & Didar, T. F. Lubricant-Infused Surfaces with Built-In Functional Biomolecules Exhibit Simultaneous Repellency and Tunable Cell Adhesion. *ACS Nano* **12**, 10890–10902 (2018).
79. Osborne, M., Aryasomayajula, A., Shakeri, A., Selvaganapathy, P. R. & Didar, T. F. Suppression of Biofouling on a Permeable Membrane for Dissolved Oxygen Sensing Using a Lubricant-Infused Coating. *ACS Sens* **4**, 687–693 (2019).
80. Badv, M. *et al.* Biofunctional Lubricant-Infused Vascular Grafts Functionalized with Silanized Bio-Inks Suppress Thrombin Generation and Promote Endothelialization. *ACS Biomater Sci Eng* **5**, 6485–6496 (2019).
81. Badv, M., Weitz, J. I. & Didar, T. F. Lubricant-Infused PET Grafts with Built-In Biofunctional Nanoprobes Attenuate Thrombin Generation and Promote Targeted Binding of Cells. *Small* **15**, 1905562 (2019).
82. Shakeri, A. *et al.* Contamination and carryover free handling of complex fluids using lubricant-infused pipette tips. *Scientific Reports 2022 12:1* **12**, 1–10 (2022).
83. Villegas, M., Zhang, Y., Abu Jarad, N., Soleymani, L. & Didar, T. F. Liquid-Infused Surfaces: A Review of Theory, Design, and Applications. *ACS Nano* **13**, 8517–8536 (2019).
84. Wong, T.-S. *et al.* Bioinspired Selfrepairing Slip. *Nature* **477**, 443–447 (2011).
85. Mackie, G., Gao, L., Yau, S., Leslie, D. C. & Waterhouse, A. Clinical Potential of Immobilized Liquid Interfaces: Perspectives on Biological Interactions. *Trends in Biotechnology* vol. 37 268–280 Preprint at https://doi.org/10.1016/j.tibtech.2018.08.003 (2019).
86. Yousefi, H. *et al.* LISzyme Biosensors: DNAzymes Embedded in an Anti-biofouling Platform for Hands-free Real-Time Detection of Bacterial Contamination in Milk. *ACS Nano* **16**, 29–37 (2022).
87. Kasapgil, E. *et al.* Polysiloxane Nanofilaments Infused with Silicone Oil Prevent Bacterial Adhesion and Suppress Thrombosis on Intranasal Splints. *ACS Biomater Sci Eng* **7**, 541–552 (2021).
88. Szaraniec, B., Pielichowska, K., Pac, E. & Menaszek, E. Multifunctional polymer coatings for titanium implants. *Materials Science and Engineering C* **93**, (2018).
89. Harris, L. G., Tosatti, S., Wieland, M., Textor, M. & Richards, R. G. Staphylococcus aureus adhesion to titanium oxide surfaces coated with non-functionalized and peptide-functionalized poly(L-lysine)-grafted- poly(ethylene glycol) copolymers. *Biomaterials* **25**, (2004).
90. Qin, S., Xu, K., Nie, B., Ji, F. & Zhang, H. Approaches based on passive and active antibacterial coating on titanium to achieve antibacterial activity. *J Biomed Mater Res A* **106**, 2531–2539 (2018).
91. Olmo, J. A. Del, Ruiz-Rubio, L., Pérez-Alvarez, L., Sáez-Martínez, V. & Vilas-Vilela, J. L. Antibacterial Coatings for Improving the Performance of Biomaterials. *Coatings 2020, Vol. 10, Page 139* **10**, 139 (2020).

92. Guo, C. *et al.* Poly-l-lysine/Sodium Alginate Coating Loading Nanosilver for Improving the Antibacterial Effect and Inducing Mineralization of Dental Implants. *ACS Omega* **5**, 10562–10571 (2020).
93. Vester, H., Wildemann, B., Schmidmaier, G., Stöckle, U. & Lucke, M. Gentamycin delivered from a PDLLA coating of metallic implants: In vivo and in vitro characterisation for local prophylaxis of implant-related osteomyelitis. *Injury* **41**, 1053–1059 (2010).
94. Wu, S. *et al.* Long-lasting renewable antibacterial porous polymeric coatings enable titanium biomaterials to prevent and treat peri-implant infection. *Nat Commun* **12**, 1–14 (2021).
95. Xing, R. *et al.* Antibacterial effect of doxycycline-coated dental abutment surfaces. *Biomed Mater* **10**, (2015).
96. Ding, L., Zhang, P., Wang, X. & Kasugai, S. A doxycycline-treated hydroxyapatite implant surface attenuates the progression of peri-implantitis: A radiographic and histological study in mice. *Clin Implant Dent Relat Res* **21**, 154–159 (2019).
97. Rahmati, M. *et al.* Coating doxycycline on titanium-based implants: Two in vivo studies. *Bioact Mater* **5**, 787–797 (2020).
98. Song, W. *et al.* Doxycycline-loaded coaxial nanofiber coating of titanium implants enhances osseointegration and inhibits Staphylococcus aureus infection. *Biomedical Materials* **12**, 045008 (2017).
99. Nie, B., Ao, H., Zhou, J., Tang, T. & Yue, B. Biofunctionalization of titanium with bacitracin immobilization shows potential for anti-bacteria, osteogenesis and reduction of macrophage inflammation. *Colloids Surf B Biointerfaces* **145**, 728–739 (2016).
100. Shahi, R. G. *et al.* Novel bioactive tetracycline-containing electrospun polymer fibers as a potential antibacterial dental implant coating. *Odontology* **105**, 354–363 (2017).
101. Amankwah, S., Adisu, M., Gorems, K., Abdella, K. & Kassa, T. Assessment of Phage-Mediated Inhibition and Removal of Multidrug-Resistant Pseudomonas aeruginosa Biofilm on Medical Implants. (2022) doi:10.2147/IDR.S367460.
102. Morimoto, T. *et al.* Development of Silver-Containing Hydroxyapatite-Coated Antimicrobial Implants for Orthopaedic and Spinal Surgery. *Medicina 2022, Vol. 58, Page 519* **58**, 519 (2022).
103. Shimabukuro, M. Antibacterial Property and Biocompatibility of Silver, Copper, and Zinc in Titanium Dioxide Layers Incorporated by One-Step Micro-Arc Oxidation: A Review. *Antibiotics 2020, Vol. 9, Page 716* **9**, 716 (2020).
104. Ray, P. D., Huang, B. W. & Tsuji, Y. Reactive oxygen species (ROS) homeostasis and redox regulation in cellular signaling. *Cell Signal* **24**, 981–990 (2012).
105. Sen, A. & Imlay, J. A. How Microbes Defend Themselves From Incoming Hydrogen Peroxide. *Front Immunol* **12**, 1104 (2021).
106. Honda, M. *et al.* Bactericidal and Bioresorbable Calcium Phosphate Cements Fabricated by Silver-Containing Tricalcium Phosphate Microspheres. *International Journal of Molecular Sciences 2020, Vol. 21, Page 3745* **21**, 3745 (2020).
107. Noda, I. *et al.* Development of novel thermal sprayed antibacterial coating and evaluation of release properties of silver ions. *J Biomed Mater Res B Appl Biomater* **89B**, 456–465 (2009).
108. Zhang, W. *et al.* Effects of strontium in modified biomaterials. *Acta Biomater* **7**, 800–808 (2011).

109. Aykul, S. & Martinez-Hackert, E. Determination of half-maximal inhibitory concentration using biosensor-based protein interaction analysis. *Anal Biochem* **508**, 97–103 (2016).
110. Kuehl, R. *et al.* Preventing Implant-Associated infections by silver coating. *Antimicrob Agents Chemother* **60**, 2467–2475 (2016).
111. Mokabber, T., Cao, H. T., Norouzi, N., Van Rijn, P. & Pei, Y. T. Antimicrobial Electrodeposited Silver-Containing Calcium Phosphate Coatings. *ACS Appl Mater Interfaces* **12**, 5531–5541 (2020).
112. Ziąbka, M. *et al.* Antibacterial composite hybrid coatings of veterinary medical implants. *Materials Science and Engineering: C* **112**, 110968 (2020).
113. Devasconcellos, P., Bose, S., Beyenal, H., Bandyopadhyay, A. & Zirkle, L. G. Antimicrobial particulate silver coatings on stainless steel implants for fracture management. *Materials Science and Engineering C* **32**, 1112–1120 (2012).
114. Zhang, B., Braun, B. M., Skelly, J. D., Ayers, D. C. & Song, J. Significant Suppression of Staphylococcus aureus Colonization on Intramedullary Ti6Al4V Implants Surface-Grafted with Vancomycin-Bearing Polymer Brushes. *ACS Appl Mater Interfaces* **11**, 28641–28647 (2019).
115. Esteban, J., Vallet-Regí, M. & Aguilera-Correa, J. J. Antibiotics-and heavy metals-based titanium alloy surface modifications for local prosthetic joint infections. *Antibiotics* **10**, (2021).
116. Bargavi, P. *et al.* Drug infused Al2O3-bioactive glass coatings toward the cure of orthopedic infection. *Prog Biomater* **11**, 79–94 (2022).
117. Stigter, M., Bezemer, J., De Groot, K. & Layrolle, P. Incorporation of different antibiotics into carbonated hydroxyapatite coatings on titanium implants, release and antibiotic efficacy. *Journal of Controlled Release* **99**, 127–137 (2004).
118. Ballarre, J. *et al.* Versatile bioactive and antibacterial coating system based on silica, gentamicin, and chitosan: Improving early stage performance of titanium implants. *Surf Coat Technol* **381**, 125138 (2020).
119. Garg, D., Matai, I. & Sachdev, A. Toward Designing of Anti-infective Hydrogels for Orthopedic Implants: From Lab to Clinic. *ACS Biomater Sci Eng* **7**, 1933–1961 (2021).
120. Zhang, L. *et al.* Electrospun vancomycin-loaded coating on titanium implants for the prevention of implant-associated infections. *Int J Nanomedicine* **9**, 3027–3036 (2014).
121. Djošić, M., Janković, A. & Mišković-Stanković, V. Electrophoretic deposition of biocompatible and bioactive hydroxyapatite-based coatings on titanium. *Materials* **14**, (2021).
122. Song, J. *et al.* Electrophoretic Deposition of Chitosan Coatings Modified with Gelatin Nanospheres to Tune the Release of Antibiotics. *ACS Appl Mater Interfaces* **8**, 13785–13792 (2016).
123. Rajesh, K. *et al.* Surface Modified Metallic Orthopedic Implant for Sustained Drug Release and Osteocompatibility. *ACS Appl Bio Mater* **2**, 4181–4192 (2019).
124. Aguilera-Correa, J. J. *et al.* A New Antibiotic-Loaded Sol-Gel Can Prevent Bacterial Prosthetic Joint Infection: From in vitro Studies to an in vivo Model. *Front Microbiol* **10**, 1–14 (2020).
125. Jaafar, A., Hecker, C., Árki, P. & Joseph, Y. Sol-gel derived hydroxyapatite coatings for titanium implants: A review. *Bioengineering* **7**, 1–23 (2020).

126. Nichol, T. *et al.* The antimicrobial activity and biocompatibility of a controlled gentamicin-releasing single-layer sol-gel coating on hydroxyapatite-coated titanium. *Bone and Joint Journal* **103 B**, 522–529 (2021).
127. Zhang, L. *et al.* Polymeric nanoarchitectures on Ti-based implants for antibacterial applications. *ACS Appl Mater Interfaces* **6**, 17323–17345 (2014).
128. Ferreira, M. B., Myiagi, S., Nogales, C. G., Campos, M. S. & Lage-Marques, J. L. Time- and concentration-dependent cytotoxicity of antibiotics used in endodontic therapy. *Journal of Applied Oral Science* **18**, 259 (2010).
129. Zhang, H. *et al.* Vancomycin-loaded titanium coatings with an interconnected micro-patterned structure for prophylaxis of infections: An: in vivo study. *RSC Adv* **8**, 9223–9231 (2018).
130. Chouirfa, H., Bouloussa, H., Migonney, V. & Falentin-Daudré, C. Review of titanium surface modification techniques and coatings for antibacterial applications. *Acta Biomater* **83**, 37–54 (2019).
131. Antoci, V. *et al.* The inhibition of Staphylococcus epidermidis biofilm formation by vancomycin-modified titanium alloy and implications for the treatment of periprosthetic infection. *Biomaterials* **29**, 4684–4690 (2008).
132. Mattioli-Belmonte, M. *et al.* Characterization and cytocompatibility of an antibiotic/chitosan/ cyclodextrins nanocoating on titanium implants. *Carbohydr Polym* **110**, 173–182 (2014).
133. Jennings, J. A. *et al.* Novel Antibiotic-loaded Point-of-care Implant Coating Inhibits Biofilm. *Clin Orthop Relat Res* **473**, 2270–2282 (2015).
134. Gibb, B. P. & Hadjiargyrou, M. Bacteriophage therapy for bone and joint infections an instructional review. *Bone and Joint Journal* **103 B**, 234–244 (2021).
135. Li, B. & Webster, T. J. Bacteria antibiotic resistance: New challenges and opportunities for implant-associated orthopedic infections. *Journal of Orthopaedic Research* **36**, 22–32 (2018).
136. Abedon, S. T., Kuhl, S. J., Blasdel, B. G. & Kutter, E. M. Phage treatment of human infections. *Bacteriophage* **1**, 66 (2011).
137. Merril, C. R., Scholl, D. & Adhya, S. L. The prospect for bacteriophage therapy in Western medicine. *Nat Rev Drug Discov* **2**, 489–497 (2003).
138. Kortright, K. E., Chan, B. K., Koff, J. L. & Turner, P. E. Phage Therapy: A Renewed Approach to Combat Antibiotic-Resistant Bacteria. *Cell Host Microbe* **25**, 219–232 (2019).
139. Mushegian, A. R. Are There 1031 Virus Particles on Earth, or More, or Fewer? *J Bacteriol* **202**, 2192–2197 (2020).
140. Fard, R. M. N. A Short Introduction to Bacteriophages. *Trends in Peptide and Protein Sciences* **1**, 7–13 (2016).
141. Bayat, F., Didar, T. F. & Hosseinidoust, Z. Emerging investigator series: bacteriophages as nano engineering tools for quality monitoring and pathogen detection in water and wastewater. *Environ Sci Nano* **8**, 367–389 (2021).
142. Melo, L. D. R., Oliveira, H., Pires, D. P., Dabrowska, K. & Azeredo, J. Phage therapy efficacy: a review of the last 10 years of preclinical studies. *Crit Rev Microbiol* **46**, 78–99 (2020).
143. Petrovic Fabijan, A. *et al.* Phage therapy for severe bacterial infections: a narrative review. *Medical Journal of Australia* **212**, 279–285 (2020).

144. Tian, L. *et al.* Phage display for the detection, analysis, disinfection, and prevention of Staphylococcus aureus. *Smart Medicine* **1**, e20220015 (2022).
145. Xie, Y., Wahab, L. & Gill, J. J. Development and validation of a microtiter plate-based assay for determination of bacteriophage host range and virulence. *Viruses* **10**, (2018).
146. Tian, L. *et al.* Self-assembling nanofibrous bacteriophage microgels as sprayable antimicrobials targeting multidrug-resistant bacteria. *Nature Communications 2022 13:1* **13**, 1–12 (2022).
147. Akanda, Z. Z., Taha, M. & Abdelbary, H. Current review—The rise of bacteriophage as a unique therapeutic platform in treating peri-prosthetic joint infections. *Journal of Orthopaedic Research* **36**, 1051–1060 (2018).
148. Kalatzis, P. G., Castillo, D., Katharios, P. & Middelboe, M. Bacteriophage interactions with marine pathogenic vibrios: Implications for phage therapy. *Antibiotics* **7**, 1–23 (2018).
149. Onsea, J. *et al.* Bacteriophage therapy as a treatment strategy for orthopaedi c-devi ce-related i nfecti ons: Where do we stand? *Eur Cell Mater* **39**, 193–210 (2020).
150. León, M. & Bastías, R. Virulence reduction in bacteriophage resistant bacteria. *Front Microbiol* **6**, 1–7 (2015).
151. Oechslin, F. Resistance development to bacteriophages occurring during bacteriophage therapy. *Viruses* **10**, (2018).
152. Onsea, J. *et al.* Bacteriophage therapy as a treatment strategy for orthopaedi c-devi ce-related i nfecti ons: Where do we stand? *Eur Cell Mater* **39**, 193–210 (2020).
153. Gibb, B. P. & Hadjiargyrou, M. Bacteriophage therapy for bone and joint infections an instructional review. *Bone and Joint Journal* **103 B**, 234–244 (2021).
154. Morris, J. L. *et al.* Evaluation of bacteriophage as an adjunct therapy for treatment of peri-prosthetic joint infection caused by Staphylococcus aureus. *PLoS One* **14**, 1–18 (2019).
155. Wroe, J. A., Johnson, C. T. & García, A. J. Bacteriophage delivering hydrogels reduce biofilm formation in vitro and infection in vivo. **108**, 39–49 (2020).
156. Barros, J. A. R. *et al.* Encapsulated bacteriophages in alginate-nanohydroxyapatite hydrogel as a novel delivery system to prevent orthopedic implant-associated infections. *Nanomedicine* **24**, 102145 (2020).
157. Cobb, L. H. *et al.* CRISPR-Cas9 modified bacteriophage for treatment of Staphylococcus aureus induced osteomyelitis and soft tissue infection. *PLoS One* **14**, 1–17 (2019).
158. Cobb, L. H. *et al.* CRISPR-Cas9 modified bacteriophage for treatment of Staphylococcus aureus induced osteomyelitis and soft tissue infection. *PLoS One* **14**, 1–17 (2019).
159. Park, J. Y. *et al.* Genetic engineering of a temperate phage-based delivery system for CRISPR/Cas9 antimicrobials against Staphylococcus aureus. *Sci Rep* **7**, 1–13 (2017).
160. Morris, J. L. *et al.* Evaluation of bacteriophage as an adjunct therapy for treatment of peri-prosthetic joint infection caused by Staphylococcus aureus. *PLoS One* **14**, 1–18 (2019).
161. Yilmaz, C. *et al.* Bacteriophage Therapy in Implant-Related Infections. *The Journal of Bone and Joint Surgery-American Volume* **95**, 117–125 (2013).
162. Ferry, T. *et al.* Phage Therapy as Adjuvant to Conservative Surgery and Antibiotics to Salvage Patients With Relapsing S. aureus Prosthetic Knee Infection. *Front Med (Lausanne)* **7**, 1–9 (2020).

163. Fischetti, V. A. Bacteriophage endolysins: A novel anti-infective to control Gram-positive pathogens. *International Journal of Medical Microbiology* **300**, 357–362 (2010).
164. Turnbull, G. *et al.* 3D bioactive composite scaffolds for bone tissue engineering. *Bioactive Materials* vol. 3 278–314 Preprint at https://doi.org/10.1016/j.bioactmat.2017.10.001 (2018).
165. DAC® | What is DAC®. http://www.dac-coating.com/dac/what-is-dac/.
166. EXPERT™ Tibial Nail and EXPERT™ Tibial Nail PROtect™. https://www.jnjmedtech.com/en-EMEA/product/expert-tibial-nail-etn.
167. The Bactiguard technology - Bactiguard. https://www.bactiguard.com/about-bactiguard/the-bactiguard-technology/.
168. Zimmer Natural Nail System. https://znnbactiguard.com/wp-content/uploads/2021/06/3405.1-EMEA-en-ZNN-with-Bactiguard-Brochure.pdf.
169. Zhang, E. *et al.* Antibacterial metals and alloys for potential biomedical implants. *Bioact Mater* **6**, 2569–2612 (2021).